FUNCTIONAL CHARACTERISATION OF HUMAN MUS81 COMPLEXES

Alessandra Pepe

London Research Institute, Cancer Research UK

and

University College London

PhD Supervisor: Dr Stephen C West

A thesis submitted for the degree of

Doctor of Philosophy

University College London

September 2013

DECLARATION

I Alessandra Pepe confirm that the work presented in this thesis is my own. Where information has been derived from other sources, I confirm that this has been indicated in the thesis.

'We live on an island surrounded by a sea of ignorance.

As our island of knowledge grows, so does the shore of our ignorance.'

John Archibald Wheeler

ABSTRACT

Human cells employ a variety of mechanisms to repair DNA damage and maintain genomic integrity. Structure-specific endonucleases play crucial roles in the repair of DNA lesions by removing secondary DNA structures that can lead to chromosome mis-segregation, aneuploidy and cancer. MUS81 is the catalytic subunit of two human structure-specific endonucleases, MUS81-EME1 and MUS81-EME2. MUS81 nuclease has been shown to function in the resolution of homologous recombination (HR) intermediates, in the repair of stalled replication forks (RFs) and in the maintenance of telomere length in alternative lengthening of telomeres (ALT)-positive cells. However, it is unknown whether the two MUS81 complexes differ in their biological functions.

To address this question, we carried out *in vivo* and *in vitro* studies to determine the roles of MUS81-EME1 and MUS81-EME2 in human cells. We found that EME2 interacts with MUS81 preferentially during the S-phase of the cell cycle, when MUS81 is important for the repair of stalled RFs. Cells treated with HU and depleted of MUS81 or EME2, but not of EME1, showed high levels of chromosomal aberrations, suggesting that the MUS81-EME2 complex is important for the maintenance of genomic stability following HU exposure. Also, depletion of EME2 or MUS81, but not of EME1, resulted in telomere loss, decreased rate of telomere sister chromatid exchanges (T-SCEs) and increased telomere fragility in ALT-positive cells. Consistent with the *in vivo* functional differences, we found that purified MUS81 complexes have different DNA substrate specificities *in vitro,* with the activity of MUS81-EME2 being 10-fold greater than that of MUS81-EME1.

Together, these results indicate that MUS81-EME1 and MUS81-EME2 have different biochemical properties and distinct, non-overlapping functions, with MUS81-EME2 being important in the repair of stalled RFs and in telomere maintenance of ALT cells, whereas MUS81-EME1 plays an important role in the resolution of HJs in the context of HR-mediated DNA repair.

ACKNOWLEDGEMENTS

First, I would like to thank my supervisor Steve West for giving me the opportunity to work in his lab and for guiding me throughout my PhD. I am also grateful to the members of my thesis committee, Simon and Mark, for their support and their suggestions on my experiments.

I would like to thank all the present and past 'Westies' for being always very helpful and supportive. My special thanks go to Tina T., Ip, Andrew, Thomas and my two angels, Miguel and Joao: there are no words to describe how grateful I am for all your patience, support and friendship. Many people have made Clare Hall a special place in these four years: Claudia, Toñi, JB, Raf, Khalid, Ross, Difo and Marco (of course!). Also, thanks to the people that made this PhD a life lesson.

Last, but not least, I thank my partner Gabriele for his big support in the (many) periods of deep personal and scientific frustration and my family: my mother, whose advices have helped me through many bad times, my father and my aunt Silvana. You are my strength.

CONTENTS

Declaration 2

Abstract 4

Acknowledgements 5

Contents 6

List of figures 11

List of tables 14

Abbreviations 15

CHAPTER 1

Introduction

1.1 DNA damage 18

1.1.1 Cellular effects of DNA lesions 19

1.2 DNA repair mechanisms 20

1.2.1 Nucleotide excision repair 20

1.2.2 Double strand break repair 22

1.2.3 Role of HR in replication fork repair and ICL repair 40

1.3 The role of MUS81 in DNA repair 46

1.3.1 Role of MUS81-EME1 in HJ resolution 47

1.3.2 Role of MUS81 at stalled RFs 57

1.4 Telomere maintenance and DNA repair 63

1.4.1 Telomerase-mediated telomere elongation 65

1.4.2 Alternative Lengthening of Telomeres (ALT) pathway 67

1.4.3 Telomere maintenance proteins in ALT-cells 74

1.4.4 The role of MUS81 in telomere maintenance of ALT-positive cells 75

1.5 Aim of the study 76

CHAPTER 2

Materials and methods

2.1 Enzymes and reagents 77
2.1.1 Enzymes 77
2.1.2 General reagents 77
2.1.3 Antibodies 78
2.2 Buffers and solutions 79
2.2.1 Media and protein buffers 79
2.2.2 DNA buffers 80
2.2.3 Reaction buffers 80
2.2.4 Immunofluorescence (IF), sister chromatid exchanges (SCEs) and telomeric fluorescence *in situ* hybridisation (FISH) buffers 80
2.2.5 Pulse-field gel electrophoresis (PFGE) buffers 81
2.3 Bacterial strains 81
2.3.1 Bacterial strains 81
2.3.2 Transformation of chemically competent cells 81
2.4 DNA primers 82
2.5 Plasmids 83
2.6 Cell lines and cell culture methods 85
2.6.1 siRNA transfection 86
2.6.2 Establishment of stable tetracycline-inducible cell lines 87
2.6.3 Bacterial Artificial Chromosome (BAC)-mediated expression of MUS81 in HeLa Kyoto cells 87
2.6.4 Cell synchronisation with double-thymidine block 88
2.7 Gel electrophoresis 88
2.7.1 SDS-polyacrylamide gel electrophoresis (PAGE) 88
2.7.2 Agarose gel electrophoresis 89
2.7.3 Neutral PAGE 89

2.7.4 Denaturing PAGE 89
2.7.5 InstantBlue staining 90
2.7.6 SYPRO® Ruby staining 90
2.7.7 Autoradiography 90
2.7.8 Phosphorimager analysis 90
2.7.9 Pulse-field gel electrophoresis 90
2.8 General methods of DNA and protein manipulation 91
2.8.1 Amplification of EME2 isoforms 91
2.8.2 DNA concentration determination 91
2.8.3 Ethanol precipitation 92
2.8.4 Whole cell extracts (WCEs) 92
2.8.5 Protein concentration determination 92
2.8.6 Generation of polyclonal antibodies 92
2.8.7 Western blotting 93
2.9 Baculovirus and insect cells 93
2.9.1 Production of the bacmid DNA 93
2.9.2 Baculovirus production 94
2.10 Protein purification 94
2.10.1 Purification of MUS81-$_{SF}$EME1, MUS81-$_{SF}$EME2A, MUS81-$_{SF}$EME2B and MUS81^{D307A}-$_{SF}$EME2A 94
2.10.2 GFP-pull-down of BAC-MUS81$_{FLAP}$ 95
2.10.3 FLAG pull-downs of $_{SF}$MUS81, $_{SF}$EME1, $_{SF}$EME2A and $_{SF}$EME2B 96
2.11 Preparation of DNA substrates and cleavage assays 97
2.11.1 Gel purification of oligonucleotides 97
2.11.2 Preparation of non-radiolabelled DNA substrates 98
2.11.3 5'-^{32}P-end labelling of oligonucleotides and substrate preparation 98
2.11.4 Preparation of 5'-^{32}P-end-labeled length marker oligonucleotides 100
2.11.5 Endonucleolytic cleavage assay 101
2.12 Preparation of metaphase spreads and stainings 102
2.12.1 Metaphase spreads 102
2.12.2 Sister Chromatid Exchanges (SCEs) 102
2.12.3 Telomeric quantitative-FISH (Q-FISH) on metaphase chromosomes

.....103
2.12.4 Telomeric chromosome orientation-FISH (CO-FISH).....103
2.12.5 Immunofluorescence 104
2.12.6 Immunofluorescence-FISH 105
2.13 Fluorescence-activated cell sorting (FACS) analysis.....105
2.13.1 Propidium Iodide (PI) staining.....105
2.13.2 BrdU staining 106
2.13.3 Phospho histone H3 staining 106

CHAPTER 3

Biochemical characterisation of MUS81-EME1 and MUS81-EME2 complexes

3.1 Two isoforms of EME2 are expressed in human cells 107
3.2 EME2A and EME2B associate with MUS81 *in vivo* 109
3.3 Purification of the MUS81 complexes 113
3.3.1 Determination of the cofactor requirements for optimal activity of the three purified MUS81 complexes.....116
3.4 Substrate specificities of MUS81-$_{SF}$EME1, MUS81-$_{SF}$EME2A and MUS81-$_{SF}$EME2B.....118
3.5 Purification of the catalytically inactive MUS81^{D307A}-EME2A.....119
3.6 MUS81-EME1 and MUS81-EME2A exhibit distinct DNA cleavage mechanisms 120
3.7 Conclusions.....139

CHAPTER 4

Functional analysis of MUS81-EME1 and MUS81-EME2 complexes in DNA repair

4.1 Generation and validation of an anti-EME2 antibody 141

4.2 Analysis of the interdependence between MUS81 and its non-catalytic partners EME1 and EME2 142
4.3 The MUS81-EME2 complex is required for the processing of stalled replication forks 142
4.4 MUS81 interacts with EME2 during the S-phase of the cell cycle 145
4.5 MUS81-EME2 is required for genomic stability after HU treatment 149
4.6 MUS81-EME2 interacts with SLX1-SLX4 and XPF-ERCC1 151
4.7 MUS81-EME2 does not significantly contribute to SCE formation 155
4.8 Conclusions..... 158

CHAPTER 5

MUS81-EME2 is required for telomere maintenance of ALT cells

5.1 Depletion of EME2 affects the cell cycle progression of ALT-cells 159
5.2 $_{SF}$EME1 and $_{SF}$EME2 localise to ALT-associated PML bodies 164
5.3 MUS81-EME2 is required for telomere maintenance of ALT-positive cells 167
5.4 Loss of EME2 increases telomere fragility in ALT-positive cells . 174
5.5 Depletion of MUS81-EME2 causes mitotic aberrations in ALT-positive cells..... 178
5.6 Conclusions..... 178

CHAPTER 6

Discussion..... 180

BIBLIOGRAPHY 192

LIST OF FIGURES

CHAPTER 1

Figure 1.1 Schematic representation of nucleotide excision repair 21

Figure 1.2 Schematic representation of two-ended DSB repair pathways 24

Figure 1.3 DSB end resection and RAD51 nucleofilament formation 31

Figure 1.4 Schematic representation of HJ resolution by symmetric or asymmetric cleavage..... 39

Figure 1.5 Schematic representation of the HR-mediated repair of stalled and collapsed RFs 43

Figure 1.6 The XPF/MUS81 family of endonucleases 48

Figure 1.7 Cell-cycle regulation of HJ dissolution and resolution pathways 58

Figure 1.8 Structural organisation of the MUS81-EME1 complex..... 60

Figure 1.9 Telomerase-mediated telomere elongation 69

Figure 1.10 Schematic representation of ALT-dependent telomere elongation models 72

CHAPTER 3

Figure 3.1 Identification of two isoforms of EME2..... 108

Figure 3.2 Sequence alignment between EME2A, EME2B, EME1 and MUS81 111

Figure 3.3 $_{SF}$EME2A and $_{SF}$EME2B interact with endogenous MUS81 112

Figure 3.4 Construction of baculovirus expression vectors for production of bacmid DNA and protein expression in insect cells..... 114

Figure 3.5 Affinity purification of MUS81-$_{SF}$EME1, MUS81-$_{SF}$EME2A and MUS81-$_{SF}$EME2B..... 115

Figure 3.6 Determination of the optimal Mg^{2+} concentration for MUS81-$_{SF}$EME1, MUS81-$_{SF}$EME2A and MUS81-$_{SF}$EME2B nuclease activity on a 3'-flap 117

Figure 3.7 Substrate specificities of MUS81-$_{SF}$EME1, MUS81-$_{SF}$EME2A and MUS81-$_{SF}$EME2B..... 121

Figure 3.8 Quantification of the nuclease activities of MUS81-$_{SF}$EME1, MUS81-$_{SF}$EME2A and MUS81-$_{SF}$EME2B 121

Figure 3.9 Affinity purification of the catalytically inactive MUS81^{D307A}-$_{SF}$EME2A 124
Figure 3.10 Cleavage of a 3'-flap substrate by MUS81-$_{SF}$EME1 and MUS81-$_{SF}$EME2A 127
Figure 3.11 MUS81-$_{SF}$EME2A cleaves a 5'-flap substrate 128
Figure 3.12 Comparison of the activities of purified MUS81-$_{SF}$EME1, MUS81-$_{SF}$EME2A and MUS81-$_{SF}$EME2B on a 3'-flap, nicked HJ and 5'-flap 130
Figure 3.13 Comparison of the activities of MUS81-$_{SF}$EME1 and MUS81-$_{SF}$EME2A on a 5'-flap using $MnCl_2$ as a cofactor 132
Figure 3.14 Comparison of the activities of MUS81-$_{SF}$EME1 and MUS81-$_{SF}$EME2A on an immobile HJ 133
Figure 3.15 Comparison of the activities of MUS81-$_{SF}$EME1 and MUS81-$_{SF}$EME2A on a D-loop structure 135
Figure 3.16 Analysis of the activities of MUS81-$_{SF}$EME1 and MUS81-$_{SF}$EME2A on a D-loop structure 137

CHAPTER 4

Figure 4.1 Design of siRNAs targeting EME2 143
Figure 4.2 Cell cycle profiles of control and EME2 siRNA-transfected cells after treatment with HU or cisplatin 146
Figure 4.3 The MUS81-EME2 complex contributes to the formation of DSBs in response to treatment with HU 147
Figure 4.4 The MUS81-EME2 complex contributes to the conversion of ICLs into DNA DSBs 148
Figure 4.5 EME2 preferentially binds to MUS81$_{FLAP}$ during the S-phase of the cell cycle 150
Figure 4.6 MUS81-EME2 complex is required for maintaining genomic stability after HU treatment 152
Figure 4.7 Depletion of EME2 increases the frequency of endoreduplication in RPE-1 hTERT cells 154
Figure 4.8 $_{SF}$EME2 interacts with SLX1-SLX4 and XPF-ERCC1 156

Figure 4.9 The MUS81-EME2 complex does not significantly contribute to SCE formation in BS cells 157

CHAPTER 5

Figure 5.1 EME2 depletion causes a delay in the G2/M phase of the cell cycle of ALT-positive cells 160
Figure 5.2 BrdU and phospho histone H3 staining of U2OS cells transfected with two EME2 siRNAs 162
Figure 5.3 163
Figure 5.4 $_{SF}$EME2 localises to APBs 165
Figure 5.5 $_{SF}$EME1 localises to APBs 166
Figure 5.6 Depletion of EME2 or MUS81 causes telomere loss in ALT-positive cells 168
Figure 5.7 Quantification of telomere loss and telomere intensity in siRNA-transfected U2OS cells 169
Figure 5.8 Depletion of EME2 or MUS81 does not cause telomere loss in ALT-negative cells 170
Figure 5.9 Depletion of EME2 or MUS81 causes a significant decrease of T-SCEs in ALT-positive cells 172
Figure 5.10 Quantification of chromosome ends with T-SCEs 173
Figure 5.11 Depletion of EME2 causes an increase in telomere fragility in ALT-positive cells 175
Figure 5.12 Depletion of EME2 or MUS81 causes a significant increase in mitotic aberrations in ALT-positive cells 176
Figure 5.13 Quantification of mitotic aberrations in ALT-positive and ALT-negative 177

CHAPTER 6

Figure 6.1 Model for MUS81-EME2 and MUS81-EME1 functions in the repair of stalled RFs 191

LIST OF TABLES

CHAPTER 2

Table 2.1 List of plasmids 83
Table 2.2 List of cell lines used in this study 85
Table 2.3 List of oligonucleotides 97
Table 2.4 Oligonucleotides sequences of synthetic DNA substrates 99
Table 2.5 Sequences of the length marker oligonucleotides 100

CHAPTER 4

Table 4.1 Frequency of chromosomal aberrations in control, EME1-, EME2- and MUS81-depleted cells, before and after treatment with HU 153

ABBREVIATIONS

A. pernix	*Aeropyrum pernix*
ALT	alternative lengthening of telomeres
APBs	ALT-associated PML bodies
ATP	adenosine triphosphate
BAC	bacterial artificial chromosome
BER	base excision repair
bp	base pair
BrdU	bromodeoxyuridine
BS	Bloom's syndrome
CFS	common fragile site
CO-FISH	chromosome orientation-FISH
CPT	camptothecin
CS	Cockayne syndrome
dGTP	deoxyguanosine triphosphate
dHJ	double HJ
DNA	deoxyribonucleic acid
dNTPs	deoxynucleotide triphosphate
DSB	double-strand break
DSBR	double-strand break repair
dsDNA	double-stranded DNA
DTT	dithiothreitol
E. coli	*Escherichia coli*
EDTA	ethylenediaminetetraacetic acid
ES cells	embryonic stem cells
FA	Fanconi anaemia
FBS	fetal bovine serum
FISH	fluorescence *in situ* hybridisation
G1-phase	gap1 phase
G2-phase	gap2 phase

GFP	green fluorescent protein
HhH	helix-hairpin-helix
Hi5	High five
HJ	Holliday junction
HR	homologous recombination
hr	hour
HtH	helix-turn-helix
HU	hydroxyurea
ICL	interstrand cross-link
IF	immunofluorescence
IPTG	isopropyl-β-D-thiogalactoside
IR	ionising radiation
kDa	kilo Daltons
KIN	karyomegalic interstitial nephritis
LOH	loss of heterozygosity
M phase	mitotic phase
MEF	mouse embryonic fibroblast
MMC	mitomycin C
MMS	methyl methanesulfonate
NCBI	National Centre for Biotechnology Information
NER	nucleotide excision repair
NHEJ	non-homologous end joining
NP-40	nonidet P40
nt	nucleotide
OB	oligonucleotide/oligosaccharide binding
OD	optical density
P. furiosus	*Pyrococcus furiosus*
PAGE	polyacrylamide gel electrophoresis
PBS	phosphate buffer saline
PCR	polymerase chain reaction
PI	propidium iodide
PML	promyelocytic laeukemia

PSI-BLAST	Position Specific Iterated–Basic Local Alignment Search Tool
Q-FISH	quantitative-FISH
RF	replication fork
ROS	reactive oxygen species
RT	room temperature
RT-PCR	reverse transcriptase-PCR
RTS	Rothmund-Thomson syndrome
s	second
S-phase	synthesis phase
S. cerevisiae	*Saccharomyces cerevisiae*
S. pombe	*Schizosaccharomyces pombe*
SCE	sister chromatid exchange
SDS	sodium dodecyl sulfate
SDSA	synthesis-dependent strand annealing
Sf9	*Spodoptera frugiperda 9*
siRNA	small interfering RNA
ssDNA	single-stranded DNA
TEMED	N,N,N',N'-(tetramethylethylenediamine)
Tris	Tris (hydroxymethyl) aminomethane
TTD	trichothiodystrophy
U	unit
UV	ultra violet
V	Volts
W	Watts
WCE	whole cell extract
WRN	Werner helicase
WS	Werner syndrome
X-gal	5-bromo-4-chloro-3-indolyl-beta-D-galactopyranoside
XP	xeroderma pigmentosum

CHAPTER 1

Introduction

1.1 DNA damage

The faithful conservation of our genetic information is critical for the maintenance of genomic stability and for the prevention of cancer development. DNA needs to be constantly protected from different kinds of DNA damage induced by endogenous cellular processes and by exogenous (or environmental) factors. One of the major causes of spontaneous DNA damage is the incorporation of incorrect bases during DNA replication. DNA polymerases incorporate nucleotides that are non-complementary to the template DNA strand with a frequency of one mis-incorporation in 10^7 nucleotides synthesised (McCulloch and Kunkel, 2008). Therefore, considering the size of the human genome (approximately 3 x 10^9 base pairs), they generate hundreds of base mismatches during each round of DNA replication (Echols and Goodman, 1991). Other causes of DNA mismatches include spontaneous deamination of bases (i.e. cytosine to uracil, adenine to hypoxanthine and guanine to xanthine) (Lindahl, 1993) and incorporation of damaged nucleotides, such as oxidated 8-oxo-dGTP (Pavlov et al., 1994). Furthermore, the by-products of cellular metabolism such as reactive oxygen species (ROS) also contribute to endogenous DNA damage (Pavlov et al., 1994). For example, ROS (peroxide, hydrogen peroxide and hydroxyl radicals) can react with DNA and fragment the component base and sugar moieties, thus generating single strand breaks (Imlay and Linn, 1988).

Exogenous DNA damage can come from either physical or chemical sources. Physical DNA damaging factors include ionising radiation (IR) and ultraviolet (UV)-light. The main sources of IR are naturally occurring radionuclides (e.g. cosmic radiation) and X-rays used for medical diagnosis. Exposure to IR results in base oxidation and in the formation of single- and double-stranded DNA breaks (Goodhead, 1989; Hutchinson, 1985; Teoule, 1987). UV light is an electromagnetic radiation found in sunlight. Extensive exposure to UV light can lead to covalent

linkages between two adjacent pyrimidines and to the formation of cyclobutane pyrimidine dimers (Setlow, 1966) and (6-4) photoproducts (Mitchell and Nairn, 1989). Examples of chemical DNA damaging agents include alkylating agents (e.g. methyl methanesulfonate or MMS), which insert alkyl groups on DNA bases (Singer, 1975), and interstrand crosslinking agents (e.g. cisplatin, mitomycin C), which can covalently link the two DNA strands (interstrand crosslinks; ICLs) and prevent their correct separation during cell division (Iyer and Szybalski, 1963; Roberts and Pascoe, 1972). Both types of chemicals have been widely used as chemotherapic drugs because they interfere with DNA replication, transcription and cell division. Other DNA damaging drugs include topoisomerase inhibitors such as camptothecin (CPT), which inhibits DNA topoisomerase I (Froelich-Ammon and Osheroff, 1995), and hydroxyurea (HU), which inhibits ribonucleotide reductase and thereby depletes the pool of dNTPs required for DNA replication (Bianchi et al., 1986).

1.1.1 Cellular effects of DNA lesions

DNA lesions lead to many adverse cellular effects and, if left unrepaired, result in irreversible mutations and can drive tumourigenesis. Many endogenous and exogenous factors described in the previous section generate lesions that block DNA replication and transcription and affect chromosome segregation during mitosis. For example, unrepaired DNA double strand breaks (DSBs) can result in the uneven distribution of genetic material between the two daughter cells, causing chromosomal deletions, translocations and aneuploidy, all of which represent hallmark features of cancer cells (Hoeijmakers, 2001). In order to allow the repair of the lesion, cells trigger a transient cell cycle arrest called “checkpoint”, during the G1/S, G2 or M phase of the cell cycle (Painter and Young, 1980). However, when the damage load is too great and cannot be repaired, cells undergo apoptosis and thereby prevent the accumulation of permanent mutations (Rich et al., 2000).

Eukaryotic cells have developed a range of different mechanisms in order to cope with the variety of DNA damages and maintain genomic integrity. For example, mis-incorporated DNA bases are recognised and replaced with correct bases by the DNA mismatch repair pathway (Kunkel, 1995), whereas small, non-helix-distorting lesions are repaired by the base excision repair (BER) pathway through

excision of the damaged bases (Lindahl and Wood, 1999). Helix-distorting damages, such as UV-induced lesions and intrastrand crosslinks, which are formed by the covalent linkage of two bases on the same DNA strand, are repaired by the nucleotide excision repair (NER) pathway through the removal of an approximately 30 nucleotides-long DNA fragment (Section 1.2.1). DSBs can be repaired by either non-homologous end joining (NHEJ), through the re-ligation of the broken ends, or by the homologous recombination (HR) machinery. Cells employ NHEJ or HR depending on the cell cycle phase during which DSBs are generated: HR is the primary repair pathway during S- and G2-phase, when the newly synthesised sister chromatid can be used as template for repair, whereas NHEJ takes place throughout the cell cycle but it is particularly important during G1-phase, when HR does not occur (Rothkamm et al., 2003). NER, NHEJ and HR will be discussed in greater detail in the future sections.

1.2 DNA repair mechanisms

1.2.1 Nucleotide excision repair

NER is the most versatile of the repair mechanisms because it recognises DNA lesions by the local structural distortions they induce in the DNA helix (Gunz et al., 1996). NER is particularly important for the repair of UV-induced lesions such as cyclobutane pyrimidine dimers and (6-4) photoproducts but it can also deal with damage created by crosslinking agents (e.g. cisplatin) or by chemicals that covalently bind DNA bases and form bulky DNA adducts (e.g. benzo[a]pyrenes contained in cigarettes smoke). This multistep repair mechanism involves (i) the recognition of DNA damage, (ii) the denaturation of DNA surrounding the lesion, (iii) cleavage of the damaged strand, and (iv) gap filling and DNA ligation reactions (Figure 1.1). First, XPC-HR23B-centrin2, a complex with high affinity for damaged DNA, identifies the lesion (Araki et al., 2001; Sugasawa et al., 1998). Second, the transcription factor TFIIH is recruited to the site of damage and its helicase subunits, XPB and XPD, open the two DNA strands around the lesion, creating a single-stranded bubble (Coin et al., 2007; Winkler et al., 2000). The next step involves the incision and removal of the damaged DNA. The XPG endonuclease incises the DNA bubble on the 3'-side of the lesion (O'Donovan et al., 1994), while the XPF-ERCC1 complex performs the incision on the 5'-side (Mu et al., 1996).

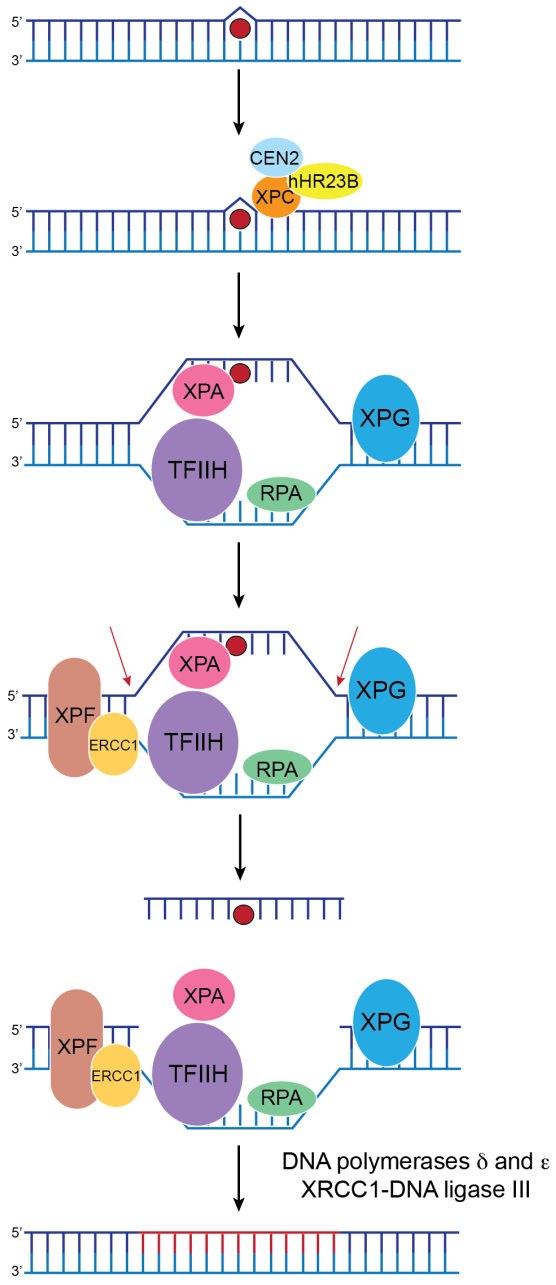

Figure 1.1 Schematic representation of nucleotide excision repair

The initial step of nucleotide excision repair is recognition and binding of the DNA lesion (red circle) by the multi-subunit protein complex XPC-hHR23B-CEN2. The TFIIH complex is subsequently recruited to the lesion and the XPB and XPD helicase subunits unwind the DNA helix, thus forming a single-stranded bubble that is stabilised by RPA. The XPG and XPF-ERCC1 flap endonucleases cleave the bubble at the junctions between single-stranded and double-stranded DNA on the 5'- and 3'-sides of the lesion (indicated by red arrows), respectively. This results in the excision of the DNA lesion and approximately 25 to 30 nucleotides of adjacent DNA. The final steps of NER involve restoration of the intact DNA duplex. More specifically, this requires the combined activities of DNA polymerases δ and ε, which catalyse gap-filling, and the XRCC1-DNA ligase III complex that joins adjacent DNA ends. The red-coloured DNA in the bottom panel indicates newly synthesised DNA.

Once a DNA fragment of approximately 25-30 nucleotides has been excised (Moggs et al., 1996), DNA polymerases δ and ε fill the single-stranded gap (Popanda and Thielmann, 1992) and the XRCC1-DNA ligase III complex ligates the remaining nicks (Moser et al., 2007). Inherited defects in the NER pathway are associated with the onset of human disorders that include Xeroderma pigmentosum (XP), Cockayne syndrome (CS) and tricothiodystrophy (TTD). As NER is an essential pathway for the repair of UV-induced DNA lesions, it is not surprising that these syndromes are all characterised by photohypersensitivity of the skin (Diderich et al., 2011).

1.2.2 Double strand break repair

DNA DSBs are the most toxic and mutagenic forms of DNA lesions. DSBs occur when both strands of the DNA duplex are broken and two physically separated DNA ends are created. These ends have the ability to recombine with other sites in the genome leading to gross chromosomal rearrangements (up to 100 million base pairs) and often to cell death (Richardson and Jasin, 2000). Despite their high mutagenic potential, cells program the formation of DSBs in the context of specific cellular processes like V(D)J recombination and meiosis. The V(D)J recombination pathway takes place in B and T-lymphocytes and promotes the production of diverse antigen receptors (Alt et al., 2013). These DNA DSBs are induced at specific loci by the lymphocyte-specific RAG endonuclease (Oettinger et al., 1990) and repaired by proteins of the non-homologous end-joining (NHEJ) pathway (Boboila et al., 2012) (Section 1.2.2). In meiosis, the programmed production of DSBs and their repair by HR (Section 1.2.2) is essential for proper chromosome segregation and for the generation of genetic diversity. Prior to the onset of meiosis I, the topoisomerase-like transesterase Spo11 creates DSBs via the formation of an intermediate in which Spo11 forms a covalent linkage with the 5'-phosphate of the DNA backbone (Keeney et al., 1997). Induction of DSB formation is essential for the initiation of meiotic recombination and the formation of inter-homologue joint molecules in which the interacting DNA strands are physically linked (Schwacha and Kleckner, 1995). Structure-specific endonucleases resolve these joint molecules (i.e. cleave these structures into two linear duplex DNA molecules) and promote the exchange of genetic material required to generate a different allele combination to that of the parental germline. Formation and resolution of these

structures is required for the bi-polar segregation of homologous chromosomes in anaphase I (Petronczki et al., 2003).

For many years, endonucleolytic cleavage and environmental DNA damaging agents were considered the only sources of DSBs. DSBs that are generated during V(D)J recombination and meiosis have two free DNA ends and are termed two-ended DSBs. However, in mitotic cells, the formation of two-ended DSBs is a rare event. The majority of the DSBs have one free DNA end (i.e. one-ended DSBs) and are generated either directly or indirectly during DNA replication (Saleh-Gohari et al., 2005), when a replication fork (RF) encounters an unrepaired single-strand break or a lesion (e.g. ICLs) (Hanada et al., 2006; Strumberg et al., 2000). Eukaryotic cells have developed two major pathways to repair two-ended and one-ended DSBs and hence maintain genomic integrity: NHEJ and HR.

Non-homologous end joining

NHEJ is a mechanism of DSB repair whereby the two broken DNA ends are re-joined in a sequence-independent manner (Lieber, 2010) and can be divided into three stages: (i) binding and tethering of the DSB ends, (ii) DNA end processing and (iii) DNA ligation. As illustrated in Figure 1.2A, NHEJ is initiated by the binding of the Ku70/80 (Ku) heterodimer and DNA-PK_{CS}, a serine/threonine protein kinase that belongs to the phosphatidylinositol 3-kinase-like protein kinase family, to the broken DNA ends (Mimori and Hardin, 1986), where Ku forms a ring-like structure that promotes the alignment of the two DNA extremities (Ma et al., 2004). The second step involves the enzymatic processing of the DSB ends. NHEJ-mediated repair of blunt DNA DSBs is very precise, i.e. it occurs without loss of any nucleotide (van Heemst et al., 2004). However, the configuration of DNA ends at DSBs varies according to the source of the lesion and affects the fidelity of the ligation process. Many DNA ends contain damaged backbone sugars or DNA bases, 5'-hydroxyl or 3'-phosphate groups as well as 5'- or 3'-single-stranded extensions. As a result, cells employ a variety of DSB ends-processing enzymes and DNA polymerases to ensure that DNA ends are restored prior to re-ligation. For example, Artemis, a member of the metallo-beta–lactamase superfamily of enzymes, interacts with DNA-PK_{CS} and cleaves DNA hairpins (intermediates of

Figure 1.2 Schematic representation of two-ended DSB repair pathways

A. During NHEJ, DSB DNA ends are first tethered by Ku-DNA-PK_{CS}. DNA end-processing factors such as Artemis, XRCC4-PNK, DNApolμ and λ and WRN bind and process DNA ends, thereby facilitating XLF-XRCC4-DNA ligase IV-dependent re-ligation.
B. In HR-mediated repair, the damaged DNA is re-synthesised using a homologous DNA sequence as the template. DSB DNA end-resection results in the formation of single-stranded 3'-overhangs, which serve as substrates for the DNA-binding protein RAD51. The RAD51-coated DNA filament initiates the search for homology and catalyses strand invasion, which forms a D-loop structure. The free 3'-end of the D-loop provides a primer for the synthesis of nascent DNA. In the SDSA pathway, DNA helicases like BLM, RTEL and FANCM unwind the D-loop and displace the invading strand, which results in the formation of non-crossover products. In contrast, the DSBR pathway of HR involves the formation of a dHJ that can be processed by BTR-mediated dissolution, which exclusively generates non-crossover products, or by SLX-MUS/GEN1-mediated resolution, which can result in either crossover or non-crossover products, depending on the orientation of HJ cleavage.
C. The SSA pathway is engaged when the DSB occurs in a region of repetitive DNA sequences (indicated by green boxes). Resected DSB DNA ends are bound by RAD52, which promotes the annealing of the repetitive elements. The non-homologous DNA that is located between the repeats forms flap structures that are cleaved by the structure-specific 3'-flap endonuclease XPF-ERCC1, resulting in the loss of genetic information.

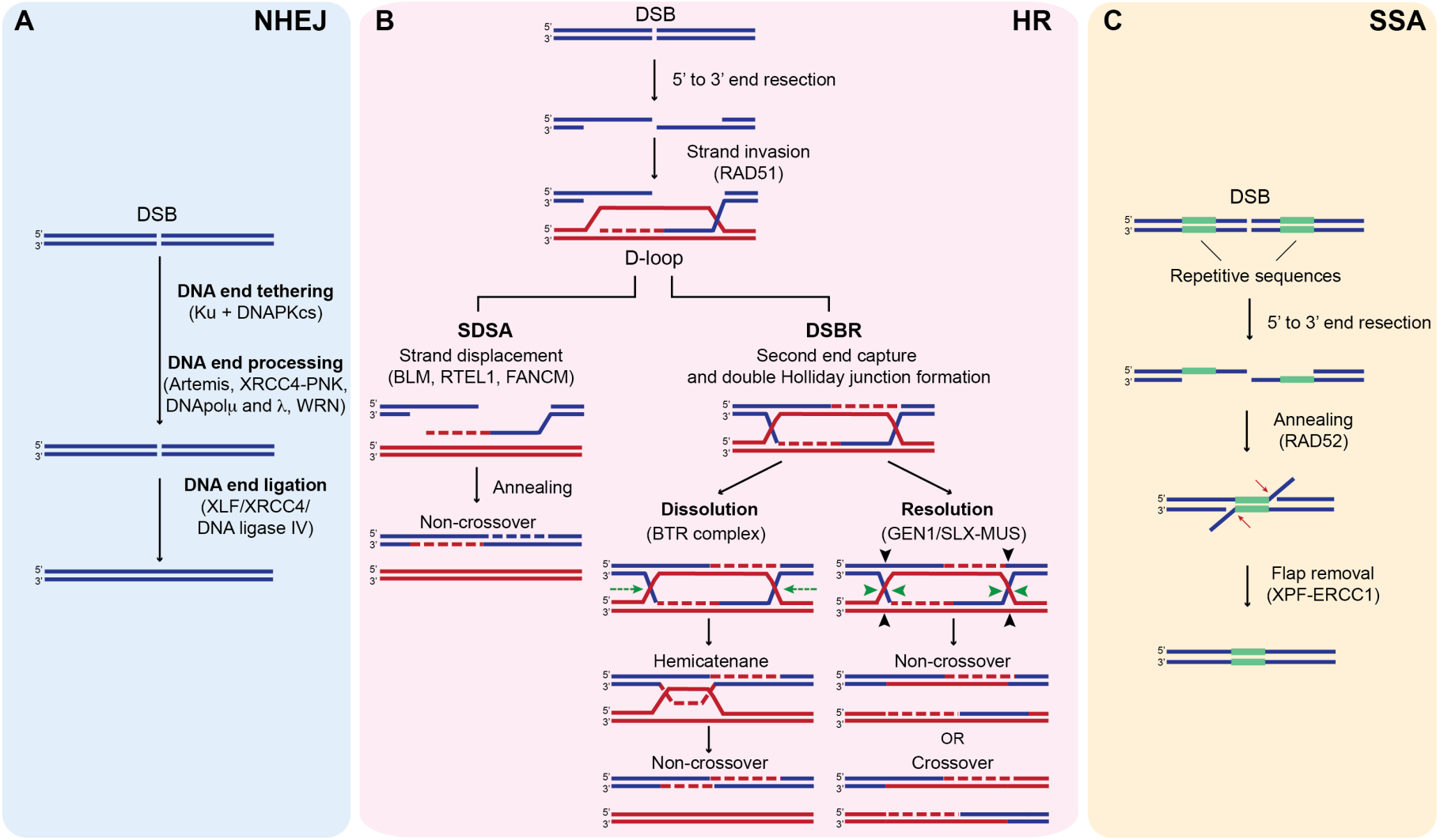
A
NHEJ
DSB
DNA end tethering
(Ku + DNAPKcs)
DNA end processing
(Artemis, XRCC4-PNK,
DNApolμ and λ, WRN)
DNA end ligation
(XLF/XRCC4/
DNA ligase IV)
B
HR
DSB
5' to 3' end resection
Strand invasion
(RAD51)
D-loop
SDSA
Strand displacement
(BLM, RTEL1, FANCM)
Annealing
Non-crossover
DSBR
Second end capture
and double Holliday junction formation
Dissolution
(BTR complex)
Hemicatenane
Non-crossover
Resolution
(GEN1/SLX-MUS)
Non-crossover
OR
Crossover
C
SSA
DSB
Repetitive sequences
5' to 3' end resection
Annealing
(RAD52)
Flap removal
(XPF-ERCC1)

V(D)J recombination) and 3'-single-stranded overhangs (Ma et al., 2002; Ma et al., 2005). X-ray cross-complementing gene 4 (XRCC4) interacts with polynucleotide kinase (PNK) to remove 3'-phosphate groups and 5'-hydroxyl groups (Chappell et al., 2002), whereas DNA polymerases μ and λ, two members of the Pol X family of DNA polymerases, fill gaps formed by partially complementary DNA ends (McElhinny et al., 2005). Finally, WRN (Werner) helicase, a member of the RecQ family of helicases mutated in Werner syndrome, possesses an exonucleolytic activity that is stimulated by the interaction with the Ku complex and that is required for efficient DNA end joining (Perry et al., 2006). The last step of NHEJ consists in the ligation of the juxtaposed DNA ends, which is performed by the XLF-XRCC4–DNA ligase IV complex, a very flexible ligase with the ability to ligate gaps of several nucleotides as well as incompatible DNA ends *in vitro* (Grawunder et al., 1997; Gu et al., 2007).

NHEJ versus HR

Sequence alterations deriving from the processing of incompatible DNA ends make NHEJ an error-prone DSB repair pathway. Also, the presence of more than one DSB could induce inappropriate NHEJ-mediated ligation of non-contiguous sequences, resulting in chromosomal deletions, insertions, translocations and hence genomic instability. In contrast, homologous recombination (HR) is an accurate, error-free mechanism of DSB repair (San Filippo et al., 2008), whereby the damaged DNA sequence is re-synthesised using a homologous DNA molecule as a template for repair. The requirement for a homologous sequence makes HR the preferred DSB repair pathway during the S- and G2-phases of the cell cycle, where recombination can occur with the available intact sister chromatid (Rothkamm et al., 2003). Conversely, NHEJ operates throughout the cell cycle and is especially important during G1. Indeed, NHEJ-deficient DT40 cells are more sensitive to IR during G1 and early S, whereas HR-deficient cells are primarily sensitive during S and G2 (Takata et al., 1998). In addition, the repair of one-ended DSBs that arise during DNA replication can only be performed by HR, as the mechanism of NHEJ-mediated DSB repair requires the presence of two DNA ends. As a result, HR-deficient cells are sensitive to many anti-cancer drugs that block DNA replication whereas NHEJ-deficient cells are mostly sensitive to those that induce DSBs (Helleday, 2010).

Homologous recombination

DSB end resection

The initial stages of HR involve 5'-3' nucleolytic resection of the damaged DNA ends and the formation of 3'-single-stranded DNA (ssDNA) overhangs (Figure 1.2B). The mechanism of end resection is conserved from yeast to humans and current models suggest that resection is a two-step process (Mimitou and Symington, 2008; Zhu et al., 2008). The first step, called resection initiation, is essential when the DNA ends have covalent modifications or bulky DNA adducts that need to be processed in order to allow extensive resection (Gravel et al., 2008; Hartsuiker et al., 2009; Nicolette et al., 2010). Resection initiation requires the MRN complex, which is formed by the MRE11 nuclease, RAD50, a member of the SMC (structural maintenance of chromosomes) superfamily, and NBS1. MRN is recruited to the DSB, where two MRE11 and two RAD50 molecules associate to form a heterotetramer, which stabilises and tethers DNA ends to facilitate the repair of the break (Buis et al., 2008; Williams and Tainer, 2005). DNA-bound MRN interacts with CtIP (C-terminal-binding protein-interacting protein), which is recruited upon phosphorylation of the NBS1 component (Buis et al., 2012; Dodson et al., 2010; Sartori et al., 2007), and the MRN-CtIP complex initiates 5'-3' resection of the DNA ends (Nicolette et al., 2010; Sartori et al., 2007). The second step, called resection extension, can be performed either by (i) the combined actions of the BLM helicase and the DNA2 nuclease, whereby DNA2 resects the DNA unwound by BLM, or by (ii) the activity of the 5'-3' exonuclease EXO1 (Figure 1.3) (Nimonkar et al., 2011; Zakharyevich et al., 2010; Zhu et al., 2008). These two mechanisms, however, are not completely independent, as BLM has been shown to interact directly with EXO1 and to stimulate its dsDNA resection activity *in vitro* (Nimonkar et al., 2008).

Cell-cycle regulation of NHEJ and HR occurs mainly through the control of DSB end resection. In particular, CtIP appears to have an essential regulatory role in this process: the protein levels of CtIP are kept low during G1-phase of the cell cycle (*via* proteosomal degradation), but increase as cells progress through S and G2 (Buis et al., 2012). Furthermore, during S/G2, cyclin-dependent kinase (CDK)-dependent phosphorylation of CtIP at Ser327 promotes its interaction with the MRN complex and its phosphorylation at Thr847 triggers DSB end resection (Chen et al.,

2008a; Huertas and Jackson, 2009). DNA end resection is also regulated by the interplay between the tumour suppressor 53BP1 and BRCA1. 53BP1 binds chromatin at the DSB site and prevents the initiation of DNA resection, thus promoting NHEJ (Bunting et al., 2010; Nakamura et al., 2006). However, the HR inhibitory activity of 53BP1 must be suppressed during S/G2-phase of the cell cycle, when HR takes place. This is achieved by the binding of BRCA1 to the DSB, which counteracts the activity of 53BP1 and promotes HR (Moynahan et al., 1999). The mechanism by which 53BP1 and BRCA1 ensure an equilibrium between HR and NHEJ is unclear, although it is likely that the interaction between BRCA1 and DNA alters the chromatin state at the site of the DSB, thereby preventing the accumulation of 53BP1 (Chapman et al., 2012).

RAD51-mediated strand exchange

The core reactions of HR, strand exchange and homologous pairing, are mediated by the RecA/RAD51 family of recombinases. RAD51, the human ortholog of the *Escherichia coli* RecA protein, is a 38 kDa protein that polymerises on ssDNA to form an evolutionarily conserved right-handed helical structure formed by 6.4-6.5 RAD51 monomers per helical turn, which cover approximately 18 nucleotides of ssDNA (Figure 1.3) (Benson et al., 1994; Conway et al., 2004; Ogawa et al., 1993; Yu et al., 2001). The formation of the RAD51 nucleofilament is required to initiate the strand exchange reaction and occurs in two steps referred to as (i) nucleation and (ii) filament extension. Filament nucleation involves the initial association of 4 to 5 RAD51 monomers with ssDNA (van der Heijden et al., 2007). Multiple nucleation events occur along a ssDNA molecule in a stochastic manner and, although nucleation does not require ATP hydrolysis, the binding of ATP to the RAD51 monomer-monomer interface favours nucleation by stabilising protein-protein interactions (Chi et al., 2006). Filament extension involves the binding of additional RAD51 monomers to the nucleated patches of ssDNA. Given that nucleation is a stochastic event, the RAD51 filaments that result from the extension reaction are not continuous but contain gaps of ssDNA that are not bound by recombinase molecules (Modesti et al., 2007; van der Heijden et al., 2007). Hence, each nucleoprotein filament is formed by filament patches that are approximately 35 RAD51 monomers long, which confer high structural flexibility, thus favouring the strand exchange (van der Heijden et al., 2007).

Unlike *E. coli* RecA, which shows high affinity for ssDNA (West et al., 1980), human RAD51 binds both ssDNA and double-stranded DNA (dsDNA) with equal affinities (Thorslund et al., 2010; Yu et al., 2001) and needs to be targeted to ssDNA in order to promote strand invasion. In addition, the formation of the RAD51:DNA nucleoprotein filament (or presynaptic filament) is hampered by the binding of RPA to ssDNA following end resection. Although RPA can remove secondary structures in ssDNA and facilitate the loading of RAD51, its binding affinity for ssDNA is stronger than that of RAD51 and therefore, it represents a physical impediment to the nucleoprotein filament formation (Sugiyama et al., 1997). As a result, mammalian cells employ several recombination mediator proteins to counteract the inhibitory activity of RPA and target RAD51 to ssDNA. These include (i) the tumour suppressor BRCA2 and its interacting protein PALB2, (ii) RAD52, (iii) RAD54 and (iv) the RAD51 paralogs.

BRCA2 is the product of the human breast cancer susceptibility gene and is a tumour suppressor protein (Wooster et al., 1995). Mutations in the *BRCA2* gene predispose individuals to breast, ovarian and other cancer types. Its biallelic inactivation results in the onset of Fanconi anaemia (FA) (Howlett et al., 2002; Roy et al., 2012), an autosomal recessive disorder characterised by bone marrow failure, susceptibility to cancer and hypersensitivity to ICL agents (D'Andrea, 2010). Indeed, when *BRCA2*$^{-/-}$ cells were exposed to DNA cross linkers, they exhibited chromosomal breakages and tri-radial chromosomes, which are hallmark features of FA (Patel et al., 1998). BRCA2 (also called FANCD1) is a 3418 amino acids protein that interacts with RAD51 and promotes its localisation to DNA damage sites, as cell lines deficient in BRCA2 fail to form RAD51 foci in response to DNA damage (Yuan et al., 1999). The BRCA2 protein contains eight conserved BRC motifs and a DNA binding domain composed of three oligonucleotide/oligosaccharide-binding (OB) folds, a helix-turn-helix (HtH) motif and an alpha-helical domain (Bork et al., 1996). BRCA2 binds ssDNA and interacts with RAD51 primarly via the BRC repeats (Chen et al., 1998; Wong et al., 1997), but interaction via an unrelated C-terminal motif can occur in response to DNA damage or in a cell cycle-dependent manner (Ayoub et al., 2009; Esashi et al., 2005). *In vitro* analysis of the interaction between full length purified BRCA2 and

RAD51 revealed that BRCA2 is able to target RAD51 to ssDNA, thus stimulating RAD51-mediated strand invasion (Jensen et al., 2010; Thorslund et al., 2010).

The function of BRCA2 is largely dependent on its interaction with PALB2 (partner and localiser of BRCA2) (Sy et al., 2009). Like BRCA2, mutations in PALB2 predispose individuals to breast and ovarian cancer and its biallelic inactivation promotes the onset of FA (Rahman et al., 2007; Reid et al., 2007). Hence, PALB2 is also known as FANCN. The BRCA2-PALB2 interaction occurs between the C-terminal domain of PALB2 and the N-terminus of BRCA2 (Oliver et al., 2009) and it is essential for the loading of RAD51 onto RPA-bound ssDNA and for the stabilisation and localisation of BRCA2 to the sites of DNA damage (Xia et al., 2006). Additionally, PALB2 interacts directly with both BRCA1 and BRCA2, providing a physical link between the two tumour suppressor proteins (Zhang et al., 2009).

In human cells, BRCA2 is the major mediator of RAD51 nucleoprotein filament formation. However, recent studies have revealed that human RAD52 mediates a BRCA2-independent pathway of RAD51 filament formation (Feng et al., 2011; Lok et al., 2013). Indeed, depletion of RAD52 in BRCA2- or PALB2-deficient cells causes severe proliferation defects and chromosomal fragility, indicating a synthetic lethal relationship between RAD52, BRCA2 and PALB2. Furthermore, in the absence of BRCA2 or PALB2, RAD52 promotes HR and RAD51 foci formation in response to DNA damage (Feng et al., 2011; Lok et al., 2013). Consistent with the *in vivo* data, RAD52 has been shown to interact with RAD51 to promote homologous pairing and strand exchange *in vitro* (Benson et al., 1998; McIlwraith et al., 2000).

RAD54 belongs to the Swi2/Snf2 family of chromatin remodelling factors, which contain a motor domain that promotes its ATP-dependent translocation on dsDNA (Ristic et al., 2001). The functions of RAD54 in HR include: (i) stabilisation of the RAD51 nucleoprotein filament, (ii) stimulation of DNA strand exchange and (iii) branch migration of recombination intermediates. Mammalian RAD54 interacts

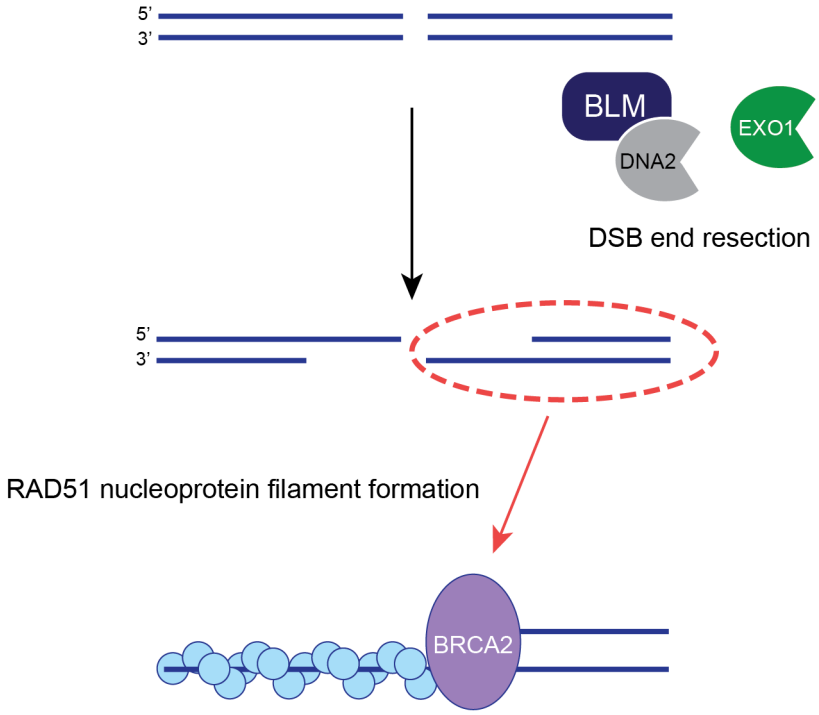

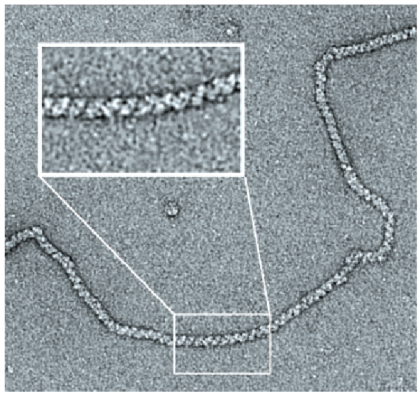

Electron microscopy image of human RAD51 nucleoprotein filament

Figure 1.3 DSB end resection and RAD51 nucleofilament formation

DSB DNA end resection can be performed either by (i) BLM and DNA2 through a mechanism in which DNA2 resects the DNA unwound by BLM or by (ii) the exonucleolytic activity of EXO1. Subsequently, RAD51 is loaded on resected DNA ends by the recombination mediator protein BRCA2. Electron microscopy image of the human RAD51 nucleoprotein filament (taken from (West, 2003))

directly with RAD51 (Golub et al., 1997) and its depletion has been shown to impair RAD51 foci formation in response to DNA damage (Tan et al., 1999), demonstrating the biological significance of the interaction. It functions as a recombination mediator by stabilising the RAD51 nucleoprotein filament in an ATP-independent manner (Agarwal et al., 2011). Indeed, the interaction between RAD54 and the RAD51 nucleoprotein filament has been shown to protect the filament against dissociation at elevated salt concentrations and to increase the RAD51-dependent protection of dsDNA from restriction endonucleases (Mazin et al., 2003). In addition, RAD54 is able to stimulate RAD51-mediated DNA strand exchange *in vitro* in an ATP-dependent manner, although the mechanism of stimulation remains to be determined (Sigurdsson et al., 2002). Importantly, RAD54 may also contribute to the late stages of HR, as it has been shown that human purified RAD54 is able to branch migrate Holliday junctions (HJs) and dissociate displacement loops (D-loops) *in vitro* (Bugreev et al., 2007; Bugreev et al., 2006). Finally, it is important to mention that Mus81, the catalytic subunit of the *S. cerevisiae* structure-specific endonuclease Mus81-Mms4, was first identified in a two-hybrid screen using *S. cerevisiae* Rad54 protein as bait (Interthal and Heyer, 2000; Mazina and Mazin, 2008). Human RAD54 also interacts with the human ortholog of Mus81-Mms4, MUS81-EME1, and stimulates its endonucleolytic activity *in vitro* (Mazina and Mazin, 2008). However, the biological significance of this interaction in human cells has not been investigated.

Human cells contain five RAD51 paralogs, namely RAD51B, RAD51C, RAD51D, XRCC2 and XRCC3, all of which function in HR repair. Chicken DT40 cells depleted of any of the RAD51 paralogs exhibit sensitivity to DNA cross linkers and IR, as well as defects in HR repair, as indicated by an increased frequency of chromosomal aberrations, a reduced frequency of HR-mediated gene targeting and DSB repair, and reduced sister chromatid exchanges (Fuller and Painter, 1988; Jones et al., 1987; Pierce et al., 1999; Takata et al., 2000; Takata et al., 2001). Human cells depleted of RAD51C, RAD51B or XRCC3 exhibited increased frequencies of mitotic aberrations and centrosomal defects, with XRCC3 being particularly important for chromosome segregation during anaphase (Rodrigue et al., 2013). Furthermore, RAD51D has been shown to localise to the telomeres of meiotic and telomerase-positive somatic cells, where its activity is required to

prevent telomere shortening and chromosomal end-to-end fusions (Tarsounas et al., 2004).

RAD51 paralogs form two functionally distinct complexes in human cells: RAD51B-RAD51C-RAD51D-XRCC2 (BCDX2) and RAD51C-XRCC3 (CX3) (Masson et al., 2001). Due to difficulties in the purification of the BCDX2 complex, the activities of the BC and DX2 sub-complexes were analysed separately. BC was found to exhibit a RAD51 mediator activity (Sigurdsson et al., 2001) and its depletion resulted in (i) increased gene conversion tract lengths, (ii) increased rate of discontinuous tracts and (iii) more frequent local rearrangements associated with HR (Brenneman et al., 2002). Interestingly, recent studies demonstrated that the BCDX2 and CX3 complexes act at different stages of the HR pathway, with BCDX2 acting upstream and CX3 acting downstream of RAD51 recruitment to DNA damage foci (Chun et al., 2013). Indeed RAD51D-depleted cells, but not XRCC3-depleted cells, showed defects in DNA damage-dependent RAD51 foci formation.

The RAD51:DNA nucleoprotein filament recognises homologous duplex DNA and catalyses DNA strand exchange (Baumann et al., 1996). Specifically, the invading ssDNA base pairs with its complementary sequence in the duplex DNA, thus generating heteroduplex DNA. The strand exchange reaction results in the formation of an intermediate structure called a displacement loop (D-loop) (Figure 1.2B), whereby the invading 3'-end primes the synthesis of new DNA using the duplex DNA as a template. *In vitro* studies have shown that D-loop extension reaction can be catalysed by both DNA polymerase η (Pol η) (McIlwraith et al., 2005) or DNA polymerase δ (Pol δ) (Li et al., 2009). DNA synthesis by Pol δ is stimulated by PCNA and is more efficient than that catalysed by Pol η, suggesting that Pol δ might be the major DNA polymerase performing D-loop extension *in vivo* (Li et al., 2009).

The fate of the D-loop intermediate defines the HR sub-pathway that the cell is going to employ to repair the DSB (Figure 1.2). D-loops formation can lead to the formation of a four-stranded DNA intermediate called the Holliday junction (HJ). HJs are named after Robin Holliday, who was the first to hypothesize their existence in 1964 (Holliday, 1964). These structures physically connect two homologous DNA sequences and must be processed to maintain genomic stability

and ensure cell viability (Lilley and White, 2001). HJs are mobile structures that can move along the DNA by a process called branch migration (Tsaneva et al., 1992). In the context of a D-loop, the HJ can branch migrate towards the 3'-end and disengage the invading strand from the duplex DNA (Johnson and Jasin, 2000). Unwinding of the D-loop structure can also be promoted by a group of helicases called antirecombinases, so named for their ability to revert the HR reaction. Examples of these helicases include the BLM protein (Karow et al., 2000; van Brabant et al., 2000), human regulator of telomere length RTEL1 (Barber et al., 2008) and FANCM (Fanconi anaemia group M) (Gari et al., 2008a). Whenever the newly synthesised DNA strand is released, owing to branch migration or to the activity of antirecombinases, it re-anneals with the single-stranded overhang of the second DSB end. This model of HR-mediated DSB repair is called synthesis-dependent strand annealing (SDSA) (Figure 1.2B) (Johnson and Jasin, 2000).

In contrast, when the extended invading strand engages the processed second end of the DSB, a double HJ (dHJ) structure is formed (Bzymek et al., 2010). This model of DSB repair is referred to as canonical DSB repair (DSBR) and can result in both crossover and non-crossover products (Szostak et al., 1983) (Figure 1.2B). Crossovers are generated when processing of the dHJ results in the reciprocal exchange of DNA between the two DNA molecules. Non-crossovers occur in the absence of genetic exchange. In meiotic cells, crossover formation is required to create genetic diversity (Petronczki et al., 2003). In mitotic cells, crossovers must be avoided as they can result in loss of heterozygosity (LOH), whereby activation of oncogenes and inactivation of tumour suppressor genes could promote tumourigenesis (Cavenee et al., 1983). The production of crossovers or non-crossovers depends on whether cells process dHJs by a dissolution or resolution pathway.

Holliday junction dissolution

The multi-protein BLM-TOPOIIIα-RMI1-RMI2 (BTR) complex catalyses dHJ dissolution, thus ensuring that only non-crossover products are generated (Singh et al., 2008; Wu and Hickson, 2003). BLM is one of the five members of the RecQ family of 3'-5' helicases, which also includes WRN, RECQ1, RECQ4 and RECQ5 (Bohr, 2008; Ellis et al., 1995). Mutations in three RecQ helicases, namely BLM,

WRN and RECQ4, have been associated with rare recessive genetic disorders characterised by premature aging and predisposition to cancer (Monnat, 2010). Specifically, mutations in WRN cause Werner's syndrome (Yu et al., 1996) while defects in the activity of RECQ4 cause Rothmund-Thomson syndrome (RTS) (Siitonen et al., 2009). Bloom's syndrome (BS) is an autosomal recessive disorder associated with mutations in the BLM protein and is characterised by dwarfism, infertility, hypersensitivity to sunlight and high predisposition to cancer (Bachrati and Hickson, 2003; German, 1993). At the molecular level, cells from BS patients exhibit hypersensitivity to DNA damaging agents, chromosomal aberrations and genomic instability (Chan et al., 2007; Cheok et al., 2005). Moreover, the hallmark feature of BS cells is an elevated frequency of sister chromatid exchanges (SCEs) (approximately 10-fold higher than normal cells) (Chaganti et al., 1974), which occur when there is a reciprocal exchange of genetic material (i.e. crossovers) between the two sister chromatids. Recent studies indicate that defects in BTR-mediated dHJ dissolution lead to the processing of persistent HJs by resolution pathways that promote crossover formation, thereby resulting in an increased frequency of SCEs (Wechsler et al., 2011).

The process of dHJ dissolution is initiated by the convergent branch migration of two HJs, which requires interactions between BLM and DNA topoisomerase IIIα (TOPOIIIα) (Figure 1.2) (Plank et al., 2006). In this reaction, BLM migrates the two HJs towards each other while TOPOIIIα removes the positive supercoils created in between (Plank et al., 2006). This process results in the formation of a hemicatenane that needs to be dissolved in order to separate the two DNA strands. The decatenation reaction is catalysed by TOPOIIIα and promoted by the other two components of the BTR complex, namely RMI1 and RMI2 (Cejka et al., 2010). These two OB-fold containing proteins directly interact with TOPOIIIα, stabilize the BTR complex and stimulate dHJ dissolution (Raynard et al., 2006; Singh et al., 2008).

Holliday junction resolution

The resolution of dHJs involves the endonucleolytic cleavage of the covalently linked DNA strands and results in the formation of crossover or non-crossover products, depending on the orientation of cleavage. The first evidence for the

existence of a nuclease that promotes HJ resolution was obtained from studies performed with bacteriophage T4. Mutations in gene *49* of bacteriophage T4 caused the accumulation of replicating DNA exhibiting very high sedimentation rates (Frankel et al., 1971) because of the presence of highly branched DNA molecules (Kemper and Brown, 1976). When extracts from bacteria infected with gene 49^+ and gene 49^- phages were mixed, this aberrant DNA was cleaved into a slower sedimenting DNA form, similar to that produced during wild-type phage infection (Frankel et al., 1971). The endonuclease encoded by gene *49* was then purified and is referred to as T4 endonuclease VII (Nishimoto et al., 1979). T4 endonuclease VII is able to cleave a variety of DNA structures and HJ resolution results in the production of nicked linear duplexes that can be readily re-ligated by DNA ligase (Mizuuchi et al., 1982). In addition to T4 endonuclease VII, the product of gene *3* of bacteriophage T7, T7 endonuclease I, was also discovered to be involved in the resolution of branched recombination intermediates (Tsujimoto and Ogawa, 1978) and, as observed with T4 endo VII, T7 endo I was found to cleave HJ structures to generate ligatable nicked duplex DNA (Dickie et al., 1987).

Later, the formation and resolution of HJs was extensively studied in bacteria. In *E. coli*, the bacterial homolog of RAD51, RecA, catalyses DNA strand exchange and the formation of HJs (West et al., 1983). The RuvABC proteins constitute the bacterial 'resolvasome' that processes HJs (West, 1997), by orchestrating HJ branch migration (catalysed by RuvAB) and resolution (catalysed by RuvC). RuvA is a tetrameric protein that binds HJs with high affinity and in a sequence-independent manner (Iwasaki et al., 1992; Parsons et al., 1992; Rafferty et al., 1996). By binding to DNA, RuvA recruits RuvB and promotes branch migration by causing structural changes to the HJ (Parsons et al., 1995; Parsons and West, 1993). The HJ-bound RuvAB complex is a tripartite structure in which the RuvA tetramer is flanked by the two oppositely-oriented RuvB hexamers (Parsons et al., 1995). The branch migration reaction is catalysed by the ATPase activity of RuvB, which rotates opposing arms of the HJ in such a way that the DNA passes out through each ring (Iwasaki et al., 1992; Parsons et al., 1995; Tsaneva et al., 1992). RuvC is a 19 kDa protein that binds HJs with a 10^3- to 10^4-fold higher affinity than dsDNA (Bennett et al., 1993). It binds DNA as a dimer and cleaves HJs by inserting symmetrically related nicks in strands of like polarity, thus generating a pair of nicked duplexes that can be religated (Dunderdale et al., 1991; Iwasaki et al.,

1991). RuvC resolves HJs in a sequence-specific manner, preferentially cleaving at the consensus sequence 5'-$^{A}/_{T}$TT↓$^{C>G}/_{A}$-3' and with optimal resolution occurring when a 5'-TT↓-3' incision site is located at, or one nucleotide away from, the point of strand exchange (Bennett et al., 1993; Bennett and West, 1996; Shah et al., 1994a, b). Hence, by catalysing HJ branch migration and resolution, the activities of RuvAB and RuvC provide a very efficient mechanism whereby RuvAB-mediated branch migration provides RuvC with a system to scan DNA for cleavable sequences.

RuvC is referred to as 'canonical' HJ resolvase because it resolves HJs in a symmetric manner (Figure 1.4). Canonical HJ resolvases have been identified in budding yeast (Yen1), *Caenorhabditis elegans* (GEN-1), Drosophila melanogaster (Gen1) and human cells (GEN1), providing evidence that that the RuvC model of HJ resolution is conserved in eukaryotes (Bailly et al., 2010; Ip et al., 2008; Ishikawa et al., 2004). *Saccharomyces cerevisiae* Yen1 and human GEN1 belong to the Rad2/XPG family of structure-specific endonucleases, which also includes the NER protein XPG, EXO1 (Sections 1.2.1 and 1.2.2) and the 5'-flap endonuclease FEN1 (Harrington and Lieber, 1994). Members of this family harbour an N-terminal and an internal XPG nuclease motif and a helix-hairpin-helix (HhH) domain (Hosfield et al., 1998). Like all the other XPG family nucleases, Yen1 and GEN1 are 5'-flap structure-specific endonucleases but, unlike the other family members, they preferentially cleave HJs (Rass et al., 2010). More specifically, Yen1 and GEN1 catalyse the cleavage of HJs by introducing two symmetrical incisions located 1 nucleotide on the 3'-side of the branch point to produce nicked duplex products that can be re-ligated efficiently (Ip et al., 2008).

GEN1's ability to cleave HJs was supported by the observation that ectopic expression of an N-terminal fragment of human GEN1, GEN1$^{1-527}$, promotes the processing of recombination intermediates that accumulate in MMS-treated *S. cerevisiae* cells mutated in *sgs1* or *top3*, the yeast orthologs of BLM and TOPOIIIα, respectively (Mankouri et al., 2011). Also, given that a gene encoding for Yen1 is absent in *S. pombe* and HJ resolution is solely performed by the 3'-flap endonuclease Mus81-Eme1, the observation that ectopically expressed GEN1$^{1-527}$ can promote HJ resolution in *S. pombe mus81Δ* cells represented further evidence for its role as a HJ resolvase (Lorenz et al., 2010). However, genetic studies

performed in *S. cerevisiae* showed that *yen1Δ* mutant cells are resistant to DNA damaging agents (e.g. MMS, HU, phleomycin, cisplatin), fail to show chromosome segregation defects and exhibit wild-type levels of cell growth and crossover formation, indicating that Yen1 may act redundantly with other nucleases (Blanco et al., 2010; Ho et al., 2010; Tay and Wu, 2010). Moreover, the observation that *yen1Δ mus81Δ* double mutants accumulate unresolved joint molecules and exhibit a synthetic phenotype, suggested that Yen1 and Mus81-Mms4 work in redundant pathways of HJ resolution *in vivo* (Blanco et al., 2010; Ho et al., 2010; Tay and Wu, 2010).

Importantly, a similar mechanism exists in human cells, where HJs can be processed by either GEN1 or a multi-protein complex that contains the MUS81-EME1 (the human ortholog of Mus81-Mms4) and SLX1-SLX4 structure-specific endonucleases (catalytic subunits are indicated first) (Andersen et al., 2009; Fekairi et al., 2009; Munoz et al., 2009; Svendsen et al., 2009). To uncover the roles of these proteins in HJ resolution, genetic studies were performed in BS cells by determining the contribution of GEN1, MUS81, SLX1 and SLX4 to SCE formation. Specifically, when GEN1 was depleted in BS cells, no significant change was observed in the frequency of SCEs and in chromosomes conformation (Wechsler et al., 2011). However, BS cells co-depleted of MUS81 and GEN1, or SLX1/SLX4 and GEN1, exhibited an SCE frequency that was lower than that observed with the individual depletions. Furthermore, BS cells depleted of MUS81 and GEN1 or GEN1 and SLX4 displayed aberrant chromosome conformations and condensation defects that were not observed with single protein depletions, providing further evidence that GEN1 and the SLX1-SLX4-MUS81-EME1 (SLX-MUS) complex work in two distinct pathways of HJ resolution (Wechsler et al., 2011; Wyatt et al., 2013). In contrast to RuvC and GEN1, the SLX-MUS complex cleaves HJs by asymmetric nicking, thereby generating mostly non-ligatable products (Figure 1.4) (Wyatt et al., 2013).

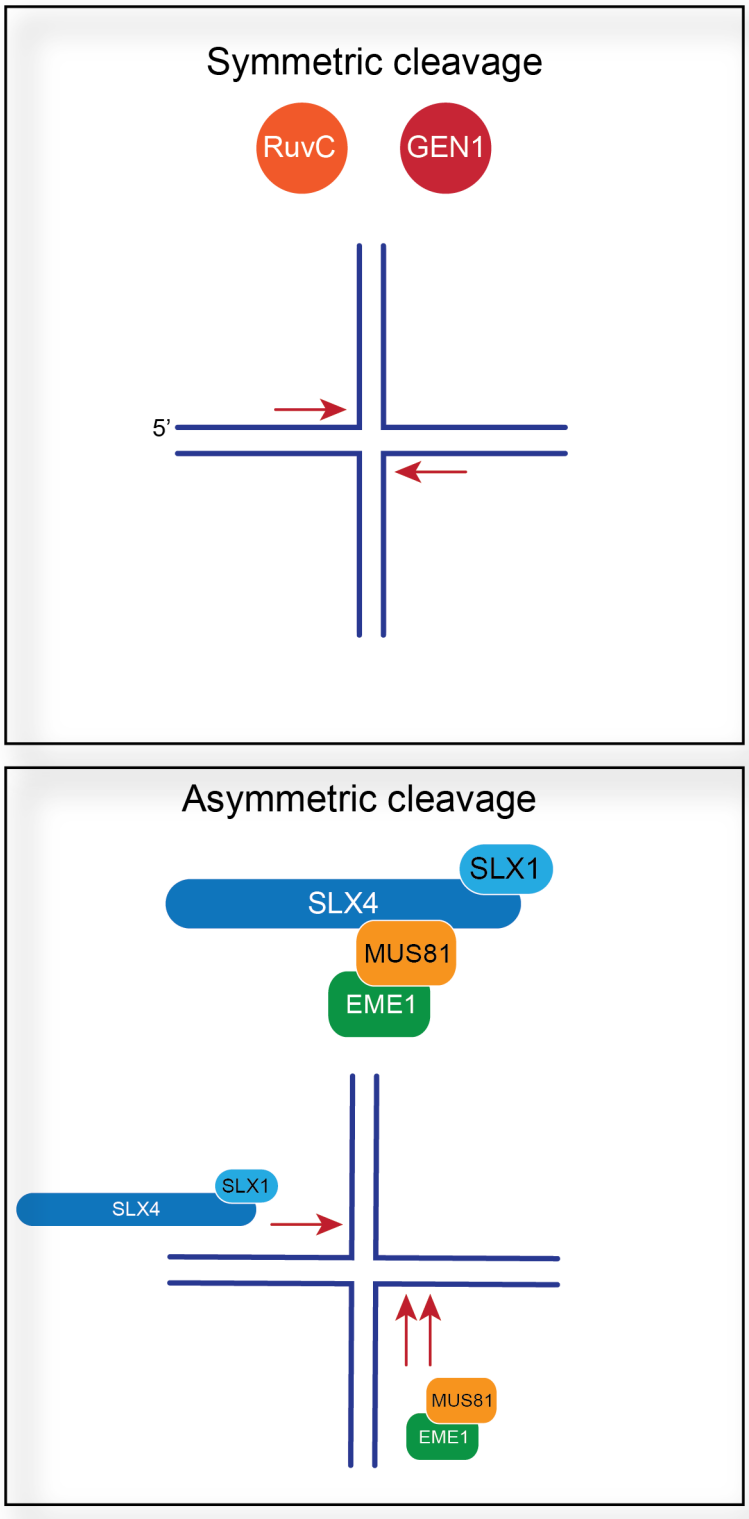

Figure 1.4 Schematic representation of HJ resolution by symmetric or asymmetric cleavage
RuvC and GEN1 are canonical HJ resolvases as they cleave HJs by inserting symmetric nicks on strands of like polarity, thus generating ligatable products. The SLX-MUS complex is an example of non-canonical HJ resolvase as it cleaves HJs by asymmetric nicking, thus generating mostly non-ligatable products.

Single strand annealing

More than 10% of the human genome is composed of repetitive sequences, which include, for example, greater than 10^6 interspersed Alu repeats (Batzer and Deininger, 2002). When a two-ended DSB occurs in a repetitive genomic region, cells activate a DSB repair mechanism called single strand annealing (SSA). This is a RAD51-independent mechanism that involves co-operation between the ssDNA-binding protein RPA and the RAD52 protein. SSA is initiated with the resection of the broken DNA ends to generate 3'-single-stranded overhangs (Figure 1.2). While RPA binds and stabilises the ssDNA tails, RAD52 binds to the ssDNA ends and promotes an annealing reaction that restores the integrity of the duplex DNA (Van Dyck et al., 2001; Wold, 1997). Annealing of the repetitive elements adjacent to the DSB causes the non-homologous sequences between the repeats to form flap structures, which are subsequently removed by the XPF-ERCC1 endonuclease (Adair et al., 2000; Sargent et al., 1997) (Section 1.2.1) (Figure 1.2C). As a result, SSA-mediated DSB repair results in the deletion of DNA sequences located between the two repeats, making this an inherently error-prone mechanism of DNA repair.

1.2.3 Role of HR in replication fork repair and ICL repair

The complete and faithful replication of DNA is essential to prevent accumulation of genetic mutations and to ensure the successful transmission of the genetic material to daughter cells. DNA secondary structures, topological stress in the DNA template, protein-DNA complexes (e.g. transcription factors bound to DNA), or chemical agents (e.g. hydroxyurea and ICL agents), constitute physical obstacles to the DNA replication machinery and can result in the stalling and/or collapse of RFs (Petermann and Helleday, 2010). Stalled RFs retain the ability to resume DNA replication when the impediment is removed, whereas collapsed forks result in one-ended DSBs and in the dissociation of the replication machinery.

The restart of stalled and collapsed RFs has been well characterised in bacteria and requires a close cooperation between the DNA replication and HR machineries (Heller and Marians, 2006). The re-assembly of the replisome on the fork is

essential for cell survival because bacteria only have one replication origin and, unlike eukaryotes, cannot rely on the licencing of other origins to complete replication (Petermann et al., 2010). Replisome re-assembly is achieved by the recruitment of the replisome loading factors PriA or PriC (Jones and Nakai, 1999). PriA is a DNA helicase that recognises and binds branched DNA structures such as D-loops (Heller and Marians, 2006). Formation of a D-loop requires the initiation of HR, which can occur in a DSB-dependent or independent manner. First, stalled RFs are regressed to generate a HJ structure. Second, the free DNA end of the HJ is processed by the RecBCD nuclease to create ssDNA overhangs that promote RecA binding and template strand invasion, ultimately forming a D-loop structure (Kuzminov and Stahl, 1999). Alternatively, RuvABC can cleave the HJ to generate a one-ended DSB that is used by RecA to invade the template DNA and establish a D-loop (Seigneur et al., 1998). Finally, PriA binds the D-loop structure and promotes the loading of the replicative DnaB helicase and replication restart (Heller and Marians, 2006).

Proteins involved in replication fork restart in *E. coli* are not conserved in eukaryotes. However, HR is the primary DNA repair pathway during S-phase of mammalian cells, suggesting that recombination-mediated repair of stalled RFs is likely to be conserved in higher eukaryotes. This is supported by observations that replication-stalling agents, such as hydroxyurea (HU) and camptothecin (CPT), induce RAD51 foci formation and HR in mammalian cells (Arnaudeau et al., 2001; Saintigny et al., 2001). Indeed, human cells employ two mechanisms of HR-mediated repair of stalled RFs and choose one or the other depending on whether forks stall temporarily (i.e. are able to resume replication) or stall permanently and become inactivated (i.e. the replication machinery has dissociated) (Petermann et al., 2010).

If forks are stalled temporarily, HR can repair the fork and restore DNA replication. DNA helicases, namely BLM, WRN and FANCM, promote RF regression *in vitro*, whereby the newly synthesised DNA strands re-anneal and generate a HJ or ‘chicken foot’ structure (Figure 1.5A) (Gari et al., 2008b; Machwe et al., 2007; Ralf et al., 2006). The two free DNA ends of the ‘chicken foot’ are thought to recombine through strand invasion with the homologous DNA template ahead of the fork and

generate a D-loop. Resolution of the D-loop structure restores DNA replication. In this context, the BLM helicase has been shown to promote efficient fork restart after cells are exposed briefly to HU (2 to 6 hr) (Davies et al., 2007). However, it is unclear whether BLM stabilizes the stalled fork by inducing its regression or by branch migration of the HJ (Karow et al., 2000; Ralf et al., 2006). Conversely, WRN is not essential for RF restart but it might have a role in the efficient progression of restarted forks as, after short HU treatments, RFs progress slowly in WRN-depleted cells (Sidorova et al., 2008).

FANCM protein belongs to the XPF family of structure-specific DNA binding proteins (Ciccia et al., 2008). It harbours an inactive excision repair cross-complementation group 4 (ERCC4)-type nuclease domain and a DEAH helicase domain, which is required for its ability to catalyse DNA translocation (Gari et al., 2008b; Meetei et al., 2005). FANCM is able to regress RFs *in vitro* and promotes a key role in the recognition and repair of DNA ICLs in the context of the FA pathway (Gari et al., 2008a). As mentioned in Section 1.1, ICLs are highly toxic DNA lesions because they covalently link two strands of DNA and thus, constitute a barrier to RF progression. During S-phase, FANCM recognises ICL-blocked forks, promotes their regression into 'chicken foot' structures and recruits the FA core complex (Gari et al., 2008a; Niedernhofer, 2007). This complex is composed of seven FA proteins (FANCA, FANCB, FANCC, FANCE, FANCF, FANCG and FANCL) and displays a FANCL-dependent ubiquitin ligase activity (Meetei et al., 2004). It monoubiquitinates two additional DNA binding factors, FANCI and FANCD2 (Garcia-Higuera et al., 2001; Smogorzewska et al., 2007), which are retained on chromatin and co-localise with DNA repair proteins such as RAD51, BRCA1 and γH2AX (Bogliolo et al., 2007; Garcia-Higuera et al., 2001; Taniguchi et al., 2002). The reversed fork is then stabilised by HR. The free DNA ends of the 'chicken foot' structure undergo RAD51-mediated strand invasion of the homologous DNA ahead of the fork and generate a D-loop (Figure 1.5B). However, re-establishment of the replication fork requires 'unhooking' of the ICL, which involves (i) unwinding of the DNA helix, (ii) incision of the DNA backbone on the 3'- and 5'-side of the lesion and (iii) displacement of the ICL. Recently, several studies led to the identification of a new DNA repair nuclease referred to as Fanconi-associated nuclease 1 (FAN1),

Figure 1.5 Schematic representation of the HR-mediated repair of stalled and collapsed RFs

A. HR promotes the restart and repair of stalled or collapsed RFs. When forks stall temporarily (top panel), fork reversal and formation of the 'chicken foot' structure promotes the invasion of the duplex DNA ahead of the fork and the formation of a dHJ. Processing of the intermediate structure allows the restart of DNA replication. Conversely, when forks stall permanently (bottom panel), MUS81-dependent cleavage of the fork results in its collapse, which generates a one-ended DSB that can be repaired by HR. Also, the progression of RFs from newly fired origins towards the break can lead to second-end capture and to the formation of a dHJ that can be processed by dissolution or resolution. **B.** When RFs stall at ICLs, FANCM is recruited to the lesion and subsequently catalyses fork reversal to form a 'chicken foot' structure that is stabilised by HR. The excision or 'unhooking' of the ICL is thought to require the activities of the SLX1-SLX4 and XPF-ERCC1 structure-specific endonucleases. The processing of recombination intermediates and synthesis of new DNA at the site of the lesion will ultimately promote RF restart. Adapted from (Petermann and Helleday, 2010).

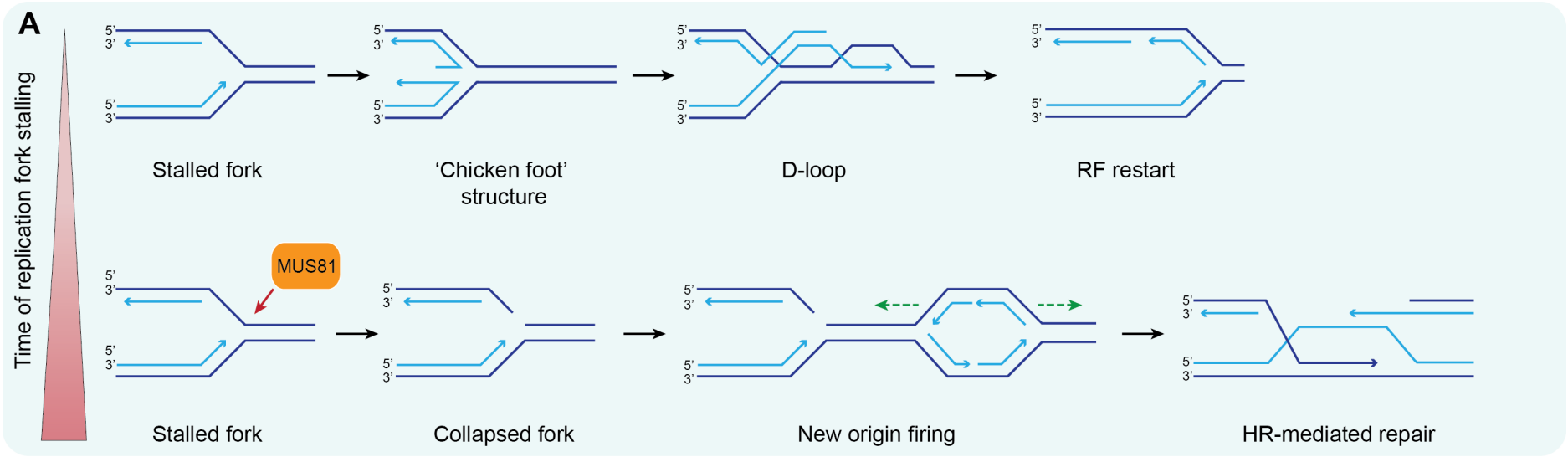
A
Time of replication fork stalling
5'
3'
Stalled fork
'Chicken foot' structure
D-loop
RF restart
MUS81
Stalled fork
Collapsed fork
New origin firing
HR-mediated repair

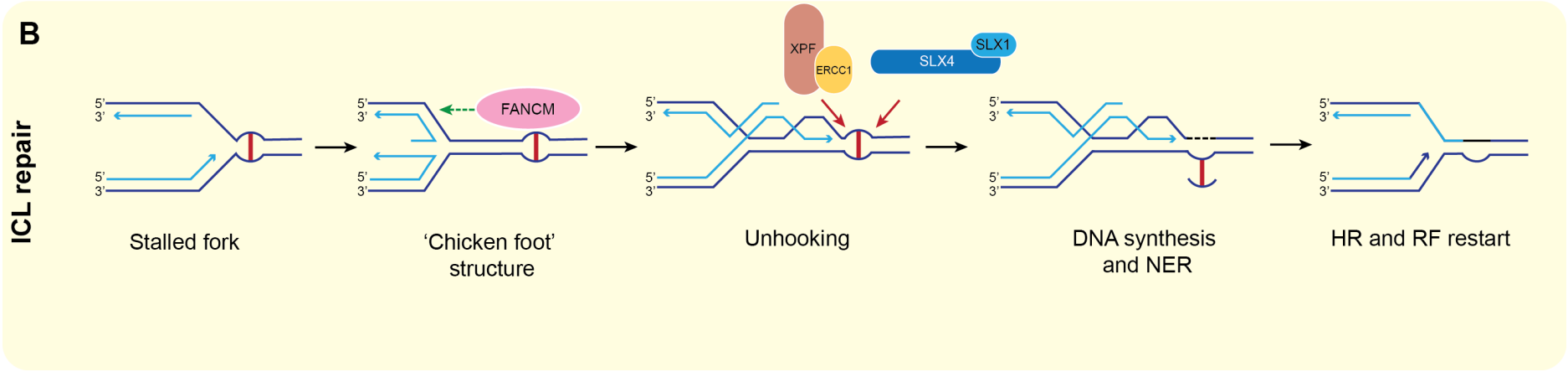
B
ICL repair
XPF
ERCC1
SLX4
SLX1
FANCM
Stalled fork
'Chicken foot' structure
Unhooking
DNA synthesis and NER
HR and RF restart

which confers cellular resistance to ICL agents (Kratz et al., 2010; Liu et al., 2010; MacKay et al., 2010; Smogorzewska et al., 2010). FAN1 is a structure-specific endonuclease with a 5'-exonuclease activity that localises to the sites of DNA damage by interacting with FANCI and monoubiquitinated FANCD2. Given that experiments conducted in a cell-free system showed that FANCD2 monoubiquitination is required for ICL unhooking (Knipscheer et al., 2009), a role for FAN1 in this step of ICL repair was hypothesized. However, although FAN1-deficient cells exhibit hypersensitivity to ICL agents, their cellular phenotypes differ from those of FA cells, thus FAN1 does not appear to be a susceptibility gene for FA (Trujillo et al., 2012; Zhou et al., 2012). Instead, mutations in FAN1 have been related to the onset of karyomegalic interstitial nephritis (KIN) (Zhou et al., 2012), a rare progressive disorder characterised by kidney failure and dysfunction of other tissues, including brain and liver (Palmer et al., 2007). Hence, how FAN1 contributes to ICL repair is still unknown. Nevertheless, given that (i) cells defective for the XPF-ERCC1 endonuclease exhibit hypersensitivity to ICL agents (Wood, 2010), (ii) SLX4 is a FA gene (Stoepker et al., 2011) and (iii) the interaction between SLX1-SLX4 and XPF-ERCC1 is essential for ICL repair (Kim et al., 2013), it is likely that the ICL unhooking step requires the cooperation of XPF-ERCC1 and SLX1-SLX4 (Figure 1.5B). The properties and functions of SLX1-SLX4 will be discussed in Section 1.3.

When RFs stall for many hours (e.g. 24 hr) they are inactivated and cells utilise a second repair mechanism that involves endonucleolytic cleavage and collapse of the RF (Figure 1.5A). This process is dependent on the activity of the MUS81 structure-specific endonuclease and results in the generation of a one-ended DSB (Hanada et al., 2007). Whether MUS81 contributes to RF restart or not is still controversial. *Mus81*$^{-/-}$ mouse embryonic stem (ES) cells exposed to HU show defects in RF restart (Hanada et al., 2007). However, it is likely that replication recovery in human cells is not dependent on MUS81 and it occurs by the activation of new replication origins (Petermann et al., 2010), suggesting that in human cells, the MUS81 endonuclease may be required for the repair of stalled RFs, but not RF restart.

Collapsed RFs that have been cleaved by MUS81 are further processed by HR (Arnaudeau et al., 2001). DNA end-resection of the one-ended DSB is followed by

RAD51 nucleoprotein filament formation, which promotes strand invasion and generation of a D-loop (Section 1.2.2). RFs progressing from a newly fired origin towards the DSB can lead to second end capture and formation of a dHJ that can be processed as discussed in Section 1.2.2 (Figure 1.5A) (Petermann et al., 2010).

RFs also collapse when they encounter a single strand break, which is converted into a one-ended DSB by DNA replication 'run-off' (Strumberg et al., 2000). Indeed, mammalian cells with defective single strand break repair (i.e. *XRCC1*$^{-/-}$) show an increased frequency of DSBs, SCEs and RAD51 foci formation specifically during the S-phase of the cell cycle (Saleh-Gohari et al., 2005; Schreiber et al., 1995; Thompson et al., 1982).

1.3 The role of MUS81 in DNA repair

MUS81 is a member of the XPF/MUS81 family of structure-specific endonucleases (Figure 1.6). Enzymes belonging to this family form heterodimeric complexes composed of a catalytic and a non-catalytic subunit and include XPF-ERCC1 (Section 1.2.1), FANCM-FAAP24 (Section 1.2.3) (Coulthard et al., 2013), MUS81-EME1 and MUS81-EME2 (catalytic subunits are indicated first) (Ciccia et al., 2008). As illustrated in Figure 1.6, each subunit contains an ERCC4 endonuclease domain and a $(HhH)_2$ domain (Nishino et al., 2003; Shao and Grishin, 2000). In the catalytic subunits, the ERCC4 domain contains a GDX_nERKX_3D motif that harbours conserved Asp and Glu residues that co-ordinate the divalent metal ion required for catalysis. In contrast, the amino acid sequence of this motif has diverged in the non-catalytic subunits, thus rendering these proteins nucleolytically inactive (Enzlin and Scharer, 2002). The $(HhH)_2$ domain is composed of two copies of the HhH motif and is required for sequence-independent DNA binding and enzyme stability (Newman et al., 2005; Shao and Grishin, 2000). In contrast to the other members of the XPF/MUS81 family, the $(HhH)_2$ domain of MUS81 is separated, with one HhH located at the N-terminus and the other one found at the C-terminus. In mammalian cells, MUS81 forms a complex with EME1 or EME2 (Ciccia et al., 2003; Ciccia et al., 2007; Ögrünc and Sancar, 2003). The interaction between MUS81 and EME1 is conserved from yeast to humans and has been the subject of many biochemical and genetic studies. However, no yeast ortholog of EME2 has been identified, potentially indicating a role for MUS81-EME2 that is specific to higher eukaryotes.

1.3.1 Role of MUS81-EME1 in HJ resolution

S. pombe Mus81-Eme1 and S. cerevisiae Mus81-Mms4

Genetics

S. pombe Mus81 was first identified through its interaction with the replication checkpoint kinase Cds1 (Boddy et al., 2000) and it forms a functional heterodimer with a non-catalytic subunit called Eme1 (Boddy et al., 2001). Genetic studies in meiotic cells revealed that Mus81-Eme1 has a crucial function in the resolution of recombination intermediates. Meiotic *mus81Δ* and *eme1Δ* cells show severe chromosome segregation defects during meiosis I, which result in the generation of inviable spores (<1% survival) (Boddy et al., 2000; Interthal and Heyer, 2000; Osman et al., 2003). In agreement with a role in HJ resolution, this phenotype can be rescued by the ectopic expression of the bacterial HJ resolvase RusA, or by depletion of the SPO11 yeast ortholog *rec12*, which, as described in Section 1.2.2, is required for the formation of programmed meiotic DSBs and for the initiation of HR (Boddy et al., 2001; Osman et al., 2003). Also, *mus81Δ* cells exhibited a lower frequency of crossovers (8 to 25 fold) compared to that of wild-type cells, indicating that meiotic crossover formation in *S. pombe* is mainly dependent on the activity of Mus81-Eme1 (Boddy et al., 2001; Osman et al., 2003).

In mitotic cells, Mus81-Eme1 is required for the resolution of HJs arising during the repair of stalled RFs. Indeed, *mus81Δ* and *eme1Δ* cells exhibit hypersensitivity to RF stalling agents, such as CPT, HU, UV light and MMS (Boddy et al., 2001; Doe et al., 2002). Also, depletion of Mus81 or Eme1 is synthetically lethal with the loss of Rqh1, the *S. pombe* ortholog of human BLM (Boddy et al., 2000; Doe et al., 2002). Both the viability of *mus81Δ rqh1Δ* double mutants and the resistance of *mus81Δ* or *eme1Δ* cells to RF stalling agents are restored by the ectopic expression of RusA, indicating that the requirement for Mus81-Eme1 in RF repair is related to its ability to resolve HR intermediate structures (Boddy et al., 2001; Doe et al., 2002).

In *S. cerevisiae*, Mus81 was first identified through its interaction with the recombination protein Rad54 (Interthal and Heyer, 2000) and in a synthetic lethal

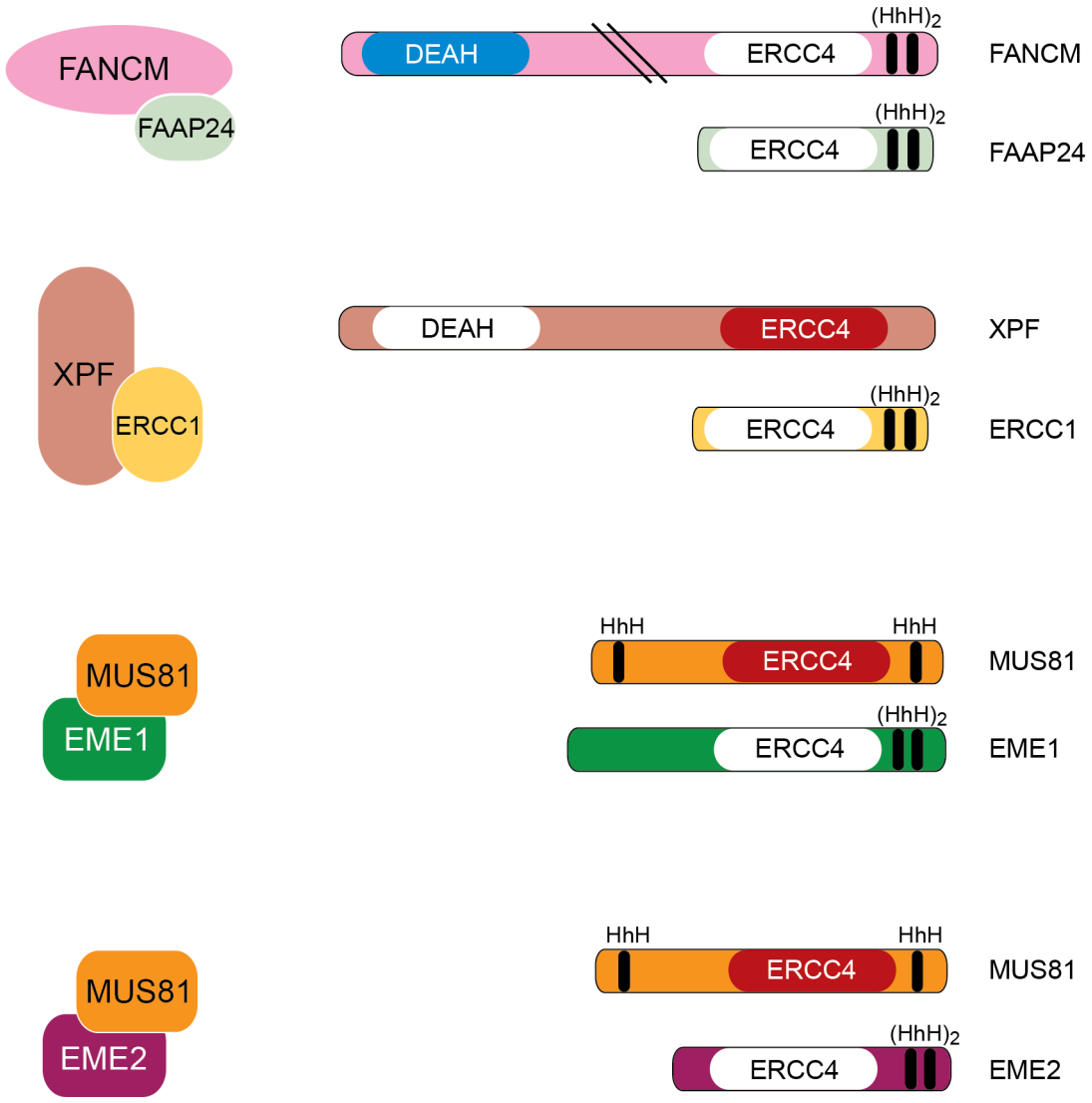

Figure 1.6 The XPF/MUS81 family of endonucleases

Schematic representation of the primary structure of XPF/MUS81 family members. As shown on the left, each protein forms a heterodimeric complex containing one catalytic subunit (i.e. MUS81, XPF, FANCM) and one non-catalytic subunit (i.e. EME1, EME2, ERCC1, FAAP24). The ERCC4 nuclease domains (red), Helix-hairpin-Helix (HhH) DNA binding domains (black) and the DEAH helicase domains (blue) are indicated. The inactive ERCC4 and DEAH domains are coloured in white.

screen for genes that are essential in the absence of Sgs1, the ortholog of human BLM (Mullen et al., 2001). In contrast to fission yeast, *S. cerevisiae* meiotic cells lacking Mus81 exhibited a small reduction in crossover formation and reduced viability (approximately 50% of the spores were viable), suggesting that Mus81-Mms4 (the ortholog of Mus81-Eme1) contributes modestly to HJ resolution and crossover formation (de los Santos et al., 2003). Indeed, Mlh1-Mlh3, Exo1 and Sgs1 are responsible for the majority of crossovers arising during meiotic recombination in this organism (Zakharyevich et al., 2010; Zakharyevich et al., 2012). Moreover, a functional redundancy exists between Mus81-Mms4 and Yen1, such that *mus81Δ yen1Δ* cells exhibit less than 1% viability (Matos et al., 2011). Therefore, the lack of an ortholog of Yen1 in *S. pombe* explains the difference in viability between fission and budding yeast *mus81Δ* cells. The functional redundancy between Mus81-Mms4 and Yen1 has also been identified in the context of DNA repair (Blanco et al., 2010; Ho et al., 2010; Munoz-Galvan et al., 2012). Indeed, depletion of Yen1 in a *mus81Δ* background increases cellular sensitivity to DNA damaging agents (e.g. MMS, HU, CPT, cisplatin) and causes cells to accumulate toxic recombination intermediates.

Biochemistry

Despite genetic evidence indicating that *S. pombe* Mus81-Eme1 and *S. cerevisiae* Mus81-Mms4 process HJs *in vivo*, biochemical analyses carried out with the purified heterodimers did not support this hypothesis, thus generating a controversy on whether the Mus81 endonuclease was a HJ resolvase (Haber and Heyer, 2001). Indeed, recombinant *S. pombe* Mus81-Eme1 purified from *E. coli* cleaves HJs with very low efficiency compared to 3'-flaps and RFs (Doe et al., 2002; Whitby et al., 2003). In general, Mus81-Eme1 preferentially cleaves three-way branched structures by inserting nicks 3 to 6 nucleotides on the 5'-side of the branch point, with the nicked HJ being its preferred substrate (Gaillard et al., 2003; Osman et al., 2003; Whitby et al., 2003). Similarly, recombinant Mus81-Mms4 purified from *E. coli* was found to be a poor HJ resolvase (Ehmsen and Heyer, 2008, 2009; Fricke et al., 2005; Kaliraman et al., 2001; Whitby et al., 2003). Conversely, three-way branched structures, including 3'-flaps and RFs, were readily converted into nicked duplex products by Mus81-Mms4 through a mechanism that is similar to that described for *S. pombe* Mus81-Eme1 (Bastin-Shanower et al., 2003; Whitby et al.,

2003). Mus81-Mms4 processes a 3'-flap substrate by recognising the 5'-end of the DNA strand located downstream of the flap and by cleaving the duplex DNA 3 to 7 nucleotides on the 5'-side of the branch point (Bastin-Shanower et al., 2003). Also, 3'-flaps with a gap of more than 4 nt were not cleaved efficiently by Mus81-Mms4, indicating that the presence of a 5'-end positioned less than 4 nt away from the branch point represents the minimal requirement for Mus81-Mms4 cleavage (Bastin-Shanower et al., 2003).

Regulation

Partially purified Mus81-Eme1 from *S. pombe* was found to efficiently cleave HJs *in vitro* (Boddy et al., 2001; Gaillard et al., 2003). Specifically, cleavage by Mus81-Eme1 occurred by asymmetric nicking, thus generating mostly non-ligatable products (Boddy et al., 2001; Gaillard et al., 2003). Such observations led to the hypothesis that the activity of the Mus81 endonuclease on HJs *in vivo* could be modulated by post-translational modifications. In agreement with this, recent studies in *S. cerevisiae* revealed that the activities of the HJ resolvases Mus81-Mms4 and Yen1 are tightly regulated. During S-phase, the cleavage of HJs by Mus81-Mms4 and Yen1 is low and increases as cells progress in the cell cycle, with Mus81-Mms4 being activated at G2/M and Yen1 being activated in anaphase (Matos et al., 2011). The increase in HJ resolution correlated with the hyper-phosphorylation of Mms4 by the cell cycle kinases Cdc28 (i.e. the budding yeast ortholog of human CDK1) and Cdc5 (i.e. the ortholog of human PLK1) and with the de-phosphorylation of Yen1 (Gallo-Fernandez et al., 2012; Matos et al., 2011; Matos et al., 2013). Indeed, phosphorylation-defective *mms4* mutants exhibit reduced nuclease activity and increase the sensitivity of *sgs1Δ* cells to DNA damaging agents (Gallo-Fernandez et al., 2012; Matos et al., 2013). On the same note, premature activation of Mus81-Mms4 achieved by expression of phosphomimic Mms4 variants or by misregulated expression of Cdc5 resulted in an increased frequency in crossover formation and chromosomal translocations (Matos et al., 2013; Szakal and Branzei, 2013). Through this cell cycle-dependent mechanism of phosphorylation/de-phosphorylation-mediated activation of HJ resolvases, cells control the interplay between HJ dissolution and resolution, thus restricting the activity of crossover-promoting enzymes to the G2/M phase of the cell cycle.

Importantly, although the activity of Mus81-Mms4 is required for complete chromosome replication and cell viability after treatment with RF stalling agents, the presence of DNA damage during S-phase does not induce its activation (Saugar et al., 2013). Instead, the action of Mus81-Mms4 is kept restricted to G2/M, thus preventing the deleterious cleavage of RFs during DNA replication (Saugar et al., 2013). In contrast to budding yeast, *S. pombe* Mus81-Eme1 is activated in a phosphorylation-dependent manner in response to DNA damage (Dehe et al., 2013). In particular, the sequential phosphorylation of Eme1 by the cell cycle kinase Cdc2 (i.e. the fission yeast ortholog of human CDK1) and by Rad1 (i.e. the fission yeast ortholog of human ATR) in response to CPT or bleomycin treatment provides a fast mechanism for Mus81-Eme1 activation in order to resolve HJs that have escaped dissolution prior to the onset of mitosis. The importance of Eme1 phosphorylation is further confirmed by the observation that *rqh1Δ* (Rqh1 being the fission yeast ortholog of human BLM) cells expressing a phosphorylation-resistant Eme1 variant exhibit gross chromosomal rearrangements in the absence of exogenous DNA damage (Dehe et al., 2013).

Mammalian MUS81-EME1

The evidence for a role of mammalian MUS81 in DNA repair comes from studies conducted in mice, where its depletion has been associated with loss of genomic integrity and cancer development (McPherson et al., 2004). Metaphase spreads of activated T-cells from *Mus81*$^{-/-}$ and *Mus81*$^{+/-}$ mice were scored for chromosomal aberrations and showed an elevated rate of chromosomal breaks, fusions and aneuploidy. Moreover, both *Mus81*$^{-/-}$ and *Mus81*$^{+/-}$ mice were predisposed to the development of a wide range of lymphomas and other cancer types, including breast and ovarian carcinomas. Interestingly, both heterozygous and homozygous mice exhibited the same phenotypes, suggesting that the biallelic expression of Mus81 is essential for the fulfilment of its function in maintaining genome stability (McPherson et al., 2004). Haploinsufficiency of MUS81 was also observed in human cells, where both *MUS81*$^{-/-}$ and *MUS81*$^{+/-}$ cells displayed increased rates of chromosomal aberrations. In some of these cells, depletion of MUS81 promoted endoreduplication, a phenotype characterised by the association of re-duplicated chromosomes into diplochromosomes (Hiyama et al., 2006). Although diplochromosomes have been already observed in cells lacking other HR genes

such as XRCC3, the cause of this phenotype is still unknown (Yoshihara et al., 2004). Importantly, the *MUS81* gene is down-regulated in hepatocellular and colon carcinoma, providing further evidence for a role of MUS81 in the maintenance of genomic stability in human cells (Wu et al., 2008; Wu et al., 2011). Finally, transient depletion of MUS81 in human cells resulted in reduced mitotic recombination (Blais et al., 2004) and sensitivity to DNA damaging agents such as CPT, cisplatin and MMS (Hiyama et al., 2006). Moreover, MUS81 has been shown to localise to regions of UV-damage, as indicated by its co-localisation with cyclobutane pyrimidine dimers (Gao et al., 2003).

Biochemistry

As found for *S. pombe* Mus81-Eme1 and *S. cerevisiae* Mus81-Mms4, recombinant human MUS81-EME1 purified from *E. coli* was found to cleave HJs with very low efficiency (Ciccia et al., 2003). Conversely, 3'-flaps, RFs and nicked HJs were readily converted into nicked duplex products (Ciccia et al., 2003; Taylor and McGowan, 2008). Only the purified complex constituted by truncated versions of MUS81 and EME1 was able to cleave HJs efficiently, albeit it should be noted that 20- to 100-fold excess of protein over DNA was used in these experiments (Taylor and McGowan, 2008). In contrast, however, immuno-precipitated or partially-purified MUS81 from human cells showed efficient cleavage of HJs *in vitro* (Chen et al., 2001; Gaillard et al., 2003). Hence, the possibility that the activity of MUS81-EME1 on HJs could be regulated by (i) unknown interacting partners, and/or (ii) post-translational modifications has been a focus of recent investigation.

The SLX-MUS complex

In agreement with the first hypothesis, MUS81-EME1 was found to interact with two other endonucleases: the NER enzyme XPF-ERCC1 (Section 1.2.1) and SLX1-SLX4 (Andersen et al., 2009; Fekairi et al., 2009; Munoz et al., 2009; Svendsen et al., 2009). Slx4 and its partner protein Slx1 were first identified in a synthetic lethal screen for proteins that are required for cell viability in the absence of the Sgs1 helicase (Mullen et al., 2001). Slx1-Slx4 is a structure-specific endonuclease that cleaves various types of branched DNA structures, including 5'- and 3'-flaps, RFs and HJs (Fricke and Brill, 2003). However, although Slx1-Slx4 can cleave HJs *in*

vitro, yeast s*lx1Δ* and s*lx4Δ* mutants do not exhibit severe meiotic defects, suggesting that Slx1-Slx4 may not function as a HJ resolvase *in vivo* (Mullen et al., 2001). Slx1 is the catalytic subunit of the complex, harbouring a N-terminal GIY-YIG nuclease domain and a C-terminal Plant Homeo Domain (PHD)-type zinc finger domain (Aravind and Koonin, 2001). Slx4 contains a SAF-A/B, Acinus and PIAS (SAP) DNA-binding domain in its C-terminus and, unlike Slx1, it does not have any catalytic domain (Aravind and Koonin, 2000). Slx4 promotes the targeting of the Slx1-Slx4 complex to DNA substrates and, given that Slx1 alone is inactive, it appears to be important for the endonucleolytic activity of the complex (Fricke and Brill, 2003).

The human Slx4 ortholog, named BTBD12/SLX4, has an N-terminal BR-C, TTK and BAB (BTB)/Pox virus and Zinc finger (POZ) protein-protein interaction domain and C-terminal SAP and HtH DNA binding domains (Fekairi et al., 2009; Munoz et al., 2009; Svendsen et al., 2009). SLX4 interacts with SLX1 and with the MUS81-EME1 and XPF-ERCC1 endonucleases, acting as a scaffold for the formation of a multi-endonuclease complex (Andersen et al., 2009; Fekairi et al., 2009; Munoz et al., 2009; Svendsen et al., 2009). Other SLX4-interacting partners include: TRF2-RAP1, PLK1, MSH2-MSH3 (Svendsen et al., 2009) and hSNM1B/Apollo (Salewsky et al., 2012). The interaction between SLX1-SLX4 and MUS81-EME1 appears to be exclusive to higher eukaryotes, whereas the interaction between SLX4 and XPF-ERCC1 is conserved from yeast to humans. In yeast, Slx4 forms an Slx1-independent complex with Rad1-Rad10, the yeast orthologs of XPF-ERCC1, which is important for the removal of 3'-flaps during SSA (Flott et al., 2007) (Section 1.2.2). In human and mouse cells, both XPF-ERCC1 and SLX1-SLX4 have been implicated in ICL repair (Fekairi et al., 2009; Munoz et al., 2009; Svendsen et al., 2009). Consistent with this observation, biallelic mutations of *SLX4* have been found in FA patients and thus, SLX4 has been designated FANCP (Kim et al., 2011; Stoepker et al., 2011).

SLX4 immunoprecipitates from human cells cleave 3'-flaps, 5'-flaps, RFs and HJs (Munoz et al., 2009; Svendsen et al., 2009). However, when HJs were exposed to SLX4 immunoprecipitates, the cleavage product profile corresponded to the additional cleavage activities of SLX1-SLX4 and MUS81-EME1, suggesting that these two enzymes might co-operate for the resolution of HJs *in vivo* (Fekairi et al.,

2009; Munoz et al., 2009; Svendsen et al., 2009). To test this hypothesis, the contribution of MUS81, SLX1-SLX4 and GEN1 to SCE formation in BS cells was studied (Wyatt et al., 2013). This analysis led to the observation that two pathways of HJ resolution exist in human cells: one mediated by GEN1 and the other mediated by the SLX-MUS complex (Wyatt et al., 2013). In particular, co-depletion of GEN1 with SLX1, SLX4 or MUS81 in BS cells resulted in a decrease in SCEs that was higher than that promoted by the single depletions. This additive effect was not observed when MUS81 was co-depleted with SLX4 or SLX1, suggesting that MUS81 and SLX1-SLX4 work in the same pathway of HJ resolution. Consistent with this observation, analysis of the HJ cleavage mechanism by the SLX-MUS complex revealed that SLX1-SLX4 and MUS81-EME1 cleave HJs by a coordinated nick and counter-nick mechanism, whereby SLX1-SLX4 performs the first, rate-limiting cut on the junction while MUS81-EME1 cleaves the nHJ by-product to produce nicked duplex DNA molecules (Wyatt et al., 2013).

Regulation

As observed with budding yeast Mms4, phosphorylation of human EME1 by CDK1 correlates with increased HJ resolution at G2/M (Matos et al., 2011; Wyatt et al., 2013). In contrast to yeast, however, phosphorylation does not directly activate the nuclease activity of the enzyme, but promotes the interaction between MUS81-EME1 and SLX1-SLX4 (Wyatt et al., 2013). Thus, these two heterodimers interact predominantly during the G2/M phase of the cell cycle and the activity of the SLX-MUS complex causes the observed increase in HJ resolution (Wyatt et al., 2013). GEN1 also appears to be activated during mitosis, but its activity is mostly regulated by the subcellular localisation of the protein (Matos et al., 2011). Indeed, GEN1 is retained into the cytoplasm throughout the cell cycle and can gain access to DNA only during mitosis, when the nuclear envelope breaks down (Figure 1.7A).

The activity of the MUS81 endonuclease is also negatively-regulated by the CDK1-inhibitor WEE1 (Dominguez-Kelly et al., 2011). Cells depleted of WEE1 activate the DNA damage response (DDR) and exhibit an S-phase progression delay (Dominguez-Kelly et al., 2011). Loss of MUS81 in WEE1-depleted cells rescues the cell cycle progression and inhibits the DDR, indicating that the damage induced in the absence of WEE1 is dependent on the activity of the MUS81 endonuclease

(Dominguez-Kelly et al., 2011). In the proposed scenario, the direct inhibition exerted by WEE1 on MUS81 is lost in WEE1-depleted cells, thereby causing the de-regulated processing of RFs by MUS81 and resulting in DDR activation and S-phase delay (Dominguez-Kelly et al., 2011). However, the mechanism by which WEE1 regulates the activity of the MUS81 endonuclease is still undetermined.

Together, these results reveal a complex mechanism in which cells restrict the crossover-promoting activity of HJ resolvases to late stages of the cell cycle. Indeed, in mitotic S-phase cells, dHJs are primarily processed by HJ dissolution, which, by promoting the formation of non-crossover products, decreases the incidence of potentially harmful genomic rearrangements. Hence, cells appear to use HJ resolution as a safeguard mechanism to process joint molecules that have escaped BTR-mediated processing (Figure 1.7B).

Structural organisation of the MUS81-EME1 complex

Structural analysis of MUS81-EME1 has been carried out on a chimeric complex composed of truncated forms of zebrafish MUS81 (zMUS81ΔN) and human EME1 (hEME1ΔN), in which the N-terminal region of each subunit was removed (Chang et al., 2008). zMUS81ΔN and hEME1ΔN contain an N-terminal α/β nuclease domain and a C-terminal $(HhH)_2$ domain (Figure 1.8A). The structure of zMUS81ΔN is more compact than the structure of hEME1ΔN because, while the interdomain region of zMUS81ΔN contains a helix H8 and a loop with four residues, the interdomain region of hEME1ΔN contains a helix H8' and two loops, resulting in a more extended structure. Because of the differences between the linker regions of the two proteins, the interaction between zMUS81ΔN and hEME1ΔN results in an asymmetric dimer. Interestingly, unlike zMUS81ΔN, hEME1ΔN contains a highly flexible linker region (36R) that connects strand S5' with helix H6', which is required to stabilise the interaction between zMUS81ΔN and the substrate DNA. The nuclease and the $(HhH)_2$ domain of zMUS81ΔN form a shallow groove, whose size (10 Å in height and 5 Å in depth) allows the accommodation of ssDNA. In addition, a deep cleft (approximately 15 Å in diameter) is formed between the nuclease domain of zMUS81ΔN and the $(HhH)_2$ domain of hEME1ΔN, and between the inactive nuclease domain of hEME1ΔN and the $(HhH)_2$ domain of zMUS81ΔN (Figure 1.8B). The GDX_nERKX_3D motif is located at the centre of the deep cleft,

with the Asp398 and Glu392 residues, which are required for divalent metal ion-mediated catalysis, located at the bottom of the pocket (Figure 1.8C) (Chang et al., 2008).

zMUS81ΔN binds hEME1ΔN through three interfaces, which are equally important for dimerization and include: (i) one between the nuclease domain of zMUS81ΔN and the inactive nuclease domain of hEME1ΔN (Figure 1.8D), (ii) one between the $(HhH)_2$ domains of zMUS81ΔN and hEME1ΔN (Figure 1.8E), and (iii) one between the nuclease and $(HhH)_2$ domains of zMUS81ΔN and the 36R linker region of hEME1ΔN (Figure 1.8F). Briefly, the nuclease interface is formed by van der Waals contacts between Val413 and Leu417 of hEME1ΔN with the side chains of Tyr389, Met475, Tyr478 and Leu479 of zMUS81ΔN and by hydrophobic interactions between Phe435 and Phe439 of hEME1ΔN and Val449 and Val453 of zMUS81ΔN (Figure 1.8D). The $(HhH)_2$ interface forms through the interaction between helices H9, H11 and H13 of zMUS81ΔN and helices H9', H11' and H13' of hEME1ΔN (Figure 1.8E). Finally, the third interface mainly forms through ring stacking between the Phe459 ring of hEME1ΔN and the Phe413 ring of zMUS81ΔN, and between the Phe457 ring of hEME1ΔN and the side chain of Arg533 of zMUS81ΔN (Figure 1.8F) (Chang et al., 2008).

Both human MUS81-EME1 and *S. cerevisiae* Mus81-Mms4 have been shown to exist as single heterodimers both in solution and when bound to DNA (Chang et al., 2008; Schwartz et al., 2012). This observation is consistent with the biochemical data showing that both budding yeast and human heterodimers preferentially cleave three-way branched structures. Indeed, efficient cleavage of HJs would require the presence of two active sites at the branch point. Given that Mus81-Mms4 is activated by Cdc5-mediated phosphorylation, the possibility that the enzyme would form a heterotetramer following its phosphorylation was investigated (Schwartz et al., 2012). However, phosphorylation by Cdc5 was found to increase the overall activity of the enzyme without triggering its multimerization, thus excluding the possibility that the increased activity of phosphorylated Mus81-Mms4 is due to the coordinated action of two heterodimers on DNA.

1.3.2 Role of MUS81 at stalled RFs

The first evidence for a role of Mus81 in the repair of stalled RFs came from studies in both *S. pombe* and *S. cerevisiae*, where *mus81Δ* cells displayed hypersensitivity to DNA damaging agents that interfere with RF progression (Bastin-Shanower et al., 2003; Boddy et al., 2000; Doe et al., 2002). Also, *S. pombe mus81Δ* showed synthetic lethality when combined with *rqh1Δ*, which is critical for the repair of damaged or stalled RFs (Boddy et al., 2000; Doe et al., 2002). In contrast to yeast cells, mouse and human cells depleted of MUS81 only exhibit hypersensitivity to ICL agents (e.g. cisplatin and MMC), while they show milder sensitivity to other DNA damaging agents such as CPT or HU (Abraham et al., 2003; Hanada et al., 2006; Hiyama et al., 2006; McPherson et al., 2004). Although the DNA structures that form at stalled RFs are poorly understood, there is clear evidence for the role of the MUS81 endonuclease in the formation of DSBs after treatment with replication stalling agents (Fugger et al., 2013; Hanada et al., 2007; Hanada et al., 2006; Regairaz et al., 2011). Given the hypersensitivity of *Mus81*$^{-/-}$ and *Ercc1*$^{-/-}$ mouse ES cells to ICL agents, *Mus81*$^{-/-}$ and *Ercc1*$^{-/-}$ mouse ES cells were treated with cisplatin or MMC and the formation of DSBs was analysed. Cells lacking Mus81 exhibited significantly fewer DSBs than wild-type cells, whereas no difference was observed between *Ercc1*$^{-/-}$ and wild-type cells, indicating that ICL-associated DSB formation is dependent on the activity of the Mus81 endonuclease and not on that of Xpf-Ercc1 (Hanada et al., 2006). Similar results were obtained when *Mus81*$^{-/-}$ cells were exposed to increasing concentrations of HU or aphidicolin. DSB formation was significantly decreased in Mus81-depleted cells compared to wild-type cells, suggesting that, upon replication inhibition, murine Mus81-associated endonuclease cleaves stalled RFs to generate a one-sided DSB, which is required for RF HR-mediated repair and DNA replication restart (Hanada et al., 2007).

In human cells, MUS81 was found to be required for the cleavage of stalled RFs after treatment with CPT or HU (Fugger et al., 2013; Regairaz et al., 2011). Interestingly, the formation of MUS81-dependent DSBs after HU treatment is affected by the activity of FBH1, a member of the UvrD family of 3'-5' DNA helicases (Fugger et al., 2013). Owing to the fact that the substrate of MUS81 at stalled RFs is unknown, it is possible that the helicase activity of FBH1 contributes

Figure 1.7 Cell-cycle regulation of HJ dissolution and resolution pathways
A. In normal mitotic human cells, dHJs encountered during S-phase of the cell cycle are primarily processed by the BTR-mediated dHJ dissolution pathway into non-crossover products (few SCEs). The activities of the crossover-promoting enzymes SLX-MUS and GEN1 are restricted to the G2 and M phase of the cell cycle, respectively and only dHJs that escape the BTR-mediated dissolution are processed by the HJ resolution pathways. **B.** In BS cells, the dHJ dissolution pathway is not functional and dHJs are exclusively processed by the resolution pathway, which generates both crossovers (i.e. SCEs) and non-crossover products.

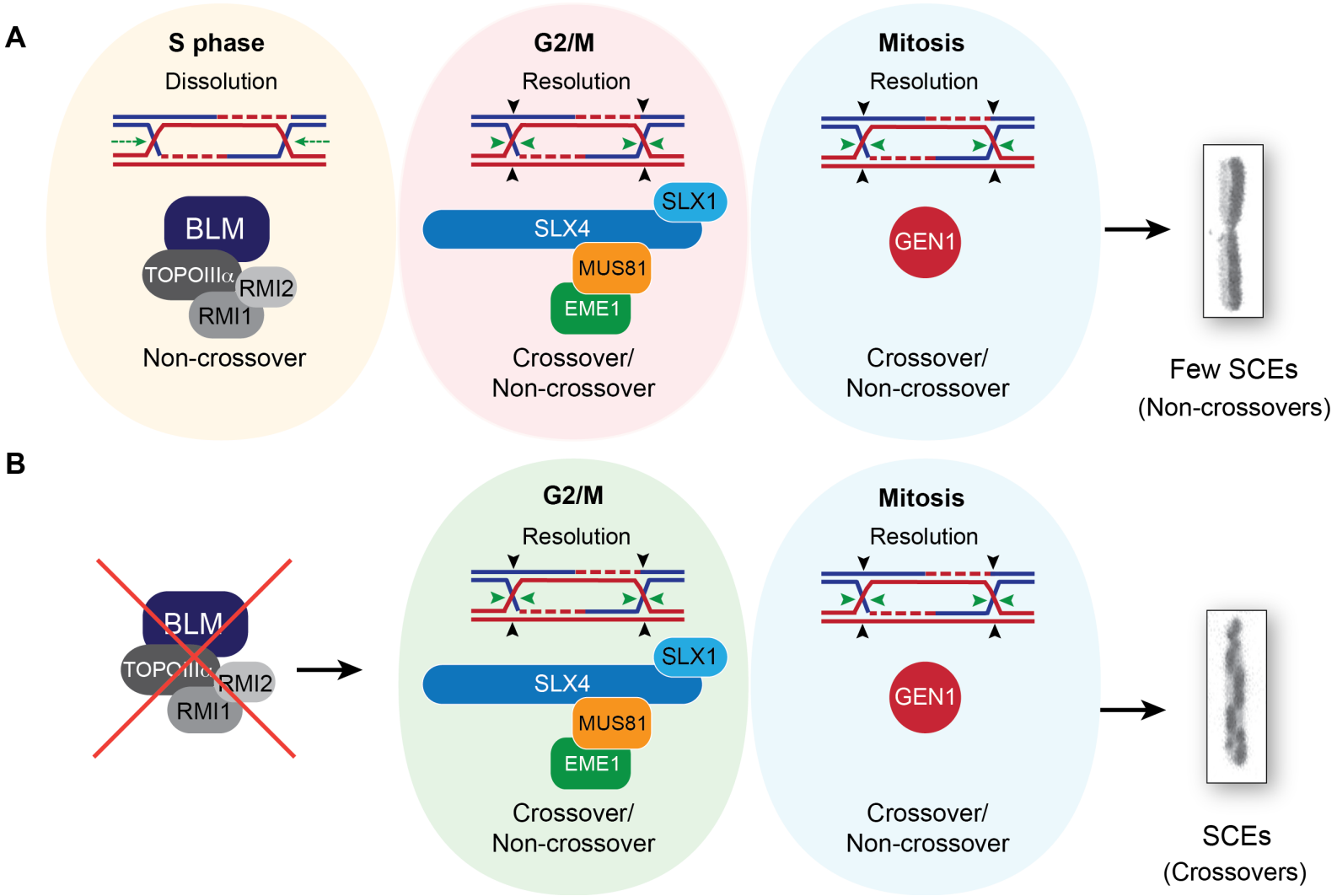
A
S phase
Dissolution
BLM
TOPOIIIα
RMI2
RMI1
Non-crossover
G2/M
Resolution
SLX1
SLX4
MUS81
EME1
Crossover/
Non-crossover
Mitosis
Resolution
GEN1
Crossover/
Non-crossover
Few SCEs
(Non-crossovers)
B
BLM
TOPOIIIα
RMI2
RMI1
G2/M
Resolution
SLX1
SLX4
MUS81
EME1
Crossover/
Non-crossover
Mitosis
Resolution
GEN1
Crossover/
Non-crossover
SCEs
(Crossovers)

Figure 1.8 Structural organisation of the MUS81-EME1 complex
A. Structure of the zMUS81ΔN- hEME1ΔN complex determined at 2.7 Å resolution. zMUS81ΔN is coloured in yellow with the active site residues and the interdomain linker helix H8 shown in magenta and orange, respectively. hEME1ΔN is coloured in cyan, with the interdomain linker helix H8' shown in blue. The dotted green line represents the 36R linker region. **B**. Surface representation of the deep cleft and central groove of the complex. The active site cleft and groove are marked. The red sphere represents the divalent metal ion required for catalysis. **C**. Structure of the active site of the complex. The side chains of zMUS81ΔN are coloured in magenta and the green sphere indicates modelled Mn^{2+} from the structure of the Hef nuclease domain. Oxygen and nitrogen atoms are shown in red and blue, respectively. The dotted green lines indicate hydrogen bonds. **D**. View of the interface between the nuclease domain of zMUS81ΔN and the nuclease-like domain of hEME1ΔN. **E**. View of the interface between the $(HhH)_2$ domain of zMUS81ΔN and the $(HhH)_2$ domain of hEME1ΔN. **F**. View of the interface between the nuclease and $(HhH)_2$ domains of zMUS81ΔN and the 36R linker region of hEME1ΔN. Figures taken from (Chang et al., 2008).

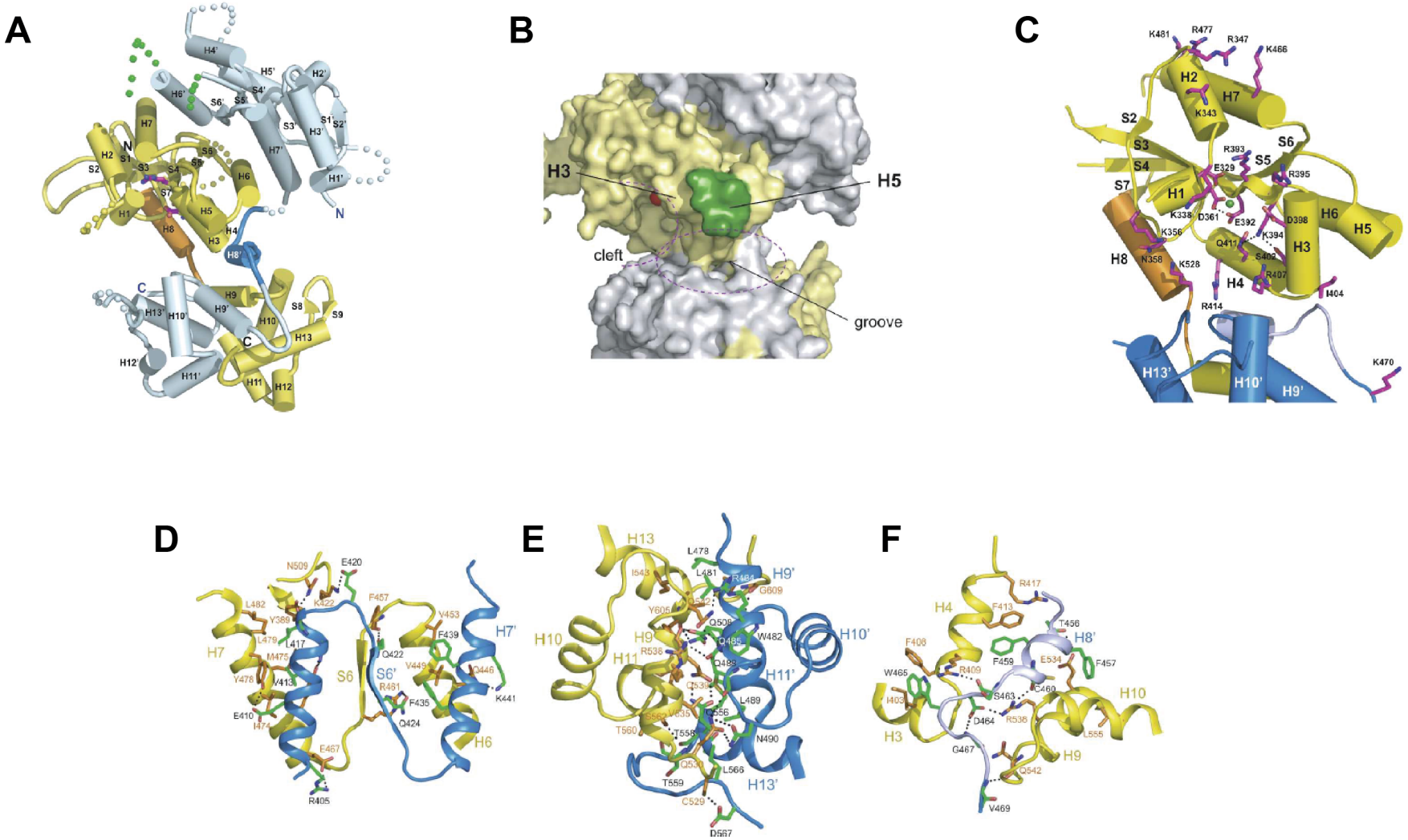
A
B
H3
H5
cleft
groove
C
K481
R477
R347
K466
H2
H7
K343
S2
S3
S6
S4
S5
R393
E329
R395
S7
H1
K338
D361
E392
D398
H6
H5
K356
K394
Q417
H3
H8
N358
S402
K528
R407
H4
I404
R414
H13'
H10'
H9'
K470
D
N509
E420
K422
F457
L482
Y389
V453
F439
H7'
H7
L479
L417
Q422
M475
S6
S6'
V449
Q446
Y478
V413
R481
K441
F435
E410
H74
Q424
H6
E467
R405
E
H13
L478
I543
L481
R484
H9'
G609
Y605
Q508
H10
H9
Q485
W482
H10'
R538
H11
Q488
H11'
C539
L489
C556
V635
S563
T560
T558
N490
Q537
L566
T559
H13'
C529
D567
F
R417
H4
F413
T456
H8'
F408
E534
F457
W465
R409
F459
C460
S463
H10
I403
D464
R536
H3
L555
G467
H9
Q542
V469

to the generation of the DNA structure required for MUS81-mediated cleavage (Fugger et al., 2013). Whether the action of MUS81 at stalled RFs is required for DNA replication restart in human cells is still controversial (Naim et al., 2013; Petermann et al., 2010; Ying et al., 2013).

Furthermore, MUS81 plays a role in the repair of damage-induced stalled RFs that arise after depletion of WRN (Franchitto et al., 2008). As described in Section 1.2.3, the activity of the WRN helicase is required for efficient progression of restarted RFs after DNA damage (Sidorova et al., 2008). Treatment of WRN-depleted cells with HU causes the accumulation of DSBs that are dependent on the activity of MUS81 (Franchitto et al., 2008). Also, depletion of MUS81 in Werner syndrome (WS) cells results in decreased levels of RAD51 focus formation and reduces the recovery of WS cells after replication arrest, indicating that cleavage by MUS81 endonuclease is required for HR-mediated repair of stalled RFs in the absence of WRN (Franchitto et al., 2008). More recently, similar results were obtained in wild-type cells following oncogene activation (Murfuni et al., 2013). Several studies have shown that over-expression of some oncogenes (e.g. E2F) induces replication stress (Halazonetis et al., 2008). In the context of oncogene-induced replication stress, WRN depletion results in the formation of DSBs that are dependent on the activity of the MUS81 endonuclease (Murfuni et al., 2013). Hence, taken together, these observations indicate that MUS81 endonuclease activity is required following replication stress, when the cleavage of the structures arising at stalled RFs is essential for DNA repair.

Importantly, two recent studies have reported a role for MUS81 in the processing of late replication intermediates at common fragile sites (CFSs) (Naim et al., 2013; Ying et al., 2013). CFSs are large genomic loci that are particularly difficult to replicate and often display gaps and breaks, especially after exposure to the DNA polymerase inhibitor aphidicolin (Debatisse et al., 2012). Also, CFSs are the source of a subset of ultrafine DNA bridges (UFBs), i.e. BLM- and PICH-positive DNA bridges that arise during anaphase (Baumann et al., 2007; Chan et al., 2007; Chan et al., 2009). These CFS-derived UFBs are denoted by the presence of FANCI-FANCD2 foci at the bridge termini, with one focus located on each sister chromatid (Chan et al., 2009; Naim and Rosselli, 2009). MUS81 has been shown to co-

localise with such FANCD2 foci at CFSs and its depletion in aphidicolin-treated cells resulted in a significant increase in fragile sites-associated chromosome mis-segregation compared to wild-type cells (Naim et al., 2013; Ying et al., 2013). These results indicate that the activity of MUS81 might be required for the cleavage of unreplicated CFSs in order to allow the correct segregation of sister chromatids during anaphase.

1.4 Telomere maintenance and DNA repair

Telomeres are nucleoprotein structures that define and protect the ends of linear chromosomes (Sfeir, 2012). Human telomeres are composed of tandem double-stranded (TTAGGG/AATCCC) hexanucleotide repeats (between 5 and 15 kilobases (kb) in length) and a shorter single-stranded G-rich overhang at the 3'-end that is approximately 30 to 500 nucleotides long (Chai et al., 2005; Sfeir, 2012). The 3'-single-stranded overhangs are found on lagging-strands after the removal of the RNA primer of the last Okazaki fragment (Makarov et al., 1997; McElligott and Wellinger, 1997). Conversely, leading strands have blunt ends. However, EXO1- and Apollo-mediated post-replicative resection generates 3'-single-stranded overhangs (Lam et al., 2010; Wu et al., 2012; Wu et al., 2010). The double-stranded/single-stranded structure of telomere ends is essential to overcome two main problems that arise from the linearity of eukaryotic chromosomes: the 'end-protection' and the 'end-replication' problem.

The 'end-protection' problem stems from the risk of chromosome ends being recognised as DSBs by the cellular DNA damage response and repair pathways. The ability of telomeres to protect chromosome ends mainly relies on the binding of a protective six-subunit protein complex called shelterin (Palm and de Lange, 2008). The shelterin complex includes TRF1 and TRF2 (telomeric repeat binding factors 1 and 2), which bind to the double-stranded region of telomeres, TIN2 (i.e. TRF1- and TRF2-interacting nuclear protein 2), RAP1 (i.e. repressor/activator protein 1, also known as TRF2-interacting protein or TERF2IP), TPP1 (i.e. TIN2- and POT1-interacting protein 1, also known as adrenocortical dysplasia homolog or ACD) and POT1 (i.e. protection of telomere 1 protein), which binds the single-stranded

TTAGGG repeats of the 3'-overhang (Baumann and Cech, 2001; Bianchi et al., 1997; Bilaud et al., 1997; Broccoli et al., 1997; Lei et al., 2002; Loayza and De Lange, 2003). TIN2 is an essential component of the shelterin complex as it binds TRF2 through its N-terminus and TRF1 through its C-terminus, thereby acting as a bridge between the two proteins (Chen et al., 2008b; Ye et al., 2004a). Also, TIN2 connects TRF1 and TRF2 to the POT1-TPP1 heterodimer by binding to the C-terminus of TPP1, thus recruiting it to telomeres (Liu et al., 2004; Ye et al., 2004b). By binding specifically to telomeres throughout the cell cycle, the shelterin complex constitutes a protective cap that allows cells to distinguish between natural chromosome ends and DNA DSBs (Palm and de Lange, 2008). Indeed, removal of the shelterin complex by conditional knockout of *TRF1* and *TRF2* revealed that shelterin-free telomeres are processed by six independent DNA damage response pathways (Sfeir and de Lange, 2012). Moreover, some shelterin subunits have been implicated in the repression of DNA signalling and repair reactions. For example, TRF2 suppresses the activation of ATM-mediated DNA damage signalling, as indicated by the accumulation of DNA damage factors like γH2AX and 53BP1 on telomeres of *TRF2*$^{-/-}$ cells (Celli and de Lange, 2005; Denchi and de Lange, 2007; Dimitrova and de Lange, 2009). Also, depletion of TRF2 promotes the activation of the Ku-dependent NHEJ pathway of DSB repair and results in telomere end-to-end fusions (Celli and de Lange, 2005). On the same note, POT1 blocks the activity of ATR by preventing the binding of the DNA damage sensor protein RPA to the single-stranded telomeric overhangs (Gong and de Lange, 2010).

A second level of end protection is provided by the presence of a lariat-like structure called a T-loop (Griffith et al., 1999), whose formation requires the activity of HR factors such as RAD51, RAD52 and XRCC3 (Verdun and Karlseder, 2006). Electron microscopic analysis of psoralen cross-linked telomeric DNA from human and mouse cells provided the first physical evidence for the existence of T-loops (Griffith et al., 1999). T-loops are generated when the G-rich 3'-overhang loops back on itself and invades the duplex telomeric DNA. Importantly, the T-loop architecture is thought to hide the telomere single-stranded termini from the end-recognition components of the DNA repair machinery (e.g. the Ku complex) and

thus, it prevents illegitimate processing of the telomere as a DNA DSB. However, the molecular mechanisms that regulate T-loop formation remain to be determined.

The 'end-replication' problem refers to the inability of semi-conservative DNA replication to completely duplicate the ends of linear chromosomes. When the RF reaches the end of the chromosome, the removal of the RNA primer of the last Okazaki fragment on the lagging strand results in the incomplete replication of the terminal sequence of the telomeric DNA. Hence, part of the telomere is lost during each cell cycle (Olovnikov, 1971, 1973; Watson, 1972). This proliferation-dependent telomere shortening process ultimately generates telomeres that are too short to be protected by the binding of the shelterin complex or by formation of T-loops. As a consequence, the DNA damage response machinery recognises telomere ends as DSBs and causes a permanent growth arrest called replicative senescence (or M1, mortality stage 1) (d'Adda di Fagagna et al., 2003; Harley et al., 1990; Wright et al., 1989). As such, telomere attrition controls the proliferative lifespan of human somatic cells (Harley et al., 1990; Olovnikov, 1971, 1973; Watson, 1972). However, replicative senescence can be overcome through the inactivation of the tumour suppressors p53 and pRB (Retinoblastoma protein), which allow cells to continue proliferating before reaching crisis (or M2, mortality stage 2). At M2, most of the cells undergo apoptosis but rare clones (approximately 1×10^7) can escape this process and generate an immortal culture (Harley et al., 1990). Cancer cells have developed two mechanisms that allow them to maintain functional telomeres and proliferate indefinitely: telomerase-mediated telomere elongation and alternative lengthening of telomeres (ALT).

1.4.1 Telomerase-mediated telomere elongation

Telomerase is a ribonucleoprotein reverse transcriptase (RT) composed of a catalytic protein subunit, the telomerase RT (TERT), a telomerase RNA (TR) subunit (Cohen et al., 2007; Greider and Blackburn, 1985) and species-specific accessory proteins (Fu and Collins, 2007; Venteicher et al., 2009; Venteicher et al., 2008). The main function of telomerase *in vivo* is the *de novo* synthesis of telomeric DNA, which counteracts progressive telomere shortening that occurs during consecutive cell divisions. Telomerase activity can be reconstituted *in vitro* by co-

expressing hTERT and hTR in rabbit reticulocyte lysates, demonstrating that hTERT and hTR represent the minimal catalytic core of human telomerase (Beattie et al., 1998; Weinrich et al., 1997). Telomerase is recruited to telomeres by binding to the OB-fold domain of the shelterin component TPP1 (Abreu et al., 2010). Indeed, human cells depleted of TPP1 or TIN2 fail to recruit telomerase to chromosome ends. Similarly, the conditional deletion of TPP1 in mice prevented the recruitment of telomerase to telomeres (Nandakumar et al., 2012; Tejera et al., 2010; Zhong et al., 2012). Since telomerase is observed at telomeres predominantly during S-phase (Jady et al., 2006; Tomlinson et al., 2006), it is likely that its recruitment to chromosome ends is cell cycle-regulated. However, the mechanism of regulation is still undetermined.

Unlike prototypical RTs, which convert genomic RNA into a single molecule of complementary DNA (cDNA), telomerase catalyses multiple rounds of telomere extension using an RNA template embedded in the TR subunit. As shown in Figure 1.9, processive telomere elongation involves multiple steps, including: (i) recognition and alignment of the telomeric DNA primer with the RNA template and the TERT subunit, (ii) synthesis of the first telomeric repeat and (iii) translocation of the telomerase in order to re-position the DNA 3'-end and initiate the next round of telomere synthesis (Wyatt et al., 2010). Recent studies have determined that both telomerase processivity and telomere elongation *in vivo* are stimulated by the same OB-fold domain of TPP1 that is required for telomerase recruitment (Nandakumar et al., 2012; Zhong et al., 2012). Indeed, *in vitro* analysis of the effect of TPP1-POT1 on telomerase reaction cycle showed that binding of TPP1-POT1 increases telomerase processivity by decreasing the primer dissociation rate and by increasing the efficiency and rate of the template-primer translocation (Latrick and Cech, 2010).

Depletion of TERT or TR from mice results in telomere shortening and end-to-end fusions, genomic instability, aneuploidy, and premature ageing (Blasco et al., 1996; Liu et al., 2000). Conversely, overexpression of TERT dramatically increased the lifespan of mice that are made cancer-resistant by enhanced expression of the tumour suppressor proteins p53, p16 and p19ARF (Tomas-Loba et al., 2008). In humans, telomerase is expressed in highly proliferative tissues such as ovaries and

testis and during embryogenesis (Wright et al., 1996). In somatic tissues, however, hTERT transcription is strongly repressed and thus, cells experience proliferation-dependent telomere erosion (Cong et al., 1999; Horikawa et al., 1999; Takakura et al., 1999). Given the highly proliferative nature of cancer cells, it is not surprising that telomerase has been found to be up-regulated in 85% of human cancers and telomerase inhibitors have entered clinical trials (Kim et al., 1994; Ruden and Puri, 2013; Shay and Bacchetti, 1997). Cells that re-activate telomerase to retain an infinite proliferative potential are referred to as 'telomerase-positive', in order to distinguish them from cells that employ the telomerase-independent ALT pathway of telomere elongation.

1.4.2 Alternative Lengthening of Telomeres (ALT) pathway

The existence of a telomerase-independent mechanism of telomere elongation was inferred from the observation that human telomerase-negative cells could maintain telomere lengths after hundreds of population doublings (Bryan et al., 1995). This mechanism is referred to as ALT and is found in approximately 15% of human cancer types, although ALT activity has also been detected in normal mouse somatic tissues (Neumann et al., 2013). Examples of tumours that utilise the ALT pathway include osteosarcomas, liposarcomas, astrocytomas and glioblastoma multiforme and they all share a very poor prognosis (Henson and Reddel, 2010).

ALT cells are characterised by several distinct features, some of which are used as diagnostic assays to detect ALT in human tumours. One of the most striking feature is the abundance of extra-chromosomal telomeric DNA in the form of double-stranded telomeric circles (T-circles) (Cesare and Griffith, 2004; Wang et al., 2004), linear dsDNA, partially single-stranded circles (called C- or G-circles depending on the nature of the continuous sequence) and 't-complexes', a form of highly branched telomeric DNA (Nabetani and Ishikawa, 2009). C-circles are highly specific to ALT cells and can be detected in patient's blood samples, thereby serving as a diagnostic marker of ALT-positive tumours (Henson et al., 2009). Their origin, however, is still unclear. Conversely, T-circles might be generated through the resolution of T-loops in order to counteract excessive ALT-mediated telomere

elongation (Compton et al., 2007; Wang et al., 2004). Other hallmark features of ALT-positive cells include the heterogeneity of telomere lengths, which range from 5 to 50 Kb, and the presence of ALT-associated promyelocytic leukaemia bodies (APBs) (Bryan et al., 1995; Yeager et al., 1999).

APBs are a subset of promyelocytic leukaemia (PML) nuclear bodies that co-localise with telomeric DNA. Their formation is triggered by the sumoylation of the shelterin components TRF1, TRF2, TIN2 and RAP1 by the SUMO E3 ligase MMS21 (Potts and Yu, 2007). Indeed, cells expressing mutants of TRF1 and TRF2 that cannot be sumoylated do not form APBs. These sumoylation events are required for the binding of PML and SP100 proteins, which constitute the shell of the APBs and promote the recruitment of DNA repair and recombination factors (Lang et al., 2010). Several lines of evidence suggest that APBs are involved in the ALT pathway of telomere elongation. First, APBs are highly specific to ALT-positive cells and constitute a strong marker for the identification of ALT-tumours (Henson et al., 2005). Second, the repression of the ALT pathway in cell hybrids of ALT-positive with telomerase-positive cells resulted in the disappearance of APBs, whereas activation of the ALT-pathway promoted their formation (Perrem et al., 2001). Third, the HR-associated MRN complex is required for APB assembly (Jiang et al., 2007; Wu et al., 2000). Despite the strong correlation between the formation of APBs and ALT-mediated telomere elongation, the function of APBs in the ALT pathway is still unclear. Interestingly, analysis of artificially enlarged APBs showed that these bodies contain clusters of telomeres and are sites of inter-telomeric recombination, as indicated by the presence of filamentous telomere bridges in metaphase spreads (Draskovic et al., 2009). Also, many DNA repair and recombination proteins, including the MRN complex, FANCA, FANCD2, BLM, RAD51, RAD51D, FEN1 and MUS81, are recruited to APBs (Bhattacharyya et al., 2009; Draskovic et al., 2009; Fan et al., 2009; Jiang et al., 2007; Saharia and Stewart, 2009; Tarsounas et al., 2004; Zeng et al., 2009). Hence, APBs might be sites of telomere elongation that provide both the physical proximity between telomeres and the proteins required for HR-mediated telomere lengthening.

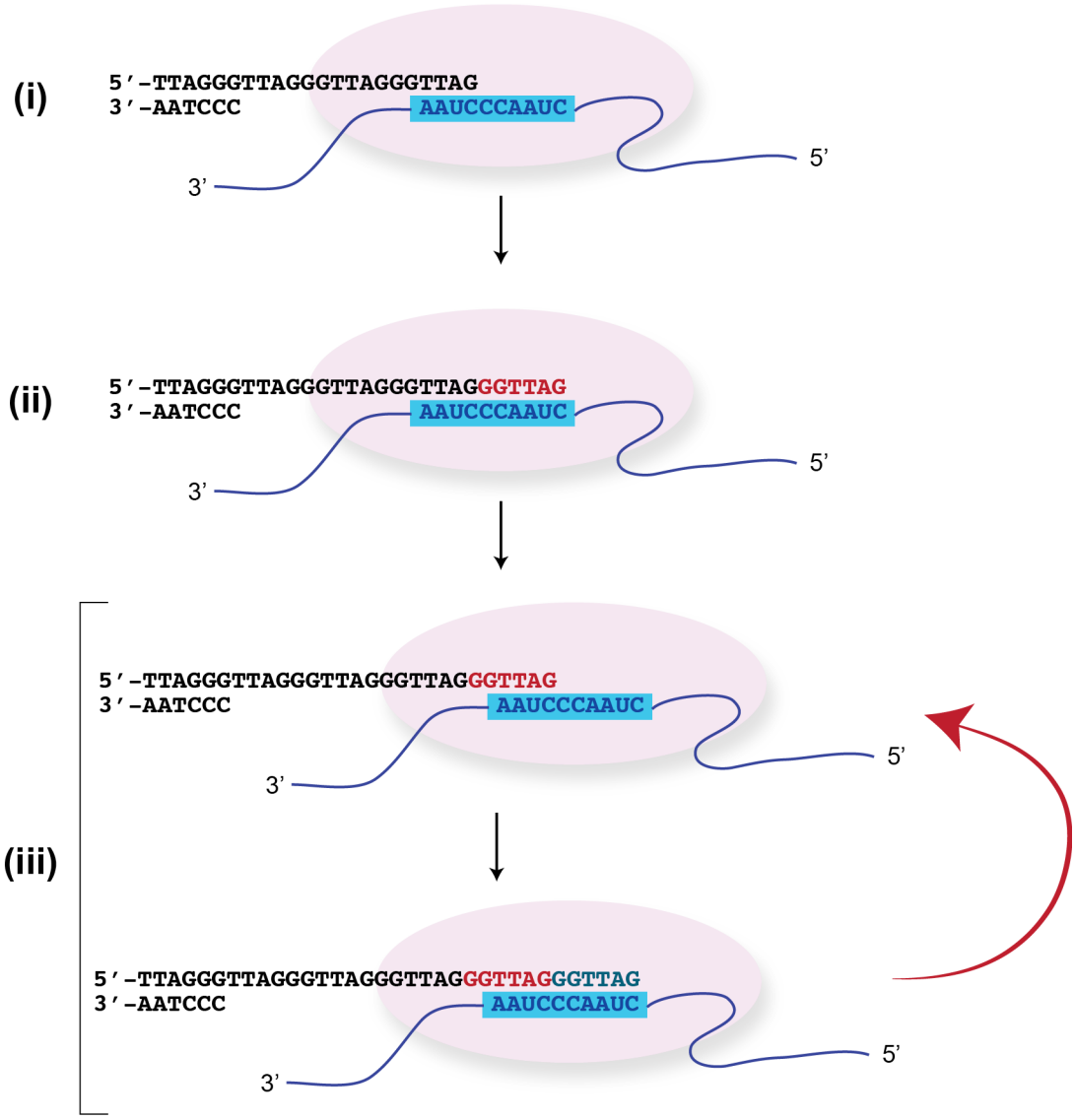

Figure 1.9 Telomerase-mediated telomere elongation

The processive extension of the telomeric DNA is a multi-step process that involves: (i) the binding and alignment of telomerase (hTERT is indicated in pink, hTR is depicted as a blue line for simplicity) to the single-stranded G-rich overhang at the telomere 3’-end; (ii) synthesis of the first telomeric repeat (i.e. GGTTAG) and (iii) translocation of telomerase and initiation of the next round of telomere synthesis. Adapted from (Autexier and Lue, 2006)

The ALT mechanism involves the HR-dependent synthesis of new telomeric DNA. The first evidence of HR at telomeres resulted from a study where a DNA tag inserted in the telomere repeats of one chromosome was duplicated to other chromosome ends in ALT-positive cells and not in telomerase-positive cells (Dunham et al., 2000). Also, ALT-positive cells display a level of telomere sister chromatid exchanges (T-SCEs) that is several orders of magnitude higher than that displayed by ALT-negative cells, without showing any increase in SCE frequency elsewhere in the genome (Londono-Vallejo et al., 2004). However, the origin of the template DNA used in the HR reaction remains uncertain and several HR-dependent elongation models have been proposed. The duplication of a DNA tag from one telomere to other chromosome ends suggests that the synthesis of new telomeric DNA occurs using an adjacent chromosome telomere as a template (inter-telomeric recombination) (Dunham et al., 2000) (Figure 1.10A). However, telomere elongation can also occur via intra-telomeric recombination, whereby T-loops and sister-chromatid telomeres can be used as templates (Muntoni et al., 2009) (Figure 1.10B-C). In the context of a T-loop, the branch migration of the junction could prime the leading strand synthesis of new DNA using the complementary strand as a template (Figure 1.10C). Also, given the high concentration of extra chromosomal telomeric DNA, it is possible that C-circles, T-circles and linear duplex DNA could be involved in the HR-dependent replication of telomeres (Figure 1.10D-E). In yeast, telomere lengthening occurs through a rolling-circle mechanism in which 3'-telomeric overhangs invade the extra chromosomal T-circles and use them as templates for telomeric extension (Tomaska et al., 2009). *In vitro*, C-circles from human ALT-positive cells are excellent substrates for rolling circle amplification of telomeres, suggesting that they might fulfil the same function *in vivo* (Henson et al., 2009) (Figure 1.10E).

Interestingly, a recent study revealed that ALT-positive cells contain single-stranded 5'-C-rich overhangs in amounts that are comparable to 3'-G-rich overhangs (Oganesian and Karlseder, 2011). Notably, the abundance of these 5'-C-rich overhangs in ALT cells correlated with aberrant recombination as depletion of RAD51, RAD52 and XRCC3 resulted in an increase of C-overhang levels at the expense of the number of G-overhangs. Although such 5'-C-rich overhangs have

been proposed to be a mark of cells undergoing aberrant HR, their origin remains undetermined (Oganesian and Karlseder, 2011).

The ability of telomeres of ALT cells to undergo HR-mediated lengthening is an indication of defective telomere protection by the shelterin complex that is essential for ALT cells survival. Such defects do not arise from mutations of TRF2, RAP1 or POT1, as they are all wild type and expressed at a normal level in ALT cells (Lovejoy et al., 2012). However, the total quantity of telomeric DNA is significantly higher in ALT cells compared to telomerase-positive cells (Lau et al., 2013). Hence, it is likely that the ratio between the shelterin components and telomeric DNA is significantly decreased in ALT cells, which might result in a functional deficiency and in a more HR-permissive telomeric state. For example, given the role of TRF2 in T-loop formation and protection against enzymatic cleavage (Fouche et al., 2006; Poulet et al., 2009), a decreased TRF2:telomeric DNA ratio would cause an increased frequency of unprotected chromosome ends. In addition, telomeres of ALT cells carry high levels of interspersed variant repeats, with the more abundant being the C-type variant (i.e. TCAGGG) (Conomos et al., 2012). C-type variant repeats are bound with high affinity by nuclear receptors such as TR4 and COUP-TF2. The interaction between nuclear receptors and telomeric DNA is usually hindered by the binding of shelterin components because, for example, TRF2 binds the canonical G-type variant repeats more strongly than TR4. Hence, in the presence of C-type variant sequences it is likely that the amount of shelterin components bound to telomeres is altered by the binding of nuclear receptors. Importantly, depletion of TR4 or COUP-TF2 diminishes several ALT characteristics, such as the generation of APBs, T-SCEs and extrachromosomal C-circles (Conomos et al., 2012). Conversely, insertion of C-type variants in the telomeres of telomerase-positive cells results in the recruitment of nuclear receptors and in the appearance of ALT hallmark features, but does not trigger HR-mediated elongation, indicating that the presence of variant repeats and nuclear receptors is not sufficient to activate the ALT mechanism in telomerase-positive cells (Conomos et al., 2012).

Figure 1.10 Schematic representation of ALT-dependent telomere elongation models
The origin of the template DNA used for ALT-mediated telomere elongation is still unclear. The various models that have been proposed involve: (**A**) intratelomeric recombination, in which an adjacent chromosomal telomere is used as template, (**B** and **C**) intratelomeric recombination, in which either the telomere of the sister chromatid (**B**) or the T-loop (**C**) can be used as templates and (**D** and **E**) recombination with extrachromosomal telomeric DNA, in which any of the forms of extrachromosomal telomeric DNA present in ALT cells can be used as template. For example, (**D**) illustrates recombination with a linear DNA template while (**E**) summarises recombination with a C-circle template. Adapted from (Cesare and Reddel, 2010)

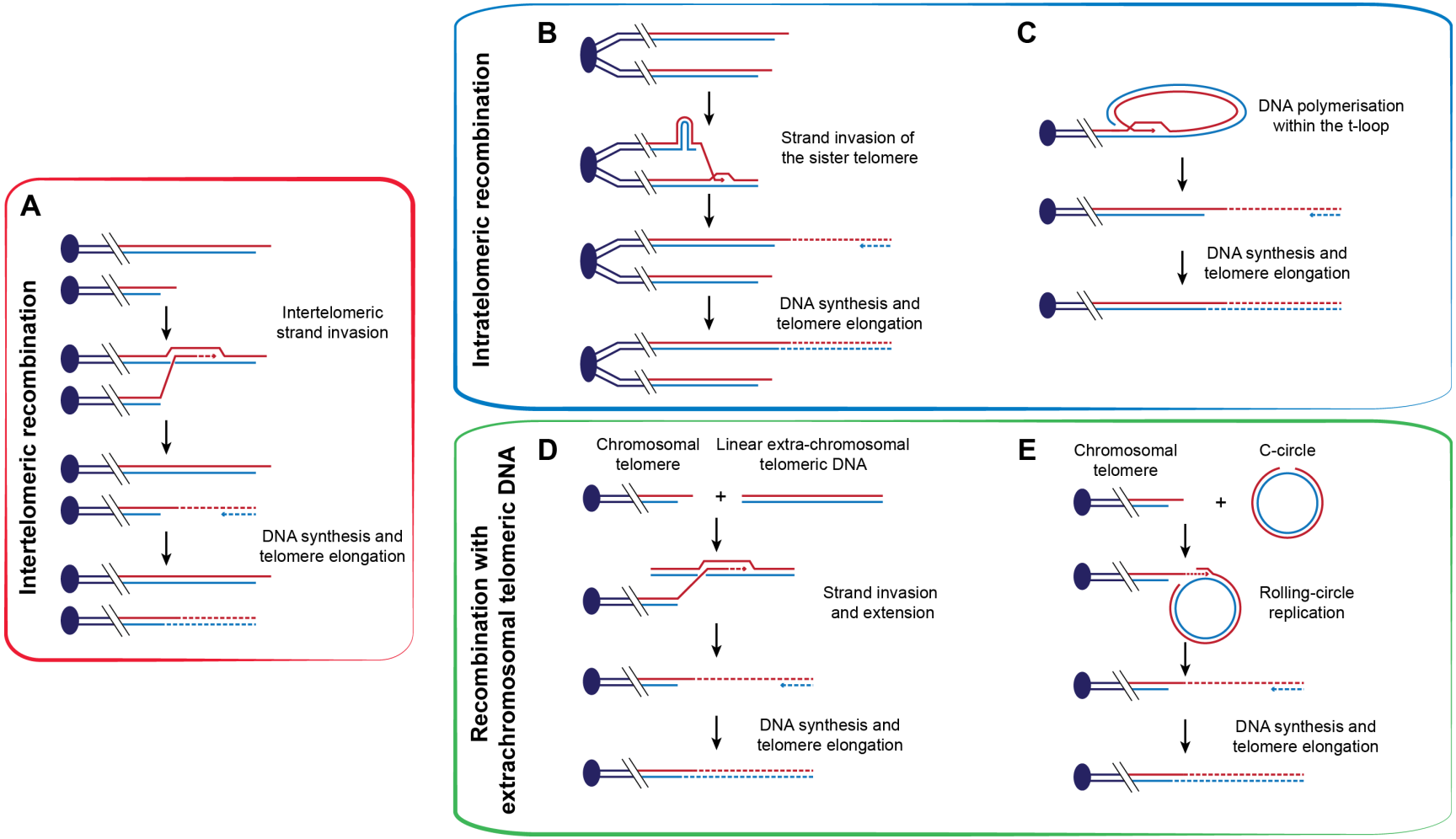
A
Intertelomeric recombination
Intertelomeric strand invasion
DNA synthesis and telomere elongation
B
Intratelomeric recombination
Strand invasion of the sister telomere
DNA synthesis and telomere elongation
C
DNA polymerisation within the t-loop
DNA synthesis and telomere elongation
D
Recombination with extrachromosomal telomeric DNA
Chromosomal telomere
Linear extra-chromosomal telomeric DNA
+
Strand invasion and extension
DNA synthesis and telomere elongation
E
Chromosomal telomere
C-circle
+
Rolling-circle replication
DNA synthesis and telomere elongation

1.4.3 Telomere maintenance proteins in ALT-cells

Telomere maintenance encompasses mechanisms for telomere elongation as well as processes that prevent telomere loss. The repetitive nature of the telomeric DNA makes telomeres a difficult substrate for the DNA replication machinery and their incomplete duplication can result in rapid telomere shortening. Because replication of telomeres is unidirectional and starts from the sub-telomeric region, the presence of unrepaired stalled or collapsed RFs can result in the complete loss of the distal telomeric sequences. Hence, it is not surprising that many proteins involved in the repair of stalled or collapsed RFs are also involved in telomere maintenance. The first proteins to be identified as essential for telomere maintenance in ALT-positive cells were the components of the MRN complex (Jiang et al., 2005; Zhong et al., 2007). Indeed, the inhibition of the MRN function by siRNA-mediated knockdown of the individual proteins or by sequestration of NBS1 by SP100 overexpression resulted in telomere shortening (Jiang et al., 2005; Zhong et al., 2007). Also, two members of the RecQ family of DNA helicases, namely WRN and BLM, are involved in telomere maintenance of ALT cells and their individual depletion results in rapid telomere shortening (Bhattacharyya et al., 2009; Crabbe et al., 2004; Du et al., 2004; Stavropoulos et al., 2002). This phenotype may be related to the ability of BLM and WRN to unwind four-stranded DNA secondary structures called G4 quadruplexes *in vitro* (Mohaghegh et al., 2001). These structures contain four guanine bases that associate through Hoogsten hydrogen bonds to form a square planar structure termed the guanine tetrad. G4 quadruplexes are formed when two tetrads stack on top of each other (Biffi et al., 2013; Sundquist and Klug, 1989; Williamson et al., 1989) and represent the most frequent impediment to RF progression at telomeres (Rizzo et al., 2009). However, studies performed on mouse cells showed that G4 quadruplexes are processed by RTEL1 (Vannier et al., 2012) and DNA2 (Lin et al., 2013) *in vivo*. Indeed, *Rtel*$^{-/-}$ and *Dna2*$^{-/-}$ cells exhibit telomere replication defects, as indicated by the presence of elevated telomere fragility and telomere loss (Lin et al., 2013; Vannier et al., 2012). However, their contribution to telomere maintenance of human ALT cells remains undetermined.

Additional proteins that have been implicated in the ALT mechanism include: (i) RPA, which prevents the accumulation of G-rich single-stranded DNA (Fan et al., 2009; Grudic et al., 2007), (ii) BRCA2, whose depletion decreases the frequency of T-SCEs (Sapir et al., 2011), (iii) flap endonuclease 1 (FEN1), a structure-specific endo/exonuclease that functions in lagging strand DNA replication by processing the 5'-end of the Okazaki fragments (Balakrishnan and Bambara, 2013), (iv) FANCA, a component of the FA core complex (Joenje et al., 1997), and FANCD2 (Section 1.2.3) (Fan et al., 2009). Importantly, FEN1 interacts directly with WRN and ALT-positive cells depleted of FEN1 exhibit telomere dysfunction (Saharia and Stewart, 2009). Similarly, the depletion of either FANCA or FANCD2 results in decreased T-SCEs level and increased frequency of telomere-free chromosome ends (Fan et al., 2009).

1.4.4 The role of MUS81 in telomere maintenance of ALT-positive cells

In mitotic human cells, the MUS81 endonuclease is required for HJ resolution and for the HR-mediated repair of stalled RFs (Sections 1.3.1 and 1.3.2). Human MUS81 also has an important role in telomere maintenance in ALT, but not telomerase-positive cells (Zeng et al., 2009). More specifically, MUS81 localises to APBs during the G2-phase of the cell cycle and its depletion is associated with a significant increase in telomere-free chromosome ends (Zeng et al., 2009). Moreover, the high frequency of T-SCEs characteristic of ALT-positive cells is significantly reduced in the absence of MUS81, which could reflect defects in the repair of RFs that stall in telomeric DNA (Zeng et al., 2009). Interestingly, MUS81 interacts with telomeric DNA in ALT cells but not in telomerase-positive cells. Also, telomere loss was not observed following its depletion in telomerase-positive cells, indicating that the function of MUS81 is restricted to telomere maintenance in ALT-cells. In agreement with these observations, MUS81 knockdown resulted in reduced viability in ALT-positive but not in ALT-negative cells. The overexpression of the human TERT subunit of the telomerase partially rescued the viability of the MUS81-depleted ALT cells but did not restore the high T-SCEs frequency, suggesting that the rescue of the cellular viability is independent from the telomeric recombination pathway (Zeng et al., 2009).

It has been proposed that the telomeric functions of MUS81 could be related to its ability to cleave recombination intermediates. Hence, synthetic D-loop substrates were exposed to MUS81 immunoprecipitates from ALT-positive cells (Zeng et al., 2009). Interestingly, the activity of the immunoprecipitated MUS81 was increased by depletion of TRF2. TRF2 has a well-known function in the suppression of telomere recombination in ALT-positive cells, as indicated by the increased frequency of T-SCEs in TRF2-depleted cells, and it interacts with MUS81 to regulate its binding to telomeric secondary structures (Zeng et al., 2009). However, because both MUS81 and TRF2 interact with SLX4 *in vivo* and *in vitro*, it is likely that their interaction is mediated through SLX4 (Svendsen et al., 2009).

1.5 Aim of the study

As detailed in the previous sections, the activity of the MUS81 endonuclease is required for HR-mediated repair of DSBs (Section 1.3.1), repair and restart of stalled RFs (Section 1.3.2) and telomere maintenance (Section 1.4.4). In mammalian cells, MUS81 can form two heterodimeric complexes, one with EME1 and another with EME2 (Section 1.3). The studies conducted so far on the function of the MUS81 endonuclease in human cells have often disregarded whether the activity and/or phenotype being observed was related to the function of the MUS81-EME1 or MUS81-EME2 complex. With particular attention to what is known about the cellular roles of the MUS81-associated endonuclease, this study was aimed to determine what are the differences (if any) in the biochemical activities and the biological functions of the MUS81-EME1 and MUS81-EME2 complexes.

CHAPTER 2

Materials and methods

2.1 Enzymes and reagents

2.1.1 Enzymes

All the restriction enzymes used in this study and T4 polynucleotide kinase were purchased from New England Biolabs Inc. (NEB). Exonuclease III was purchased from Promega. Proteinase K, recombinant PCR grade, was purchased from Roche. RNase A was purchased from Qiagen.

2.1.2 General reagents

All chemical reagents were purchased from Sigma unless stated otherwise.
Amersham: Hyperfilm™ ECL High Performance Chemiluminescence film
Bio-Rad: 30% Acrylamide/Bis Solution, 37.5:1; 40% Acrylamide/Bis Solution 19:1; bromophenol blue and xylene cyanol; All Blue Precision Plus Protein™ Standards.
bioSYNTHESIS: TelG-TMR probe and TelC-FITC probe
Chromotek: GFP-TRAP®_A beads
Clontech: In-Fusion® cloning kit
EMD Millipore: KOD Hot Start DNA polymerase
Electron Microscopy Sciences: Paraformaldehyde 16%
Expedeon: InstantBlue™
Fermentas: GeneRuler 1kb DNA ladder
Fisher BioReagents: DPX mounting medium; urea.
FLUKE: GIEMSA stain, modified solution
GE Healthcare: HiTrap™ Heparin HP 1ml columns; ECL western blotting detection reagents
Gene Bridges: Quick & Easy BAC Modification Kit

GIBCO: Tetracycline-free Fetal Bovine Serum (FBS)

IBA: Strep-Tactin® Superflow®

Kodak: BioMax MR films

Life technologies™: SYPRO® Ruby Protein gel stain; NuPAGE® 10% Bis-Tris gels and NuPAGE® 7% Tris-Acetate gels; NuPAGE® MOPS and Tris-Acetate SDS running buffer (20x); UltraPure™ agarose; NuPAGE® LDS sample buffer; ProLong® Gold Antifade Reagent with DAPI; Lipofectamine RNAiMAX; zeocin; geneticin; SOC medium; Gateway® LR and BP reactions

Macherey-Nagel: Polygram® CEL 300 PEI/UV_{245}

Millipore: Immobilon®-P transfer membrane

NBS Biologicals: SafeView

Promega: Fugene HD transfection reagent

Roche: Colcemid; complete EDTA-free protease inhibitor cocktail tablets; blocking reagent (11096176001);

Stratagene: QuickChange Lightning Multi Site-Directed Mutagenesis Kit

Qiagen: Effectene® transfection reagent

Sigma: Anti-FLAG M2 Affinity Gel resin; Hoechst 33342; 5-bromo-2'-deoxyuridine (BrdU); phosphatase inhibitor cocktail 2 and 3; propidium iodide (PI); formamide, >99.5%; Fetal Bovine Serum (FBS); pepsin from porcine gastric mucosa; Stains-all; polyethylene glycol (PEG)-3350; dimethyl sulfoxyde (DMSO); thymidine.

2.1.3 Antibodies

Primary antibodies

FITC mouse anti-BrdU (BD Pharmingen™); mouse anti-Phospho Histone H3 (Ser10) (9701, Cell Signalling); rabbit anti-FLAG (Sigma, 1:500); mouse anti-XPF (Ab-1 clone 219, Thermo Scientific, 1:1000); mouse anti-TRF1 (ab10579, Abcam, 1:200); mouse anti-TRF2 (ab13579, Abcam, 1:200); mouse anti-CENPF (ab90, Abcam, 1:1000); mouse anti-MUS81 (ab14387, Abcam, 1:500); mouse anti-EME1 (clone MTA31 7H2, Santa Cruz, 1:500); mouse anti-β-Actin (ab8226, Abcam, 1:10000). Sheep anti-SLX1 (1:500) and sheep anti-SLX4 (1:2000) were a kind gift from Prof. John Rouse.

Secondary antibodies

Polyclonal swine anti-rabbit immunoglobulins/HRP and polyclonal goat anti-mouse immunoglobulins/HRP (Dako); polyclonal rabbit to sheep IgG (HRP) (ab6747, Abcam); Alexa Fluor® 488 goat anti-mouse IgG (H+L), Alexa Fluor® 488 F(ab')$_2$ fragment of goat anti-rabbit IgG (H+L), Alexa Fluor® 555 donkey anti-mouse IgG (H+L) and Alexa Fluor® 546 goat anti-rabbit IgG (H+L) (Molecular probes).

2.2 Buffers and solutions

2.2.1 Media and protein buffers

Western blot blocking buffer: 4% (w/v) skimmed milk powder in PBS + 0.1% (v/v) Tween-20
PBS: 140 mM NaCl, 3.4 mM KCl, 10 mM Na_2HPO_4, 18 mM KH_2PO_4
Luria broth (LB): 1% (w/v) bactotryptone, 0.5% (w/v) yeast extract, 0.05% (w/v) NaCl
Tris-buffered saline (TBS): 30 mM Tris-HCl (pH 7.4), 150 mM NaCl
Lysis buffer: TBS supplemented with 1x phosphatase inhibitor cocktail 2, 1x phosphatase inhibitor cocktail 3, 1x protease inhibitor cocktail, 0.5% (v/v) NP-40
Immunoprecipitation (IP) wash buffer: TBS supplemented with 0.5% (v/v) NP-40
FLAG elution buffer: TBS supplemented with 200 µg/ml 3xFLAG peptide (Peptide synthesis facility, Cancer Research UK)
Western blot transfer buffer: 25 mM Tris base, 190 mM glycine, 20% (v/v) methanol
Protein loading buffer (2x): NuPAGE® LDS loading buffer supplemented with 10% (v/v) β-mercaptoethanol
TGN buffer: 20 mM Tris-HCl (pH 7.5), 10% (v/v) glycerol, 0.01% (v/v) NP-40
Storage buffer: 50 mM Tris-HCl (pH 8.0), 10% (v/v) glycerol, 100 mM NaCl, 1 mM DTT
Protein dilution buffer: 50 mM Tris-HCl (pH 8.0), 10% (v/v) glycerol, 100 mM NaCl, 1 mM DTT, 0.1 mg/ml purified BSA
TSB: 10% (w/v) PEG-3350, 5% (v/v) DMSO, 10 mM $MgCl_2$, 10 mM $MgSO_4$, LB (pH 6.1)
KCM (5x): 0.5 M KCl, 0.15 M $CaCl_2$, 0.25 M $MgCl_2$

2.2.2 DNA buffers

Formamide loading buffer: 90% (v/v) deionised formamide, 0.05% (w/v) xylene cyanol, 0.05% (w/v) bromophenol blue, 1% (v/v) TBE
TBE: 89 mM Tris base, 89 mM boric acid, 2 mM EDTA
TE: 10 mM Tris-HCl (pH 8.0), 1 mM EDTA
DNA loading buffer (6x): 0.35% (w/v) bromophenol blue, 0.35% (w/v) xylene cyanol, 30% (v/v) glycerol
Stains-all solution: 20% (v/v) isopropanol, 10% (v/v) formamide, 0.01% (w/v) Stains-all
Annealing buffer: 150 mM NaCl, 15 mM sodium citrate
TN buffer: 10 mM Tris-HCl (pH 8.0), 50 mM NaCl
TNE buffer: 50 mM Tris-HCl (pH 8.0), 50 mM NaCl, 0.1 mM EDTA

2.2.3 Reaction buffers

Cleavage buffer: 50 mM Tris-HCl (pH 8.0), 0.1 mg/ml purified BSA, 3 mM $MgCl_2$, 1 mM DTT
Stop buffer (5x): 100 mM Tris-HCl (pH 7.5), 10 mg/ml proteinase K, 50 mM EDTA, 2.5% (v/v) SDS

2.2.4 Immunofluorescence (IF), sister chromatid exchanges (SCEs) and telomeric fluorescence *in situ* hybridisation (FISH) buffers

Pre-extraction buffer: PBS supplemented with 0.1% (v/v) Triton X-100
Permeabilisation buffer: 0.1% (w/v) sodium citrate, 0.1% (v/v) Triton X-100
IF washing solution: PBS supplemented with 0.25% (w/v) BSA and 0.1% (v/v) Tween-20
IF blocking solution: PBS supplemented with 2.65% (w/v) BSA, 0.1% (v/v) Tween-20 and 10% (v/v) FBS
FISH blocking solution (10%): blocking reagent dissolved in 100 mM maleic acid and 150 mM NaCl (pH 7.5).
Hybridising solution: 10 mM Tris-HCl (pH 7.2), 70% (v/v) deionised formamide, 0.5% (w/v) FISH blocking solution

Hybridisation wash #1: 10 mM Tris-HCl (pH 7.2), 70% (v/v) formamide
Hybridisation wash #2: 100 mM Tris-HCl (pH 7.2), 150 mM NaCl, 0.08% (v/v) Tween-20
Soerensen buffer (pH 6.8): 38% (v/v) 133 mM Na_2HPO_4, 62% (v/v) 133 mM KH_2PO_4.
20x SSC: 3 M sodium citrate (pH 7.0), 0.3 M NaCl

2.2.5 Pulse-field gel electrophoresis (PFGE) buffers

Washing buffer: 10 mM Tris-HCl (pH 8.0), 100 mM EDTA
Lysis buffer: 10 mM Tris-HCl (pH 8.0), 100 mM EDTA, 1% (w/v) sodium lauryl sarcosine, 0.2% (w/v) sodium deoxycholate, 1 mg/ml proteinase K
RNase buffer: 10 mM Tris-HCl (pH 8.0), 10 mM EDTA, 1 mg/ml RNase A (Section 2.1.2)

2.3 Bacterial strains

2.3.1 Bacterial strains

E. coli DH5α competent cells were used for all plasmid transformations.
E. coli One Shot® TOP10 chemically competent cells (Life Technologies™) were used for the transformation of DNA ligation reactions.
E. coli MAX Efficiency DH10BAC chemically competent cells (Life Technologies™) were used to generate recombinant baculovirus DNA.

2.3.2 Transformation of chemically competent cells

E. coli cells were grown to an OD~0.5, centrifuged, resuspended in 500 µl of ice-cold TSB (Section 2.2.1) and incubated on ice for 10 min or aliquoted at -80°C.
For transformation with 1 µg of plasmid DNA, 50 µl of competent cells were incubated with DNA, 1x KCM (Section 2.2.1) and water (up to 50 µl) on ice for 20 min and then at RT for 20 min. Cells were incubated with 500 µl of SOC media

(Section 2.1.2) for 40-60 min in a shaking 37°C incubator and plated on LB agar plates.

2.4 DNA primers

1. $^{5'}$GGGGACAAGTTTGTACAAAAAAGCAGGCTTCATGGCTCTAAAGAAGTCATA$^{3'}$
2. $^{5'}$GGGGACCACTTTGTACAAGAAAGCTGGGTCGTCAGCACTATCTAAAGA$^{3'}$
3. $^{5'}$GGGGACAAGTTTGTACAAAAAAGCAGGCTTCATGGCGCGGGTTGGACCCGGG$^{3'}$
4. $^{5'}$GGGGACCACTTTGTACAAGAAAGCTGGGTCGGAGCCCAGGTCCAGCAG$^{3'}$
5. $^{5'}$GGGGACAAGTTTGTACAAAAAAGCAGGCTTCATGGCGGCCCCGGTCCGCCTG$^{3'}$
6. $^{5'}$GGGGACCACTTTGTACAAGAAAGCTGGGTCGGTCAAGGGGCCGTAGCT$^{3'}$
7. $^{5'}$CTCTGAGCAGGACCTTATCCCAGCTCTACTGCAGCTACGGCCCCTTGACCGATTATGATATTCCAACTACTG$^{3'}$
8. $^{5'}$CCTGGGTTGGGGGACAGACGGGGGCTGGGGGCTGTTTCACGGCATAAGCTTCAGAAGAACTCGTCAAGAAG$^{3'}$
9. $^{5'}$CAGAGGTGAGGGCAAGAGAC$^{3'}$
10. $^{5'}$ATGAGCCCTCTGCACTCCTA$^{3'}$
11. $^{5'}$CACCCGGGATCTCGAGATGGCGGCCCCGGTCCG$^{3'}$
12. $^{5'}$AGCACCATGGCTCGAGTCAGGTCAAGGGGCCGTAG$^{3'}$
13. $^{5'}$GAAGCGCGGAATTCATGGCTCTAAAGAAGTCATCAC$^{3'}$
14. $^{5'}$GTAGGCCTTTGAATTCTCAGTCAGCACTATC$^{3'}$
15. $^{5'}$GAAGCGCGGAATTCATGGATTATAAAGATGATGATG$^{3'}$
16. $^{5'}$GTAGGCCTTTGAATTCTCAGGAGCCCAGGTC$^{3'}$
17. $^{5'}$AAGCTGCACGTTGGAGCTTTTGTGTGGGTGGCC$^{3'}$
18. $^{5'}$GGCCACCCACACAAAAGCTCCAACGTGCAGCTT$^{3'}$
19. $^{5'}$ATGGCGCGGGTTGGACCCGGGAGGG$^{3'}$
20. $^{5'}$TCAGGAGCCCAGGTCCAGCAGGAGA$^{3'}$

All oligonucleotides used in this study were synthesised by SIGMA.

2.5 Plasmids

Table 2.1 List of plasmids

PLASMID	DESCRIPTION
pDONR221-EME1	Gateway® entry vector generated by Gateway® recombination between pDONR221 (Life technologies™) and a PCR fragment (amplified with primers 1 and 2, Section 2.4) coding for EME1 cDNA
pDONR221-EME2A	Gateway® entry vector generated by Gateway® recombination between pDONR221 (Life Technologies™) and a PCR fragment (amplified with primers 3 and 4, Section 2.4) coding for EME2A cDNA
pDONR221-EME2B	Gateway® entry vector generated by Gateway® recombination between pDONR221 (Life Technologies™) and a PCR fragment (amplified with primers 3 and 4, Section 2.4) coding for EME2B cDNA
pDONR221-MUS81	Gateway® entry vector generated by Gateway® recombination between pDONR221 (Life Technologies™) and a PCR fragment (amplified with primers 5 and 6, Section 2.4) coding for MUS81 cDNA
pDEST-N-SF-TAP	Gateway® vector for mammalian expression of proteins with N-terminal STREP/FLAG (SF) tag
pDEST-N-SF-TAP-EME1	Gateway® vector for mammalian expression obtained by Gateway® recombination between pDEST-N-SF-TAP and pDONR221-EME1
pDEST-N-SF-TAP-EME2A	Gateway® vector for mammalian expression obtained by Gateway® recombination between pDEST-N-SF-TAP and pDONR221-EME2A
pDEST-N-SF-TAP-EME2B	Gateway® vector for mammalian expression

	obtained by Gateway® recombination between pDEST-N-SF-TAP and pDONR221-EME2B
pDEST-N-SF-TAP-MUS81	Gateway® vector for mammalian expression obtained by Gateway® recombination between pDEST-N-SF-TAP and pDONR221-MUS81
pcDNA4-TO-$_{SF}$EME1	Vector for tetracycline-inducible expression of proteins in mammalian cells generated by cloning $_{SF}$EME1 from pDEST-N-SF-TAP-EME1 (*HindIII* and *XbaI* digested) into *HindIII* and *XbaI* sites of pcDNA4-TO (Life Technologies^{TM})
pcDNA4-TO-$_{SF}$EME2A	Vector for tetracycline-inducible expression of proteins in mammalian cells generated by cloning $_{SF}$EME2A from pDEST-N-SF-TAP-EME2A (*HindIII* and *XbaI* digested) into *HindIII* and *XbaI* sites of pcDNA4-TO (Life Technologies^{TM})
pcDNA4-TO-$_{SF}$EME2B	Vector for tetracycline-inducible expression of proteins in mammalian cells generated by cloning $_{SF}$EME2B from pDEST-N-SF-TAP-EME2B (*HindIII* and *XbaI* digested) into *HindIII* and *XbaI* sites of pcDNA4-TO (Life Technologies^{TM})
pcDNA4-TO-$_{SF}$MUS81	Vector for tetracycline-inducible expression of proteins in mammalian cells generated by cloning $_{SF}$MUS81 from pDEST-N-SF-TAP-MUS81 (*HindIII* and *XbaI* digested) into *HindIII* and *XbaI* sites of pcDNA4-TO (Life Technologies^{TM})
pFL-MUS81	Bicistronic vector for baculovirus expression generated by cloning PCR amplified MUS81 into the pFL vector with In-Fusion® primers 11 and 12 (Section 2.4)
pFL-MUS81 -$_{SF}$EME1	Bicistronic vector for baculovirus co-expression of MUS81 and EME1 generated by cloning PCR amplified $_{SF}$EME1 in pFL-MUS81 with In-Fusion® primers 13 and 14 (Section 2.4)

pFL-MUS81 -$_{SF}$EME2A	Bicistronic vector for baculovirus co-expression of MUS81 and EME2A generated by cloning PCR amplified $_{SF}$EME2A in pFL-MUS81 with In-Fusion® primers 15 and 16 (Section 2.4)
pFL-MUS81 -$_{SF}$EME2B	Bicistronic vector for baculovirus co-expression of MUS81 and EME2B generated by cloning PCR amplified $_{SF}$EME2B in pFL-MUS81 with In-Fusion® primers 15 and 16 (Section 2.4)
pFL-MUS81^{D307A} -$_{SF}$EME2A	Bicistronic vector for baculovirus co-expression of MUS81^{D307A} and EME2A generated by alanine substitution of MUS81 D307 using pFL-MUS81-$_{SF}$EME2A as a template, the QuickChange Lightning Multi Site-Directed Mutagenesis Kit (Section 2.1.2) and primers 17 and 18 (Section 2.4)

The plasmid pDEST-N-SF-TAP was a kind gift from Dr Christian Gloeckner and Prof Marius Ueffing from the Department of Protein Science, Helmholtz Zentrum München-German Research Center for Environmental Health, Nuremberg, Germany.

2.6 Cell lines and cell culture methods

Table 2.2 List of cell lines used in this study

CELL LINE	DESCRIPTION
HeLa	*Homo sapiens* cervix adenocarcinoma cell line
HeLa Kyoto	*Homo sapiens* cervix adenocarcinoma cell line, Kyoto clone
U2OS	*Homo sapiens* osteosarcoma cell line
U2OS-TREx^{TM}	*Homo sapiens* osteosarcoma cell line designed for tetracycline-regulated mammalian expression of proteins of interest

HEK 293-TREx™	*Homo sapiens* embryonic kidney cells designed for tetracycline-regulated mammalian expression of proteins of interest
HT1080	*Homo sapiens* fibrosarcoma cell line
GM847	*Homo sapiens* SV40-transformed skin fibroblasts
RPE-1 hTERT	*Homo sapiens* human TERT-immortalised retinal pigment epithelial cell line
GM08505	*Homo sapiens* SV40-transformed Bloom's syndrome skin fibroblasts
MCF-7	*Homo sapiens* breast adenocarcinoma cell line

All cells were cultured in Dulbecco's Modified Eagle Media (DMEM) supplemented with 10% (v/v) FBS (Section 2.1.2). The cultures were incubated in a 10% CO_2 humidified incubator at a temperature of 37°C.

2.6.1 siRNA transfection

The short-interfering RNAs (siRNAs) used in this study were purchased from Eurofins. EME2 siRNAs were designed using Sfold (http://sfold.wadsworth.org/cgi-bin/index.pl). The siRNAs sequences (written 5' to 3') are as follows:
Luciferase GL2: CGTACGCGGAATACTTCGA
EME1: GCUAAGCAGUGAAAGUGAA (Dharmacon) (Naim et al., 2013)
EME2 #1: GCGAGCCAGUGGCAAGAGA
EME2 #2: UGGAGCCCGAGGAGUUUCU
MUS81: CAGCCCUGGUGGAUCGAUA (Wechsler et al., 2011)

One day before transfection, 3 x 10^5 or 7 x 10^5 cells were seeded in 6 cm or 10 cm cell culture plates respectively. EME1 (40 nM), EME2 #1 (80 nM), EME2 #2 (80 nM) and MUS81 (60 nM) siRNAs were transfected using Lipofectamine® RNAiMAX (Section 2.1.2) according to the manufacturer's instructions. Cells were transfected with MUS81 siRNA 2x within 24 hr. All the other transfections were

performed once. Control Luciferase GL2 siRNA was used at equivalent concentrations. Cells were collected 72 hr after the first transfection, unless stated otherwise.

2.6.2 Establishment of stable tetracycline-inducible cell lines

One day before transfection, U2OS-TREx™ and HEK 293-TREx™ cells were plated at 50% confluency in DMEM supplemented with 10% (v/v) tetracycline-free FBS (Section 2.1.2). Cells were transfected with 500 ng of pcDNA4-TO-$_{SF}$EME1, pcDNA4-TO-$_{SF}$EME2A, pcDNA4-TO-$_{SF}$EME2B or pcDNA4-TO-$_{SF}$MUS81 (Section 2.5) using Effectene® (Section 2.1.2) and following the manufacturer's instructions. Stable clones were isolated after selection with 500 µg/ml zeocin (Section 2.1.2) and were tested for protein expression by western blotting (Section 2.8.7).

2.6.3 Bacterial Artificial Chromosome (BAC)-mediated expression of MUS81 in HeLa Kyoto cells

The BAC clone CTD-2084A20 encoding MUS81 was purchased from Life Technologies™.

BAC modification by pRed/ET recombination

BAC modification was performed as described in (Poser et al., 2008) with some variations. The BAC clone encoding for MUS81 was modified by insertion of an affinity purification cassette (FLAP) encoding green fluorescent protein (GFP) at the C-terminus of the gene (Figure 2.1). BAC modification was performed by recombineering using the Quick&Easy BAC modification kit (Section 2.1.2). Briefly, the bacteria containing the BAC clone were transformed with the pRed/ET plasmid (Quick&Easy BAC modification kit) using the protocol described in Section 2.3.2. The FLAP cassette was PCR amplified with primers 7 and 8 (Section 2.4) and transformed into pRed/ET-transformed cells in the presence of 10% (w/v) L-Arabinose. The successful integration of the FLAP cassette was checked by PCR using primers 9 and 10 (Section 2.4).

BAC transfection and generation of stable cell lines

One day before transfection, 2 x 10^5 HeLa Kyoto cells were seeded in a 6 cm cell culture plate. Cells were transfected with isolated BAC-MUS81$_{FLAP}$ using Effectene® (Section 2.1.2), according to the manufacturer's instructions. Stable clones were isolated after selection with 500 µg/ml Geneticin (Section 2.1.2) and were tested for protein expression by western blotting (Section 2.8.9).

2.6.4 Cell synchronisation with double-thymidine block

In order to synchronise cells at the G1/S-phase of the cell cycle, 2 x 10^6 BAC-MUS81$_{FLAP}$ HeLa Kyoto cells (Section 2.6.3.2) were seeded in 15 cm plates and treated with 2.5 mM thymidine for 16 hr. Cells were washed with PBS and released in fresh media for 8 hr and incubated again with the same concentration of thymidine. After 16 hr, cells were washed in PBS, treated with trypsin and harvested.

2.7 Gel electrophoresis

2.7.1 SDS-polyacrylamide gel electrophoresis (PAGE)

SDS-PAGE was performed as described (Laemmli, 1970). Briefly, protein samples were prepared by adding an equal volume of protein loading buffer (2x) (Section 2.2.1) and boiling for 5 min prior to electrophoresis. Gel electrophoresis was performed with NuPAGE® 10% Bis-Tris gels or NuPAGE® 7% Tris-Acetate gels in an XCell SureLock™ Mini-Cell Electrophoresis System (Life Technologies™) using NuPAGE® MOPS or Tris-Acetate SDS running buffer (20x). Gels were run at RT for 90 min at 180 V or 150 V. Proteins were visualised by western blotting (Section 2.8.7) or by staining with InstantBlue (Section 2.8.4) or SYPRO® Ruby (Section 2.8.5).

2.7.2 Agarose gel electrophoresis

Gels were prepared in Sub-Cell® GT Agarose Gel Electrophoresis System (Bio-Rad) and contained 1% (w/v) Agarose in TBE buffer supplemented with a 1:10 dilution of SafeView (Section 2.1.2). Samples were loaded in 1x DNA loading buffer (Section 2.2.2) and run at 100 V for 1 hr at RT. Gels were imaged and photographed using the Molecular Imager® GelDoc^{TM} XR+ (Bio-Rad).

2.7.3 Neutral PAGE

Gels were prepared using a Cambridge gel apparatus and contained 10% acrylamide (30% Acrylamide/Bis Solution, 37.5:1) in TBE, supplemented with 0.12% (v/v) of ammonium persulfate and 0.06% (v/v) of TEMED. Samples were prepared by addition of 1/6 vol DNA loading buffer (Section 2.2.2). Gels were run at RT in TBE for 75 min at 150 V and then dried onto 3MM filter paper (Whatman). Following electrophoresis, ^{32}P-labelled DNA was detected by autoradiography (Section 2.7.5) or phosphorimaging (Section 2.7.6).

2.7.4 Denaturing PAGE

Gels were prepared in a Sequi-Gen® sequencing gel apparatus (Bio-Rad) and contained 7 M urea, 12% acrylamide (40% Acrylamide/Bis Solution 19:1), 0.035% (v/v) APS and 0.075% (v/v) TEMED in TBE. Samples were supplemented with an equal volume of formamide loading buffer (Section 2.2.2) and boiled for 3 min prior to loading. Before electrophoresis of DNA samples, the sequencing gels were preheated to 50°C and run in TBE buffer. After sample loading, gels were run for 90 min at 60 W and then dried onto anion exchanger filter paper (Whatman). ^{32}P-labelled DNA was detected by autoradiography (Section 2.7.5) or phosphorimaging (Section 2.7.6).

2.7.5 InstantBlue staining

After SDS-PAGE (Section 2.7.1), gels were incubated with InstantBlue® for up to 12 hr and destained in water.

2.7.6 SYPRO® Ruby staining

After SDS-PAGE (Section 2.7.1), protein gels were incubated in a solution containing 50% (v/v) methanol and 7% (v/v) acetic acid for 15 min at RT. SYPRO® Ruby Protein gel stain was added to cover the gels, microwaved for 30 s, agitated for 30 s at RT and then microwaved for an additional 30 s. The gel was covered with aluminium foil and incubated in the SYPRO® Ruby Protein gel stain for 30 min at RT before washing with a solution containing 10% (v/v) methanol and 7% (v/v) acetic acid (3x for 15 min each). Proteins were visualised using the Molecular Imager® GelDoc^{TM} XR+ (Bio-Rad).

2.7.7 Autoradiography

Dried polyacrylamide gels were exposed to Biomax® MR films. When necessary, dried gels were exposed to intensifying screens and placed at -80°C. Exposed films were developed using a JPI automatic X-ray film processor (model JP-33).

2.7.8 Phosphorimager analysis

Dried gels were exposed to GE Healthcare storage phosphor screens for up to 5 hr. Screens were analysed on a Molecular Dynamics Phosphorimager (model 425E) and quantified using ImageQuant software.

2.7.9 Pulse-field gel electrophoresis

PFGE was performed essentially as described (Hanada et al., 2007). HeLa cells were transfected with siRNAs targeting Luciferase control, EME1, EME2 or MUS81 as described in Section 2.6.1. Various concentrations of hydroxyurea (HU) (0, 1, 2,

4, 8 mM) were added to the cells 48 hr post-transfection. After 24 hr, cells were collected, washed in PBS and 1 x 10^6 cells/each condition were used to make low melting point agarose plugs using CHEF Mapper® XA system plug molds (Bio-Rad). Briefly, 1 x 10^6 cells were centrifuged, resuspended in 50 µl of PFGE washing buffer (Section 2.2.5) and mixed with 50 µl 1% (w/v) low melting point agarose in water. Agarose plugs were allowed to polymerise for 30-40 min at 4°C and then lysed at 37°C in lysis buffer (Section 2.2.5). After 48 hr, plugs were washed 2x in washing buffer and incubated overnight in RNase buffer (Section 2.2.5). The next day, the plugs were washed once in washing buffer and loaded on a 1% (w/v) agarose gel in 0.5% (v/v) TBE. After the plugs were positioned, the gel was sealed with 0.5% (w/v) low melting point agarose in 0.5% (v/v) TBE and run for 23 hr at 13°C in a Gene Navigator PFGE apparatus (Amersham Biosciences) using the following parameters: voltage 180–120 V log; angle from 1201 to 1101 linear; interval 30 s to 5 s log. Gels were stained with 1.25 µg/ml ethidium bromide in 0.5% (v/v) TBE for 1 hr and visualized using the Molecular Imager® GelDoc™ XR+ (Bio-Rad). Data analysis was performed using ImageLab software.

2.8 General methods of DNA and protein manipulation

2.8.1 Amplification of EME2 isoforms

RNA was extracted from MCF-7 cells (Table 2.2) using the RNeasy kit (Qiagen), according to the manufacturer's instructions. cDNA synthesis was performed using Illustra™ Ready-To-Go™ RT-PCR beads (GE Healthcare), following the manufacturer's instructions. EME2 isoforms were amplified from MCF-7 cDNA using KOD Hot Start DNA polymerase (Section 2.1.2) and primers 19 and 20 (Section 2.4). PCR products were analysed by agarose gel electrophoresis (Section 2.7.2).

2.8.2 DNA concentration determination

DNA concentrations were determined by measuring the sample absorbance at 260 nm using a NanoDrop® ND-1000 Spectrophotometer.

2.8.3 Ethanol precipitation

DNA samples were mixed with 0.1 vol of 3 M sodium acetate (pH 5.2) and two volumes of 100% ice-cold ethanol. After 20 min incubation in dry ice, samples were centrifuged at 14000 rpm for 30 min. The precipitated DNA was washed in 70% (v/v) ethanol, air-dried and resuspended in TE buffer (Section 2.2.2).

2.8.4 Whole cell extracts (WCEs)

Cells were washed in PBS, treated with trypsin, harvested and centrifuged at 1200 rpm for 4 min. Cell pellets were washed with 5 ml of PBS, resuspended in lysis buffer (Section 2.2.1) and incubated on ice for 15 min. Lysates were sonicated in a Bioruptor® Plus (Diagenode) 3x (30 s pulses) with 30 s rest on ice between the pulses and centrifuged at 4°C for 30 min at 14000 rpm. Soluble extracts were transferred to a fresh tube and quantified as described in Section 2.8.5.

2.8.5 Protein concentration determination

Protein concentrations were quantified using Bio-Rad D_c protein assay kit. The absorbance at 750 nm was determined using µQuant (BIO-TEK instruments Inc.) and compared to a standard curve obtained with known concentrations of BSA.

2.8.6 Generation of polyclonal antibodies

Synthetic peptides for EME2 (amino acids 1-13, 13-36, 208-218 and 401-418) were generated by the Peptide Synthesis Facility, Cancer Research UK. The mixture of peptides was injected into two rabbits by Pettingill Technology Ltd. The final bleeds were tested against HeLa extracts, used as a stock antibody and designated APEP13 and APEP14. The antibody used in this study (APEP13) was purified using protein A-agarose by Cell Services, Cancer Research UK.

2.8.7 Western blotting

After SDS-PAGE (Section 2.7.1), gels were transferred onto Immobilon®-P transfer membrane (Section 2.1.2) (pre-activated in 100% methanol for 5 min at RT) in western blot transfer buffer (Section 2.2.1) at 100 V for 90 min at 4°C. Membranes were incubated in blocking buffer (Section 2.2.1) for 1 hr at RT. Primary antibodies (Section 2.1.3.1) were diluted in blocking buffer and added to the membranes. All incubations with primary antibodies were performed overnight at 4°C. The next day, membranes were washed 3x in TBS supplemented with 0.05% (v/v) Tween-20 for 10 min each. Secondary antibodies (Section 2.1.3.2) were diluted in blocking buffer (1:5000) and added to the membranes for 1 hr at RT. The membranes were then washed 3x with TBS supplemented with 0.05% (v/v) Tween-20 for 10 min (RT). Following the application of ECL western blotting detection reagents (Section 2.1.2), membranes were exposed to Amersham Hyperfilm^{TM} ECL High Performance Chemiluminescence film (Section 2.1.2) for 30 s to 10 min.

2.9 Baculovirus and insect cells

2.9.1 Production of the bacmid DNA

pFL-MUS81-$_{SF}$EME1, pFL-MUS81-$_{SF}$EME2A, pFL-MUS81-$_{SF}$EME2B and pFL-MUS81^{D307A}-$_{SF}$EME2A were transformed into *E. coli* MAX Efficiency® DH10BAC^{TM} chemically competent cells (Section 2.3.1) according to the manufacturer's instructions. Recombinant bacmids were generated by transposing a DNA fragment (containing MUS81-$_{SF}$EME1, MUS81-$_{SF}$EME2A, MUS81-$_{SF}$EME2B or MUS81^{D307A}-$_{SF}$EME2A) flanked by Transposon 7 (Tn7) sites into the mini Tn7 of the bacmid DNA. Transformants were selected on LB plates containing 10 µg/ml tetracyline, 50 µg/ml kanamycin, 7 µg/ml gentamicin, 40 µg/ml IPTG and 100 µg/ml X-gal. As the mini Tn7 sites are placed in the middle of the *lacZ* gene, white colonies were generated by successful transposition. Bacmid DNA was purified by ethanol precipitation (Section 2.8.3).

2.9.2 Baculovirus production

Isolated bacmid DNA (1 µg) was transfected into two wells of a 6-well plate containing 2 x 10^6 *Spodoptera frugiperda* Sf9 cells using Fugene HD transfection reagent (Section 2.1.2) and FBS-free Grace's media. Transfection was performed according to Fugene HD's manufacturer's protocol and cells were cultured at 27°C. After 5 to 6 hr, FBS was added to a final concentration of 10% (v/v). The next day, growth media was replaced with fresh Grace's media supplemented with 10% (v/v) FBS. The supernatant of transfected Sf9 cells was collected 72 hr after transfection (P1 virus), centrifuged 5 min at 3000 rpm and transferred to a fresh tube covered with aluminium foil. Cells were pelleted by centrifugation, lysed in 300 µl of protein loading buffer (Section 2.2.1) and screened for optimal protein expression by western blotting (Section 2.8.7). The P1 virus from the clone with the optimal protein expression (400 µl) was used to infect 20 ml of Sf9 cells (at a density of 1 x 10^6 cells/ml). Seventy-two hours post-infection, the supernatant of Sf9 cells was harvested as described above (P2 virus). The P2 baculovirus (4 ml) was used to infect 200 ml of Sf9 cells (at 1 x 10^6 cells/ml). Seventy-two hours post-infection, the P3 baculovirus was harvested as described above and used to infect High Five cells (Hi5).

2.10 Protein purification

2.10.1 Purification of MUS81-$_{SF}$EME1, MUS81-$_{SF}$EME2A, MUS81-$_{SF}$EME2B and MUS81^{D307A}-$_{SF}$EME2A

MUS81-$_{SF}$EME1, MUS81-$_{SF}$EME2A, MUS81-$_{SF}$EME2B and MUS81^{D307A}-$_{SF}$EME2A complexes were purified from 600 ml of Hi5 cells (at 1 x 10^6 cells/ml) infected with 24 ml of P3 baculovirus for 72 hr. Cells were harvested by centrifugation at 3000 rpm, washed in ice-cold PBS and resuspended in 30 ml of TGN buffer (Section 2.2.1) supplemented with 500 mM NaCl, 1x protease inhibitor cocktail, 1x phosphatase inhibitor cocktail 2 and 3 and 1mM DTT (Section 2.1.2). Cells were lysed on ice for 45 min and homogenised with a Dounce using pestle B (20 strokes). The lysate was ultracentrifuged for 45 min at 35000 rpm (Beckman Type 45 Ti rotor) and the clarified extract was loaded overnight (0.2 ml/min) on a 1 ml

Strep-Tactin Superflow column (Section 2.1.2) using a ÄKTAprime plus chromatography system (GE Healthcare) at 4°C. The column was washed with 20 column volumes of TGN buffer (0.5 ml/min) containing 500 NaCl and proteins were eluted with the same buffer supplemented with 2.5 mM Desthiobiotin (40 x 0.5ml elution fractions, 0.5 ml/min). Eluted proteins were identified by SDS-PAGE (Section 2.7.1). Peak fractions were pooled and loaded on a 1 ml anti-FLAG M2 column (Section 2.1.2) for 2 hr at 4°C using a ÄKTAprime plus chromatography system (GE Healthcare). The column was washed with 20 column volumes of TGN buffer containing 500 mM NaCl and proteins were eluted in the same buffer containing 500 µg/ml of 3xFLAG peptides. Before eluting MUS81-$_{SF}$EME2B, the FLAG column was washed with additional 20 ml of TGN buffer (0.5 ml/min) containing 500 mM NaCl and supplemented with 1 mM ATP and 3 mM $MgCl_2$. Eluted proteins were identified by SDS-PAGE (Section 2.7.1) and the fractions containing MUS81-$_{SF}$EME2B were pooled and diluted to 100 mM NaCl using four volumes of TGN buffer. The sample was loaded on a 1 ml HiTRAP^{TM} heparin column (0.5 ml/min, Section 2.1.2) for 30 min and the column was washed with 30 ml of TGN buffer containing 100 mM NaCl (0.5 ml/min). Proteins were eluted using a 30 ml linear salt gradient that ranged between 100 mM and 1 M NaCl (30 x 1ml elution fractions, 0.5 ml/min) and an additional ten 1 ml fractions were collected at 1 M NaCl. Fractions containing MUS81-$_{SF}$EME1, MUS81-$_{SF}$EME2A, MUS81-$_{SF}$EME2B or MUS81^{D307A}-$_{SF}$EME2A were dialysed 2x for 2 hr against 2 L of storage buffer (Section 2.2.1) at 4°C, aliquoted and stored at -80°C. The described purifications yielded approximately 2ml of MUS81-$_{SF}$EME1at 7.5 µg/ml, 2 ml of MUS81-$_{SF}$EME2A at 12 µg/ml, 2ml of MUS81-$_{SF}$EME2B at 8.5 µg/ml and 600µl of MUS81^{D307A}-$_{SF}$EME2A at 15 µg/ml.

2.10.2 GFP-pull-down of BAC-MUS81$_{FLAP}$

BAC-MUS81$_{FLAP}$ HeLa Kyoto cells (Section 2.6.3.2) were synchronised in G1/S-phase of the cell cycle with a double thymidine block, as described in Section 2.6.4. Cells were washed with PBS, treated with trypsin and harvested. Cell pellets were washed with PBS and resuspended in 500 µl of lysis buffer (Section 2.2.1). DNA was sheared using a 1 ml syringe and a 0.8 mm x 40 mm needle (20 strokes

on ice). Samples were incubated on ice for 30 min and then centrifuged for 30 min at 14000 rpm at 4°C. Cleared lysates were transferred to a fresh Eppendorf tube and quantified by Bio-Rad D_c protein assay (Section 2.8.5). GFP-TRAP® beads (Section 2.1.2) were washed four times in lysis buffer and incubated in lysis buffer + 1 mg/ml BSA for 30 min on a rotating wheel at 4°C. The volumes and concentrations of the samples were normalised and 15 µl of GFP-TRAP® packed beads were added to each sample. Beads were incubated with the lysates for 1.5 hr on a rotating wheel at 4°C, washed four times with IP buffer and boiled in 25 µl of 1x protein loading buffer (Section 2.2.1) for 5 min. The pull-down of BAC-MUS81$_{FLAP}$ was analysed by loading 20 µl of the protein sample on a NuPAGE® 7% Tris-Acetate gels (Section 2.1.2) and by western blotting (Section 2.8.7).

2.10.3 FLAG pull-downs of $_{SF}$MUS81, $_{SF}$EME1, $_{SF}$EME2A and $_{SF}$EME2B

The expression of $_{SF}$MUS81, $_{SF}$EME1, $_{SF}$EME2A and $_{SF}$EME2B was induced for 24 hr in HEK 293-TREx^{TM} or U2OS-TREx^{TM} cells by addition of 1 µg/ml tetracycline. Cells were washed in PBS, treated with trypsin and harvested. After centrifugation (1200 rpm, 5 min), the cell pellets were washed in PBS and resuspended in 500 µl of lysis buffer (Section 2.2.1). DNA was sheared by using a 1 ml syringe and a 0.8 mm x 40 mm needle (20 strokes on ice). Samples were incubated on ice for 30 min and then centrifuged for 30 min at 14000 rpm at 4°C. Cleared lysates were transferred to a fresh Eppendorf tube and quantified by Bio-Rad D_c protein assay (Section 2.8.5). Anti-FLAG M2 resin was washed four times with 1 ml of lysis buffer and incubated with 1 ml of lysis buffer containing 1 mg/ml BSA for 30 min on a rotating wheel at 4°C. The volumes and concentrations of the samples were normalised and 30 µl of FLAG M2 packed resin were added to each sample. The resin-lysate mixture was incubated for 1.5 hr on a rotating wheel at 4°C and then washed four times with IP wash buffer (Section 2.2.1). Proteins were eluted by incubating the resin with 60 µl of TBS supplemented with 200 µg/ml 3xFLAG peptides. Elutions were boiled in 30 µl of 1x loading buffer (Section 2.1.2) for 5 min and loaded on a NuPAGE® 10% Bis-Tris gel (Section 2.1.2). Co-immunoprecipitated proteins were detected by western blotting (Section 2.8.9).

2.11 Preparation of DNA substrates and cleavage assays

2.11.1 Gel purification of oligonucleotides

Dried oligonucleotides (Table 2.3) were resuspended in water to give a final concentration of 200 μM. In order to purify them from shorter oligonucleotides species, approximately one third of the total volume was mixed with one volume of formamide loading buffer (Section 2.2.2), boiled for 5 min and loaded on a 15% polyacrylamide denaturing gel (Bio-Rad Protean® II xi system). The gel was run at 400 V for 2 hr, stained with Stains-all solution (Section 2.2.2) for 10 min at RT (in a glass dish) and then destained in water for 15 min at RT. In order to remove shorter DNA products, only the upper third of the oligonucleotide band was excised from the gel. DNA was eluted overnight in TE buffer (Section 2.2.2) on a rotating wheel at 4°C. The next day, the supernatant was collected, the oligonucleotides were ethanol-precipitated (Section 2.8.3) and the pellet was dissolved in 60 μl TE (Section 2.2.2). The concentration of each oligonucleotide was determined as described in Section 2.8.2.

Table 2.3 List of oligonucleotides

OLIGONUCLEOTIDE	SEQUENCE (5'-3')
X0.1	ACGCTGCCGAATTCTACCAGTGCCTTGCTAGGACATCTTTGCCCACCTGCAGGTTCACCC
X0.2	GGGTGAACCTGCAGGTGGGCAAAGATGTCCATCTGTTGTAATCGTCAAGCTTTATGCCGT
X0.3	ACGGCATAAAGCTTGACGATTACAACAGATCATGGAGCTGTCTAGAGGATCCGACTATCG
X0.4	CGATAGTCGGATCCTCTAGACAGCTCCATGTAGCAAGGCACTGGTAGAATTCGGCAGCGT
X0.2 1/2	GGGTGAACCTGCAGGTGGGCAAAGATGTCC
X0.3 1/2	ATGGAGCTGTCTAGAGGATCCGACTATCGA
X0.3 2/2	ACGGCATAAAGCTTGACGATTACAACAGATC
X26.1	GCGCTACCAGTGATCACCAATGGATTGCTAGGACATCTTTGCCCACCTGCAGGTTCACCC
X26.2	GGGTGAACCTGCAGGTGGGCAAAGATGTCCTAGCAATCCATTGTCTATGACGTCAAGCTC

X26.3	GAGCTTGACGTCATAGACAATGGATTGCTAGGACATCTTTGCC GTCTTGTCAATATCGGC
X26.4	GCCGATATTGACAAGACGGCAAAGATGTCCTAGCAATCCATTG GTGATCACTGGTAGCGC
DL-0	CGTTGGACGCTGCCGAATTCTACCACTGCGTGCCTTGCTAGG ACATCTTTGCCCACCTGCAGGTTCACCCATCGC
DL-1	GCGATGGGTGACCTGCAGGTGGGCGGCTGCTCATCGTAGGT TAGTGAATTGGTAGAATTCGGCAGCGTCCAACG
DL-2	GATCGTAAGAGCAAGATGTTCTATAAAAGATGTCCTAGCAAGG CACGCAG
DL-3	TATAGAACATCTTGCTCTTACGATC

2.11.2 Preparation of non-radiolabelled DNA substrates

Purified oligonucleotides were mixed (600 pmol of 60-mers and 1200 pmol of 30-mers, Table 2.3) in 60 µl of annealing buffer (Section 2.2.2), placed in boiling water for 2 min and annealed overnight at RT. Annealed substrates were mixed with 1x DNA loading buffer (Section 2.2.2) and analysed on a native 12% polyacrylamide gel (Bio-Rad Protean® II xi system) in TBE at 200V for 4 hr at 4°C. The gel was covered with plastic wrap and placed on TLC paper with fluorescent indicator (UV245) (Section 2.1.2). The bands were identified by exposure to 245 nm UV light, excised from the gel and eluted overnight in TNE buffer (Section 2.2.2) on a gyro-rocker at 4°C. The DNA concentration was measured as described in Section 2.8.2.

2.11.3 5'-^{32}P-end labelling of oligonucleotides and substrate preparation

Reactions contained 100 ng of oligonucleotide, approximately 10 pmol of ^{32}P-γATP and 10 U of T4 PNK in 1x NEB T4 PNK buffer (Section 2.1.1). Mixtures were incubated at 37°C for 45 min and reactions were stopped by the addition of EDTA to 50 mM. Unincorporated label was removed using Illustra^{TM} MicroSpin® G-25 columns (GE Healthcare) according to the manufacturer's instructions. Radiolabelled oligonucleotides were mixed with 300 ng of combinations of unlabelled oligonucleotides in order to obtain the DNA substrates illustrated in

SUBSTRATES	OLIGONUCLEOTIDES
 3' flap	(XO1) 5'ACGCTGCCGAATTCTACCAGTGCCTTGCTAGGACATCTTTGCCCACCTGCAGGTTCACCC3' (XO3.1/2) 5'CATGGAGCTGTCTAGAGGATCCGACTATCGA3' (XO4) 5'TCGATAGTCGGATCCTCTAGACAGCTCCATGTAGCAAGGCACTGGTAGAATTCGGCAGCGT3'
 5' flap	(XO1) 5'ACGCTGCCGAATTCTACCAGTGCCTTGCTAGGACATCTTTGCCCACCTGCAGGTTCACCC3' (XO2.1/2) 5'GGGTGAACCTGCAGGTGGGCAAAGATGTCC3' (XO4) 5'TCGATAGTCGGATCCTCTAGACAGCTCCATGTAGCAAGGCACTGGTAGAATTCGGCAGCGT3'
 Replication fork	(XO1) 5'ACGCTGCCGAATTCTACCAGTGCCTTGCTAGGACATCTTTGCCCACCTGCAGGTTCACCC3' (XO2.1/2) 5'GGGTGAACCTGCAGGTGGGCAAAGATGTCC3' (XO3.1/2) 5'CATGGAGCTGTCTAGAGGATCCGACTATCGA3' (XO4) 5'TCGATAGTCGGATCCTCTAGACAGCTCCATGTAGCAAGGCACTGGTAGAATTCGGCAGCGT3'
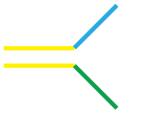 Splayed arm	(XO1) 5'ACGCTGCCGAATTCTACCAGTGCCTTGCTAGGACATCTTTGCCCACCTGCAGGTTCACCC3' (XO4) 5'TCGATAGTCGGATCCTCTAGACAGCTCCATGTAGCAAGGCACTGGTAGAATTCGGCAGCGT3'
 static HJ	(XO1) 5'ACGCTGCCGAATTCTACCAGTGCCTTGCTAGGACATCTTTGCCCACCTGCAGGTTCACCC3' (XO2) 5'GGGTGAACCTGCAGGTGGGCAAAGATGTCCATCTGTTGTAATCGTCAAGCTTTATGCCGT3' (XO3) 5'ACGGCATAAAGCTTGACGATTACAACAGATCATGGAGCTGTCTAGAGGATCCGACTATCG3' (XO4) 5'CGATAGTCGGATCCTCTAGACAGCTCCATGTAGCAAGGCACTGGTAGAATTCGGCAGCGT3'
 mobile HJ	(X26-1) 5'GCGCTACCAGTGATCACCAATGGATTGCTAGGACATCTTTGCCCACCTGCAGGTTCACCC3' (X26-2) 5'GGGTGAACCTGCAGGTGGGCAAAGATGTCCTAGCAATCCATTGTCTATGACGTCAAGCTC3' (X26-3) 5'GAGCTTGACGTCATAGACAATGGATTGCTAGGACATCTTTGCCGTCTTGTCAATATCGGC3' (X26-4) 5'GCCGATATTGACAAGACGGCAAAGATGTCCTAGCAATCCATTGGTGATCACTGGTAGCGG3'
 nicked HJ	(XO1) 5'ACGCTGCCGAATTCTACCAGTGCCTTGCTAGGACATCTTTGCCCACCTGCAGGTTCACCC3' (XO2) 5'GGGTGAACCTGCAGGTGGGCAAAGATGTCCATCTGTTGTAATCGTCAAGCTTTATGCCGTT3' (XO3.1/2) 5'[P]ATGGAGCTGTCTAGAGGATCCGACTATCG3' (XO3.2/2) 5'ACGGCATAAAGCTTGACGATTACAACAGATC (XO4) 5'TCGATAGTCGGATCCTCTAGACAGCTCCATGTAGCAAGGCACTGGTAGAATTCGGCAGCGT3'
 D-loop	(DL-0) 5'CGTTGGACGCTGCCGAATTCTACCACTGCGTGCCTTGCTAGGACATCTTTGCCCACCTGCA GGTTCACCCATCGC3' (DL-1) 5'GCGATGGGTGAACCTGCAGGTGGGCGGCTGCTCATCGTAGGTTAGTGAATTGGTAGAA TTCGGCAGCGTCAACG3' (DL-2) 5'GATCGTAAGAGCAAGATGTTCTATAAAAGATGTCCTAGCAAGGCACGCAG3' (DL-3) 5'TATAGAACATCTTGCTCTTACGATC3'

Table 2.4 Oligonucleotides sequences of synthetic DNA substrates

Identical colours indicate complementary strands. Note that 3'-flap, 5'-flap, replication fork, splayed-arm, static HJ, nicked HJ and mobile HJ have oligonucleotides X01 and X04 in common

Table 2.4. Mixtures were boiled for 2 min and annealed overnight at RT. Annealed substrates were mixed with 1x DNA loading buffer (Section 2.2.2) and electrophoresed through a native 12% polyacrylamide gel (Bio-Rad Protean® II xi system) in TBE at 200 V for 4 hr at 4°C. The gel was covered with plastic wrap, exposed to Biomax MR film for 2 min and the DNAs were excised from the gel and eluted overnight in TN buffer (Section 2.2.2) on a gyro-rocker at 4°C.

2.11.4 Preparation of 5'-^{32}P-end-labeled length marker oligonucleotides

Length marker oligonucleotides (10 µM) listed in Table 2.5 were mixed in equimolar amounts. Reactions contained the mixture of marker oligonucleotides (0.5 µM), approximately 3 pmol of ^{32}P-γATP and 10 U of T4 PNK in 1x NEB T4 PNK buffer (Section 2.1.1). Mixtures were incubated at 37°C for 45 min and reactions were stopped by the addition of EDTA to 50 mM. Unincorporated label was removed using Illustra™ MicroSpin® G-25 columns (GE Healthcare) according to the manufacturer's instructions. Formamide loading buffer (two to four volumes) was added to the labelled marker oligonucleotides and the mixture was boiled for 5 min before loading on a denaturing PAGE (Section 2.7.4).

Table 2.5 Sequences of the length marker oligonucleotides

OLIGONUCLEOTIDE	SEQUENCE (5'-3')
X01.35	ACGCTGCCGAATTCTACCAGTGCCTTGCTAGGACA
X01.30	ACGCTGCCGAATTCTACCAGTGCCTTGCTA
X01.25	ACGCTGCCGAATTCTACCAGTGCCT
X02.35	GGGTGAACCTGCAGGTGGGCAAAGATGTCCATCTG
X02.30	GGGTGAACCTGCAGGTGGGCAAAGATGTCC
X02.25	GGGTGAACCTGCAGGTGGGCAAAGA
X03.35	ACGGCATAAAGCTTGACGATTACAACAGATCATGG
X03.30	ACGGCATAAAGCTTGACGATTACAACAGAT
X03.25	ACGGCATAAAGCTTGACGATTACAA
X04.35	CGATAGTCGGATCCTCTAGACAGCTCCATGTAGCA
X04.30	CGATAGTCGGATCCTCTAGACAGCTCCATG
X04.25	CGATAGTCGGATCCTCTAGACAGCT

DL-0.57	CGTTGGACGCTGCCGAATTCTACCACTGCGTGCCTTGCTAGG ACATCTTTGCCCA
DL-0.52	CGTTGGACGCTGCCGAATTCTACCACTGCGTGCCTTGCTAGG ACATCTTT
DL-0.47	CGTTGGACGCTGCCGAATTCTACCACTGCGTGCCTTGCTAGG ACA
DL-0.32	CGTTGGACGCTGCCGAATTCTACCACTGCG
DL-0.27	CGTTGGACGCTGCCGAATTCTACCA
DL-0.22	CGTTGGACGCTGCCGAATTC
DL-1.57	GCGATGGGTGAACCTGCAGGTGGGCGGCTGCTCATCGTAGG TTAGTGAATTGGTA
DL-1.52	GCGATGGGTGAACCTGCAGGTGGGCGGCTGCTCATCGTAGG TTAGTGAAT
DL-1.47	GCGATGGGTGAACCTGCAGGTGGGCGGCTGCTCATCGTAGG TTAG
DL-1.32	GCGATGGGTGAACCTGCAGGTGGGCGGCTG
DL-1.27	GCGATGGGTGAACCTGCAGGTGGGC
DL-1.22	GCGATGGGTGAACCTGCAGG
DL-2.32	GATCGTAAGAGCAAGATGTTCTATAAAAGA
DL-2.27	GATCGTAAGAGCAAGATGTTCTATA
DL-2.22	GATCGTAAGAGCAAGATGTT
DL-3.22	TATAGAACATCTTGCTCTTA

2.11.5 Endonucleolytic cleavage assay

Reactions (10 µl) contained 100 µM of non-radiolabelled DNA (Section 2.11.2), 1 µl of 5'-^{32}P-labelled DNA (Section 2.11.3) and cleavage buffer (Section 2.2.3), unless otherwise specified. Various concentrations of MUS81-$_{SF}$EME1, MUS81-$_{SF}$EME2A, MUS81-$_{SF}$EME2B and MUS81^{D307A}-$_{SF}$EME2A complexes (Section 2.10.1) diluted in protein dilution buffer (Section 2.2.1) were added to the reaction mixtures. Reactions were initiated by incubation at 37°C, allowed to proceed for 30 min and then terminated by addition of stop buffer (5x) (Section 2.2.3). Labelled DNA products were analysed by neutral PAGE (Section 2.7.3) or by denaturing PAGE (Section 2.7.4) followed by autoradiography (Section 2.7.7) or phosphorimaging (Section 2.7.8).

2.12 Preparation of metaphase spreads and stainings

2.12.1 Metaphase spreads

To enrich for the mitotic cell population, cells were treated for 1.5 hr with 0.2 µg/ml of colcemid, a drug that depolymerises microtubules and arrests cells in metaphase (Section 2.1.2). Cells were collected by mitotic shake-off, washed in PBS and swollen in 5 ml of 750 mM KCl for 30 min at 37°C. Ice-cold methanol/acetic acid (3:1, 5 ml) was added on top of the swelling buffer and cells were centrifuged for 5 min at 1200 rpm at RT. The two-layered solution was removed from the bottom to the top and cells were resuspended in an additional 5 ml of ice-cold methanol/acetic acid (3:1). Fixation was performed for 15 min on ice. Metaphase cells were then spread on Superfrost® Microscope slides (Thermo Scientific) and air-dried overnight at RT.

2.12.2 Sister Chromatid Exchanges (SCEs)

Reciprocal exchanges of DNA between the sister chromatids was detected by the SCEs assay essentially as described (Bayani and Squire, 2005). One day before siRNA transfection, GM08505 (7×10^5) cells were seeded on 10 cm plates. On the following day, cells were transfected with siRNA as described in Section 2.6.1. After 48 hr, cells were incubated with 100 µM BrdU for 72 hr. Colcemid (0.2 µg/ml) was added for the last 1.5 hr of BrdU incubation. Metaphase spreads were performed as described in Section 2.12.1. Slides were air-dried overnight and then stained for 30 min in 50 ml Soerensen buffer (pH 6.8) (Section 2.2.4) containing 100 µg/ml Hoechst 33258. After washing with an additional 50 ml Soerensen buffer (pH 6.8), slides were placed in a shallow container, covered with Soerensen buffer (pH 6.8) and exposed to 254 nm UV light (Stratalinker 2400) for 45 min. Slides were then covered with 2x SSC buffer (Section 2.2.4), incubated at 60°C for 1 hr and stained in 50 ml 7% (v/v) GIEMSA solution (Section 2.1.2) at RT for 7 min. After washing three to four times with 50 ml water, coverslips were mounted on the slides using 80 µl DPX mounting medium (Section 2.1.2). Images were acquired with a Zeiss Axio Imager M1 microscope using a Plan-Neofluar x60, 0.4 numerical

aperture oil objective lens, and captured using an ORCA-ER camera (Hamamatsu) controlled by Volocity 6.0.1 software (Improvision).

2.12.3 Telomeric quantitative-FISH (Q-FISH) on metaphase chromosomes

Metaphase spreads were prepared as described in Section 2.12.1. Q-FISH was performed essentially as described (Blasco et al., 1997; Zijlmans et al., 1997). Briefly, slides were re-hydrated in 50 ml PBS for 5 min, fixed with 100 µl of 4% (v/v) paraformaldehyde for 2 min and treated with 100 µl of 1 mg/ml pepsin for 10 min at 37°C. Slides were washed in 50 ml PBS, fixed again with 100 µl of 4% (v/v) paraformaldehyde and dehydrated using a series of ethanol washes (5 min in 70% (v/v), 5 min in 95% (v/v) and 5 min in 100%). Hybridisation solution (80 µl) (Section 2.2.4) containing 110 nM FISH-TelC probes (Section 2.1.2) was added to the slides and denaturation was performed on a 70°C hot plate for 7 min. Slides were incubated in a humid chamber for 2 hr at RT or overnight at 4°C, washed 2x with 50 ml of hybridisation wash #1 (Section 2.2.4) for 15 min and 3x with 50 ml of hybridisation wash #2 (Section 2.2.4) for 5 min (160 ng/ml DAPI was added to the second wash) in Coplin jars. Slides were dehydrated using a series of ethanol washes (5 min in 70% (v/v), 5 min in 95% (v/v) and 5 min in 100%), air-dried and mounted using ProLong® Gold Antifade Reagent (Section 2.1.2). Images were acquired with a Zeiss Axio Imager M1 microscope using a Plan-Neofluar x60, 0.4 numerical aperture oil objective lens, and captured using an ORCA-ER camera (Hamamatsu) controlled by Volocity 6.0.1 software (Improvision).

2.12.4 Telomeric chromosome orientation-FISH (CO-FISH)

One day before siRNA transfection, U2OS cells (7 x 10^5 cells) were seeded on 10 cm plates. Cells were transfected with siRNA as described in Session 2.6.1. Twenty hours before harvesting, 10 µM BrdU was added to the cells and metaphase spreads were prepared as described in Section 2.12.1. CO-FISH was performed as described (Bailey et al., 2004; Bechter et al., 2004; Londono-Vallejo et al., 2004). Briefly, slides were re-hydrated for 5 min in PBS, treated with 0.5 mg/ml RNase A for 10 min at 37°C and stained with 0.5 µg/ml Hoechst 33258 in 2x

SSC (Section 2.2.4) for 15 min at RT. Slides were placed in a shallow container, covered with 2x SSC buffer and exposed to 365 nm UV light (Stratalinker 1800) at RT for 30 min. The BrdU-substituted DNA strands were digested by treatment with 80 µl of 10 U/ml of Exonuclease III (Section 2.1.1) at RT for 10 min. Slides were washed with 50 ml of PBS, dehydrated using a series of ethanol washes (5 min in 70% (v/v), 5 min in 95% (v/v) and 5 min in 100%) and air-dried at RT. The first hybridisation was performed by adding 80 µl of hybridising solution (Section 2.2.4) containing 10 nM TelG-TMR probe onto the slides and incubating for 2 hr at RT in a humidified chamber. Slides were rinsed in hybridisation wash #1 (Section 2.2.4) for 5 s. The second hybridisation was performed by adding 80 µl of hybridisation solution containing 110 nM FITC TelC probe onto the slides and incubating for 2 hr at RT in a humidified chamber. Slides were washed 2x with 50 ml of hybridisation buffer #1 for 30 min each, 3x with 50 ml of hybridisation buffer #2 (Section 2.2.4) for 5 min (160 ng/ml DAPI was added to the second wash) in Coplin jars, dehydrated using a series of ethanol washes (5 min in 70% (v/v), 5 min in 95% (v/v) and 5 min in 100%) and air-dried at RT. Coverslips were mounted onto the slides using ProLong® Gold Antifade Reagent (Section 2.1.2). Images were acquired with a Zeiss Axio Imager M1 microscope using a Plan-Neofluar x60, 0.4 numerical aperture oil objective lens, and captured using an ORCA-ER camera (Hamamatsu) controlled by Volocity 6.0.1 software (Improvision).

2.12.5 Immunofluorescence

Immunofluorescence was performed as described (Perez-Burgos et al., 2004) with some variations. Briefly, cells were seeded in 6 cm plates containing two 22 mm x 22 mm coverslips. On the day of the experiment, coverslips were transferred into 6-well plates, washed with 2 ml PBS and incubated with 2 ml pre-extraction buffer (Section 2.2.4) for 4 min at RT. Cells were fixed with 2 ml of 4% (v/v) paraformaldehyde for 10 min, washed 2x in PBS and permeabilised in 2 ml of permeabilisation buffer (Section 2.2.4) for 5 min at RT. Coverslips were washed 2x with PBS (2 ml, 5 min each) and then 2x in IF washing solution (Section 2.2.4, 2ml, 5 min each) before incubating with 2 ml of IF blocking solution (Section 2.2.4) for 30 min at RT. Primary antibodies (Section 2.1.3.1) were diluted in IF blocking

solution and 40 µl drops were placed on parafilm. Coverslips were positioned on the primary antibody solution drops and incubated in a humid chamber for 2 hr at RT or overnight at 4°C. After washing the coverslips 3x with 2 ml of IF washing solution (10 min each), secondary antibodies (Section 2.1.3.2) were diluted in IF blocking buffer and applied to the coverslips as described above. Excess secondary antibody was washed out with 2 ml of IF washing solution (three washes, 10 min each, RT). Coverslips were air-dried and mounted using ProLong® Gold Antifade Reagent with DAPI (Section 2.1.2).

2.12.6 Immunofluorescence-FISH

Cells were grown on 22 mm x 22 mm coverslips and IF was performed as described in Section 2.12.5. After incubation with the secondary antibody, cells were washed with 3x with 2 ml PBS (5 min each) and fixed for 2 min with 2 ml of 4% (v/v) paraformaldehyde. Coverslips were washed with 2 ml of PBS, dehydrated using a series of ethanol washes (5 min in 70% (v/v), 5 min in 95% (v/v) and 5 min in 100%) and air-dried for 30 min at RT. FISH was performed as described in Section 2.12.3.

2.13 Fluorescence-activated cell sorting (FACS) analysis

2.13.1 Propidium Iodide (PI) staining

Cells were washed with PBS, treated with trypsin and harvested in their own media. Pellets were washed with PBS and fixed with 70% (v/v) ethanol for at least 30 min on ice. Ethanol was removed by washing the cell pellets 2x with 5 ml of PBS. Cells were treated with 50 µl of 100 µg/ml RNase A (Section 2.1.2) and stained with 200 µl of 50 µg/ml PI (Section 2.1.2). DNA content was analysed on a FACSCalibur™ flow cytometer (BD Biosciences) and FACS data were analysed using FlowJo 10.1 software.

2.13.2 BrdU staining

BrdU staining was performed as described (Sasaki et al., 1989). Briefly, cells were treated for 30 min with 10 μM BrdU, washed with PBS, treated with trypsin and harvested in their own media. Pellets were washed with 5 ml of PBS and fixed with 70% (v/v) ethanol for at least 30 min on ice. Ethanol was removed by washing the cell pellets 2x with 5 ml of PBS. Cells were treated with 5 ml of 2 M HCl for 30 min at RT, washed 2x with 5 ml of PBS and once with 5 ml of PBS supplemented with 0.5% (v/v) Tween-20. FITC anti-BrdU antibody (2μl, Section 2.1.3.1) was added directly to the cell pellet and incubated in the dark for 20 min. Cells were washed with 5 ml of PBS and stained with PI as described in Section 2.13.1.

2.13.3 Phospho histone H3 staining

Cells were washed with PBS, treated with trypsin and in their own media. Pellets were washed with 5 ml of PBS and fixed with 70% (v/v) ethanol for at least 30 min on ice. Ethanol was removed by washing the cell pellets 2x with 5 ml of PBS. Cells were incubated with 2% (v/v) FBS in PBS containing mouse anti-phospho histone H3 antibody (1:500 dilution, Section 2.1.3.1) for 2 hr at RT and then washed once with 5 ml of 2% (v/v) FBS in PBS. Alexa Fluor® 488 goat anti-mouse IgG (H+L) secondary antibody (1:500 dilution, Section 2.1.3.2) was diluted in 2% (v/v) FBS in PBS and added to the cell pellet. After 1 hr, cells were washed once with 5 ml of 2% (v/v) FBS in PBS and stained with PI as described in Section 2.13.1.

CHAPTER 3

Biochemical characterisation of MUS81-EME1 and MUS81-EME2 complexes

3.1 Two isoforms of EME2 are expressed in human cells

Human EME2 was first identified using a PSI-BLAST (Position Specific Iterated – Basic Local Alignment Search Tool) search for the human ortholog of the *S. pombe* Eme1 and corresponds to a 245 amino acid protein with a molecular mass of 26 kDa (NCBI # XM_113869) (Ciccia et al., 2003). However, this sequence for EME2 was removed from the National Centre for Biotechnology Information (NCBI) database due to insufficient evidence for the existence of the transcript. Later, the database entry was replaced by a sequence predicted to encode a 444 amino acid protein (NM_001010865), but this sequence has also recently been revised to one that now encodes a 379 amino acid protein (NM_001257370.1). In addition to the sequence deletion, there are two amino acid changes compared with the earlier version.

To verify whether which, if any, transcript variants are expressed in human cells, the EME2 sequence was amplified from human cDNA. First, mRNA was extracted from MCF-7 cells and cDNA was prepared (Section 2.8.1). Second, primers 19 and 20 (Section 2.4), corresponding to the 5'- and 3'-ends of the longest gene transcript (NM_001010865), were used to PCR-amplify the EME2 sequence from MCF-7 cDNA (Section 2.8.1). PCR amplification resulted in two products of around 1100 and 1300 base pairs (bp), with the 1100bp product being more abundant (Figure 3.1A). Sequencing of the product DNA led to the identification of two splice variants of EME2: the smaller and more abundant transcript variant results from the alternative splicing of exons 4, 5 and 6, and encodes for a 379 amino acid protein, hereafter referred to as EME2A, that is identical to that in the NCBI database (NM_001257370.1); the second, less abundant splice variant represents the

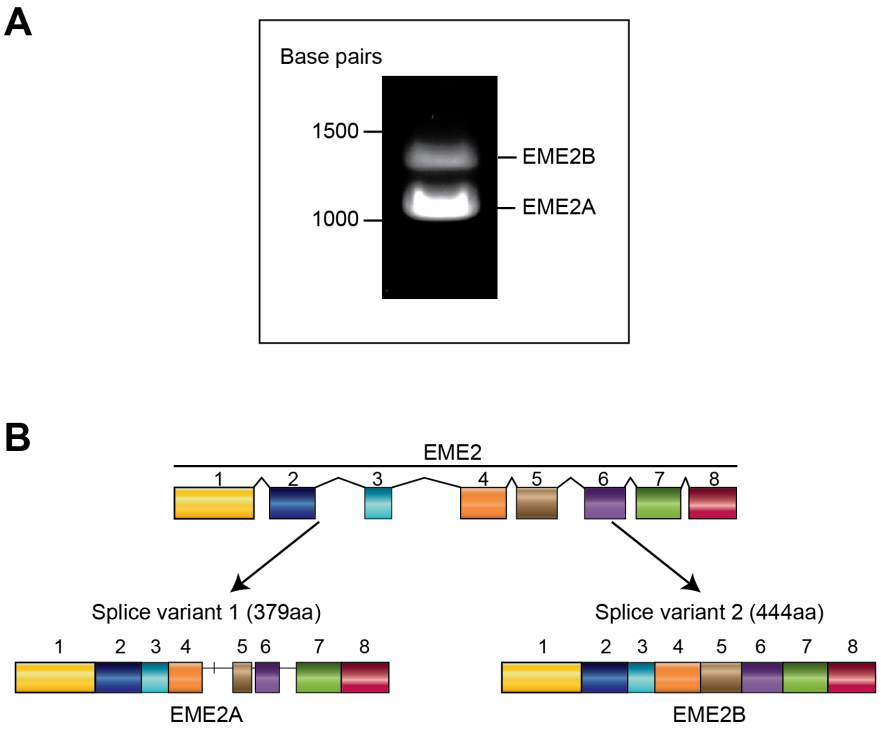

Figure 3.1 Identification of two isoforms of EME2
A. Agarose gel (Section 2.7.2) stained with SafeView showing the products of the PCR amplification of the EME2 sequence from MCF-7 cDNA (Section 2.8.1). **B.** Schematic representation of the two isoforms of EME2, EME2A and EME2B. **C.** Sequence alignment of the EME2A and EME2B proteins. Blue = non-conserved residues, yellow = highly conserved residues. Sequence alignments were performed using ClustalW and analysed in Jalview.

longest gene transcript, equivalent to NM_001010865, which encodes for a 444 amino acid protein hereafter referred to as EME2B (Figure 3.1B). Sequence alignment of the two proteins showed that EME2A and EME2B share 85.36% of identity (Figure 3.1C). Human MUS81, EME1 and EME2 have a conserved C-terminal domain, through which they are believed to interact to form active endonuclease heterodimers (Ciccia et al., 2003). Sequence alignment of MUS81, EME1, EME2A and EME2B showed that the newly identified EME2 isoforms align mainly with the C-terminal region of MUS81 and EME1 (Figure 3.2A). In addition, sequence comparisons revealed that EME1 shares 37% identity and 61.2% similarity with EME2A and 33.1% identity and 56.9% similarity with EME2B (Figure 3.2A).

In order to determine the domain architecture of EME2A and EME2B, the protein sequences were analysed by the Simple Modular Architecture Research Tool (SMART) server, which allows the identification of evolutionary conserved domains. Both isoforms were found to have an ERCC4 nuclease domain (Figure 3.2A-B, amino acids 77-326 in EME2A and amino acids 77-391 in EME2B) but, as already observed for EME1, the amino acid sequence of the ERKXXXD catalytic motif has diverged (Figure 3.2A, compare amino acids 333-339 of MUS81 with the corresponding amino acids of EME1, EME2A and EME2B) (Ciccia et al., 2003). Also, like MUS81 and EME1, EME2A and EME2B harbour a C-terminal $(HhH)_2$ domain (Figure 3.2A-B) (Ciccia et al., 2008).

3.2 EME2A and EME2B associate with MUS81 *in vivo*

To determine whether EME2A and EME2B interact with MUS81, we performed FLAG pull-downs from HEK293-TREx^{TM} cells carrying Strep-FLAG-tagged versions of either EME2A or EME2B ($_{SF}$EME2A or $_{SF}$EME2B) (Section 2.10.3). Both $_{SF}$EME2A and $_{SF}$EME2B immunoprecipitated endogenous MUS81 efficiently, as determined by SDS-PAGE and western blotting (Sections 2.7.1 and 2.8.7) (Figure 3.3). Interestingly, we did not detect EME1 in $_{SF}$EME2A or $_{SF}$EME2B immunoprecipitates, although it formed a stable complex with MUS81 under the same conditions (data not shown). These results suggest that human MUS81 can

A

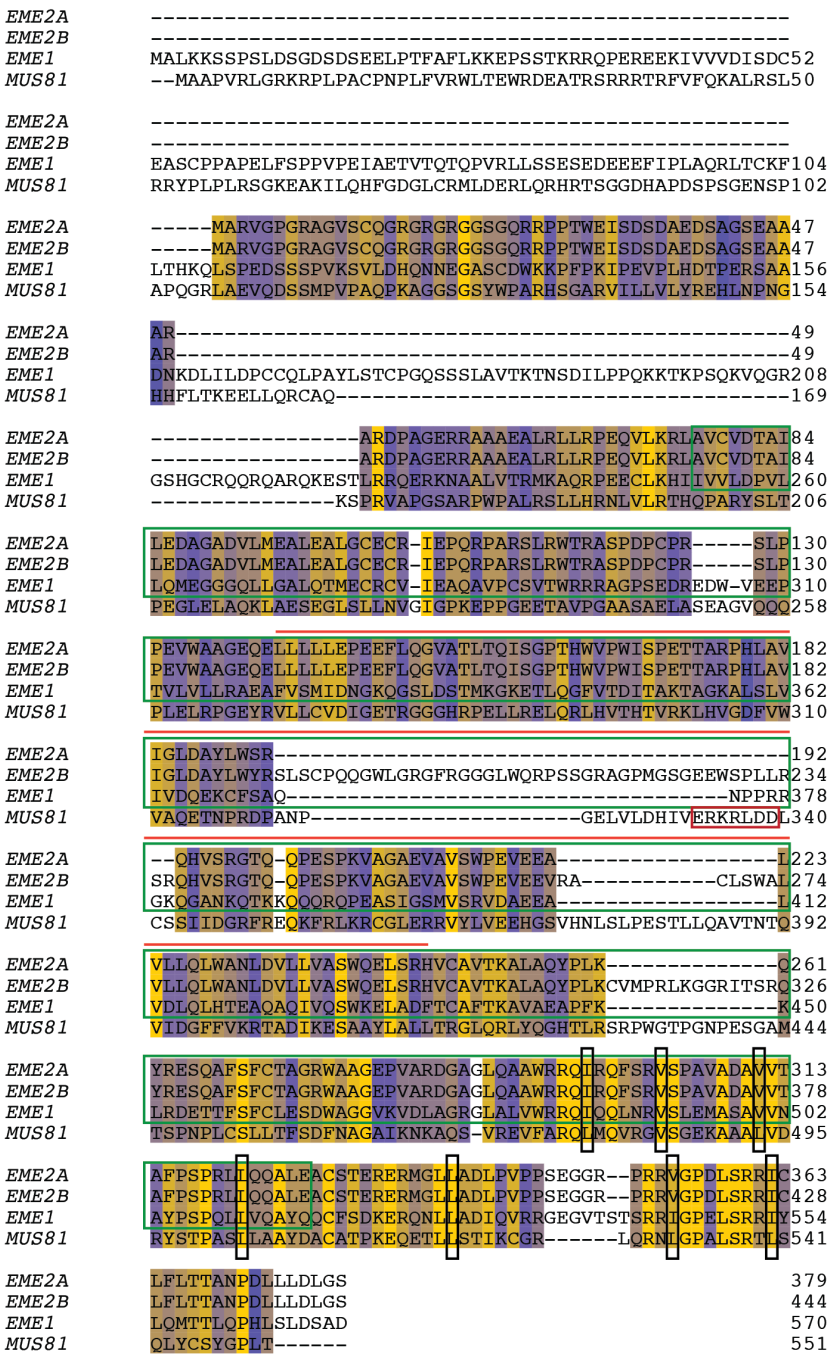
EME2A
EME2B
EME1
MUS81

B

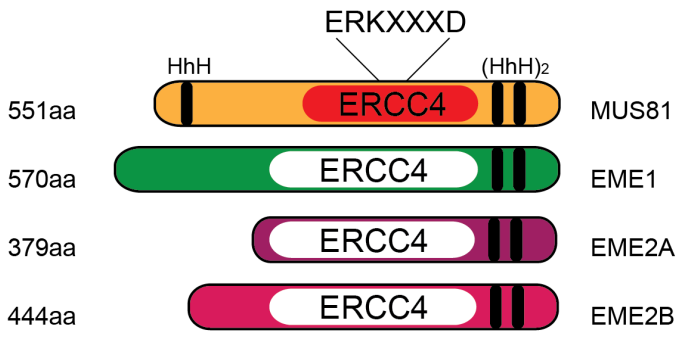
ERKXXXD
HhH
(HhH)2
551aa
ERCC4
MUS81
570aa
ERCC4
EME1
379aa
ERCC4
EME2A
444aa
ERCC4
EME2B

Figure 3.2 Sequence alignment between EME2A, EME2B, EME1 and MUS81

A. Conservation of the residues is indicated using the following colour ramp: blue = non-conserved, yellow = highly conserved. The ERKXXXD domain of MUS81 is indicated in the red box. The dark green box indicates the ERCC4 domain of EME1, EME2A and EME2B. The orange line indicates the ERCC4 domain of MUS81. Black boxes indicate important hydrophobic residues for the formation of the HhH domain. Sequence alignments were performed using ClustalW and analysed in Jalview. **B.** Schematic representation of MUS81, EME1, EME2A and EME2B. HhH and ERCC4 nuclease domains are indicated in black. The active ERCC4 domain of MUS81 is indicated in red. Inactive ERCC4 domains are indicated in white.

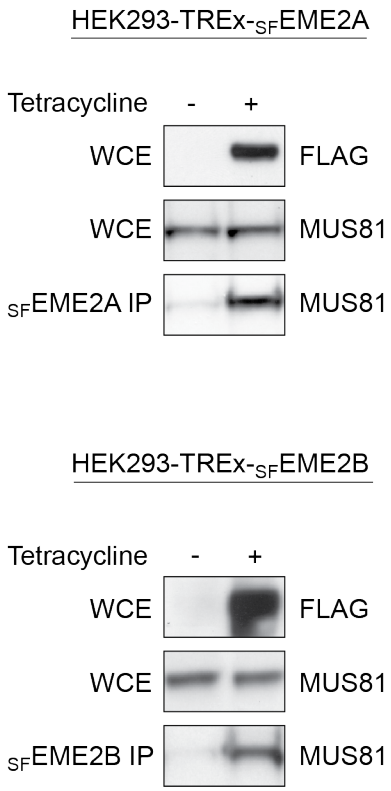

Figure 3.3 $_{SF}$EME2A and $_{SF}$EME2B interact with endogenous MUS81

Expression of $_{SF}$EME2A and $_{SF}$EME2B was induced in HEK293-TREx™ cell lines (Section 2.6.2) with 1 µg/ml tetracycline for 72 hr. FLAG pull-down was performed as described in Section 2.10.3.

form three distinct heterodimeric complexes: MUS81-EME1, MUS81-EME2A and MUS81-EME2B.

3.3 Purification of the MUS81 complexes

To determine whether MUS81-EME2A and MUS81-EME2B form active endonucleases and to compare their *in vitro* endonucleolytic activities with those of MUS81-EME1, all three MUS81 complexes were purified to near homogeneity. Co-expression of MUS81 with EME1, EME2A or EME2B in *E. coli* produced mostly insoluble proteins and attempts to purify the soluble complexes were unsuccessful. Therefore, MUS81-EME1, MUS81-EME2A and MUS81-EME2B were expressed in insect cells using the baculovirus protein expression system, which allows the production of post-translationally-modified multi-protein complexes. Furthermore, tandem affinity purification strategies were used to purify proteins quickly away from contaminants. For this purpose, we inserted a 2xStrepII-FLAG (SF) tag at the N-terminus of EME1, EME2A and EME2B. It has been reported that the combinations of Strep-tag II and a FLAG tag results in the best protein purity and recovery rates when compared to combinations of other protein tags (Gloeckner et al., 2007). In addition, the SF tag is small (4.6 kDa) and contains terminal hydrophilic residues that prevent its folding into the protein structure, thus minimising the potential interference of the tag with protein function.

MUS81-$_{SF}$EME1, MUS81-$_{SF}$EME2A and MUS81-$_{SF}$EME2B were cloned into the pFL bicistronic vectors for baculovirus protein expression and the bacmid DNA was obtained as described in Section 2.9.1 and illustrated in Figure 3.4. Baculoviruses expressing MUS81-$_{SF}$EME1, MUS81-$_{SF}$EME2A and MUS81-$_{SF}$EME2B were then generated (Section 2.9.2) and used to infect Hi5 insect cells. Hi5 whole cell extracts were cleared by high-speed centrifugation and loaded onto a Strep-Tactin® affinity column (Figure 3.5A). The MUS81 complexes were eluted by ligand competition using desthiobiotin (Figure 3.5B, lanes a), and peak fractions were collected and loaded onto an anti-FLAG-M2 column (Figure 3.5A). After elution with 3xFLAG peptides (Figure 3.5B, lanes b), fractions containing MUS81 complexes were applied to a heparin column and eluted with a 0.15 - 1 M NaCl gradient (Figure

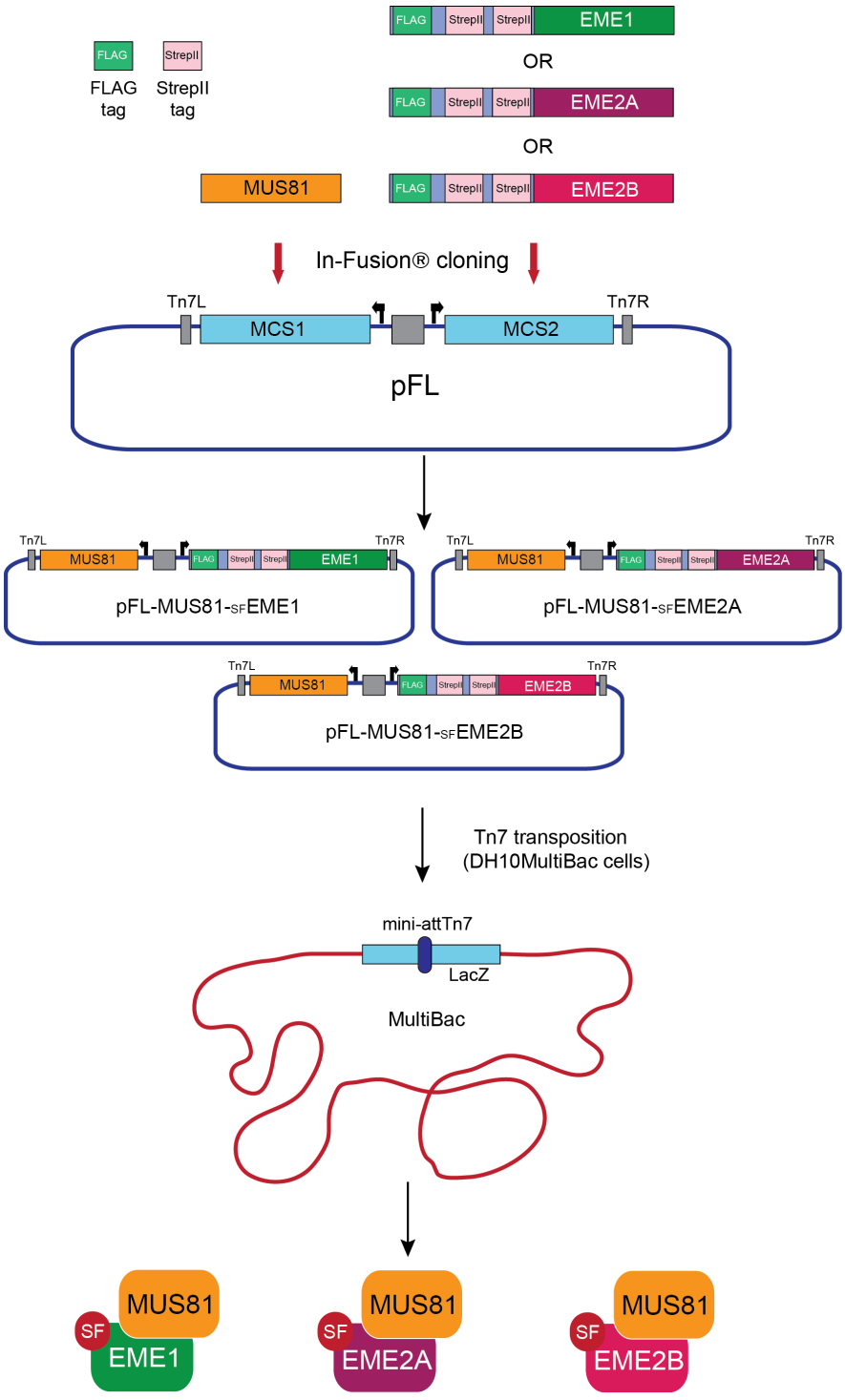

Figure 3.4 Construction of baculovirus expression vectors for production of bacmid DNA and protein expression in insect cells
Human MUS81 and STREP/FLAG (SF)-tagged EME1, EME2A and EME2B were cloned into the pFL vector with In-Fusion® cloning system. DNA fragments containing MUS81-$_{SF}$EME1, MUS81-$_{SF}$EME2A or MUS81-$_{SF}$EME2B were inserted into the bacmid DNA by Tn7 transposition. Isolated recombinant bacmid DNA was used to express the tagged protein complexes in insect cells (Section 2.9).

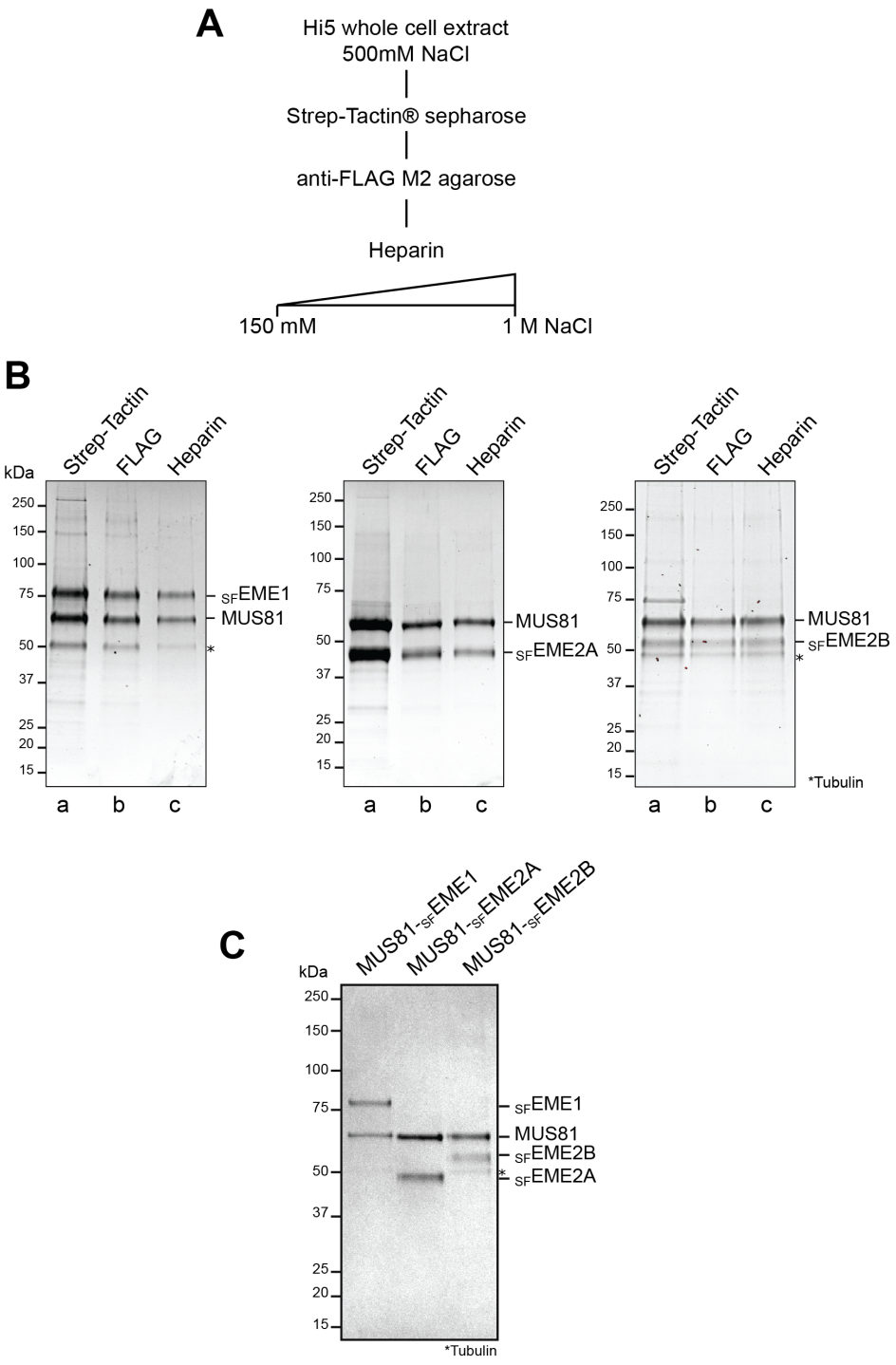

Figure 3.5 Affinity purification of MUS81-$_{SF}$EME1, MUS81-$_{SF}$EME2A and MUS81-$_{SF}$EME2B

A. Hi5 cells expressing MUS81-$_{SF}$EME1, MUS81-$_{SF}$EME2A or MUS81-$_{SF}$EME2B were lysed in high salt lysis buffer and the proteins were purified by affinity chromatography (Section 2.10.1). **B.** SYPRO® Ruby-stained SDS gel (Section 2.7.6) showing the level of purity of the proteins after elution from each column **C.** InstantBlue^{TM}-stained SDS gel (Section 2.7.5) showing purified MUS81-$_{SF}$EME1, MUS81-$_{SF}$EME2A and MUS81-$_{SF}$EME2B.

3.5B, lanes c). MUS81-$_{SF}$EME1, MUS81-$_{SF}$EME2A and MUS81-$_{SF}$EME2B were purified to near homogeneity, as shown in Figure 3.5C.

3.3.1 Determination of the cofactor requirements for optimal activity of the three purified MUS81 complexes

Most enzymes that catalyse the hydrolysis of DNA phosphodiester bonds require Mg^{2+} as a cofactor (Yang et al., 2006). Affinity purified Mus81-Mms4 endonuclease, the *S. cerevisiae* ortholog of human MUS81-EME1, shows optimal nuclease activity at a concentration of approximately 3 mM Mg^{2+} (Ehmsen and Heyer, 2008). To determine the optimal Mg^{2+} concentration for the three purified MUS81 complexes, MUS81-$_{SF}$EME1, MUS81-$_{SF}$EME2A and MUS81-$_{SF}$EME2B were incubated with a 5'-^{32}P-end-labelled 3'-flap synthetic substrate (Section 2.11) in the presence of increasing amounts of $MgCl_2$. The DNA was prepared by annealing partially complementary oligonucleotides, only one of which was ^{32}P-labelled at the 5'-end. Nuclease activities were analysed by neutral PAGE (Section 2.7.3) and the appearance of faster migrating bands indicated the generation of cleaved DNA products (Figure 3.6A). The intensity of the bands corresponding to the cleavage products was quantified by phosphorimaging analysis and product formation was plotted as a percentage of the total radiolabeled DNA (Figure 3.6B, Section 2.7.8). All heterodimers cleaved the 3'-flap substrate efficiently, indicating that, like EME1, EME2A and EME2B form catalytically active complexes with MUS81 *in vitro*. As observed with Mus81-Mms4 (Ehmsen and Heyer, 2008), optimum nuclease activity for MUS81-$_{SF}$EME1, MUS81-$_{SF}$EME2A and MUS81-$_{SF}$EME2B was observed at 2.5 mM $MgCl_2$. Importantly, we did not observe loss of label or fragmentation of the substrate due to the activities of contaminating phosphatases or exonucleases (Figure 3.6 and data not shown). This indicated that the protein preparations did not contain any contaminating activities able to modify the substrate during the incubation time of the cleavage assays.

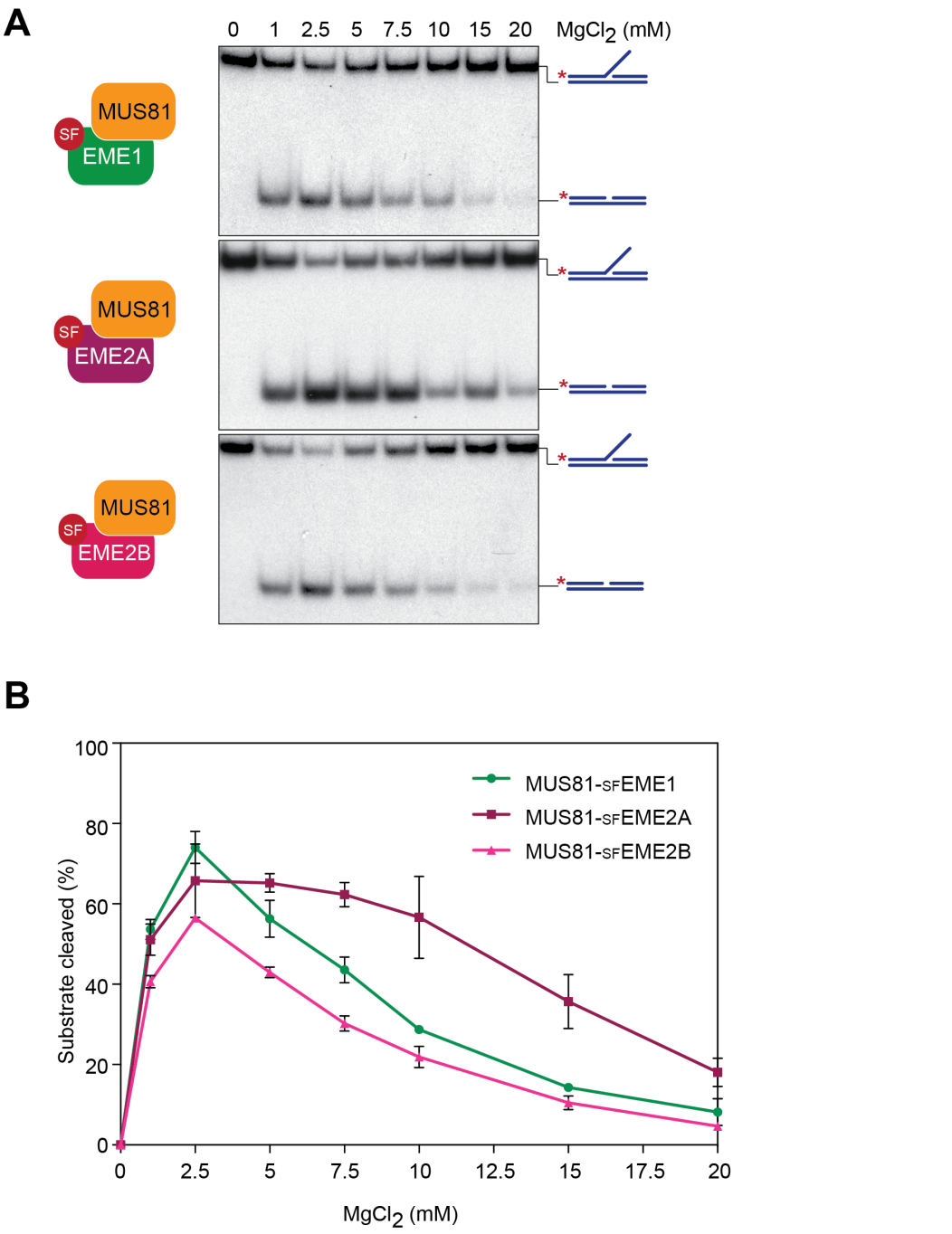

Figure 3.6 Determination of the optimal Mg^{2+} concentration for MUS81-$_{SF}$EME1, MUS81-$_{SF}$EME2A and MUS81-$_{SF}$EME2B nuclease activity on a 3'-flap

A. The 3'-flap synthetic substrate (100 nM) was incubated with purified MUS81-$_{SF}$EME1 (5 nM), MUS81-$_{SF}$EME2A (0.5 nM) or MUS81-$_{SF}$EME2B (5 nM) for 30 min at 37°C (Section 2.11.4). Reactions contained the indicated concentrations of $MgCl_2$ and the products were analysed by neutral PAGE (Section 2.7.3). Red asterisks indicate the ^{32}P-labelled oligonucleotide. **B.** Quantification of the data showed in A was performed by phosphorimaging analysis (Section 2.7.8). Product formation is expressed as a percentage of total radiolabeled DNA. Data are presented as the mean of three experiments (±SEM).

3.4 Substrate specificities of MUS81-$_{SF}$EME1, MUS81-$_{SF}$EME2A and MUS81-$_{SF}$EME2B

Previous studies showed that recombinant *S. cerevisiae* Mus81-Mms4, *S. pombe* Mus81-Eme1 and human MUS81-EME1 preferentially cleave three-way branched structures like 3'-flaps, RFs and nicked HJs (Bastin-Shanower et al., 2003; Ciccia et al., 2003; Gaillard et al., 2003). Also, as shown previously, the activity of MUS81-EME2 (XM_113869) was reported to be 10-fold greater than that of MUS81-EME1 on 3'-flap and splayed-arm substrates (Ciccia et al., 2007). However, in view of the identification of two novel MUS81 complexes, a comparative analysis of the biochemical properties of MUS81-EME1, MUS81-EME2A and MUS81-EME2B was necessary.

To study the substrate specificities of the three endonucleases, a series of model branched DNA substrates were generated by annealing partially complementary oligonucleotides (Section 2.11). These included splayed-arm, 3'-flap, 5'-flap, replication fork and Holliday junction (HJ) structures, all containing a common 5'-^{32}P-end-labelled oligonucleotide (X0.1) (Figure 3.7). Specifically, the HJs used in this analysis have a mobile homologous core (mobile HJ), an immobile non-homologous core (static HJ) or a nick adjacent to the branch point (nicked HJ). Reactions were performed with a fixed amount of non-radiolabeled substrate and 'spiked' with a negligible concentration of 5'-^{32}P-end-labelled DNA. Increasing amounts of MUS81-$_{SF}$EME1, MUS81-$_{SF}$EME2A or MUS81-$_{SF}$EME2B were mixed with the DNA substrates and the cleavage activities were analysed by neutral PAGE (Section 2.7.3).

MUS81-$_{SF}$EME1 preferentially cleaved the 3'-flap, replication fork and nicked HJ substrates, as previously described (Ciccia et al., 2003). Interestingly, the activity of MUS81-$_{SF}$EME2A was higher than that of MUS81-$_{SF}$EME1 on each of the substrates analysed (Figure 3.7). Also, cleavage of the 3'-flap and replication fork resulted in the formation of two products. Reactions performed with limiting amounts of substrate resulted in the complete conversion of one product into the other (data not shown), suggesting that MUS81-$_{SF}$EME2A processes 3'-flaps and

replication forks in a two-step reaction. The cleavage mechanism of 3'-flaps by MUS81-$_{SF}$EME2A will be described in more detail in Section 3.6. In contrast to MUS81-$_{SF}$EME1, MUS81-$_{SF}$EME2A was also able to cleave the 5'-flap substrate.

Interestingly, the activity profile of MUS81-$_{SF}$EME2B was closer to that of MUS81-$_{SF}$EME1 than to that of MUS81-$_{SF}$EME2A. MUS81-$_{SF}$EME2B cleaved the 3'-flap DNA with an efficiency that was comparable to that of MUS81-$_{SF}$EME1, but showed moderate activity towards replication fork and nicked HJ substrates. In contrast to MUS81-$_{SF}$EME2A, few cleavage products were detected when MUS81-$_{SF}$EME2B was incubated with splayed-arm, 5'-flap, mobile and static HJs. Finally, quantification of the reaction products by phosphorimaging revealed that, consistent with results obtained with Mus81-Mms4 from *S. cerevisiae* and Mus81-Eme1 from *S. pombe* (Chang et al., 2008; Fricke et al., 2005; Gaillard et al., 2003; Osman et al., 2003; Whitby et al., 2003), the nicked HJ is the preferred substrate of MUS81-$_{SF}$EME1 whereas MUS81-$_{SF}$EME2A preferentially cleaves 3'-flaps and replication forks (Figure 3.8).

3.5 Purification of the catalytically inactive MUS81^{D307A}-EME2A

To determine whether all the activities described in the previous section were intrinsic to MUS81-$_{SF}$EME2A, catalytically inactive MUS81^{D307A}-$_{SF}$EME2A complex was purified using a similar scheme to the wild-type protein. Inactive MUS81 was obtained by alanine mutagenesis of the residue D307 (D307A), as previously reported (Taylor and McGowan, 2008). Indeed, on the basis of structural studies performed on the related nucleases *Pyrococcus furiosus* Hef and *Aeropyrum pernix* XPF (Newman et al., 2005; Nishino et al., 2003), aspartic acid D307 of human MUS81 was predicted to be critical for catalysis. MUS81^{D307A} and $_{SF}$EME2A were cloned in the pFL bicistronic expression vector and the bacmid DNA was generated as described in Section 2.9. Baculovirus expression and purification of MUS81^{D307A}-$_{SF}$EME2A were performed as previously described for MUS81-$_{SF}$EME2A. The complex was purified to homogeneity and its purity was similar to that of MUS81-$_{SF}$EME2A (Figure 3.9A). The activities of MUS81-$_{SF}$EME2A and MUS81^{D307A}-$_{SF}$EME2A were compared on 3'-flap and 5'-flap

substrates under the same reaction conditions. As expected, MUS81-$_{SF}$EME2A efficiently cleaved the two DNA structures, whereas no cleavage was detected when the DNA was incubated with catalytically inactive MUS81^{D307A}-$_{SF}$EME2A (Figure 3.9B). These results indicate that all the activities observed with MUS81-$_{SF}$EME2A are strictly dependent on its catalytic site.

3.6 MUS81-EME1 and MUS81-EME2A exhibit distinct DNA cleavage mechanisms

In the previous section it was shown that the activity of MUS81-EME2B was comparable to that of MUS81-EME1. On the basis of this, and other, results we hypothesised that the nuclease activity of MUS81-EME2B might not be physiologically relevant (details will be provided in Chapter 4). Conversely, significant differences were observed in the cleavage efficiency and substrate specificities of MUS81-EME2A and MUS81-EME1. Therefore, to investigate the basis of these differences, the DNA cleavage mechanism of MUS81-EME1 and MUS81-EME2A was determined by comparing their pattern of cleavage with 3'-flap, 5'-flap, immobile HJ and D-loop substrates.

Recombinant affinity purified *S. cerevisiae* Mus81-Mms4 processes a 3'-flap substrate by recognising the 5'-end of the DNA strand located downstream of the flap and by cleaving the duplex DNA 3-7 nucleotides on the 5'-side of the branch point (Bastin-Shanower et al., 2003). To test whether MUS81-EME1 and MUS81-EME2A share the same pattern of cleavage, purified MUS81-$_{SF}$EME1 or MUS81-$_{SF}$EME2A complex were incubated with 3'-flap substrates, 5'-^{32}P-end-labelled on strand 1, 2 or 3, as indicated in Figure 3.10B. Reaction products were analysed by denaturing PAGE (Figure 3.10A, Section 2.7.4) and ^{32}P-labelled marker oligonucleotides were used to determine the position of the incisions (data not shown). Both MUS81-$_{SF}$EME1 and MUS81-$_{SF}$EME2A showed the same incision sites (5'-T↓G↓C↓C↓T↓T↓G↓C-3'), with three major consecutive cuts (5'-C↓T↓T↓G-3') (Figure 3.9A-B). All the incisions were positioned 3 to 7 nucleotides on the 5'-side of the branch point; therefore, the cleavage pattern observed on

Figure 3.7 Substrate specificities of MUS81-$_{SF}$EME1, MUS81-$_{SF}$EME2A and MUS81-$_{SF}$EME2B
The indicated DNA substrates (100 nM) were incubated with the indicated concentrations of purified MUS81-$_{SF}$EME1, MUS81-$_{SF}$EME2A and MUS81-$_{SF}$EME2B for 30 min at 37°C (Section 2.11.5). Reactions were analysed by neutral PAGE (Section 2.7.3). Red asterisks indicate ^{32}P-labelled oligonucleotides.

Figure 3.8 Quantification of the nuclease activities of MUS81-$_{SF}$EME1, MUS81-$_{SF}$EME2A and MUS81-$_{SF}$EME2B
Quantification of the data shown in Figure 4.1 was performed by phosphorimaging analysis (Section 2.7.6). Product formation is expressed as a percentage of total radiolabeled DNA. Data are presented as the mean of three experiments (±SEM).

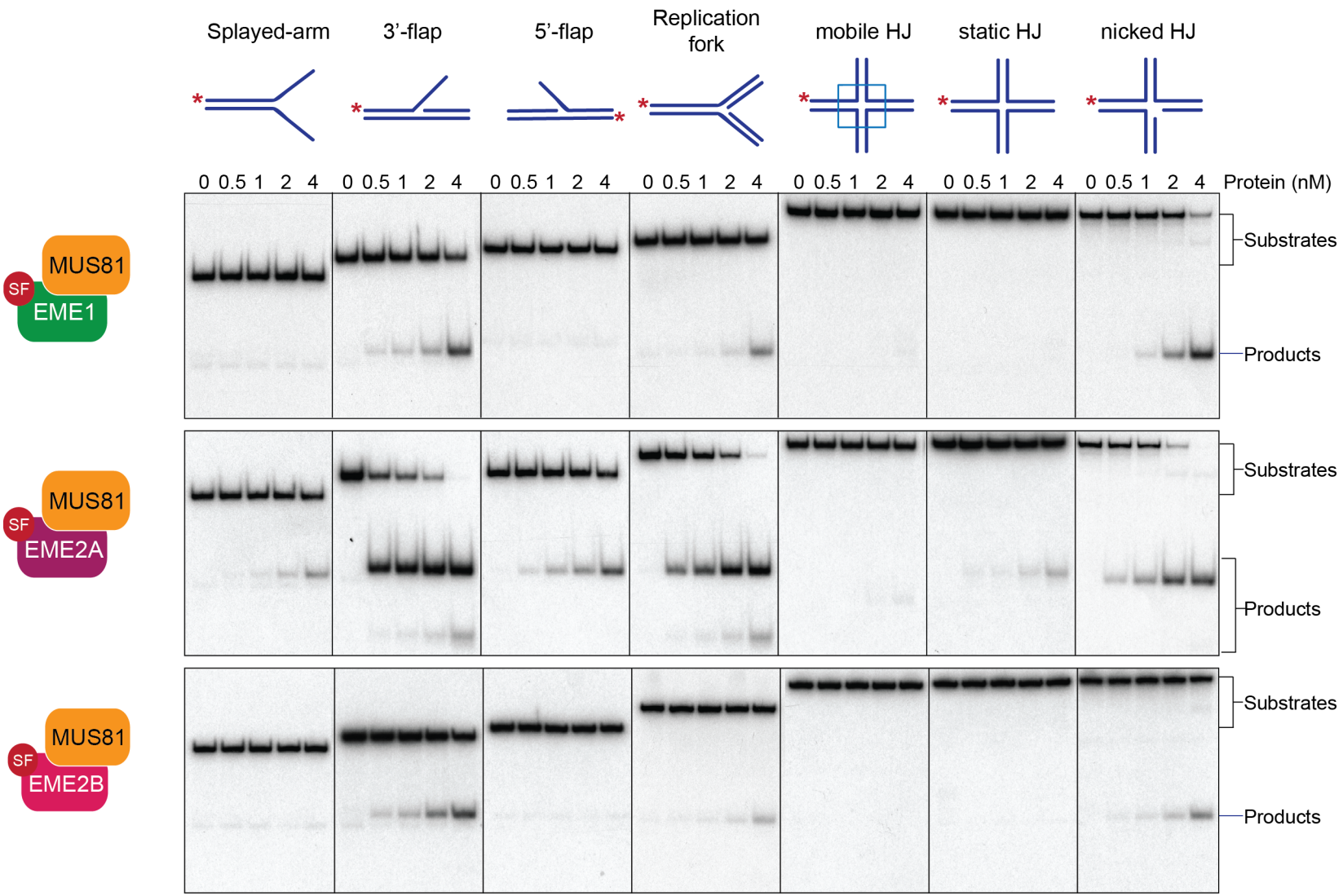
Splayed-arm
3'-flap
5'-flap
Replication fork
mobile HJ
static HJ
nicked HJ
0 0.5 1 2 4
Protein (nM)
MUS81
SF
EME1
MUS81
SF
EME2A
MUS81
SF
EME2B
Substrates
Products
Substrates
Products
Substrates
Products

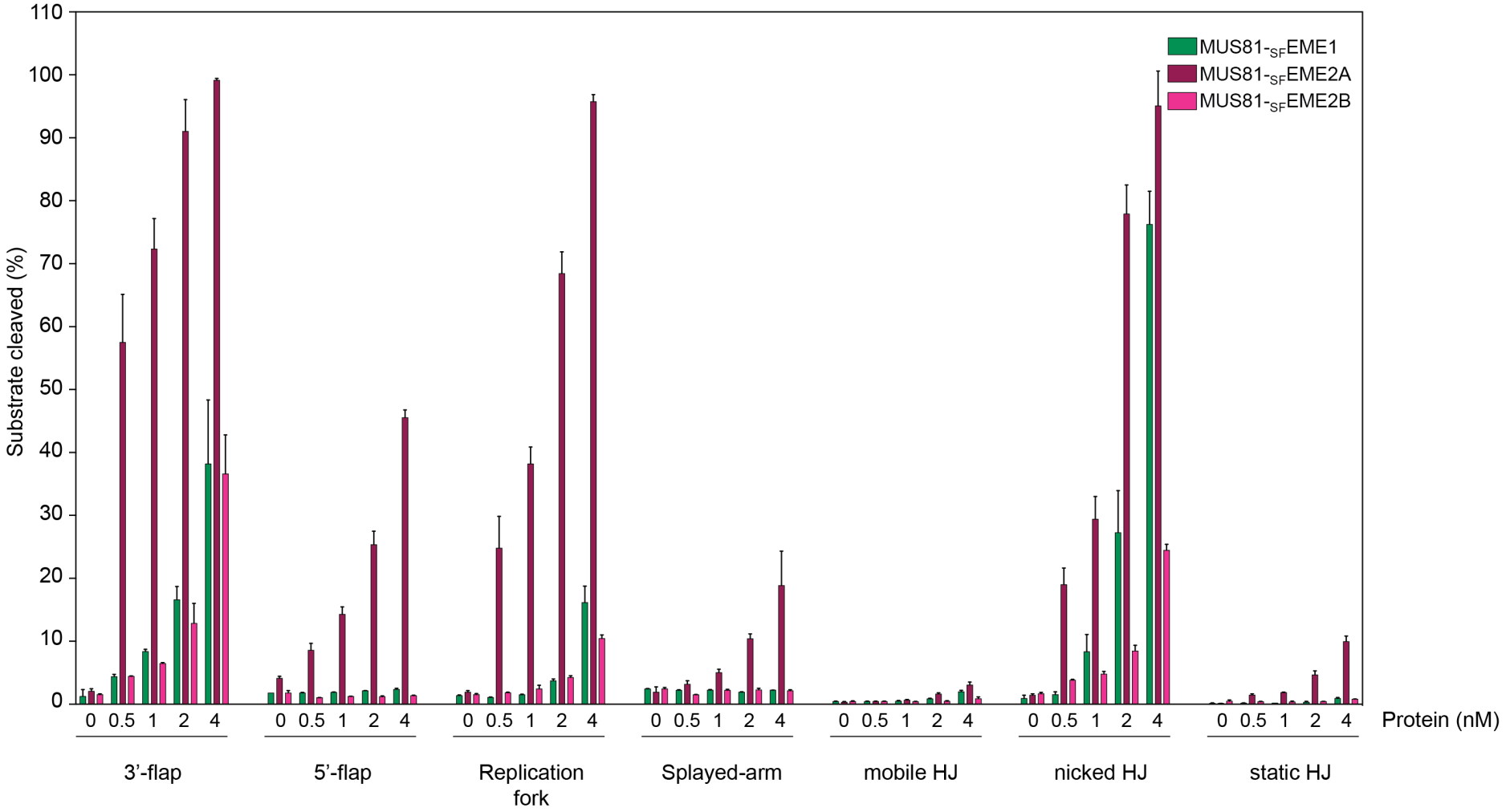
Substrate cleaved (%)
110
100
90
80
70
60
50
40
30
20
10
0
MUS81-SFEME1
MUS81-SFEME2A
MUS81-SFEME2B
0 0.5 1 2 4
Protein (nM)
3'-flap
5'-flap
Replication fork
Splayed-arm
mobile HJ
nicked HJ
static HJ

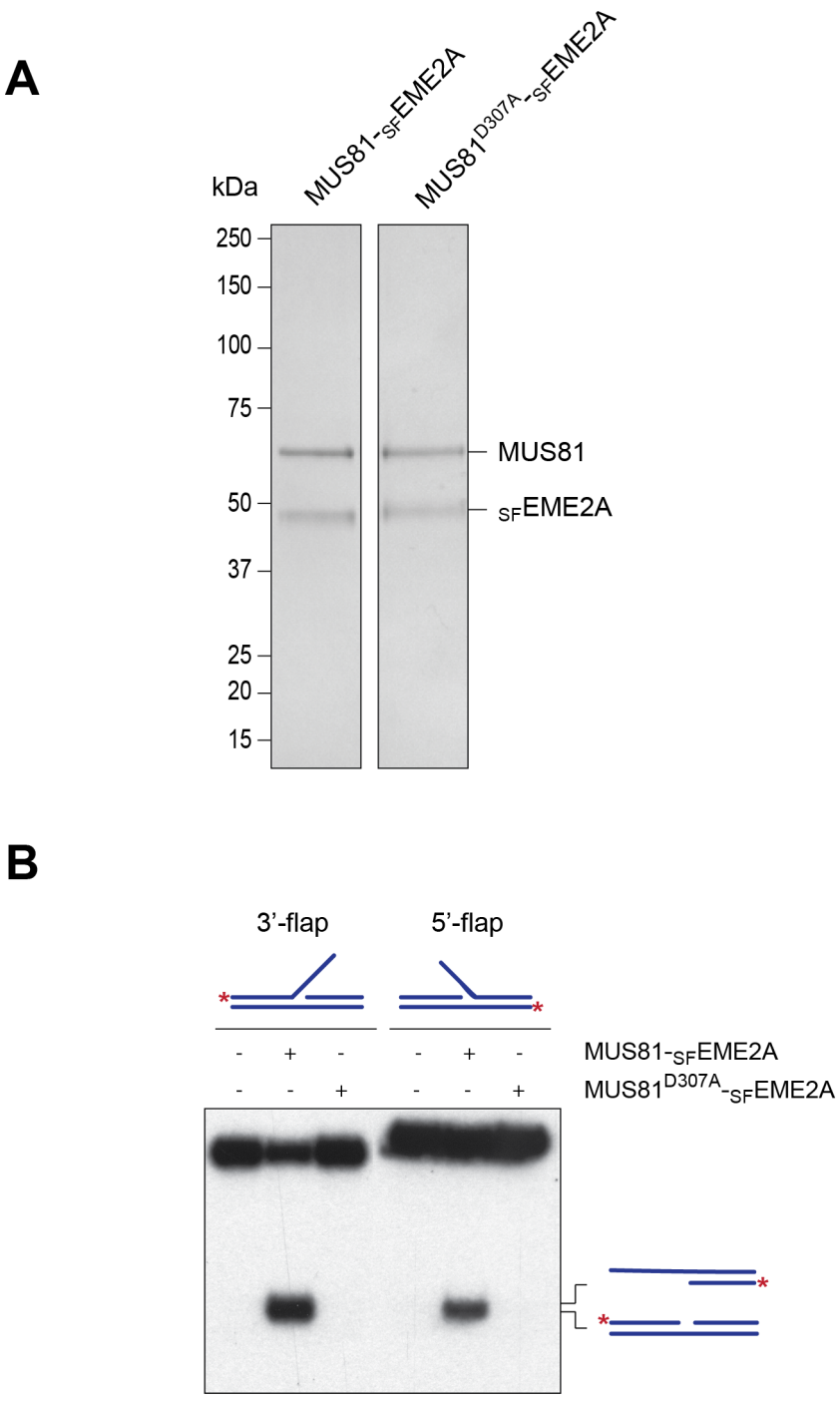

Figure 3.9 Affinity purification of the catalytically inactive MUS81^{D307A}-$_{SF}$EME2A

A. InstantBlue^{TM}-stained SDS gel (Section 2.7.5) showing purified MUS81-$_{SF}$EME2A and MUS81^{D307A}-$_{SF}$EME2A. **B.** The 3'-flap and 5'-flap synthetic substrates (100 nM) were incubated with purified MUS81-$_{SF}$EME2A (2 nM) or catalytically inactive MUS81^{D307A}-$_{SF}$EME2A (2 nM) for 30 min at 37°C (Section 2.11.4). Reaction products were analysed by neutral PAGE (Section 2.7.3). Red asterisks indicate ^{32}P-labeled oligonucleotides.

a 3'-flap structure with MUS81-$_{SF}$EME1 and MUS81-$_{SF}$EME2A was consistent with the incisions performed by yeast Mus81-Mms4. However, we observed that, unlike MUS81-$_{SF}$EME1, MUS81-$_{SF}$EME2 performed a minor incision on the strand opposite to that containing the flap at the site (5'-CT↓CC-3') (Figure 3.10B).

As shown in Section 3.4, in contrast to MUS81-$_{SF}$EME1, MUS81-$_{SF}$EME2A was found to process 5'-flap substrates. To gain further insights into its cleavage mechanism, MUS81-$_{SF}$EME2A was incubated with 5'-flap structures, 5'-^{32}P-end-labelled on strand 1, 2 or 3 (Figure 3.11C). Reactions were analysed by neutral PAGE (Figure 3.11A, Section 2.7.3) and ^{32}P-labelled marker oligonucleotides were used to map the cleavage sites using denaturing PAGE (Figure 3.11B and data not shown, Section 2.7.4). As a control, MUS81-$_{SF}$EME1 was incubated with the 5'-flaps but no DNA cleavage was observed (Section 3.4, Figure 3.11A-B). As a positive control, the cleavage mechanism of MUS81-$_{SF}$EME2A was compared to that of the purified HJ resolvase GEN1$^{1-527}$, which removes the flap strand by cleaving at one of three main sites: 5'-GC↓TCCA↓T↓GT-3' (Figure 3.11) (Rass et al., 2010). Surprisingly, the pattern of cleavage of MUS81-$_{SF}$EME2A was very different from that of GEN1$^{1-527}$ as MUS81-$_{SF}$EME2A performed multiple incisions on the duplex DNA 3-11 nucleotides on the 5'-side of the branch point (5'-G↓C↓AA↓A↓GA↓T↓G↓T-3') and on the strand opposite to the flap (5'-T↓C↓G↓TT↓C↓CGTGA↓C-3') (Figure 3.11B-C). Hence, although MUS81-$_{SF}$EME1 and MUS81-$_{SF}$EME2 are able to process a 3'-flap structure in the same conserved way, MUS81-$_{SF}$EME2A has the remarkable ability to cleave a 5'-flap substrate by incising the strand complementary to that containing the flap.

Next, we considered the possibility that the higher cleavage efficiency displayed by MUS81-$_{SF}$EME2A when compared to MUS81-$_{SF}$EME1 and MUS81-$_{SF}$EME2B could account for its ability to cleave a 5'-flap substrate. To test this hypothesis, the activities of MUS81-$_{SF}$EME1, MUS81-$_{SF}$EME2A and MUS81-$_{SF}$EME2B were first normalised on a 3'-flap and nicked HJ substrates and then compared on a 5'-flap, using a time course experiment (Figure 3.12A). In conditions in which the three MUS81 complexes exhibited the same level of activity on the 3'-flap and nicked HJ, MUS81-$_{SF}$EME2A was still able to cut the 5'-flap structure, whereas little or no

cleavage was observed with MUS81-$_{SF}$EME1 and MUS81-$_{SF}$EME2B (Figure 3.12B). In addition, we wanted to determine whether MUS81-$_{SF}$EME1 was able to process 5'-flaps in the presence of Mn^{2+}, a cofactor that decreases the stringency of the endonucleolytic reaction (Loeb and Kunkel, 1982; Vermote and Halford, 1992). MUS81-$_{SF}$EME1 and MUS81-$_{SF}$EME2A were mixed with the DNA in the presence of increasing amounts of $MnCl_2$ (Figure 3.13). Reaction products were analysed by neutral PAGE (Section 2.7.3) and quantified by phosphorimaging (Section 2.7.8). As observed with Mg^{2+}, the 5'-flap substrate was cleaved efficiently by MUS81-$_{SF}$EME2A but not by MUS81-$_{SF}$EME1, indicating that the efficiency of the reaction is independent of the divalent metal ion used as cofactor.

Given that, like the HJ resolvase GEN1, MUS81-$_{SF}$EME2A was able to process 5'-flaps, we investigated in more detail the mechanistic differences between MUS81-$_{SF}$EME1 and MUS81-$_{SF}$EME2A with a HJ substrate. MUS81-$_{SF}$EME2A cleaved the HJs more efficiently than MUS81-$_{SF}$EME1, as shown in Figures 3.7 and 3.8. In order to be able to determine and compare their patterns of cleavage, MUS81-$_{SF}$EME1 and MUS81-$_{SF}$EME2A were incubated with immobile HJs, 5'-^{32}P-end-labelled on strand 1, 2, 3 or 4, as illustrated in Figure 3.14B. Reaction products were analysed by denaturing PAGE (Section 2.7.4) and ^{32}P-labelled marker oligonucleotides were used to determine the positions of the cuts (Figure 3.14A). In contrast to GEN1, which cuts symmetrically across the junction (Ip et al., 2008), both MUS81 complexes introduced multiple incisions in all four strands of the immobile HJ (Figure 3.14A-B). Specifically, the major cleavage sites by MUS81-$_{SF}$EME1 were closer to the branch point compared to those of MUS81-$_{SF}$EME2A and both enzymes cleaved the junction 6 nucleotides to the 5'-side of the branch point of strand 3 (5'-CA↓AC-3') and 5 nucleotides on the 5'-side of the branch point of strand 4 (5'-CC↓TC-3'), as illustrated in Figure 3.14B.

D-loops are intermediate structures of HR-mediated repair of both one- and two-ended DSBs (Section 1.2.2) as they are generated by RAD51-mediated 3'-ended strand invasion. The formation of D-loop structures is also very important in the context of telomere maintenance: at telomeres, D-loops are generated when the 3'-G-rich single-stranded overhangs invade duplex telomeric DNA to form a lariat-like structure referred to as T-loop, which protects chromosome ends from being

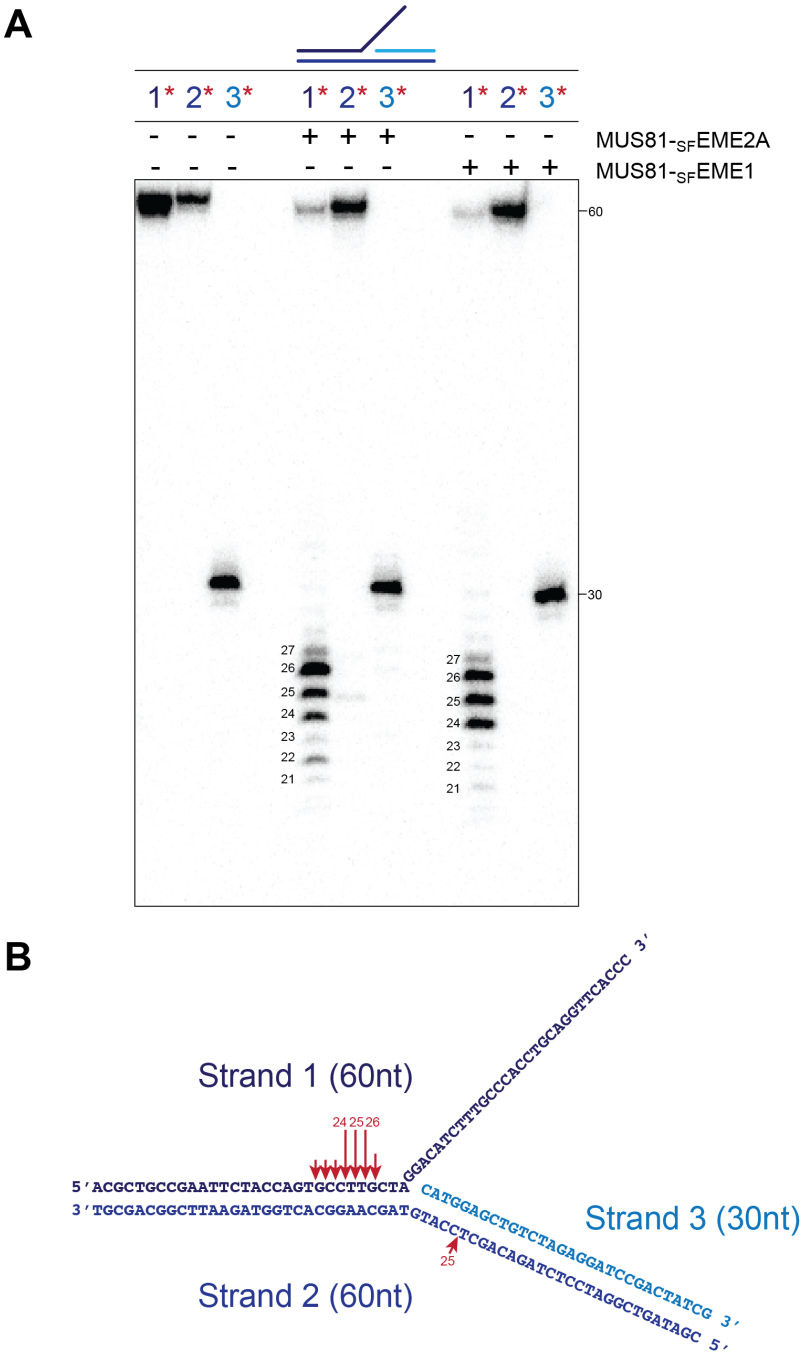

Figure 3.10 Cleavage of a 3'-flap substrate by MUS81-$_{SF}$EME1 and MUS81-$_{SF}$EME2A

A. The 3'-flap substrate (100 nM) was incubated with purified MUS81-$_{SF}$EME1 (5 nM) or MUS81-$_{SF}$EME2A (2 nM) for 15 min at 37°C (Section 2.11.5). Reaction products were analysed by denaturing PAGE (Section 2.7.4). Numbers with red asterisks indicate the ^{32}P-labelled strands. The size of the intact and cleaved oligonucleotides is indicated. **B.** Schematic representation of the 3'-flap synthetic substrate. Red arrows indicate the sites of cleavage by MUS81-$_{SF}$EME1 and MUS81-$_{SF}$EME2A. Arrow size is proportional to the relative efficiency of the cleavage.

Figure 3.11 MUS81-$_{SF}$EME2A cleaves a 5'-flap substrate
A-B. The 5'-flap substrate (3 nM) was incubated with purified MUS81-$_{SF}$EME1 (1 nM) and MUS81-$_{SF}$EME2A (1 nM) for 30 min at 37°C (Section 2.11.5). Purified GEN1$^{1-527}$ (0.5 nM) was used as a positive control (10 min incubation at 37°C). Samples were divided in half and analysed by neutral PAGE (**A**, Section 2.7.3) and denaturing PAGE (**B**, Section 2.7.4). Red asterisks indicate ^{32}P-labelled oligonucleotides. In **B**, the sizes of intact and cleaved oligonucleotides are indicated. **C.** Schematic representation of the 5'-flap synthetic substrate showing the sites of cleavage introduced by MUS81-$_{SF}$EME2A (red arrows). Green arrows indicate the sites of cleavage by GEN1$^{1-527}$. Arrow size is proportional to the relative cleavage efficiency.

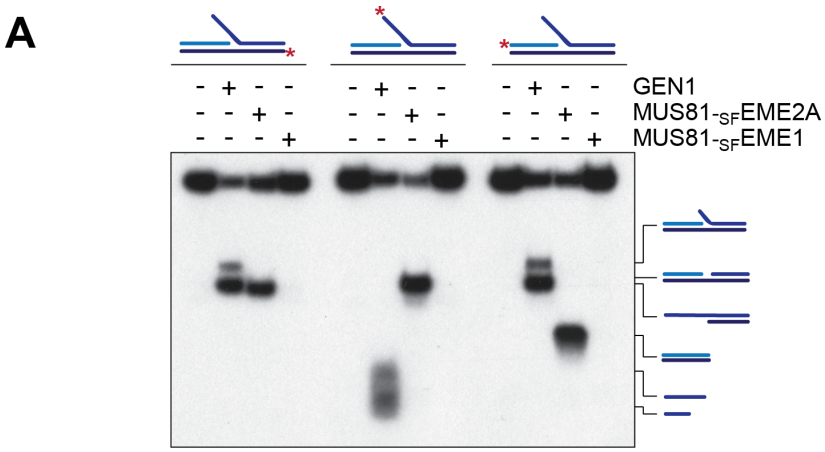
A
GEN1
MUS81-SFEME2A
MUS81-SFEME1

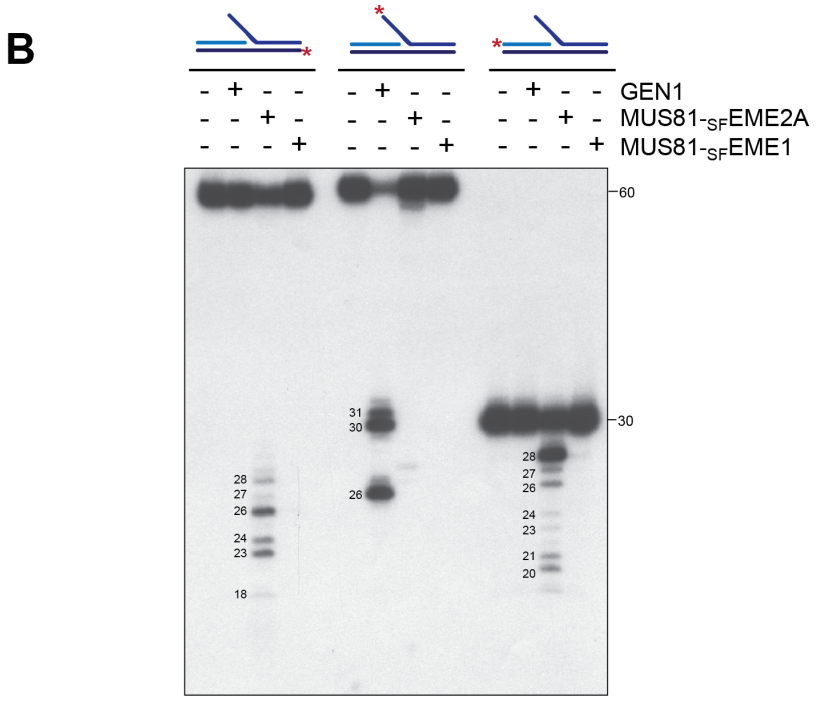
B
GEN1
MUS81-SFEME2A
MUS81-SFEME1
60
30
31
30
26
28
27
26
24
23
18
28
27
26
24
23
21
20

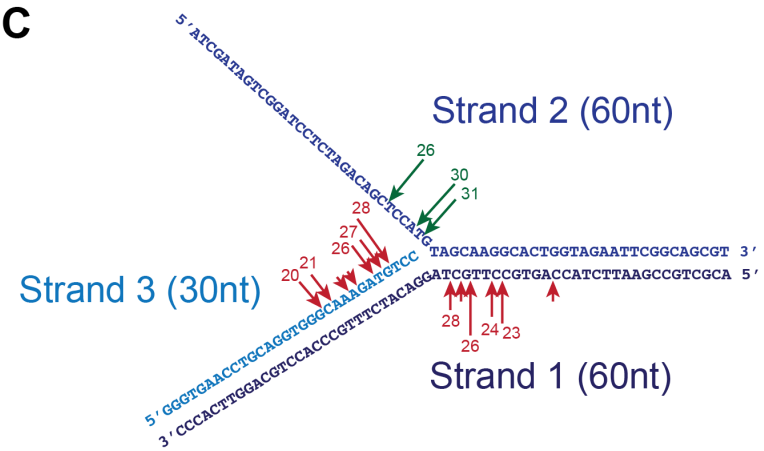
C
5′ATCGATAGTCGGATCCTCTAGACAGCTCCAAG
Strand 2 (60nt)
26
30
31
28
27
26
TAGCAAGGCACTGGTAGAATTCGGCAGCGT 3′
20
21
Strand 3 (30nt)
5′GGGTGAACCTGCAGGTGGGCAAAGATGTCC
ATCGTTCCGTGACCATCTTAAGCCGTCGCA 5′
28
24
23
26
3′CCCACTTGGACGTCCACCCGTTTCTACAGG
Strand 1 (60nt)

Figure 3.12 Comparison of the activities of purified MUS81-$_{SF}$EME1, MUS81-$_{SF}$EME2A and MUS81-$_{SF}$EME2B on a 3'-flap, nicked HJ and 5'-flap

A. The indicated substrates (100 nM) were incubated with purified MUS81-$_{SF}$EME1 (5 nM), MUS81-$_{SF}$EME2A (1 nM) or MUS81-$_{SF}$EME2B (5 nM) at 37°C for the indicated times (Section 2.11.5). Reaction products were analysed by neutral PAGE (Section 2.7.3). Red asterisks indicate ^{32}P-labelled oligonucleotides. **B.** Quantification of the data shown in A was performed by phosphorimager analysis (Section 2.7.8). Product formation is expressed as a percentage of total radiolabeled DNA. Data are presented as the mean of three experiments (±SEM).

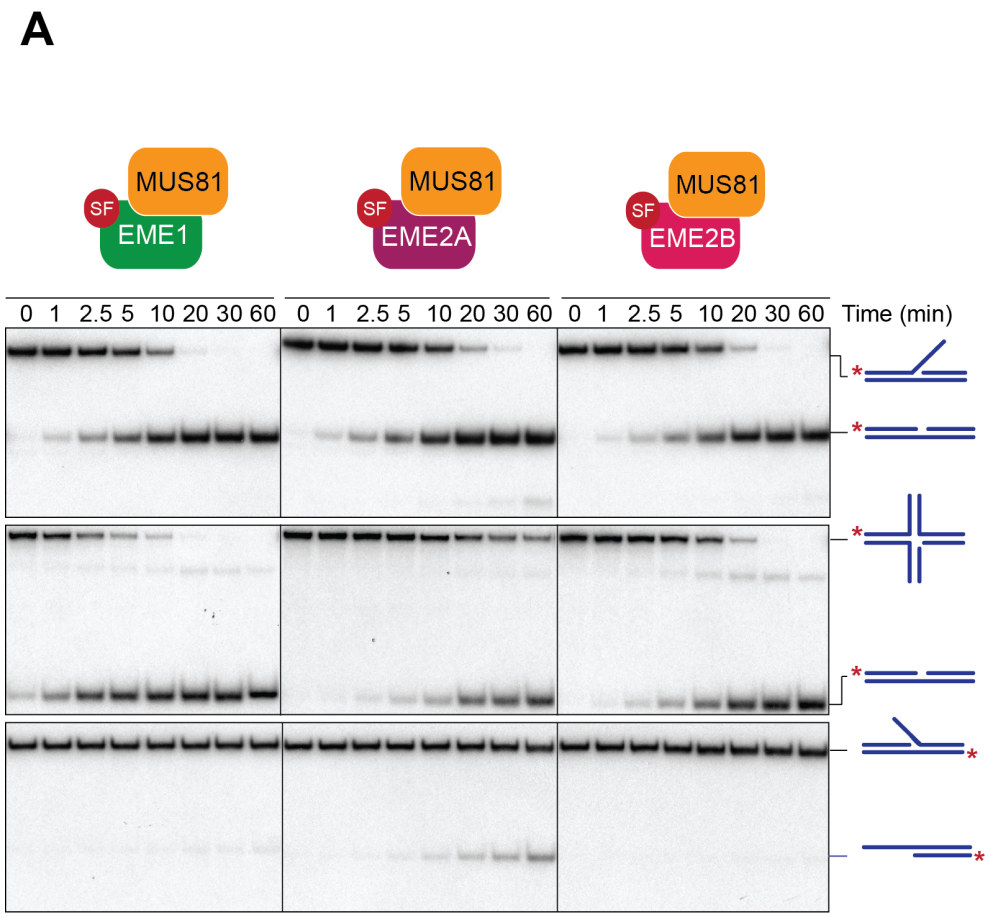
A
MUS81
SF
EME1
MUS81
SF
EME2A
MUS81
SF
EME2B
0 1 2.5 5 10 20 30 60
0 1 2.5 5 10 20 30 60
0 1 2.5 5 10 20 30 60
Time (min)
*
*
*
*
*
*

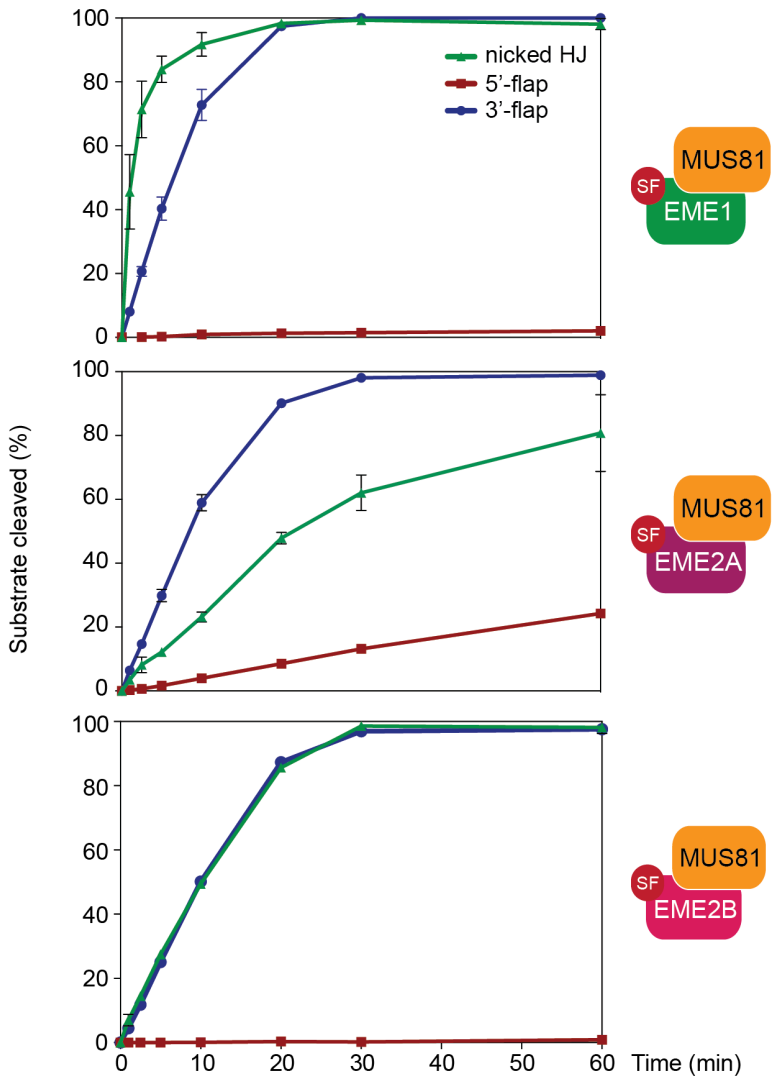
B
Substrate cleaved (%)
100
80
60
40
20
0
nicked HJ
5'-flap
3'-flap
MUS81
SF
EME1
MUS81
SF
EME2A
MUS81
SF
EME2B
0
10
20
30
40
50
60
Time (min)

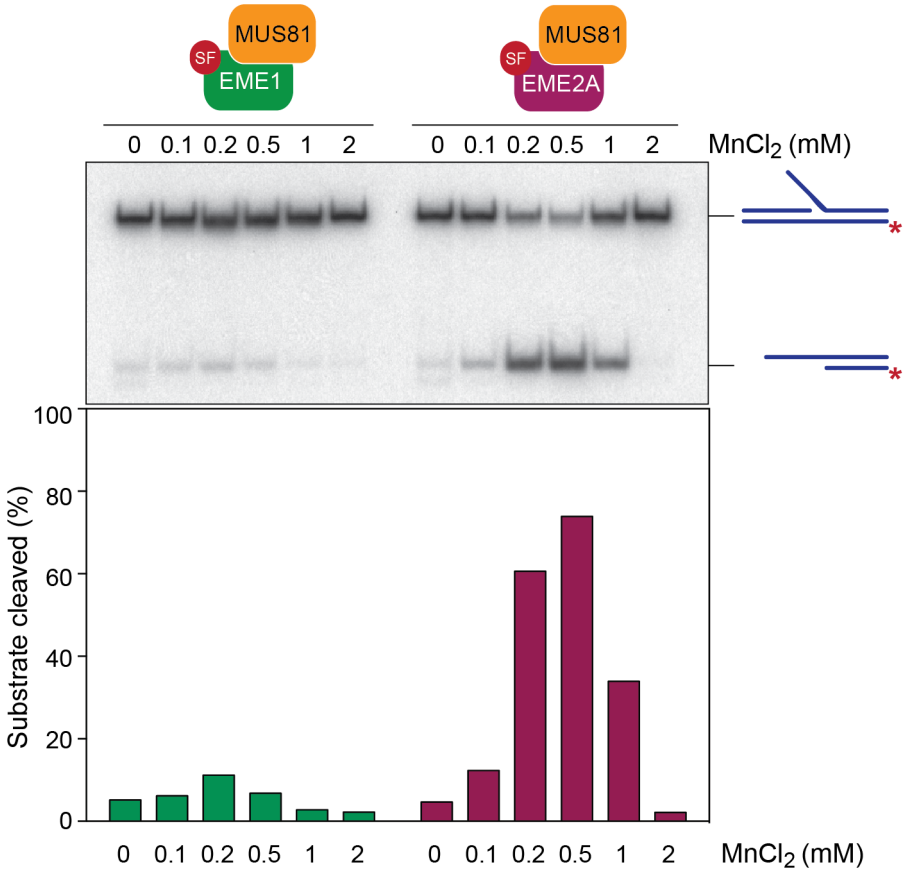

Figure 3.13 Comparison of the activities of MUS81-$_{SF}$EME1 and MUS81-$_{SF}$EME2A on a 5'-flap using $MnCl_2$ as a cofactor
The 5'-flap substrate (100 nM) was incubated with purified MUS81-$_{SF}$EME1 (4 nM) or MUS81-$_{SF}$EME2A (1 nM) for 30 min at 37°C (Section 2.11.5). Reactions contained the indicated concentrations of $MnCl_2$ and were analysed by neutral PAGE (Section 2.7.3). Red asterisks indicate ^{32}P-labelled oligonucleotides. Quantification was performed by phosphorimager analysis (Section 2.7.8). Product formation is expressed as a percentage of total radiolabeled DNA.

Figure 3.14 Comparison of the activities of MUS81-$_{SF}$EME1 and MUS81-$_{SF}$EME2A on an immobile HJ

A. The immobile HJ (approximately 3 nM), 5'-^{32}P-end-labeled on strands 1, 2, 3 or 4, was incubated with purified MUS81-$_{SF}$EME1 (5 nM) or MUS81-$_{SF}$EME2A (1 nM) for 30 min at 37°C (Section 2.11.5). Reaction products were analysed by denaturing PAGE (Section 2.7.4). Red asterisks indicate ^{32}P-labelled oligonucleotides. The sizes of intact and cleaved oligonucleotides is indicated. M = 5'-^{32}P-end-labeled marker oligonucleotides (Section 2.11.4). All the reactions shown were analysed in the same gel. **B.** Schematic representation of the static HJ. Red arrows indicate the sites of cleavage by MUS81-$_{SF}$EME1 or MUS81-$_{SF}$EME2A. Arrow size is proportional to the relative efficiency of the cleavage.

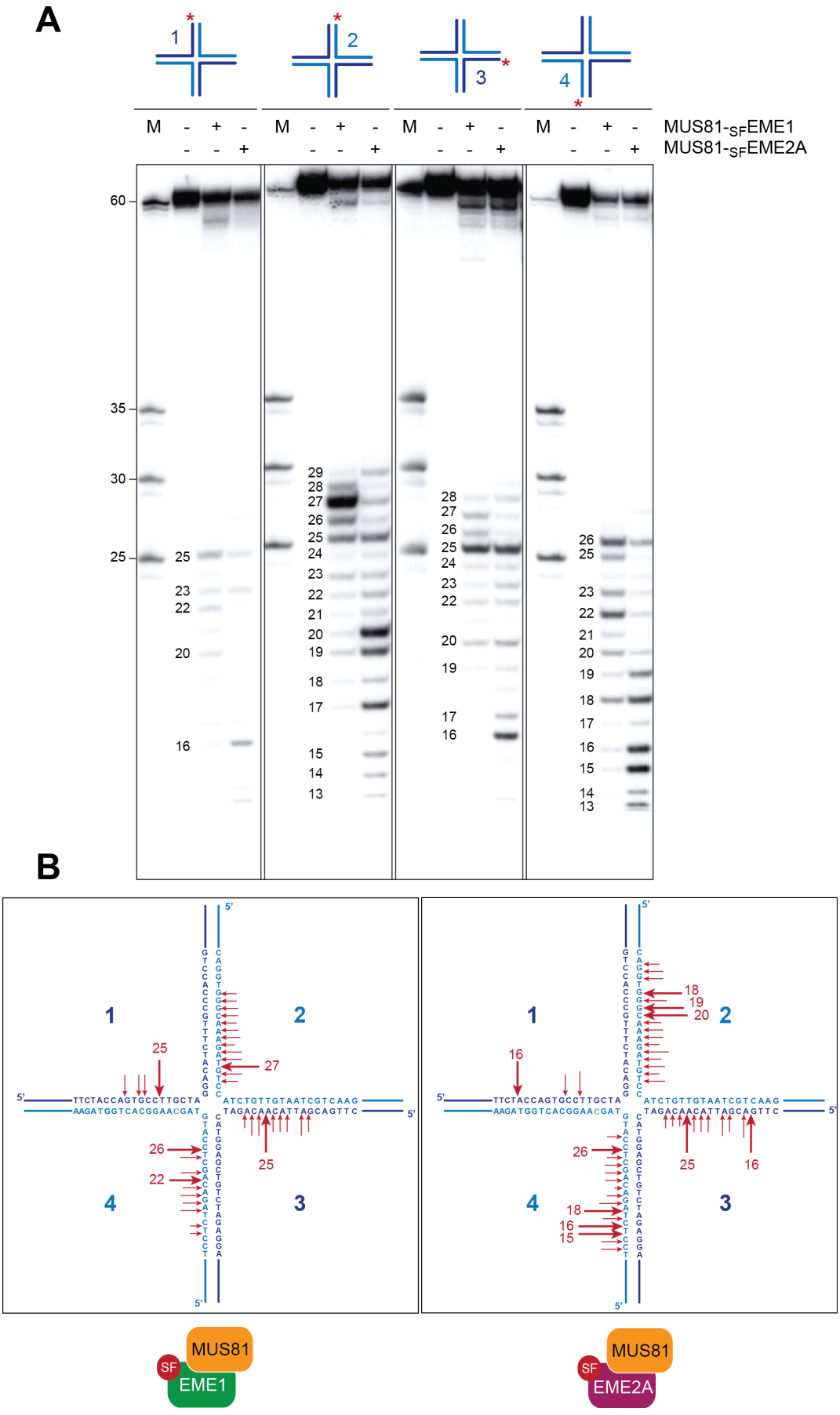
A
1
2
3
4
M - + - M - + - M - + - M - + -
MUS81-SFEME1
MUS81-SFEME2A
60
35
30
25
B
MUS81
SF
EME1
MUS81
SF
EME2A

Figure 3.15 Comparison of the activities of MUS81-$_{SF}$EME1 and MUS81-$_{SF}$EME2A on a D-loop structure

A. Schematic representation of the D-loop structure, indicating the strands and oligo lengths. **B-C.** The D-loop structure (100 nM), 5'-^{32}P-end-labeled on strands DL-0, DL-1 or DL-2, was incubated with purified MUS81-$_{SF}$EME1 (5 nM) or MUS81-$_{SF}$EME2A (5 nM) for 30 min at 37°C (Section 2.11.5). Samples were divided in half and analysed by neutral PAGE (**B**, Section 2.7.3) and by denaturing PAGE (**C**, Section 2.7.4). Red asterisks indicate ^{32}P-labelled oligonucleotides. In **C**, the size of the intact and cleaved oligonucleotides is indicated. M = 5'-^{32}P-end-labeled marker oligonucleotides (Section 2.11.4).

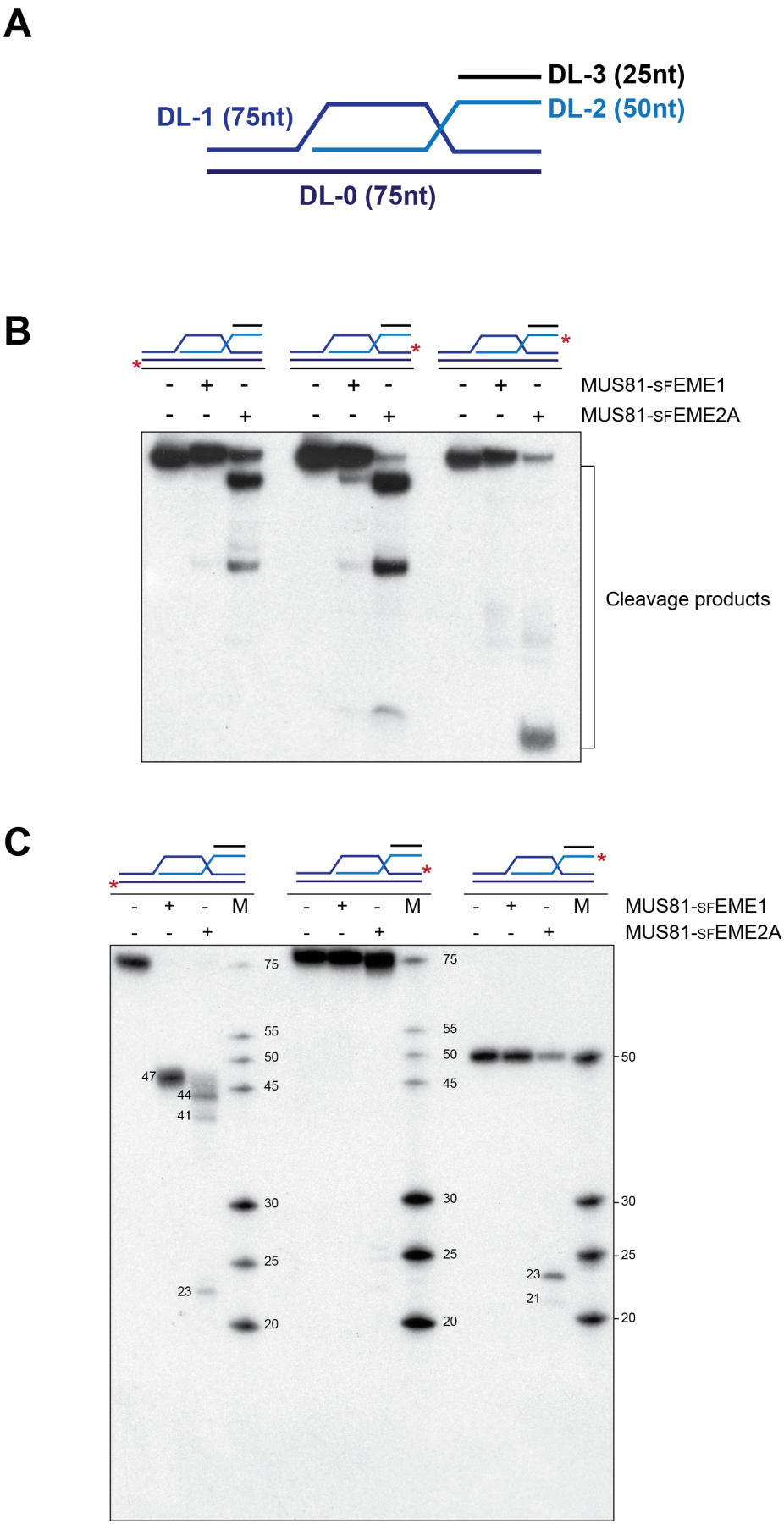
A
DL-3 (25nt)
DL-2 (50nt)
DL-1 (75nt)
DL-0 (75nt)
B
MUS81-sFEME1
MUS81-sFEME2A
Cleavage products
C
MUS81-sFEME1
MUS81-sFEME2A
M
75
55
50
45
47
44
41
30
25
23
20
21

Figure 3.16 Analysis of the activities of MUS81-$_{SF}$EME1 and MUS81-$_{SF}$EME2A on a D-loop structure

A. The D-loop structure (100 nM), 5'-^{32}P-end-labeled on strands DL-0, DL-1 or DL-2, was incubated with MUS81-$_{SF}$EME2A (5 nM) at 37°C for the indicated times (Section 2.11.5). Reactions were analysed by neutral PAGE (Section 2.7.3). Red asterisks indicate ^{32}P-labelled oligonucleotides. **B.** Schematic representation of the D-loop substrate. Red arrows indicate the sites of cleavage by MUS81-$_{SF}$EME1 or MUS81-$_{SF}$EME2A. Arrow size is proportional to the relative efficiency of the cleavage.

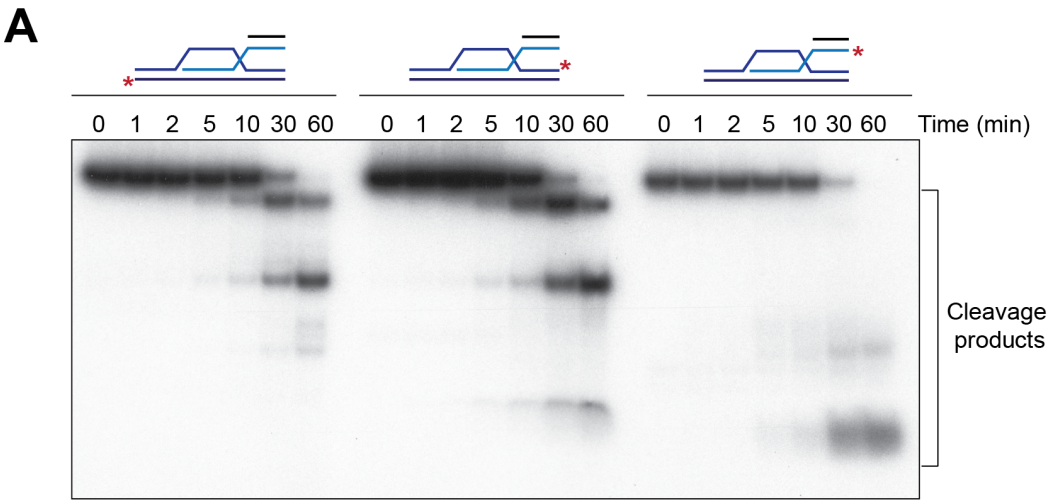
A
0 1 2 5 10 30 60
0 1 2 5 10 30 60
0 1 2 5 10 30 60
Time (min)
Cleavage products

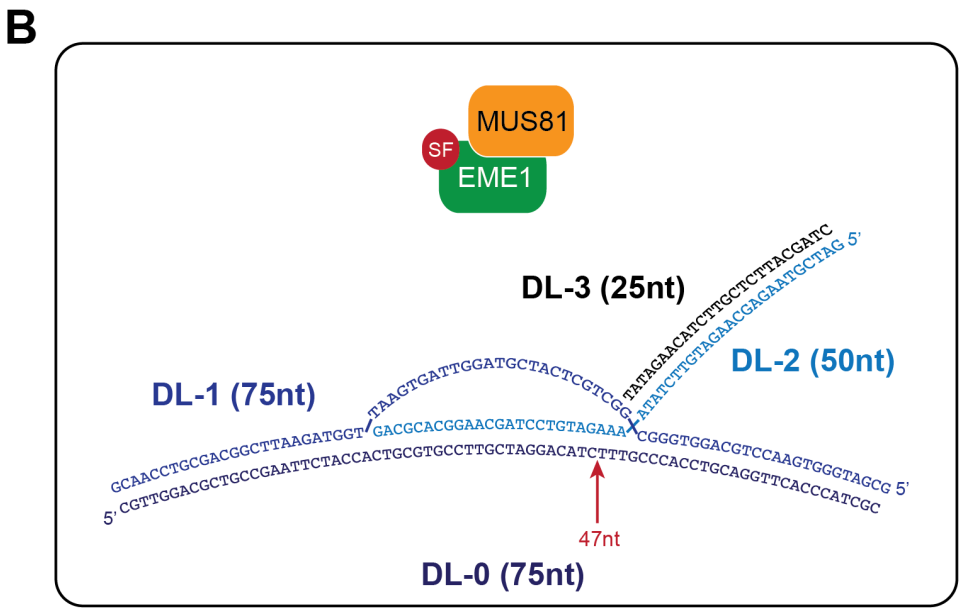
B
MUS81
SF
EME1
DL-3 (25nt)
DL-2 (50nt)
DL-1 (75nt)
TAAGTGATTGGATGCTACTCGTCGG
TATAGAACATCTTGCTCTTACGATC
ATATCTTGTAGAACGAGAATGCTAG 5'
GACGCACGGAACGATCCTGTAGAAA
CGGGTGGACGTCCAAGTGGGTAGCG 5'
GCAACCTGCGACGGCTTAAGATGGT
5' CGTTGGACGCTGCCGAATTCTACCACTGCGTGCCTTGCTAGGACATCTTTGCCCACCTGCAGGTTCACCCATCGC
47nt
DL-0 (75nt)

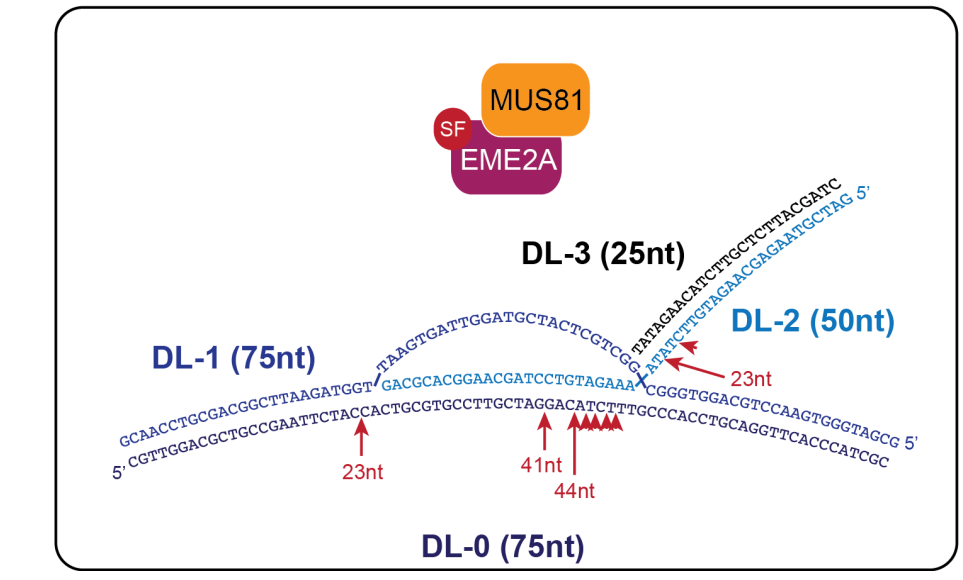
MUS81
SF
EME2A
DL-3 (25nt)
DL-2 (50nt)
DL-1 (75nt)
TAAGTGATTGGATGCTACTCGTCGG
TATAGAACATCTTGCTCTTACGATC
ATATCTTGTAGAACGAGAATGCTAG 5'
GACGCACGGAACGATCCTGTAGAAA
CGGGTGGACGTCCAAGTGGGTAGCG 5'
GCAACCTGCGACGGCTTAAGATGGT
5' CGTTGGACGCTGCCGAATTCTACCACTGCGTGCCTTGCTAGGACATCTTTGCCCACCTGCAGGTTCACCCATCGC
23nt
23nt
41nt
44nt
DL-0 (75nt)

recognised as DSBs by the cellular DNA damage response machinery (Section 1.4) (Griffith et al., 1999).

To determine whether MUS81-$_{SF}$EME1 and MUS81-$_{SF}$EME2A differ in their ability to cleave D-loop structures, equal amounts of the purified proteins were incubated with D-loops, 5'-^{32}P-end-labelled on strands DL-0, DL-1 or DL-2 (Figure 3.15A). Analysis of the reaction products by neutral PAGE (Section 2.7.3) showed that, as observed for the other model substrates analysed, MUS81-$_{SF}$EME2A was about ten times more efficient than MUS81-$_{SF}$EME1 in promoting cleavage (Figure 3.15B). To map the cleavage sites, reaction products were also analysed using denaturing PAGE (Section 2.7.4) (Figure 3.15C). MUS81-$_{SF}$EME1 performed only one incision on the strand complementary to the invading single-stranded 3'-overhang, 4 nucleotides to the 5'-side of the invasion point (Figure 3.15C and 3.16B). MUS81-$_{SF}$EME2A cleaved the D-loop on the same strand as MUS81-$_{SF}$EME1 but performed multiple incisions 2-9 and 27 nucleotides to the 5'-side of the invading site, with the major cuts being at sites 5'-G↓GAC↓A-3'. In contrast to MUS81-$_{SF}$EME1, MUS81-$_{SF}$EME2A was able to disengage the D-loop structure by cleaving the 3'-invading overhang off from the duplex DNA. The incisions occurred 2 and 4 nucleotides to the 5'-side of the invading point at the site 5'-T↓AT↓C-3' (Figure 3.15C and 3.16B). Finally, to determine whether MUS81-$_{SF}$EME2A processes D-loops by a one-step or multi-step mechanism, the activity of the purified complex was analysed in a time course experiment (Figure 3.16A). All the products observed by neutral PAGE (Section 2.7.3) were generated simultaneously, even after short incubations, suggesting that MUS81-$_{SF}$EME2A processes a D-loop in a one-step reaction.

3.7 Conclusions

In summary, these results indicate that human cells express two isoforms of EME2, referred to as EME2A and EME2B, which can form heterodimeric complexes with MUS81 *in vivo*. Comparative biochemical analysis of affinity-purified MUS81-EME1, MUS81-EME2A and MUS81-EME2B shows that the three heterodimers differ in nucleolytic cleavage efficiency and substrate specificities. Specifically,

MUS81-EME2A appears to be the most active of the complexes, exhibiting approximately a 10-fold greater activity compared to MUS81-EME1 and MUS81-EME2B on the substrates analysed. Furthermore, in contrast to MUS81-EME1, which preferentially cleaves nicked HJs, MUS81-EME2A cleaves 3'-flaps and RFs more efficiently than nicked HJs. MUS81-EME2A was also able to cleave 5'-flaps by inserting nicks on the strand complementary to that containing the flap, indicating that MUS81-EME1 and MUS81-EME2A have different enzymatic properties. Conversely, we did not observe any remarkable difference between the substrate specificities of MUS81-EME1 and MUS81-EME2B, indicating that the activity of MUS81-EME2B might not be physiologically important. Further details regarding the expression and function of MUS81-EME2B *in vivo* will be provided in the next chapter.

CHAPTER 4

Functional analysis of MUS81-EME1 and MUS81-EME2 complexes in DNA repair

4.1 Generation and validation of an anti-EME2 antibody

To determine the level of expression of EME2A and EME2B in human cells, we raised a rabbit polyclonal antibody (APEP13) using synthetic peptides common to both EME2 isoforms (Section 2.8.6). The antibody was purified using Protein-A agarose and tested for western blotting (Section 2.8.7) using WCEs (Section 2.8.4) of human cells transfected with control luciferase siRNA or with EME2 #1 siRNA (Section 2.6.1). A band at the predicted size of EME2A (~42kDa) was detected in the WCE of control-treated cells but not in the EME2 siRNA-transfected sample, confirming the specificity of the antibody (Figure 4.1A, compare lane a and c). No band corresponding to EME2B (~49kDa) was observed. Therefore, despite the synthesis of its transcript, it is unclear whether the EME2B protein is expressed in human cells or whether its expression is tissue-specific.

In all subsequent studies, RNA interference (RNAi) was used to investigate the cellular roles of EME2. Although we favour the hypothesis that EME2A is the only isoform expressed by human cells, all experiments were performed with siRNAs targeting both EME2A and EME2B (Figure 4.1B, Section 2.6.1). Hence, for simplicity, EME2A and EME2B will be hereafter referred to as EME2. Two non-overlapping siRNAs were designed using Sfold (Section 2.6.1) and were designated siEME2#1 and siEME2#2 (Figure 4.1B). The studies described in this chapter were performed using siEME2#1, whereas siEME2#2 was used in the experiments described in Chapter 5.

4.2 Analysis of the interdependence between MUS81 and its non-catalytic partners EME1 and EME2

Previous studies showed that depletion of MUS81 or EME1 affects the stability of the MUS81-EME1 heterodimeric complex (Forment et al., 2011). In order to evaluate the interdependence between MUS81 and its interacting partners EME1 and EME2, we assessed the stability of these proteins in control, MUS81, EME1 and EME2 siRNA-transfected cells (Section 2.6.1) by western blotting (Section 2.8.7). As previously described, depletion of EME1 significantly affected the cellular level of MUS81 (Figure 4.1A, lane b). The knockdown of EME2 resulted in a moderate reduction of MUS81 (Figure 4.1A, lane c). Finally, the knockdown of MUS81 resulted in a decrease in the level of EME2, indicating that the stability of EME2 depends on the formation of the MUS81-EME2 heterodimer (Figure 4.1A, lane d). Hence, depletion of EME1 or EME2 causes the destabilisation of the MUS81-EME1 or MUS81-EME2 complex, respectively. To determine the relative ratio between the MUS81-EME1 and MUS81-EME2 complex, we quantified the effect of EME1 or EME2 depletion on the cellular level of MUS81. We found that the stability of MUS81 was decreased by approximately 30% in EME2-depleted cells and by approximately 70% in EME1-depleted cells (Figure 4.1A), indicating that approximately 30% of the total MUS81 expressed in human cells interacts with EME2 whereas the remaining 70% forms a complex with EME1.

4.3 The MUS81-EME2 complex is required for the processing of stalled replication forks

Treatment of cells with agents that affect RF progression results in the production of S-phase specific DSBs (Arnaudeau et al., 2000; Saintigny et al., 2001). Interestingly, several studies showed that depletion of MUS81 results in a significant decrease in the production of DSBs, indicating a role for MUS81 in the collapse of stalled RFs (Fugger et al., 2013; Hanada et al., 2007). Unlike human cells, where the activity of MUS81 appears to be only required for the repair of stalled RFs, mouse cells rely on RF cleavage by Mus81 to restart RF progression (Petermann et al., 2010).

A

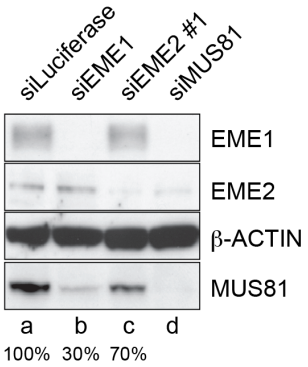

B

```
EME2A     GACCCGAGCGAGTCCCGACCCCTGCCCCCGCAGCCTGCCTCCTGAAGTGT400
EME2B     GACCCGAGCGAGTCCCGACCCCTGCCCCCGCAGCCTGCCTCCTGAAGTGT400
                                                  EME2 #2
EME2A     GGGCTGCAGGTGAACAGGAATTGCTGCTGCTGCTGGAGCCCGAGGAGTTT450
EME2B     GGGCTGCAGGTGAACAGGAATTGCTGCTGCTGCTGGAGCCCGAGGAGTTT450

EME2A     CTGCAGGGCGTCGCCACACTGACCCAGATCTCTGGCCCAACCCACTGGGT500
EME2B     CTGCAGGGCGTCGCCACACTGACCCAGATCTCTGGCCCAACCCACTGGGT500

EME2A     GCCCTGGATCTCCCCCGAGACCACCGCCCGGCCCCACCTGGCTGTCATCG550
EME2B     GCCCTGGATCTCCCCCGAGACCACCGCCCGGCCCCACCTGGCTGTCATCG550

EME2A     GGCTGGATGCCTACCTGTGGT----------------------------571
EME2B     GGCTGGATGCCTACCTGTGGTACCGCTCACTCTCATGCCCACAGCAGGGC600

EME2A     ----------------------------------------------------
EME2B     TGGCTGGGACGGGGGTTCAGGGGAGGTGGGCTCTGGCAGAGGCCAAGCTC650

EME2A     ----------------------------------------------------
EME2B     GGGCAGGGCAGGCCCCATGGGGAGCGGGGAGGAATGGTCACCTCTGCTCA700

EME2A     ---CTCGCCAGCACGTTTCCCGGGGGACACAGCAGCCAGAGAGCCCGAAG618
EME2B     GGTCTCGCCAGCACGTTTCCCGGGGGACACAGCAGCCAGAGAGCCCGAAG750

EME2A     GTGGCCGGTGCCGAGGTGGCCGTCAGCTGGCCGGAGGTGGAAGAGG----664
EME2B     GTGGCCGGTGCCGAGGTGGCCGTCAGCTGGCCGGAGGTGGAAGAGGTGAG800

EME2A     -----------------CCCTGGTACTCCTGCAGCTCTGGGCAAACCTGG697
EME2B     GGCCTGTCTGAGCTGGGCCCTGGTACTCCTGCAGCTCTGGGCAAACCTGG850

EME2A     ACGTGCTACTGGTGGCCTCTTGGCAGGAGCTGAGTCGGCACGTGTGCGCC747
EME2B     ACGTGCTACTGGTGGCCTCTTGGCAGGAGCTGAGTCGGCACGTGTGCGCC900

EME2A     GTTACCAAGGCTCTCGCCCAGTATCCCCTCAAG-----------------780
EME2B     GTTACCAAGGCTCTCGCCCAGTATCCCCTCAAGTGCGTGATGCCAAGGCT950

EME2A     ------------------------CAGTACCGGGAATCCCAGGCCTTCT805
EME2B     GAAGGGGGGCAGGATCACCTCAAGGCAGTACCGGGAATCCCAGGCCTTCT1000
                                                  EME2 #1
EME2A     CCTTCTGCACAGCAGGGCGCTGGGCAGCCGGCGAGCCAGTGGCAAGAGAC855
EME2B     CCTTCTGCACAGCAGGGCGCTGGGCAGCCGGCGAGCCAGTGGCAAGAGAC1050

EME2A     GGCGCAGGGCTGCAGGCGGCCTGGCGGAGGCAGATCAGGCAGTTCAGTCG905
EME2B     GGCGCAGGGCTGCAGGCGGCCTGGCGGAGGCAGATCAGGCAGTTCAGTCG1100
```

Figure 4.1 Design of siRNAs targeting EME2
A. U2OS cells were transfected with the indicated siRNAs for 72 hr (Section 2.6.1). WCEs (Section 2.8.4) were analysed on NuPAGE® 10% Bis-Tris gel and efficiency of the depletion was determined by western blotting (Section 2.8.7). Percentages refer to the level of MUS81 in the WCEs. **B**. Alignment of EME2A and EME2B cDNAs. The red boxes indicate the sequences targeted by EME2 #1 and EME2 #2 siRNAs (Section 2.6.1).

The role of EME1 in RF repair, however, has not been investigated and the function of MUS81 has always been related, without any supporting experimental evidence, to the MUS81-EME1 complex. Therefore, to determine whether the activity of human MUS81 at stalled RFs is dependent on MUS81-EME1 or MUS81-EME2, we analysed the contribution of MUS81, EME1 or EME2 to HU-induced DSB formation by pulse-field gel electrophoresis (PFGE). PFGE allows the separation of large DNA molecules from DNA fragments and was performed as described in Section 2.7.9. As opposed to intact DNA, broken DNA migrates into the gel and DSB formation can be quantified as the ratio of broken to intact DNA. HeLa cells were transfected with control, MUS81, EME1 or EME2 siRNAs (Section 2.6.1). The three proteins were efficiently depleted, as determined by western blotting (Figure 4.2A, Section 2.8.7). Forty-eight hours after transfection, cells were treated with increasing concentrations of HU for 24 hr. As expected, treatment with HU caused a delay during S-phase of the cell cycle, as indicated by the accumulation of cells incorporating BrdU (Figure 4.2B, Section 2.13.2). Consistent with previous observations (Fugger et al., 2013; Hanada et al., 2007), depletion of MUS81 resulted in a significant decrease in DSB formation following treatment with HU (Figure 4.3 A-B). Surprisingly, the amount of DSBs observed in EME1-depleted cells was comparable to that of control siRNA-transfected cells, whereas depletion of EME2 caused a decrease in DSB formation that was comparable to that obtained after loss of MUS81 (Figure 4.3A-B, the quantification of DSBs in Figure 4.3B represents the mean of four experiments).

Similar results were observed after treatment with the ICL agent cisplatin. Forty-eight hours after transfection with control, MUS81, EME1 or EME2 siRNAs (Section 2.6.1), cells were exposed to increasing concentrations of cisplatin for 24 hr. Treatment with cisplatin causes a delay during S-phase of the cell cycle, as indicated by the accumulation of cells incorporating BrdU (Figure 4.2C, Section 2.13.2). As already observed with HU-treated cells, MUS81 and EME2 depletion significantly affected the production of ICL-dependent DSBs (Figure 4.4 A-B). Conversely, cells transfected with control or EME1 siRNA displayed comparable levels of DSB formation (Figure 4.4 A-B, the quantification of DSBs in Figure 4.4B represents the mean of two experiments). Taken together, these results indicate that, in contrast to what was previously assumed, but not tested, MUS81-EME2,

rather than MUS81-EME1, is required for the collapse and repair of stalled RFs after prolonged HU or cisplatin treatments.

4.4 MUS81 interacts with EME2 during the S-phase of the cell cycle

Results from our laboratory have established that MUS81 and EME1 form a stable complex throughout the cell cycle and that at the G2/M transition, MUS81-EME1 cooperates with SLX1-SLX4 to efficiently resolve HJs that have escaped BTR-mediated dissolution (Section 1.3.1) (Wyatt et al., 2013). In view of the function of the MUS81-EME2 complex in the repair of stalled RFs, we decided to investigate whether MUS81 might also interact with EME2 in a cell cycle-dependent manner. To do this, we generated a HeLa Kyoto cell line expressing BAC-MUS81$_{FLAP}$ (Section 2.6.3) (Figure 4.5A). BAC-MUS81$_{FLAP}$ HeLa Kyoto cells were synchronised at G1/S by double thymidine block (Section 2.6.4) and released into fresh media. Samples were collected at intervals of 3 hr and nocodazole, a drug that interferes with the polymerization of microtubules, was added 6 hr after the thymidine release. FACS analysis of the cellular DNA content (propidium iodide staining, Section 2.13.1) showed that the majority of the cells were efficiently synchronised at G1/S (Figure 4.5C). Between 3 and 6 hr after thymidine release, cells were undergoing DNA replication and, upon addition of nocodazole, began to accumulate in prometaphase with a 4n DNA content. GFP affinity purification was performed from samples collected at the time points indicated in Figure 4.5 B and C (Section 2.10.2). Western blotting analysis was used to assess the efficiency of the MUS81$_{FLAP}$ pull-down and the presence of EME1, EME2 and SLX4 in the immunoprecipitates (Figure 4.5B, Section 2.8.7). As previously shown, EME1 interacted with MUS81 throughout the cell cycle and its phosphorylation status appeared to change according to the cell cycle stage (Figure 4.5B, lane e) (Wyatt et al., 2013). MUS81 was found to preferentially associate with SLX4 during the G2/M phase of the cell cycle (Figure 4.5B, lanes d and e) (Wyatt et al., 2013). Surprisingly, the interaction between MUS81 and EME2 also appeared to be cell cycle stage-dependent.

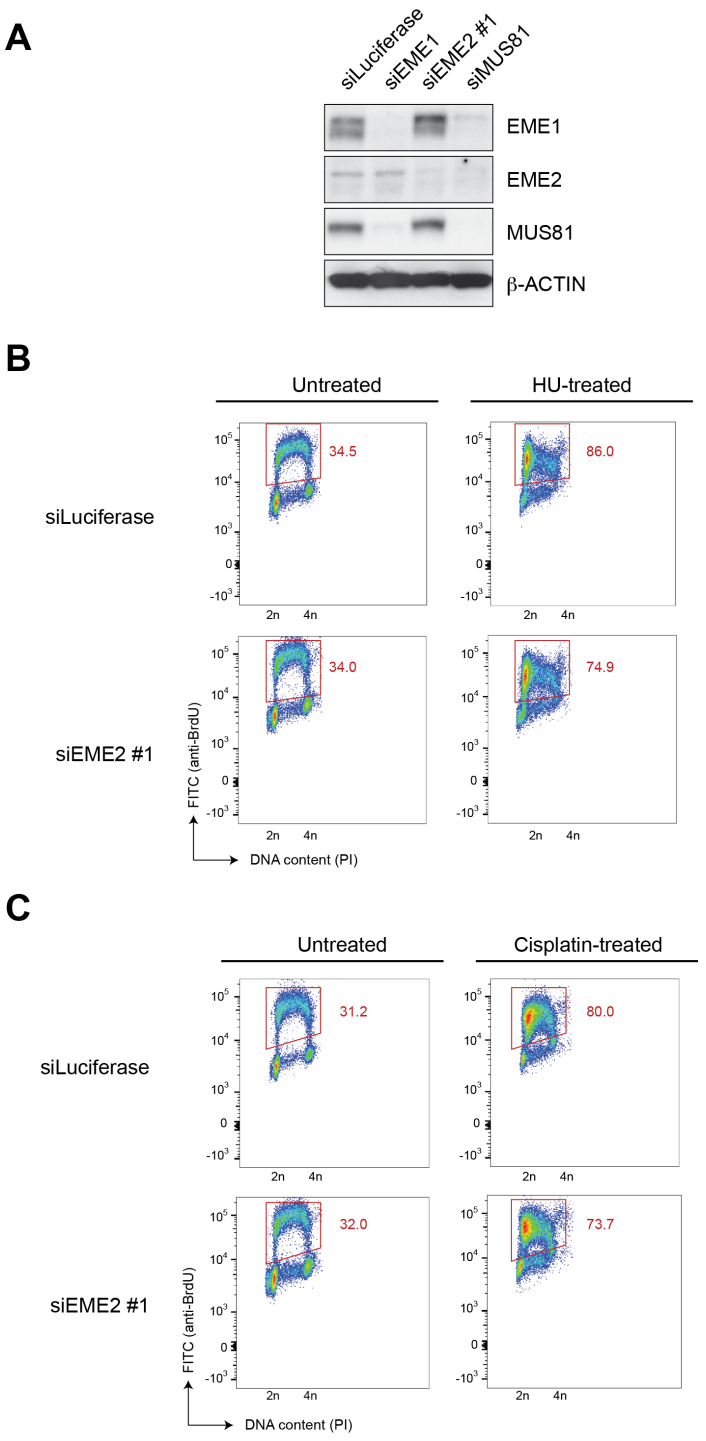

Figure 4.2 Cell cycle profiles of control and EME2 siRNA-transfected cells after treatment with HU or cisplatin

HeLa cells were transfected with the indicated siRNAs for 48 hr and then treated with 1 mM HU (**A**) or 10 μM cisplatin (**B**) for 24 hr. BrdU staining was performed as described in Section 2.13.2. Data were analysed using the analysis software FlowJo 10.1. **C.** The efficiency of MUS81, EME1 and EME2 siRNA-mediated depletion was determined by western blotting (Section 2.8.7) on HeLa WCEs (Section 2.8.4).

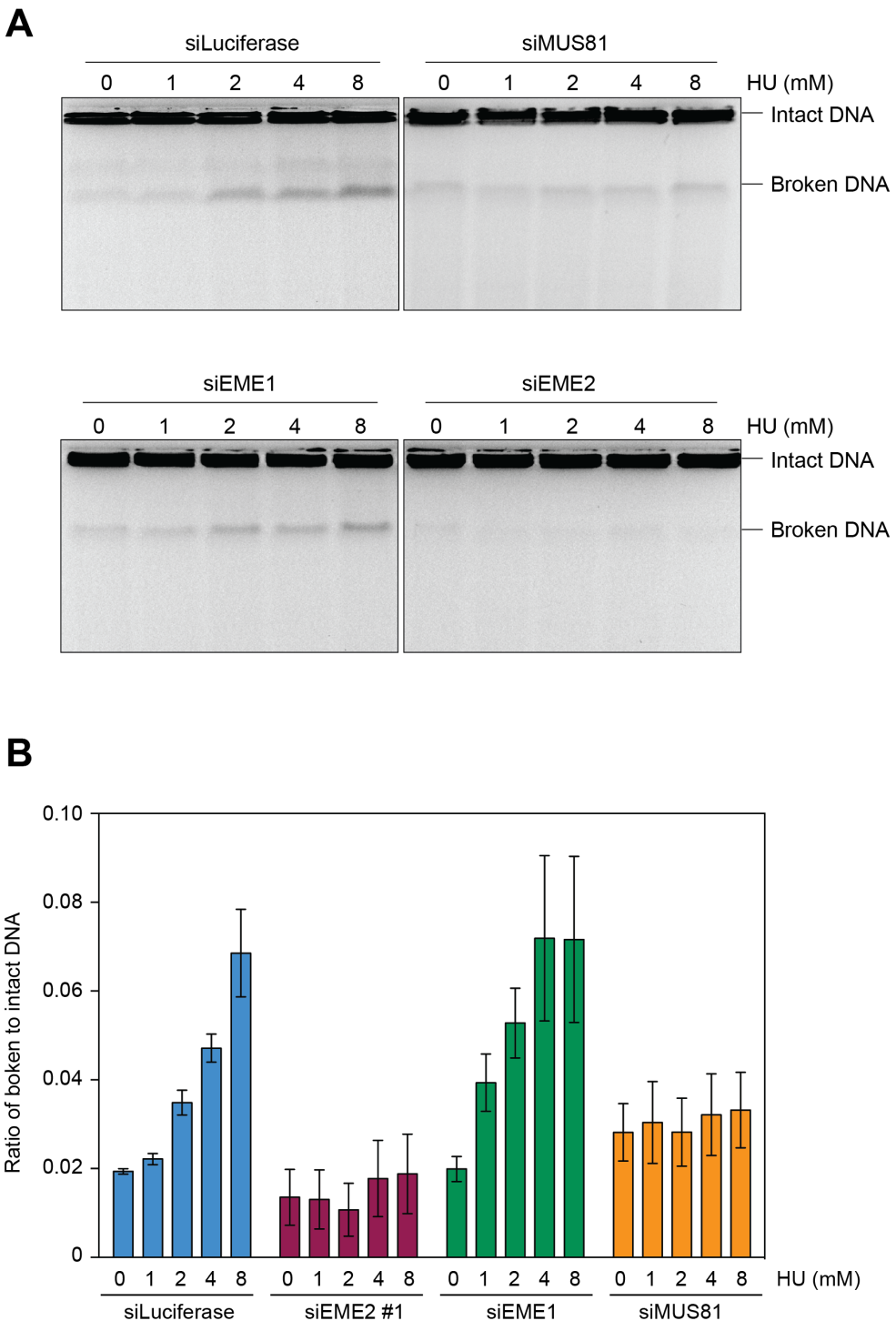

Figure 4.3 The MUS81-EME2 complex contributes to the formation of DSBs in response to treatment with HU

A. PFGE gels showing the formation of DNA DSBs after treatment with the indicated concentration of HU for 24 hr. HeLa cells were transfected with the indicated siRNAs for 48 hr before the addition of the drug. **B.** The formation of HU-induced DSBs is expressed as the ratio of broken to intact DNA. Data are presented as a mean of three experiments (±SEM).

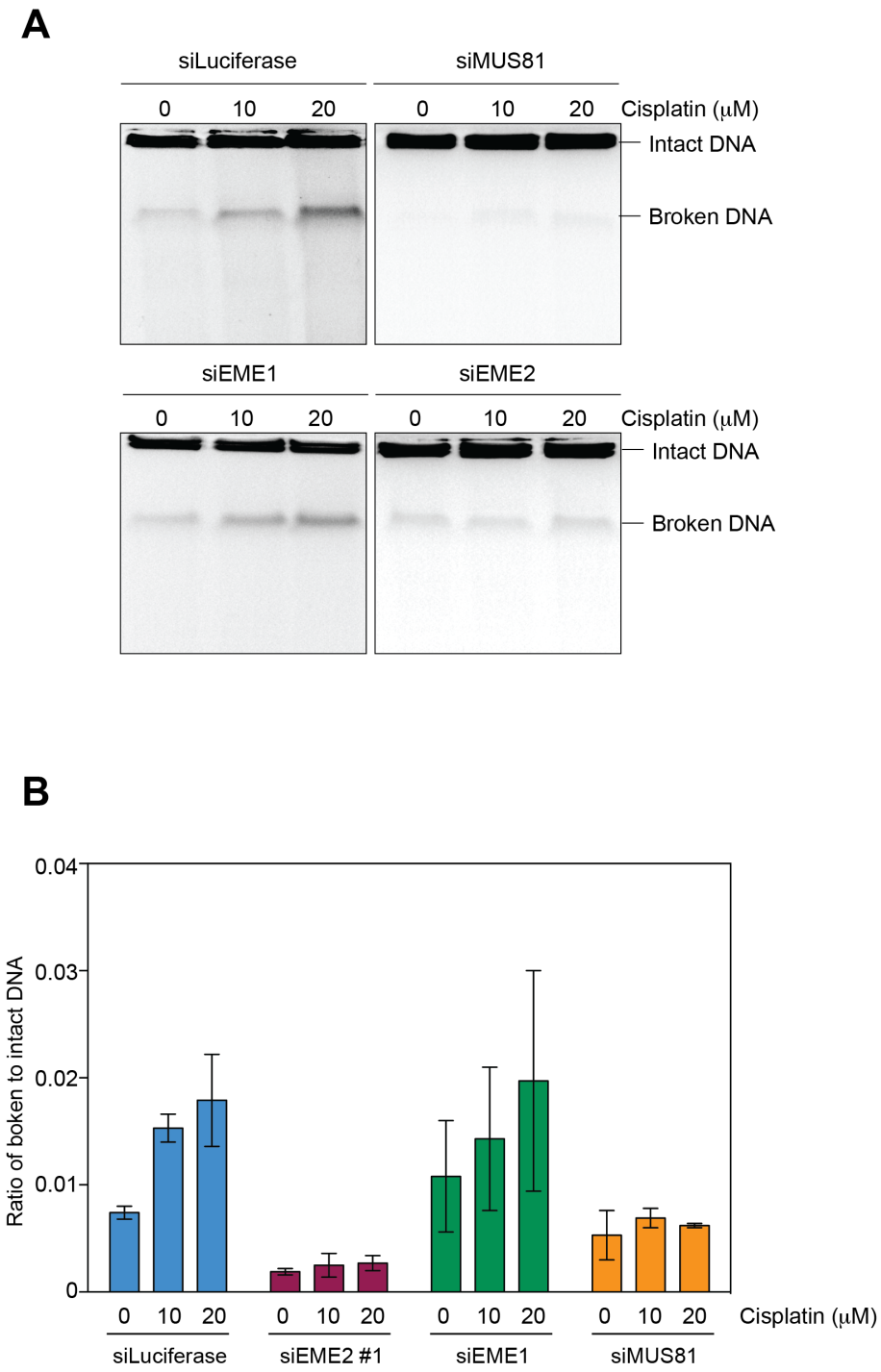

Figure 4.4 The MUS81-EME2 complex contributes to the conversion of ICLs into DNA DSBs

A. PFGE gels showing the formation of DNA DSBs after treatment with the indicated concentration of cisplatin for 24 hr. HeLa cells were transfected with the indicated siRNAs for 48 hr before the addition of the drug. **B.** The formation of cisplatin-induced DSBs is expressed as the ratio of broken to intact DNA. Data are presented as a mean of two experiments (±SEM).

Specifically, EME2 was enriched in MUS81 immunoprecipitates during S-phase, i.e. 3 to 6 hr after thymidine release (Figure 4.5B, lanes b and c). Some EME2 was also detected in the pull-down from cells arrested in G1/S (Figure 4.5B, lane a), suggesting that the MUS81-EME2 complex might start to form prior the initiation of DNA replication. Hence, in agreement with the concept that MUS81-EME2 may play a role in the repair of stalled RFs, these results show that MUS81 and EME2 interact preferentially during G1- and S-phase.

4.5 MUS81-EME2 is required for genomic stability after HU treatment

Defects in the repair of damaged RFs often lead to the accumulation of chromosomal aberrations and genomic instability. For example, Fanconi Anaemia (FA) cells, which are defective in the repair of RFs stalled at ICLs, show an elevated level of chromosomal aberrations, which include radial chromosomes and chromosome breaks (Shahid et al., 1972). Given the role of MUS81-EME2 in the repair of stalled RFs, we analysed the formation of aberrant chromosomes in untreated or HU-treated MUS81-, EME1- and EME2-depleted cells (Figure 4.6A). To do so, untransformed RPE-1 cells, immortalised by overexpression of the telomerase subunit hTERT, were transfected with luciferase, EME1, EME2 and MUS81 siRNAs (Section 2.6.1). All proteins were efficiently depleted, as determined by western blotting (Figure 4.6C, Section 2.8.7). Cells were treated with HU for 24 hr and then incubated in fresh medium for further 24 hr. Metaphase spreads were prepared as described in Section 2.12.1 and stained with GIEMSA. RPE-1 hTERT cells transfected with EME1, EME2 and MUS81 siRNAs showed a mild increase in chromosomal aberrations compared to luciferase-transfected cells (Figure 4.6B and Table 4.1). The treatment with HU promoted the formation of chromosome aberrations in all the samples analysed. However, cells depleted of MUS81 or EME2 showed a two-fold increase in the number of aberrant chromosomes compared to control or EME1-depleted cells (Figure 4.6B and Table 4.1). In line with the observations made so far in this study, this suggests that MUS81-EME2 is important for the maintenance of genomic stability of human cells after treatment with HU.

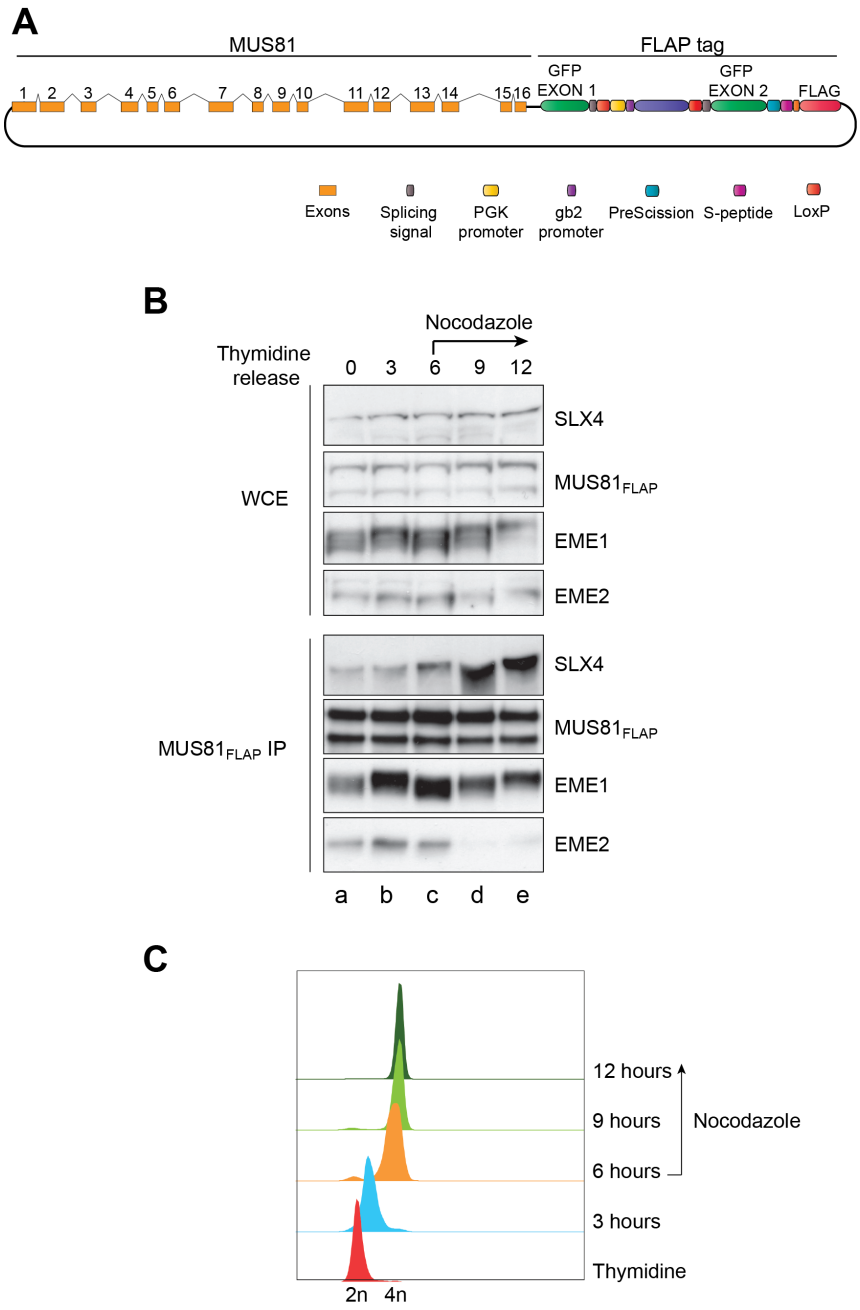

Figure 4.5 EME2 preferentially binds to MUS81$_{FLAP}$ during the S-phase of the cell cycle

A. Schematic representation of BAC-MUS81$_{FLAP}$. **B.** HeLa Kyoto BAC-MUS81$_{FLAP}$ cells were synchronised in the G1/S-phase of the cell cycle by double thymidine block (Section 2.6.4). Samples were collected after 0, 3, 6, 9 and 12 hr after thymidine release and nocodazole was added after 6 hr. GFP-pull-down of BAC-MUS81$_{FLAP}$ was performed as described in Section 2.10.2. **C.** Propidium iodide staining (Section 2.13.1) of synchronised cells described in A. Data were analysed using the analysis software FlowJo 10.1.

We also observed that EME2-depleted cells displayed a high level of endoreduplication, a phenomenon characterised by the pairing of re-replicated chromosomes into 'butterfly-like' structures called diplochromosomes (Figure 4.7A). A previous study showed that also Mus81-depleted mouse cells displayed endoreduplication but with a much lesser frequency compared to that of the EME2-depleted cells analysed in this study (Hiyama et al., 2006). Importantly, the frequency of endoreduplication in RPE-1 hTERT cells transfected with MUS81 or EME1 siRNA was considerably lower compared to EME2 depleted cells (Figure 4.7B). Therefore, we asked whether co-depletion of MUS81 and EME2 would phenocopy MUS81- or EME2-depleted cells. Surprisingly, when MUS81 was co-depleted with EME2, the number of cells showing endoreduplication was reduced to a level similar to that of the single MUS81 depletion, indicating that in the absence of MUS81-EME2, MUS81-EME1 promotes endoreduplication.

4.6 MUS81-EME2 interacts with SLX1-SLX4 and XPF-ERCC1

MUS81-EME1 forms a multi-nuclease complex with SLX1-SLX4 and the NER enzyme XPF-ERCC1 (Fekairi et al., 2009; Munoz et al., 2009; Svendsen et al., 2009; Wyatt et al., 2013). To determine whether MUS81-EME2 can also form a complex with SLX1-SLX4 and XPF-ERCC1, we performed a FLAG immunoprecipitation (Section 2.10.3) from HEK293-TREx^{TM} expressing $_{SF}$EME2A (Figure 4.8, Section 2.6.2). FLAG pull-down from HEK293-TREx^{TM} expressing $_{SF}$EME1 was used as a positive control (Section 2.6.2). Western blotting analysis (Section 2.8.7) of $_{SF}$EME1 and $_{SF}$EME2 eluates showed that, like $_{SF}$EME1, $_{SF}$EME2 interacted with MUS81, SLX1, SLX4, XPF and ERCC1 (Figure 4.8). This result indicates that in human cells SLX4 functions as a scaffold for the formation of two multi-nuclease complexes that differ in the non-catalytic subunit of the MUS81 endonuclease.

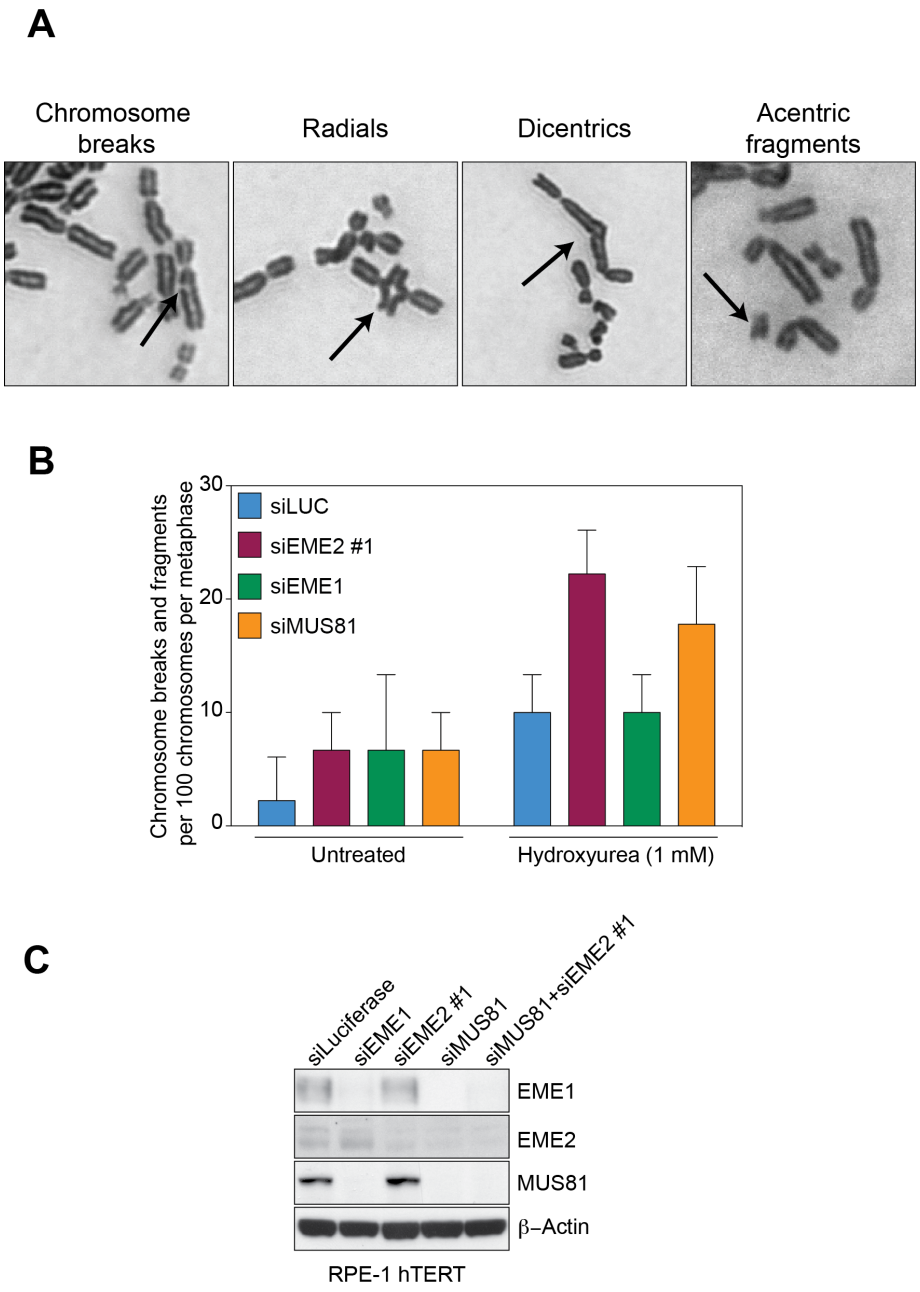

Figure 4.6 MUS81-EME2 complex is required for maintaining genomic stability after HU treatment

A. Representative images of metaphase spreads of RPE-1 hTERT cells showing the indicated chromosomal aberrations. Cells were transfected with MUS81, EME1, EME2 siRNAs or with control Luciferase siRNA (Section 2.6.1). After 48 hr, cells were treated with 1 mM HU for 24 hr and incubated in fresh media for further 24 hr. **B.** Quantification of the frequency of chromosomal breaks and fragments in siRNA-transfected cells, untreated or treated with 1 mM HU for 24 hr. Data are presented as the mean of three different experiments (±SD). **C**. RPE-1 hTERT cells were transfected with the indicated siRNAs for 72 hr (Section 2.6.1). WCEs (Section 2.8.4) were analysed on a NuPAGE® 10% Bis-Tris gel. Efficiency of the depletion was determined by western blotting (Section 2.8.7).

siRNA	Treatment	Number of metaphases analysed	Acentric fragments	Chromosome breaks	Chromatid breaks	Radials	Dicentrics	Rings
Luciferase	Mock	30	0.03	0	0	0	0	0
EME1	Mock	30	0.06	0.03	0.1	0	0	0
EME2	Mock	30	0.1	0.06	0.03	0.03	0.03	0.03
MUS81	Mock	30	0.03	0.06	0.1	0	0	0
Luciferase	Hydroxyurea	30	0.03	0	0.2	0.26	0	0
EME1	Hydroxyurea	30	0.1	0	0.2	0.13	0	0
EME2	Hydroxyurea	30	0.3	0.16	0.2	0	0.03	0.1
MUS81	Hydroxyurea	30	0.26	0.06	0.2	0.13	0	0.03

Table 4.1 Frequency of chromosomal aberrations in control, EME1-, EME2- and MUS81-depleted cells, before and after treatment with HU

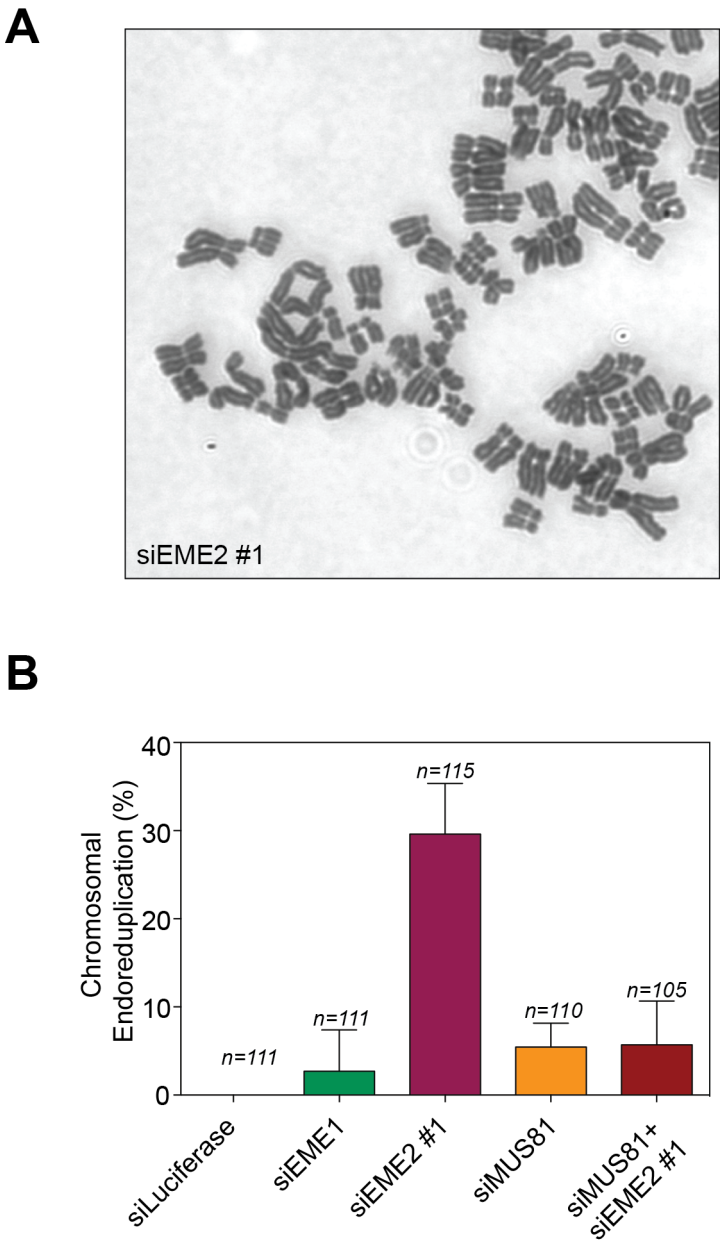

Figure 4.7 Depletion of EME2 increases the frequency of endoreduplication in RPE-1 hTERT cells

A. Representative image of a metaphase spread of EME2-depleted RPE-1 hTERT cells showing diplochromosomes as an indication of endoreduplication. **B.** Quantification of the frequency of endoreduplication in RPE-1 hTERT cells transfected with the indicated siRNAs (Section 2.6.1). Data are presented as the mean of three different experiments (±SD).

4.7 MUS81-EME2 does not significantly contribute to SCE formation

Bloom's syndrome cells are defective in the BTR-mediated dissolution of dHJs and show a high level of SCEs (Chaganti et al., 1974), which are largely MUS81-dependent (Wechsler et al., 2011; Wyatt et al., 2013). However, the contribution of EME1 and EME2 to SCE formation in BS cells has not been investigated and, without any supporting experimental evidence, the activity of MUS81 has always been related to that of the MUS81-EME1 complex. Therefore, to determine whether SCE formation depends on MUS81-EME1 or MUS81-EME2, we analysed SCE frequency in BS cells depleted for MUS81, EME1 or EME2 (Figure 4.9A). BS cells were transfected with siRNAs targeting EME1, EME2 or MUS81 (Section 2.6.1) and all proteins were efficiently depleted (data not shown). The SCE assay was performed as described in Section 2.12.2. Depletion of MUS81 significantly reduced the number of SCEs compared to cells transfected with control luciferase siRNA, as previously described (Figure 4.9B) (Wechsler et al., 2011; Wyatt et al., 2013). EME1-depleted cells showed a similar level of SCE frequencies compared to that of MUS81-depleted cells, suggesting that the MUS81-EME1 complex is responsible for SCE formation in BS cells. Conversely, depletion of EME2 did not result in a significant decrease in the number of SCEs. SLX1 and SLX4 were also implicated in the formation of SCEs in BS cells and were shown to function in the same pathway of HJ resolution as MUS81 (Wechsler et al., 2011; Wyatt et al., 2013). These results further support a model in which SLX1-SLX4 and MUS81-EME1 interact to promote efficient HJ resolution (Fekairi et al., 2009; Munoz et al., 2009; Svendsen et al., 2009; Wyatt et al., 2013). Conversely, MUS81-EME2 does not appear to play an important role in SCEs formation, in further agreement with its function in the repair of stalled replication forks.

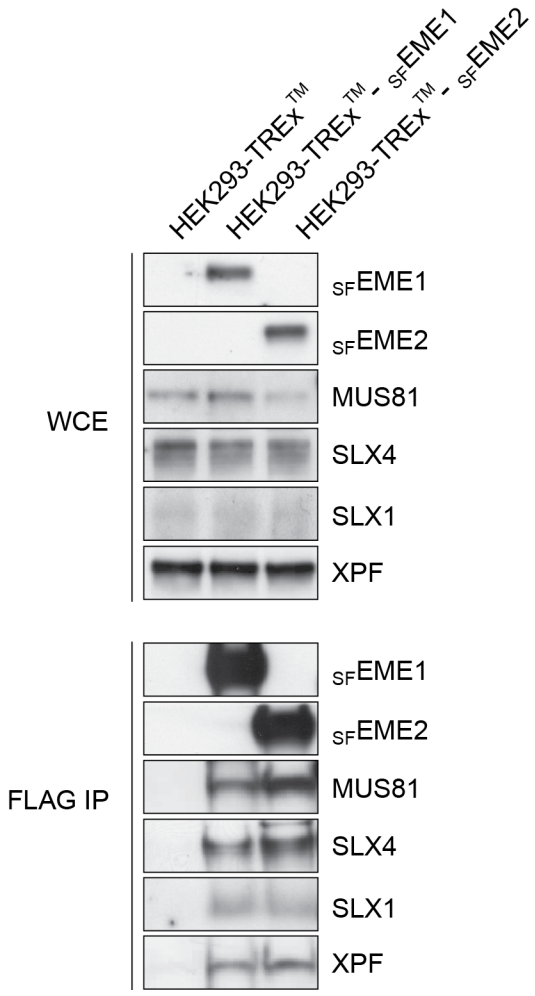

Figure 4.8 $_{SF}$EME2 interacts with SLX1-SLX4 and XPF-ERCC1
The expression of $_{SF}$EME2 and $_{SF}$EME1 was induced in HEK293-TREx™ cell lines (Section 2.6.2) with 1 µg/ml tetracycline for 72 hr. As a control, the same concentration of tetracycline was added to the HEK293-TREx™ cell line. FLAG pull-downs were performed as described in Section 2.10.3.

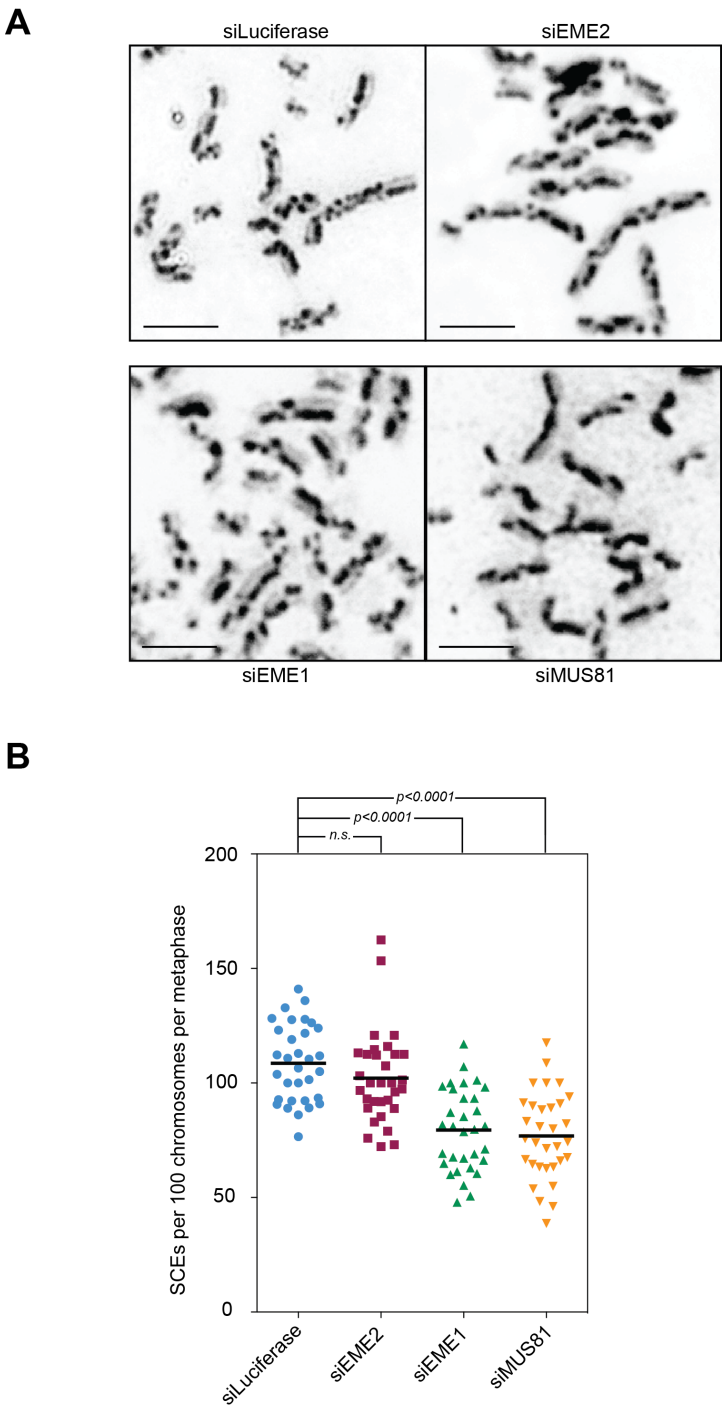

Figure 4.9 The MUS81-EME2 complex does not significantly contribute to SCE formation in BS cells

A. Representative images of metaphase spreads prepared from BLM-deficient cells (GM08505) transfected with the indicated siRNAs (Section 2.12.2). **B.** Quantification of SCE formation after siRNA transfection. Each data point represents the number of SCEs per 100 chromosomes per metaphase spread (for each condition 32 metaphases were analysed). *P* values were determined using two-tailed unpaired *t*-test with Welch correction.

4.8 Conclusions

In summary, these studies indicate that MUS81 forms two mutually exclusive heterodimers *in vivo*: MUS81-EME1 and MUS81-EME2. MUS81 interacts with EME2 preferentially during the S-phase of the cell cycle, during which it appears to be required for the restart of stalled RFs. In support of this, analysis of chromosomal aberrations reveals that MUS81-EME2 is required for the maintenance of genomic stability following treatment with HU. Furthermore, in contrast to MUS81-EME1, MUS81-EME2 is not required for SCE formation in BS cells, providing further evidence for distinct cellular functions of the two MUS81 heterodimers. Interestingly, as already observed for MUS81-EME1 (Fekairi et al., 2009; Munoz et al., 2009; Svendsen et al., 2009), MUS81-EME2 interacts with SLX1-SLX4 and XPF-ERCC1. The biological relevance of this interaction will be investigated in further studies.

CHAPTER 5

MUS81-EME2 is required for telomere maintenance of ALT cells

5.1 Depletion of EME2 affects the cell cycle progression of ALT-cells

Previously, it was shown that *MUS81*$^{-/-}$ cells displayed a spontaneous mild delay in the S/G2-phase of the cell cycle when compared to wild-type cells (Hiyama et al., 2006). Therefore, we determined the effect of EME2 depletion on the cell cycle progression of U2OS and HeLa cells by FACS analysis (Section 2.13.1). We observed that depletion of EME2 did not affect the cell cycle profile of HeLa cells, whereas EME2-depleted U2OS cells accumulated with a 4n DNA content. We hypothesised that this difference in cell cycle progression could be related to the different telomere maintenance mechanisms employed by the two cell lines, with U2OS being ALT-positive and HeLa being telomerase-positive cells. To confirm this hypothesis, we analysed the effect of EME2 depletion on the cell cycle profile of additional ALT (GM847) and telomerase-positive (HT1080) cell lines (Figure 5.1). As observed for U2OS and HeLa cells, loss of EME2 caused a cell cycle delay in ALT cells but not in the telomerase-positive cells (Figure 5.1). Specifically, FACS analysis of BrdU incorporation and histone H3 phosphorylation performed on U2OS cells (Sections 2.13.1 and 2.13.2) showed that EME2 depletion caused a delay in the late S/G2-phase of the cell cycle, but not in mitosis, as indicated by the decreased frequency of phospho-histone H3-positive cells (Figure 5.2). Importantly, the same results were obtained with two, non-overlapping EME2 siRNAs (Figure 5.1, 5.2 and 5.3C, Section 2.6.1), excluding the contribution of siRNA-mediated off-target effects. Proteins were efficiently depleted in all cell lines analysed, as determined by western blotting (Figure 5.3A-B, Section 2.8.7). When the cell cycle distribution of EME2-depleted cells was compared to that of control, EME1 and MUS81 siRNA-transfected cells, we observed that both

Figure 5.1 EME2 depletion causes a delay in the G2/M phase of the cell cycle of ALT-positive cells
Cells were transfected with the indicated siRNAs for 72 hr as described in Section 2.6.1. PI staining was performed as described in Section 2.13.1. Data were analysed using the analysis software FlowJo 10.1.

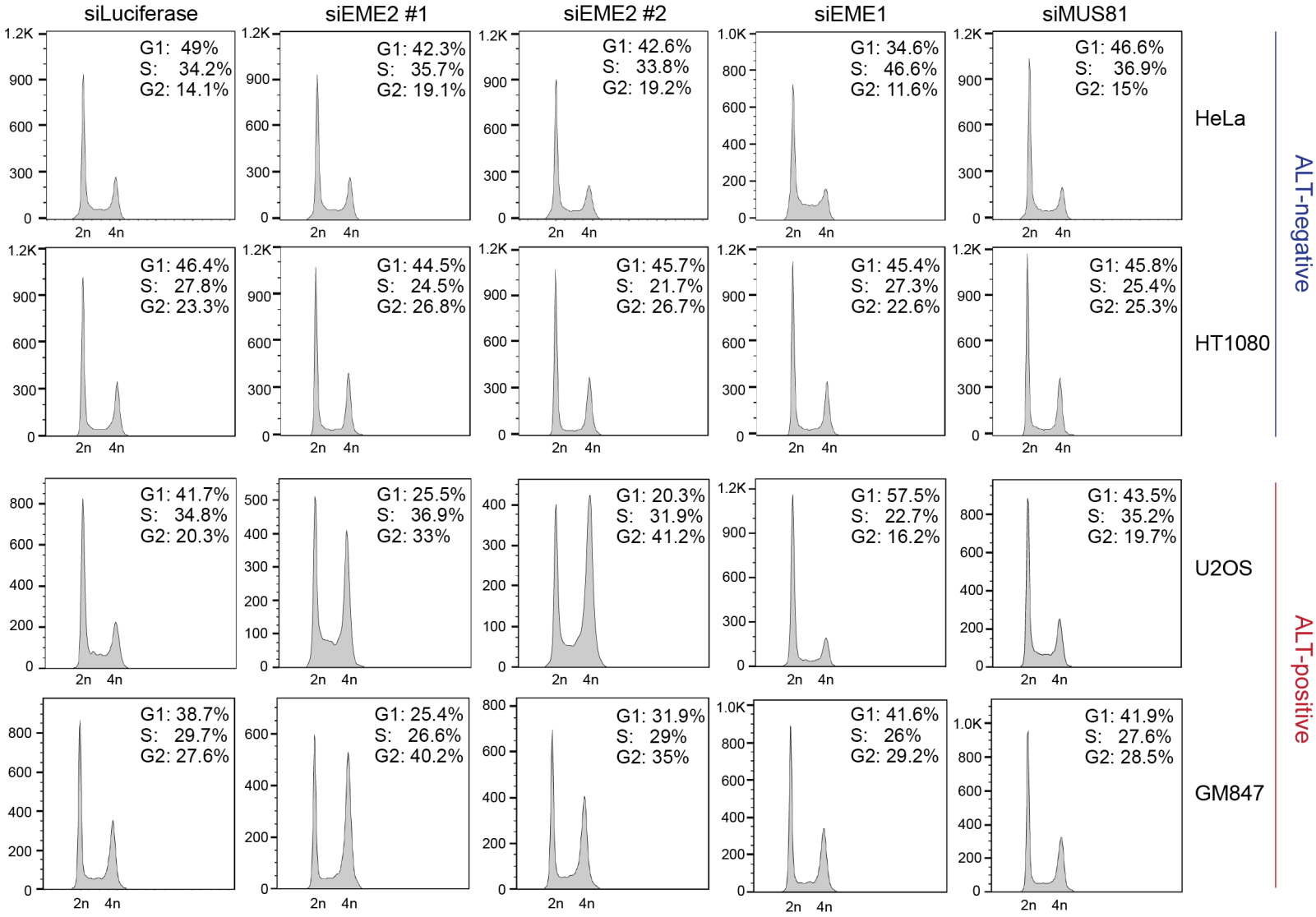
siLuciferase
siEME2 #1
siEME2 #2
siEME1
siMUS81
G1: 49%
S: 34.2%
G2: 14.1%
G1: 42.3%
S: 35.7%
G2: 19.1%
G1: 42.6%
S: 33.8%
G2: 19.2%
G1: 34.6%
S: 46.6%
G2: 11.6%
G1: 46.6%
S: 36.9%
G2: 15%
HeLa
G1: 46.4%
S: 27.8%
G2: 23.3%
G1: 44.5%
S: 24.5%
G2: 26.8%
G1: 45.7%
S: 21.7%
G2: 26.7%
G1: 45.4%
S: 27.3%
G2: 22.6%
G1: 45.8%
S: 25.4%
G2: 25.3%
HT1080
ALT-negative
G1: 41.7%
S: 34.8%
G2: 20.3%
G1: 25.5%
S: 36.9%
G2: 33%
G1: 20.3%
S: 31.9%
G2: 41.2%
G1: 57.5%
S: 22.7%
G2: 16.2%
G1: 43.5%
S: 35.2%
G2: 19.7%
U2OS
G1: 38.7%
S: 29.7%
G2: 27.6%
G1: 25.4%
S: 26.6%
G2: 40.2%
G1: 31.9%
S: 29%
G2: 35%
G1: 41.6%
S: 26%
G2: 29.2%
G1: 41.9%
S: 27.6%
G2: 28.5%
GM847
ALT-positive
2n
4n

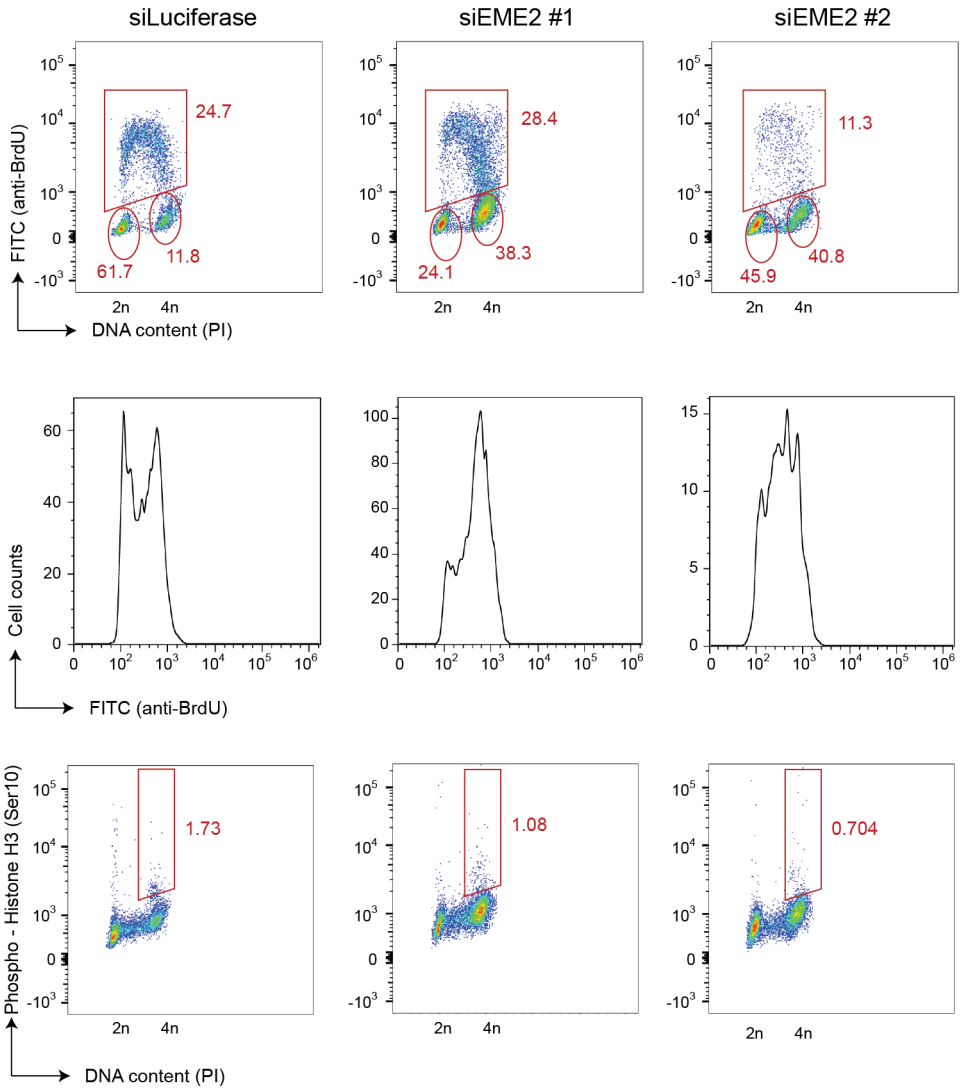

Figure 5.2 BrdU and phospho histone H3 staining of U2OS cells transfected with two EME2 siRNAs

Cells were transfected with the indicated siRNAs for 72 hr as described in Section 2.6.1. BrdU and phospho-histone H3 stainings were performed as described in Section 2.13.2 and 2.13.3, respectively. Data were analysed using the analysis software FlowJo 10.1.

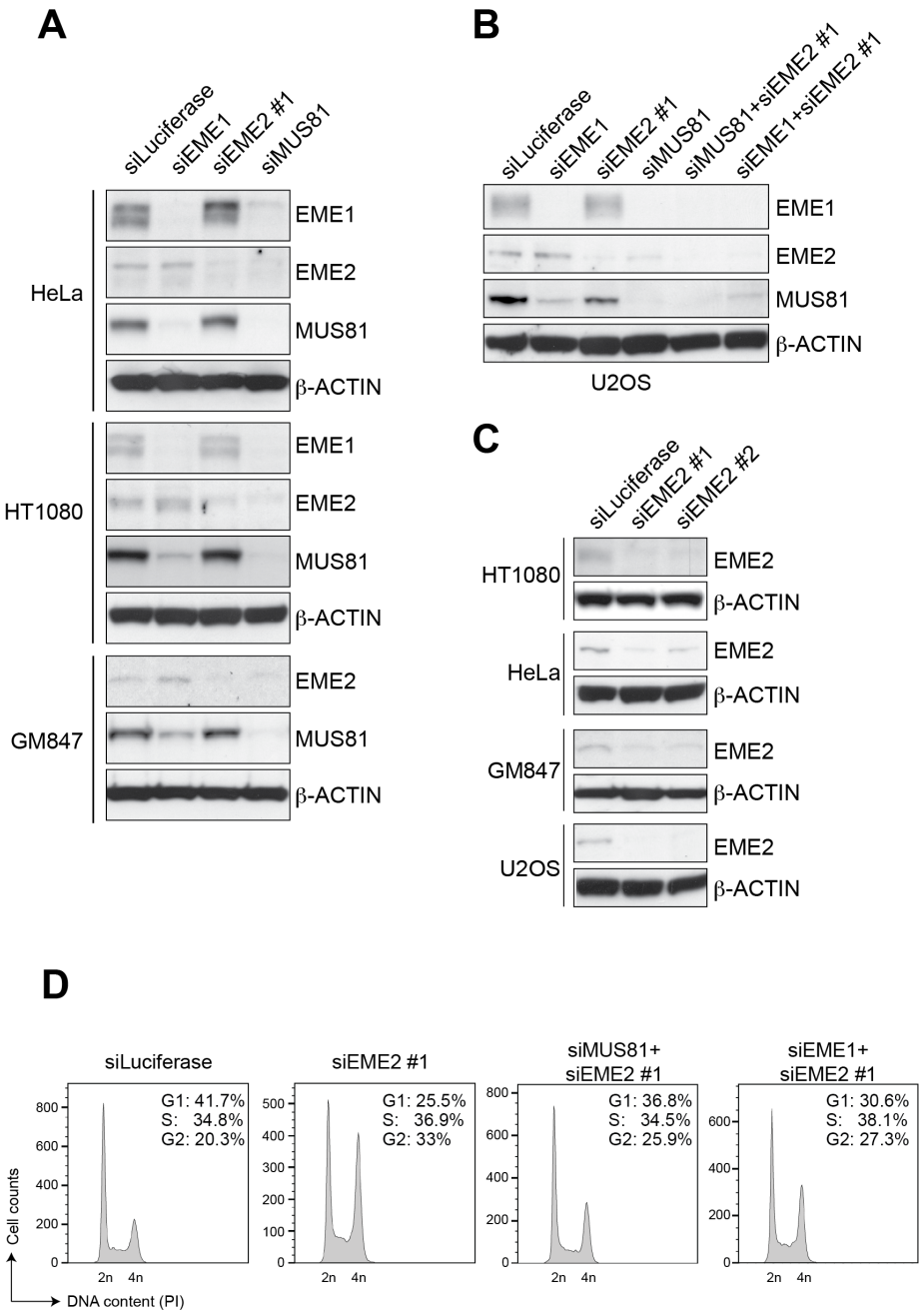

Figure 5.3

A-B-C. **Western blot analysis of siRNA-mediated depletions**
HeLa, HT1080, GM847 and U2OS cells were transfected with the indicated siRNAs for 72 hr, as described in Section 2.6.1. WCEs (Section 2.8.4) were analysed on a NuPAGE® 10% Bis-Tris gel. The efficiency of depletion was determined by western blotting (Section 2.8.7)

D. Depletion of MUS81 or EME1 rescues the G2/M delay of EME2-depleted U2OS cells
Cells were transfected with the indicated siRNAs for 72 hr as described in Section 2.6.1. PI staining was performed as described in Section 2.13.1. Data were analysed using the analysis software FlowJo 10.1.

ALT-positive and ALT-negative cells transfected with control, EME1 or MUS81 siRNA showed similar cell cycle progression profiles (Figure 5.1). Taken together, these results indicate that the cell cycle delay caused by the loss of EME2 is specific to ALT-positive cells.

Because we did not observe a defect in the cell cycle progression of MUS81- and EME1-depleted cells, we asked whether co-depletion of EME2 with MUS81 or EME1 would rescue the EME2-specific cell cycle defect. Indeed, when EME2 was co-depleted with MUS81 or EME1 in U2OS cells, the frequency of cells with 4n DNA content was significantly reduced (Figure 5.3D). As described in Section 4.2, loss of EME1 or EME2 causes the depletion of the MUS81-EME1 or MUS81-EME2 complex, respectively. Given that MUS81 protein level was reduced in cells treated with EME1 and EME2 siRNA (Figure 5.3B), we concluded that depletion of both MUS81-EME1 and MUS81-EME2 complexes rescues the delay in cell cycle progression of EME2-depleted cells.

5.2 $_{SF}$EME1 and $_{SF}$EME2 localise to ALT-associated PML bodies

ALT-associated PML bodies (APBs) accumulate in ALT-positive cells during the G2-phase of the cell cycle and are believed to be sites of telomere elongation (Bryan et al., 1995; Yeager et al., 1999). These bodies are identified by the co-localisation of telomeric DNA with the shelterin proteins TRF1 and TRF2 at nuclear foci that are larger than those formed at individual telomeres (Jiang et al., 2007; Yeager et al., 1999). As discussed in Section 1.4.2, many proteins involved in telomere maintenance and DNA repair have been visualised at APBs, including MUS81 (Zeng et al., 2009).

To determine whether the non-catalytic partners of MUS81 localise to APBs, we examined the nuclear localisation of EME1 and EME2 by immunofluorescence (IF) (Section 2.12.5). Unfortunately, the anti-EME1 (Section 2.1.3.1) and anti-EME2 (Section 2.8.8) antibodies were unable to specifically detect EME1 and EME2 in IF. For this reason, we analysed the localisation of ectopically expressed $_{SF}$EME1 and $_{SF}$EME2. The expression of $_{SF}$EME1 or $_{SF}$EME2 was induced in U2OS-TREx^{TM} cells

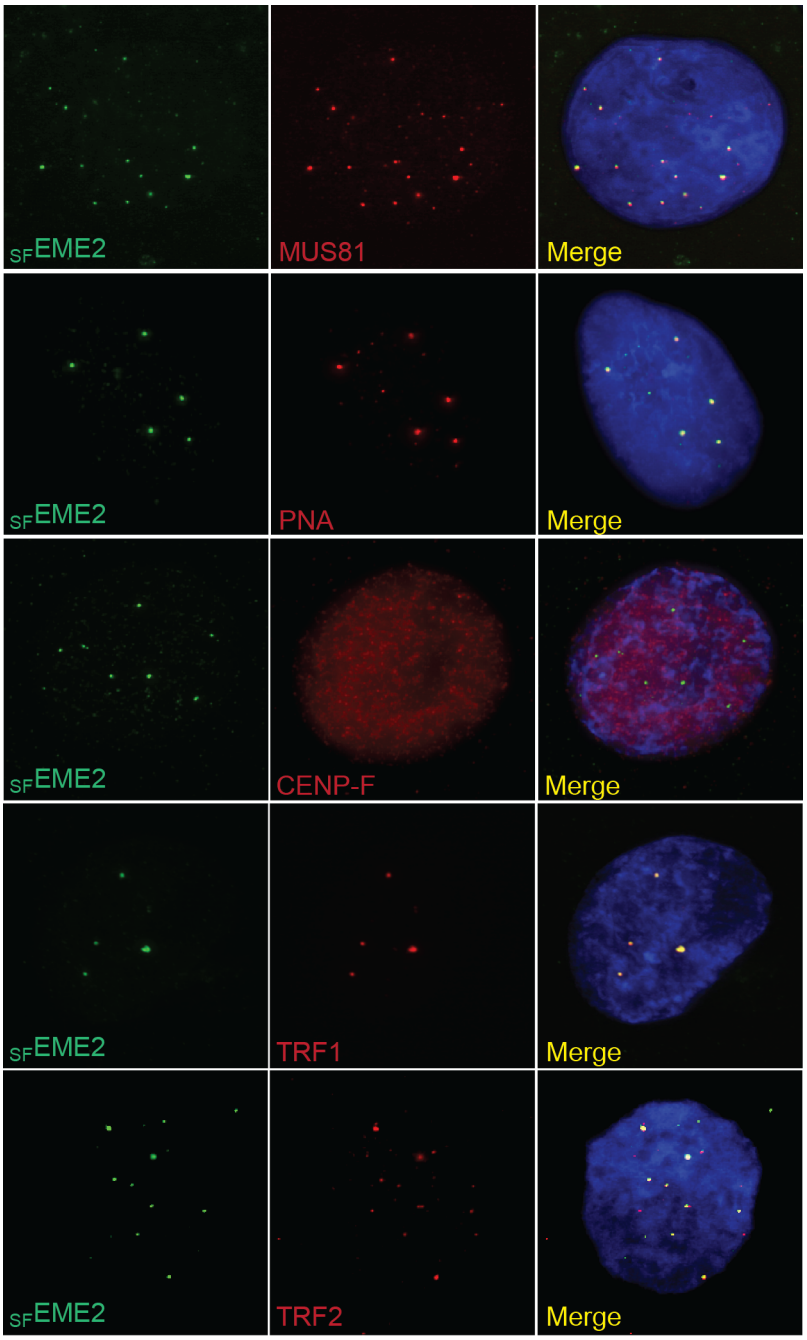

Figure 5.4 $_{SF}$EME2 localises to APBs
The expression of $_{SF}$EME2 was induced in U2OS-TREx^{TM}-$_{SF}$EME2 cells (Section 2.6.2) with 1 µg/ml tetracycline for 48 hr. IF was performed as described in Section 2.12.5. $_{SF}$EME2 was detected using the rabbit anti-FLAG primary antibody (Section 2.1.3.1). IF-FISH was performed as described in Section 2.12.6.

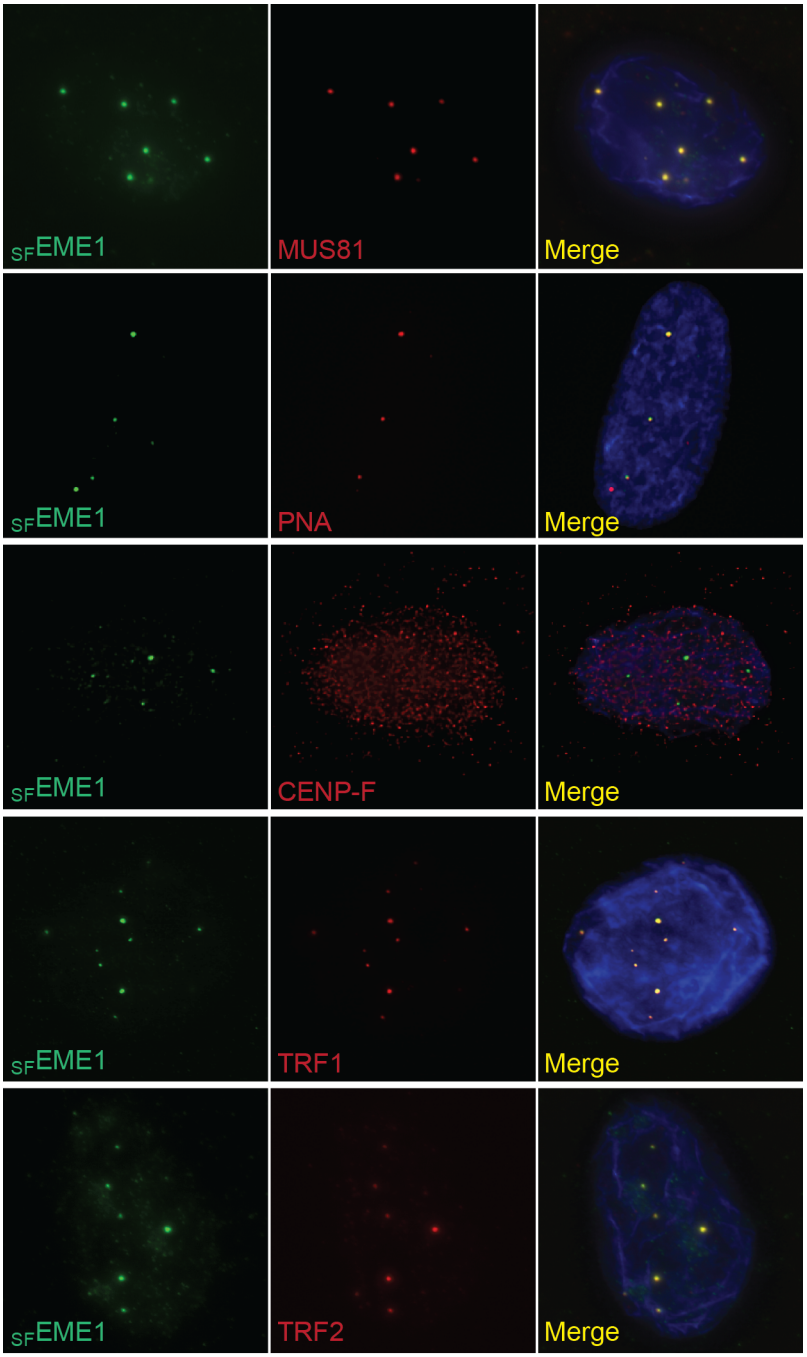

Figure 5.5 $_{SF}$EME1 localises to APBs
The expression of $_{SF}$EME1 was induced in U2OS-TREx^{TM}-$_{SF}$EME1 cells (Section 2.6.2) with 1 µg/ml tetracycline for 48 hr. IF was performed as described in Section 2.12.5. $_{SF}$EME1 was detected using the rabbit anti-FLAG primary antibody (Section 2.1.3.1). IF-FISH was performed as described in Section 2.12.6.

(Section 2.6.2) for 48 hr and IF was performed using the anti-FLAG M2 antibody (Section 2.1.3.1), as described in Section 2.12.5. We observed that both $_{SF}$EME1 and $_{SF}$EME2 formed large foci in cells showing a nuclear CENP-F staining, which is specific for the G2-phase of the cell cycle (Figure 5.4 and 5.5). These foci co-localised with MUS81 and were decorated with TRF1 and TRF2, indicating that $_{SF}$EME1 and $_{SF}$EME2 are found at APBs (Figure 5.4 and 5.5). These results indicate that both MUS81-EME1 and MUS81-EME2 complexes are recruited to APBs and might have a role in telomere maintenance of ALT-positive cells.

5.3 MUS81-EME2 is required for telomere maintenance of ALT-positive cells

Previously, it was shown that MUS81 is required for telomere maintenance of ALT-positive cells, as indicated by the increased loss of telomere signals in MUS81-depleted cells (Zeng et al., 2009). To determine whether the telomeric function of MUS81 depended on the activity of the MUS81-EME1 or MUS81-EME2 complex, we performed Q-FISH analysis (Section 2.12.3), which allows the visualisation of telomere DNA through the hybridisation of telomeric fluorescent probes on metaphase chromosomes. ALT-positive U2OS cells were transfected with control, MUS81, EME1 or EME2 siRNA (Figure 5.6) and all proteins were efficiently depleted, as determined by western blotting (Figure 5.3B, Section 2.8.9). Loss of MUS81 resulted in an increased frequency of telomere-free chromosome ends, as already described (Zeng et al., 2009) (Figure 5.7A). However, when EME1- and EME2-depleted cells were compared, we observed that the rate of telomere signal loss in cells transfected with EME1 siRNA was comparable to that of control-treated cells, whereas depletion of EME2 using two, non-overlapping siRNAs resulted in a two-fold increase in telomere-free ends. To determine the requirement for the MUS81 endonucleases in ALT-negative cells, we performed Q-FISH analysis on metaphase spreads from HT1080 cells transfected with control, MUS81, EME1 or EME2 siRNA (Section 2.6.1), but no significant difference in the rate of telomere loss was observed between the samples (Figure 5.8A-B). Taken together, these results confirm that the role of MUS81 in telomere maintenance is restricted to ALT-positive cells (Zeng et al., 2009) and reveal that MUS81-EME2,

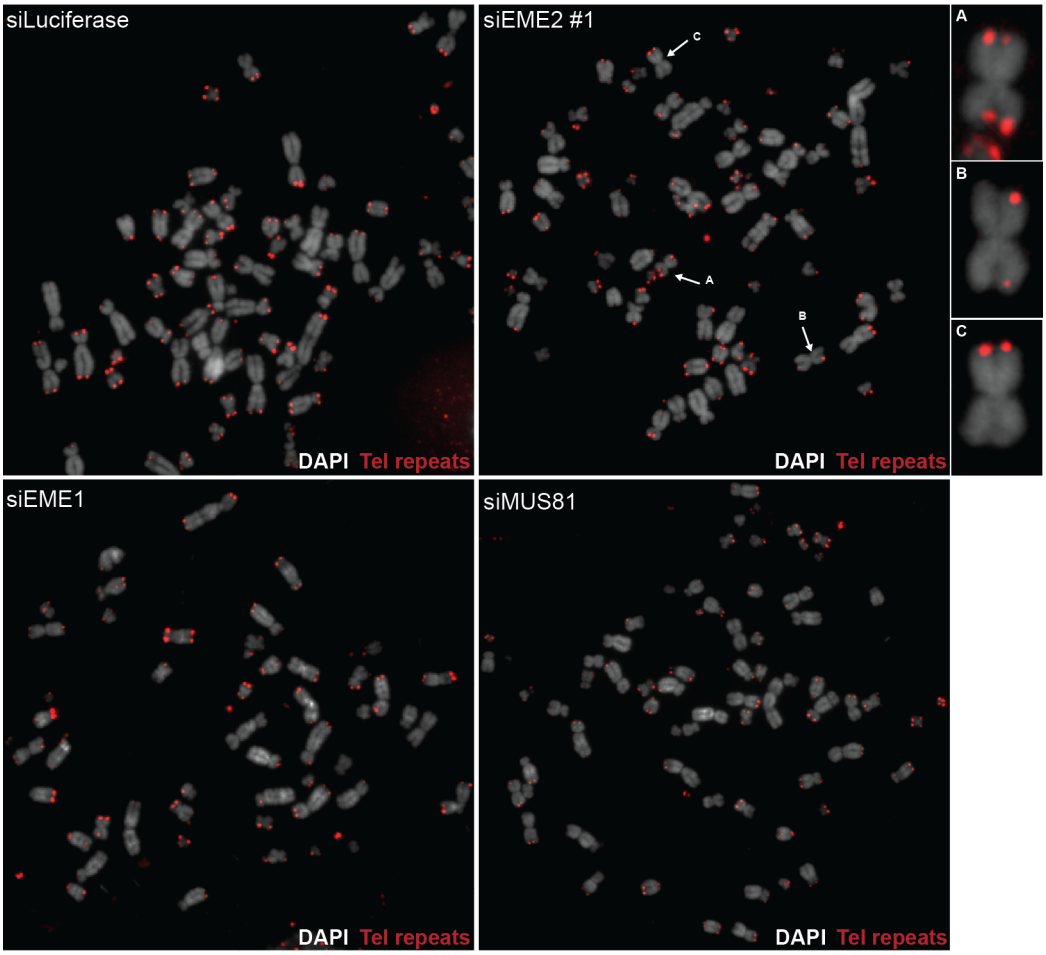

Figure 5.6 Depletion of EME2 or MUS81 causes telomere loss in ALT-positive cells
Representative images of Q-FISH (Section 2.12.3) on metaphase spreads from U2OS cells transfected with the indicated siRNAs (Section 2.6.1). The arrows point to a normal chromosome (A) or to chromosomes with telomere-free ends (B and C).

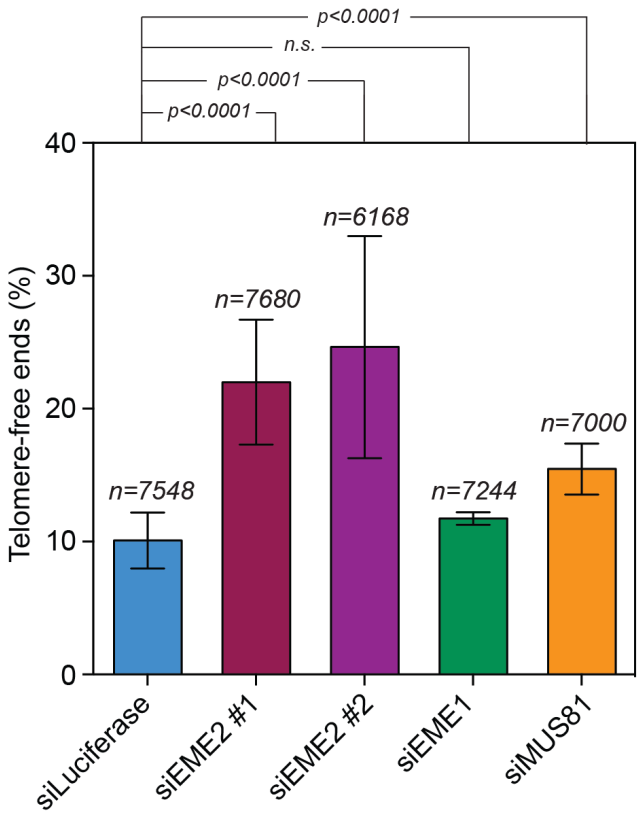

Figure 5.7 Quantification of telomere loss and telomere intensity in siRNA-transfected U2OS cells

A. Quantification of the data shown in Figure 5.6. Data are presented as the mean of three different experiments (±SD). *n* = number of telomere ends analysed. *P* values were determined using Pearson's chi-squared test.

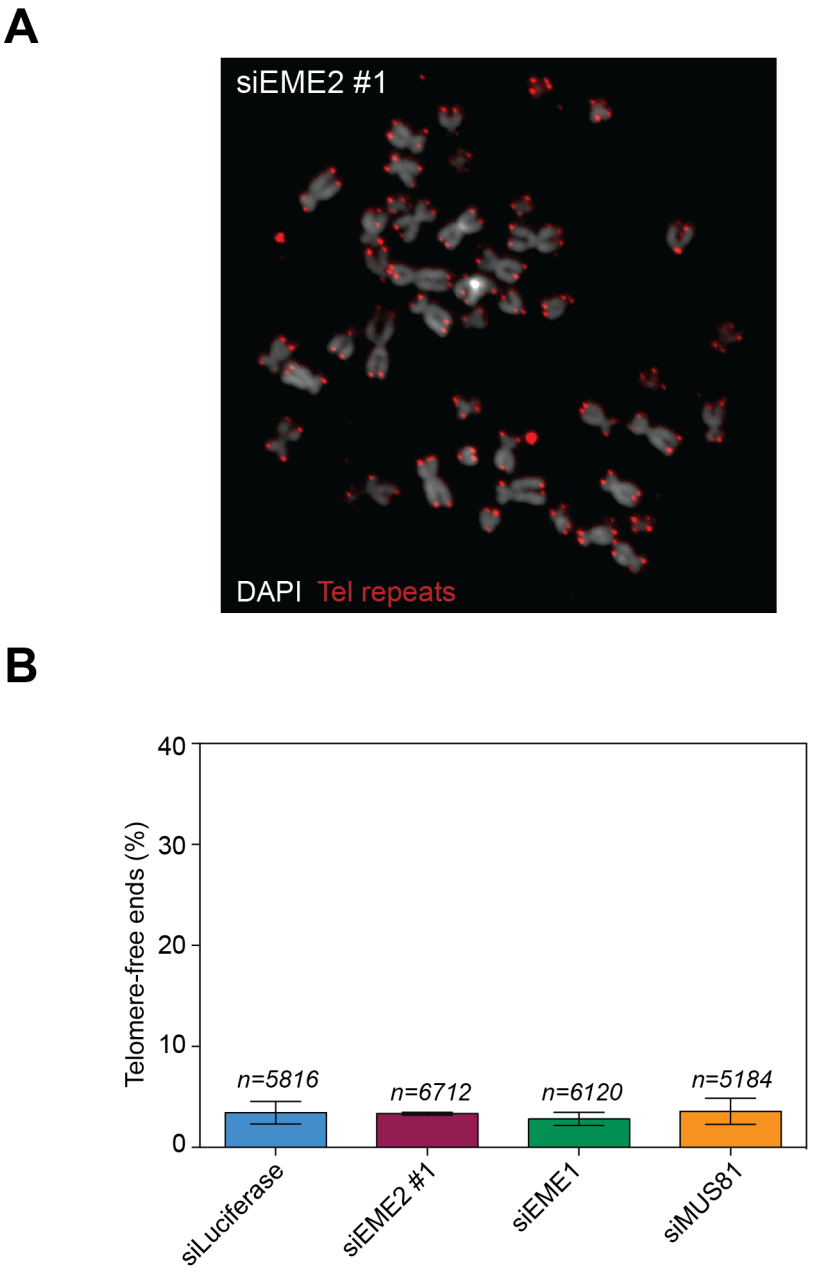

Figure 5.8 Depletion of EME2 or MUS81 does not cause telomere loss in ALT-negative cells
A. Representative images of Q-FISH (Section 2.12.3) on metaphase spreads from HT1080 cells transfected with EME2 siRNA #1 (Section 2.6.1). **B.** Quantification of telomere-free ends from Q-FISH analysis of HT1080 cells transfected with the indicated siRNAs. Data are presented as the mean of three different experiments (±SD). *n* = number of telomere ends analysed.

and not MUS81-EME1, is required for this function. Preliminary data shows that the telomere fluorescence intensity of EME2- and MUS81-depleted cells is significantly lower compared to control or EME1-depleted cells, suggesting that the loss of MUS81 or EME2 results in a decrease in the overall telomere length (data not shown). Furthermore, we did not observe chromosome end-to-end fusion in MUS81- or EME2-depleted cells (data not shown), suggesting that MUS81-EME2 might be required for telomere elongation but not for telomere end protection in ALT-positive cells.

Given that ALT-positive cells are characterised by an elevated frequency of telomere SCEs (T-SCEs) and telomere recombination (Londono-Vallejo et al., 2004), we asked whether loss of EME2 affected the rate of T-SCEs in ALT-cells. Previous studies have shown that depletion of MUS81 in GM847 cells causes a decrease in T-SCEs (Zeng et al., 2009), but it is unclear whether this phenotype resulted from the loss of the MUS81-EME1 or MUS81-EME2 complex. Therefore, to determine the role of the two MUS81 heterodimers in telomere recombination, we analysed the frequency of T-SCEs in U2OS cells depleted of MUS81, EME1 or EME2 (Section 2.6.1). To do so, we used CO-FISH analysis (Figure 5.9, Section 2.12.4), which allows the monitoring of telomere recombination by hybridisation of a G-strand (red)- and a C-strand (green)-specific fluorescent probe: when recombination occurs, the red G-strand- and the green C-strand-specific signals overlap and produce a yellow double signal (T-SCE). We observed that depletion of MUS81 and EME2 caused a significant decrease in the frequency of T-SCEs, compared to control-transfected cells (Figure 5.10). Conversely, the rate of T-SCEs in EME1-depleted cells was comparable to that of cells treated with luciferase siRNA, implicating MUS81-EME2 but not MUS81-EME1 in the production of T-SCEs in ALT-positive cells.

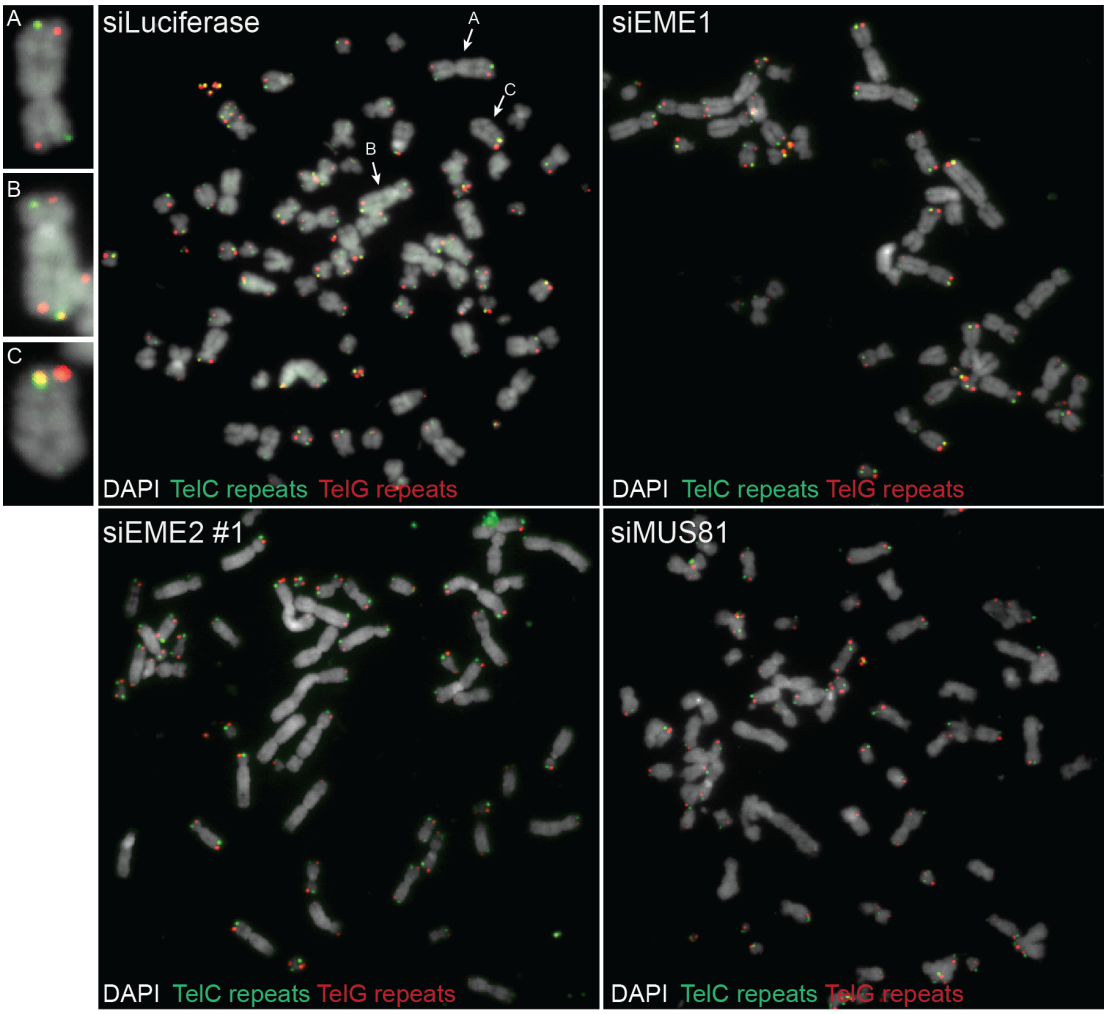

Figure 5.9 Depletion of EME2 or MUS81 causes a significant decrease of T-SCEs in ALT-positive cells

A. Representative images of CO-FISH (Section 2.12.4) on metaphase spreads from U2OS cells transfected with the indicated siRNAs (Section 2.6.1). T-SCEs were detected using a telomeric G-strand PNA probe (red) and a telomeric C-strand PNA probe (green). The arrows point to a chromosome without T-SCEs (A) and to chromosomes with telomeric exchange signals (yellow, B and C).

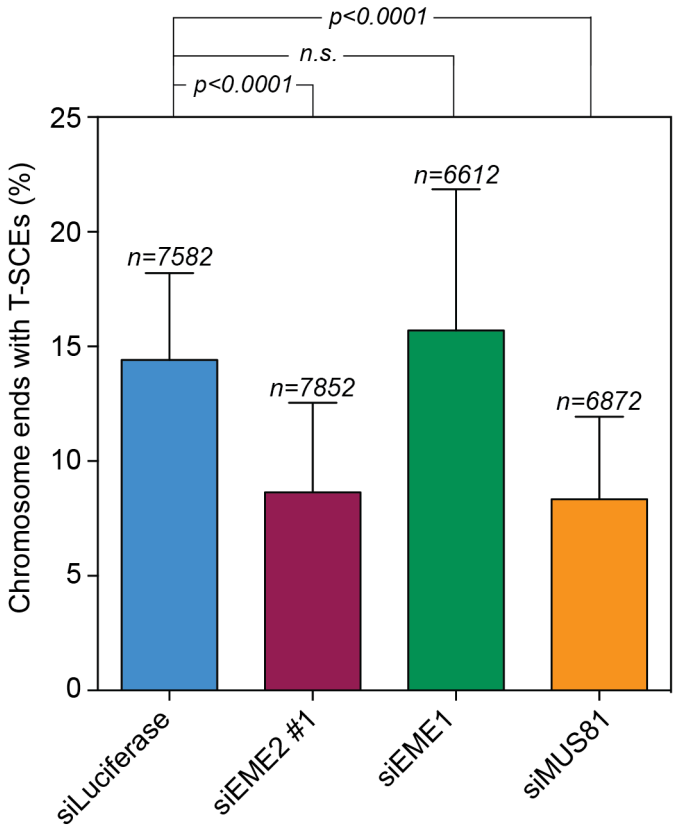

Figure 5.10 Quantification of chromosome ends with T-SCEs
Cells were transfected with the indicated siRNAs (Section 2.6.1). Data are presented as the mean of three different experiments (±SD). *n* = number of telomere ends analysed. *P* values were determined using Pearson's chi-squared test.

5.4 Loss of EME2 increases telomere fragility in ALT-positive cells

Fragile sites are specific chromosomal loci that exhibit gaps and breaks in response to treatment with aphidicolin, which causes DNA replication stress by inhibition of DNA polymerase α, δ and ε (Sheaff et al., 1991). Recently, telomeres have been identified as common fragile sites, as treatment of human and mouse cells with aphidicolin resulted in the appearance of multiple telomeric signals (Sfeir et al., 2009). Telomeric FISH analysis usually results in the visualisation of one signal per chromatid end, although ALT-positive cells exhibit a high level of telomere-free chromosome ends (approximately 10%, Figure 5.7). Upon replication stress, telomeres appear broken, as indicated by the presence of smaller, spatially separated telomeric signals (Figure 5.11A). This abnormal signal pattern has been referred to as telomere fragility and it is likely to result from the presence of regions of single-stranded DNA caused by incomplete replication (Sfeir et al., 2009). The repetitive nature of telomeric DNA constitutes an obstacle to the DNA replication machinery, most likely because of the formation of secondary structures like G4-quadruplexes (Section 1.4.3). In line with this hypothesis, the DNA helicases BLM and RTEL1, which are involved in the removal of G4 structures, repress the fragility phenotype at telomeres (Sfeir et al., 2009). Also, loss of TRF1, which is required for the recruitment of BLM and RTEL1 to telomeres, results in a dramatic increase in telomere fragility (Sfeir et al., 2009).

Given the role of MUS81-EME2 in the repair of stalled RFs, we investigated whether depletion of EME2 in U2OS cells causes an increase in telomere fragility. FISH analysis performed on EME2-depleted U2OS cells revealed that loss of EME2 caused a two-fold increase in the frequency of multiple telomeric signals compared with that observed in cells treated with luciferase or EME1 siRNAs (Figure 5.10B). The increase in chromatids exhibiting telomere fragility was not statistically significant in cells depleted of MUS81. Additionally, we did not observe an increase in telomere fragility in ALT-negative cells (data not shown). Taken together, these results suggest that the activity of MUS81-EME2 might be required to ensure complete DNA replication of telomeres in ALT-positive cells.

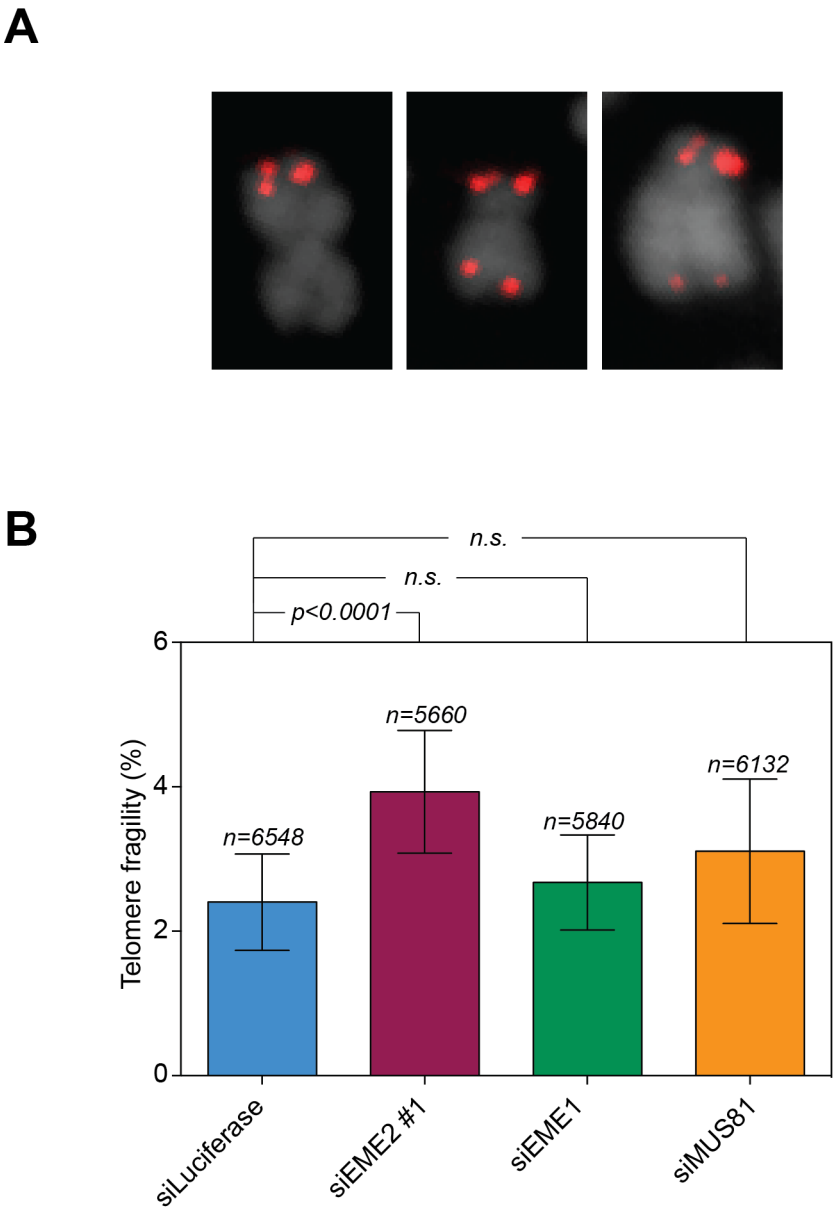

Figure 5.11 Depletion of EME2 causes an increase in telomere fragility in ALT-positive cells
A. Representative images of chromosomes from U2OS cells with multiple telomeric signals. **B.** Quantification of chromosome ends with multiple telomeric signals. Cells were transfected with the indicated siRNAs (Section 2.6.1). Data are presented as the mean of three different experiments (±SD). *n* = number of telomere ends analysed. *P* values were determined using Pearson's chi-squared test.

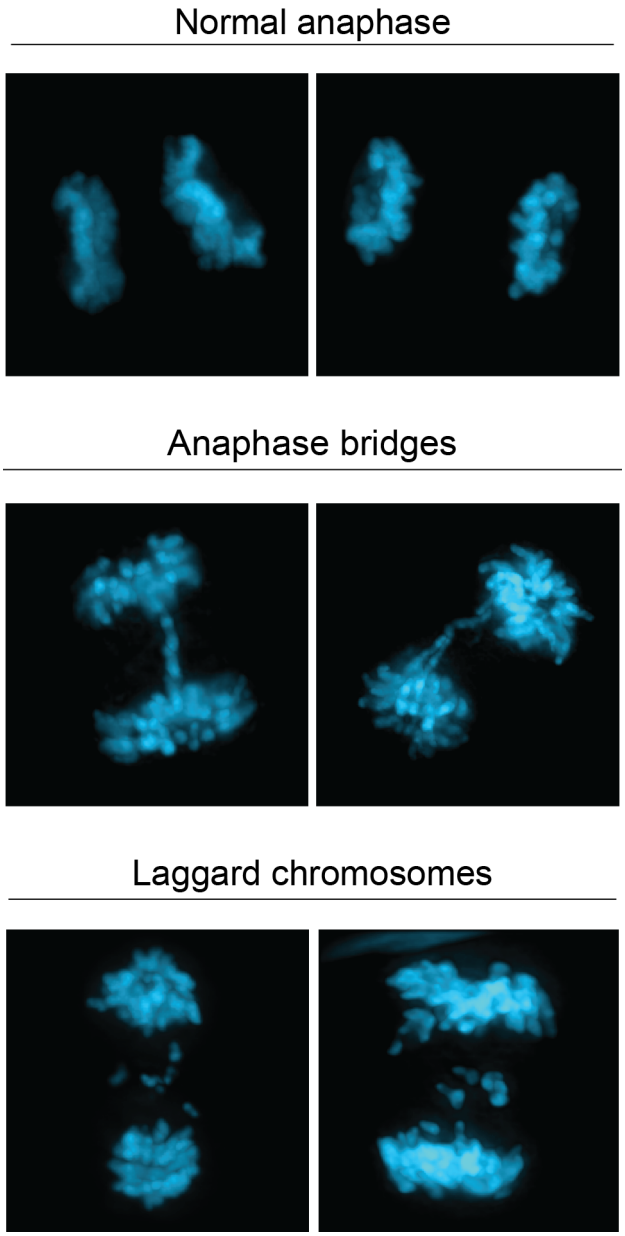

Figure 5.12 Depletion of EME2 or MUS81 causes a significant increase in mitotic aberrations in ALT-positive cells
A. Representative images of DAPI-stained dividing cells undergoing normal mitosis or showing anaphase bridges and laggard chromosomes. **B.** Quantification of mitotic aberrations showed in A in ALT-positive (U2OS) and ALT-negative (HeLa Kyoto) cells transfected with the indicated siRNAs (Section 2.6.1). A total of 150 cells per condition were counted. Data are presented as the mean of three different experiments (±SD). *P* values were determined using a two-tailed Fisher's Exact test.

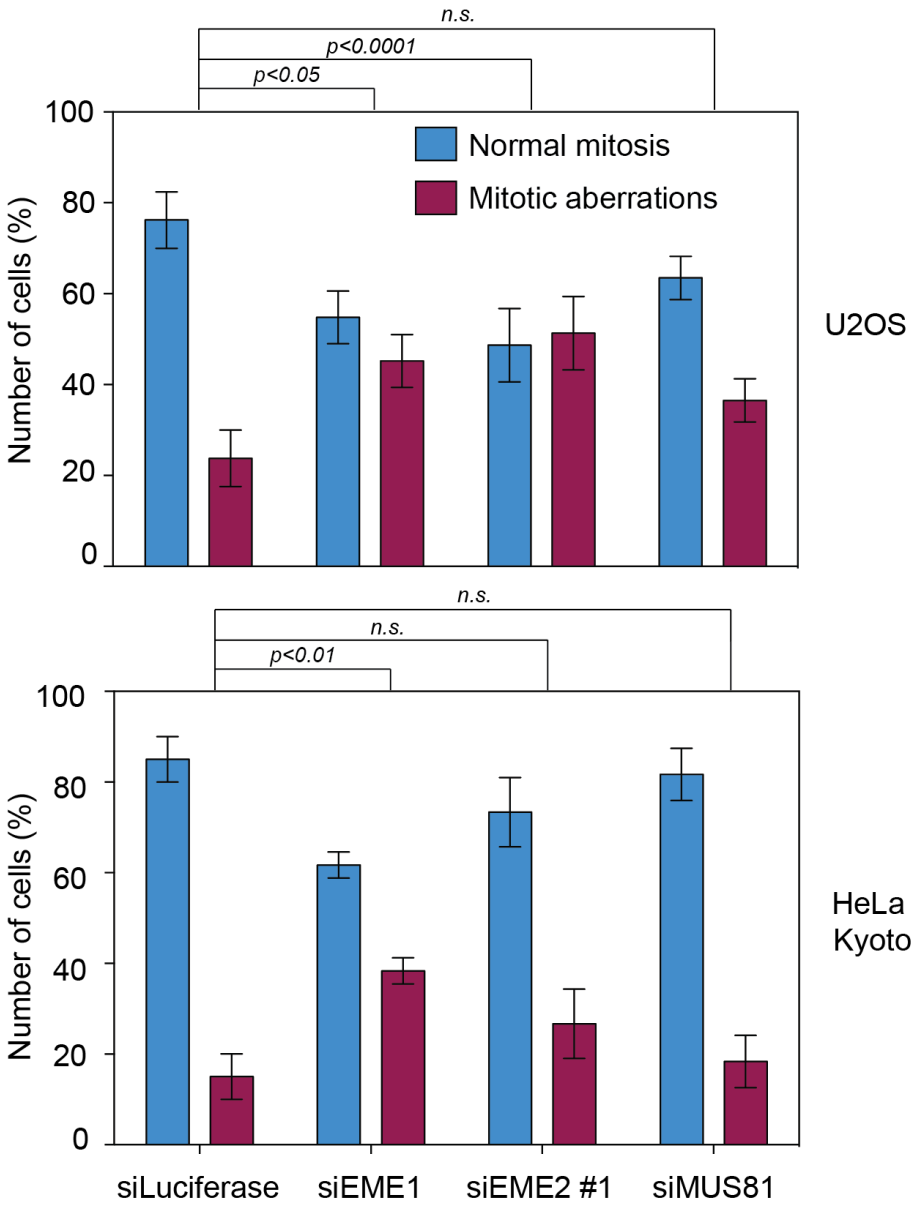

Figure 5.13 Quantification of mitotic aberrations in ALT-positive and ALT-negative
U2OS (ALT-positive) and HeLa Kyoto (telomerase-positive) cells were transfected with the indicated siRNAs (Section 2.6.1). A total of 150 cells per condition were counted. Data are presented as the mean of three different experiments (±SD). *P* values were determined using a two-tailed Fisher's Exact test.

5.5 Depletion of MUS81-EME2 causes mitotic aberrations in ALT-positive cells

Defects in DNA replication progression create regions of unreplicated DNA that represent an impediment for the proper segregation of chromatids during mitosis and result in mitotic aberrations like bulky DAPI-positive anaphase bridges and lagging chromosomes (Figure 5.12), which are indicators of genomic instability. To determine whether depletion of EME2 increased the frequency of mitotic aberrations, we counted the number of anaphase bridges and laggard chromosomes in ALT-positive (U2OS) and telomerase-positive (HeLa Kyoto) cells following treatment with control, EME1, EME2 and MUS81 siRNAs (Figure 5.13, Section 2.6.1). We observed that depletion of EME1 in both ALT-positive and ALT-negative cells caused a two-fold increase in the number of cells exhibiting mitotic aberrations compared to control-treated cells. Loss of EME2 resulted in a significant increase in the rate of mitotic defects in U2OS cells but not in HeLa Kyoto cells. Also, the difference between the frequency of mitotic aberrations in MUS81-depleted and control U2OS cells was not statistically significant. Taken together, these results suggest that depletion of the MUS81-EME2 complex causes mitotic aberrations specifically in ALT-positive cells, whereas loss of MUS81-EME1 contributes to the formation of bulky bridges and laggards in both ALT-positive and ALT-negative cells.

5.6 Conclusions

In summary, these studies indicate that MUS81-EME2, rather than MUS81-EME1, is implicated in telomere maintenance of ALT-positive cells. In support of this, ALT-cells depleted of the MUS81-EME2 complex exhibit an increased frequency in telomere-free chromosome ends and a decreased frequency in T-SCEs when compared to control cells or cells depleted of the MUS81-EME1 complex. We propose that the phenotype observed might be related to the function of MUS81-EME2 at stalled RFs that was described in Chapter 4. Indeed, depletion of EME2 in U2OS cells results in an increase in chromosome ends exhibiting multiple telomeric signals, which have been proposed to indicate defects in RF progression

(Sfeir et al., 2009). Furthermore, loss of EME2 in ALT-cells, but not in telomerase-positive cells, results in an increased rate of bulky DNA bridges and laggard chromosomes, which may derive from regions of unreplicated DNA and are indicators of genomic instability.

CHAPTER 6

Discussion

The role of MUS81 has been widely studied in both yeast and human cells. In yeast, Mus81 forms a heterodimeric complex with Eme1/Mms4 and functions in the resolution of HJs generated during meiotic and mitotic HR and in the repair of stalled RFs (Sections 1.3.1 and 1.3.2). Conversely, human MUS81 forms two heterodimeric complexes, one with EME1 and the other with EME2. However, studies conducted so far on human MUS81 have often disregarded the existence of MUS81-EME2, thereby relating all the phenotypes observed to the activity of MUS81-EME1. As a result, the biological role of MUS81-EME2 and its differences (if any) with MUS81-EME1 have not been investigated. In contrast to EME1, EME2 is exclusively expressed in vertebrates, suggesting that higher eukaryotes require two MUS81 endonucleases to fulfil specific distinct functions. In this study, we performed a detailed comparison of the biochemical properties and cellular functions of the two human MUS81 complexes, providing evidence of distinct biological roles for MUS81-EME1 and MUS81-EME2.

MUS81-EME1 and MUS81-EME2 have different biochemical properties

In this study, we reported the identification of two isoforms of EME2, referred to as EME2A and EME2B (Figure 3.1). Both isoforms align mainly with the C-terminal region of EME1 and interact with endogenous MUS81 (Figure 3.2 and 3.3). Like XPF-ERCC1 and MUS81-EME1, MUS81-EME2A and MUS81-EME2B have a single subunit (MUS81) with an active ERCC4 nuclease domain because, as already reported for EME1, the ERKXXXD catalytic motif has evolutionarily diverged in both EME2A and EME2B (Figure 3.2) (Ciccia et al., 2003). In the case of XPF-ERCC1, the nuclease domain is contained in the XPF subunit, whereas the HhH domain of ERCC1 is required for DNA binding (Tripsianes et al., 2005). It is likely that the inactive subunits of the MUS81 complexes are also necessary for the

targeting of MUS81 to DNA and that the binding of MUS81 to EME1, EME2A or EME2B defines the structure specificity of the endonuclease. Therefore, we decided to characterise the endonucleolytic activities of purified MUS81-$_{SF}$EME1, MUS81-$_{SF}$EME2A and MUS81-$_{SF}$EME2B complexes on a set of synthetic model DNA structures. Given that we observed no remarkable difference between the cleavage activities of MUS81-$_{SF}$EME1 and MUS81-$_{SF}$EME2B, we focused our attention on the comparison between MUS81-$_{SF}$EME1 and MUS81-$_{SF}$EME2A. We found that the interaction between MUS81 and EME2A results in a novel 3'-flap endonuclease, which differs from MUS81-EME1 in both efficiency and mechanisms of cleavage of model DNA substrates. Specifically, MUS81-$_{SF}$EME2A was found to be approximately 10-fold more active than MUS81-$_{SF}$EME1 on all the DNA substrates analysed and, in contrast to MUS81-$_{SF}$EME1, it was able to process a 5'-flap structure by cleaving the DNA strand complementary to that containing the flap (Figure 3.7 and 3.11).

The mechanisms by which MUS81-$_{SF}$EME1 and MUS81-$_{SF}$EME2A cleave a 3'-flap substrate is similar: both complexes cleave the structure in the duplex DNA region 3 to 7 nucleotides on the 5'-side of the branch point (Figure 3.10). This cleavage pattern is consistent with that observed with purified *S. cerevisiae* Mus81-Mms4, which binds to the 5'-end located downstream of the flap and cleaves the duplex DNA 3 to 7 nucleotides upstream of the branch point (Bastin-Shanower et al., 2003). Hence, it is likely that the cleavage mechanism of 3'-flap structures is an evolutionarily conserved feature of the MUS81 endonuclease, which does not depend on the identity of the catalytically inactive subunit. Nevertheless, we observed that, unlike MUS81-$_{SF}$EME1, MUS81-$_{SF}$EME2A was able to process the 3'-flap in a two-step reaction: in the first step, which is comparable to the cleavage by MUS81-$_{SF}$EME1, MUS81-$_{SF}$EME2A removes the flap, generating a nicked duplex molecule; in the second step, it cleaves the nicked DNA generating smaller duplex DNA products (Figure 3.7 and 3.10). MUS81-$_{SF}$EME2A employs the same mechanism to process RFs but the biological relevance of the second reaction step is unknown. We favour the hypothesis that MUS81-EME2A performs only the first step of the cleavage reaction *in vivo,* as it is likely that the complex is displaced from the substrate once the first cleavage has occurred.

MUS81-$_{SF}$EME1 and MUS81-$_{SF}$EME2A differ in the cleavage mechanism of HR intermediate structures such as HJs and D-loops. Although MUS81-$_{SF}$EME1 does not cleave HJs efficiently, it exhibits a preference for mobile over immobile HJs (Figure 3.8). It has been suggested that this preference might be due to the ability of MUS81-EME1 to recognise and cleave transient flap structures that are formed when the mobile HJ undergoes spontaneous thermal denaturation at the junction point (Ciccia et al., 2003). Conversely, MUS81-$_{SF}$EME2A exhibits a 3-fold preference for immobile over mobile HJs (Figure 3.8). This difference might be due to the fact that MUS81-$_{SF}$EME1 and MUS81-$_{SF}$EME2A recognise and bind HJs in different manners. Indeed, the cleavage mechanisms of MUS81-$_{SF}$EME1 and MUS81-$_{SF}$EME2A on immobile HJs are different, with the major cuts inserted by MUS81-$_{SF}$EME1 being closer to the branch point compared to the cleavage sites by MUS81-$_{SF}$EME2A (Figure 3.14).

When D-loops were exposed to the activities of MUS81-$_{SF}$EME1 and MUS81-$_{SF}$EME2A, we found that, unlike MUS81-$_{SF}$EME1, MUS81-$_{SF}$EME2A was able to cleave the invading strand 2 and 4 nucleotides on the 5'-side of the invasion point, thereby disengaging the D-loop structure (Figure 3.15 and 3.16). This result indicates that MUS81-EME2A might function as an anti-recombinase *in vivo.* However, in contrast to the anti-recombinogenic reaction performed by helicases (Section 1.2.2), the cleavage of the D-loop by MUS81-$_{SF}$EME2A would require further processing of the structure in order to remove either the invading or the displaced DNA strand and restore the duplex DNA. D-loops are intermediates of HR-mediated repair of DSBs but they also form at telomeres, where the invasion of duplex DNA by the G-rich single-stranded overhang causes the formation of a T-loop. The release of the single-stranded G-rich-invading overhang by MUS81-EME2A would result in the opening of the T-loop structure, which is required to ensure full telomere replication or to promote HR-mediated telomere elongation in ALT-positive cells. Recent studies show that mouse cells require the activity of the helicase RTEL-1 to dismantle T-loop structures (Vannier et al., 2012). Also, in the absence of RTEL-1, T-loops are released in the form of T-circles in a reaction catalysed by the SLX1-SLX4 endonuclease. Further investigation is required to understand whether the expression and/or the activity of RTEL-1 varies according to the cell type and whether cells defective in RTEL-1-mediated T-loop

disassembly require the endonucleolytic activity of MUS81-EME2A to dismantle the T-loop structure.

Taken together, these results indicate that MUS81-EME1 and MUS81-EME2A are 3'-flap endonucleases that differ in cleavage efficiency and substrate preference. Indeed, MUS81-$_{SF}$EME2A is more active than MUS81-$_{SF}$EME1 and it preferentially cleaves 3'-flaps and RFs, whereas the nicked HJ is the preferred substrate for MUS81-$_{SF}$EME1. To further investigate the basis of these differences, future studies will be aimed at determining the structural properties of MUS81-EME1 and MUS81-EME2A. We believe that, depending on whether MUS81 interacts with EME1 or EME2A, the complex might adopt a different structural conformation, thereby conferring distinct biochemical properties.

EME2A might be the only functional isoform

To determine whether both EME2 isoforms are translated in human cells, we raised a rabbit polyclonal antibody and tested its specificity for western blotting using human WCEs. We observed that our antibody could only recognise a band corresponding to EME2A (42 kDa), whereas no band at the predicted size of EME2B (49 kDa) was detected (Figure 4.1A). Hence, given that we could not observe any remarkable difference between the cleavage activities of MUS81-$_{SF}$EME2B and MUS81-$_{SF}$EME1 (Figure 3.7), we favour the hypothesis that, despite the presence of two transcripts, human cells translate only one isoform of EME2, i.e. EME2A. We do not, however, exclude the possibility of tissue-specific expression.

MUS81, EME1 and EME2 are interdependent

To address the biological role of EME2 and determine the functional dissection of the two MUS81 complexes, we depleted MUS81, EME1 or EME2 (i.e. EME2A and EME2B) in human cells. Previous studies had shown that the depletion of MUS81 or EME1 resulted in the destabilisation of the MUS81-EME1 complex (Forment et al., 2011). Similarly, we found that knockdown of MUS81 resulted in the depletion

of EME2, whereas the knockdown of EME2 caused approximately 30% decrease in the level of MUS81, which is likely to correspond to the fraction of the total cellular MUS81 that interacts with EME2 (Figure 4.1A). This data, together with the evidence that EME2 does not interact with EME1 (data not shown), indicates that MUS81 forms two mutually exclusive complexes with EME1 and EME2.

MUS81-EME2, rather than MUS81-EME1, appears to process stalled RFs

The biological functions of the MUS81 endonuclease have been widely studied in the past years. However, little attention has been paid to understanding whether the phenotype observed was related to MUS81-EME1 or MUS81-EME2. For example, after prolonged cisplatin or HU treatment, murine Mus81 cleaves stalled RFs in order to create one-sided DSBs that are required for the initiation of HR-mediated DNA repair (Hanada et al., 2007). Without any supporting evidence, this activity was related to the Mus81-Eme1 complex. In my work, I determined whether the role of human MUS81 at stalled RFs depends on the activity of MUS81-EME1 or MUS81-EME2. Treatment with increasing concentrations of HU or cisplatin induced DSBs in both luciferase-transfected cells and EME1-depleted cells, suggesting that EME1 was not required for DSB formation (Figure 4.3 and 4.4). Conversely, MUS81- and EME2-depleted cells displayed a significant decrease in DSBs, indicating that MUS81-EME2, rather than MUS81-EME1 is important for repair of stalled RFs.

Although DSBs are harmful to cells, their formation is essential for the HR-mediated repair of stalled RFs. If forks are left unrepaired, regions of unreplicated DNA accumulate and cause chromosomes to break when sister chromatids separate during mitosis. Given the function of Mus81 in the repair of stalled RFs, its depletion in HU-treated mouse ES cells results in an increase in chromosomal aberrations (Hanada et al., 2007). In human cells, collapse of stalled RFs appears to be dependent on the activity of the MUS81-EME2 endonuclease. Hence, it is not surprising that, 24 hr after treatment with HU, MUS81- and EME2-depleted cells accumulate more chromosomal aberrations than luciferase or EME1 siRNA-treated cells, indicating that MUS81-EME2 is required for the maintenance of genomic

stability after treatment with HU (Figure 4.6 and Table 4.1). In mouse ES cells, the activity of MUS81 is required for the restart of DNA replication (Hanada et al., 2007). Whether MUS81 is important for RF restart in human cells is unclear. DNA fiber analysis of U2OS cells after 24 hr treatment with HU revealed that restart of DNA replication occurs by new origin firing and does not depend on MUS81-mediated DSB formation (Petermann et al., 2010). However, a recent study showed that replication restart following HU treatment is impaired in MUS81-depleted cells (Ying et al., 2013). The reason of this difference is unknown and needs further investigation.

When we analysed metaphase spreads from untreated MUS81-, EME1- and EME2-depleted cells, we noticed that cells transfected with EME2 siRNA showed an elevated frequency of endoreduplication (Figure 4.7). At present, it is unclear what causes chromosomes to associate into these 'butterfly-like' structures, although it is likely that this phenotype results from repetitive failure of chromatid segregation during mitosis. Endoreduplication has been observed in human cells depleted of XRCC3 and MUS81, albeit at a much lower rate than that observed in EME2-depleted cells (Hiyama et al., 2006; Yoshihara et al., 2004). Interestingly, depletion of MUS81 dramatically reduced the frequency of diplochromosomes, indicating that the high rate of endoreduplication is exclusively due to depletion of the MUS81-EME2 complex, whereas loss of all cellular MUS81 alleviates the severity of the phenotype.

Evidence for a role of MUS81 in HJ resolution came from studies on BS cells, which are defective in the HJ dissolution pathway and display an elevated rate of SCEs. Depletion of MUS81 in these cells caused a decrease in the frequency of SCEs, indicating that MUS81 contributes to SCE formation (Wechsler et al., 2011). To test whether the activity of MUS81 on HJs was dependent on MUS81-EME1 or MUS81-EME2, we analysed SCE formation in BS cells depleted of EME1, EME2 or MUS81 (Figure 4.9). In line with the role of MUS81-EME2 in the repair of stalled RF, we found that cells depleted of EME2 showed SCE frequencies comparable to that of control-treated cells, whereas both MUS81 and EME1 depletion caused a significant decrease in the frequency of SCEs. Given that SLX4 contributes to SCE formation in BS cells and it works in the same pathway of HJ resolution as MUS81,

our results further confirm a model in which SLX1-SLX4 and MUS81-EME1 cooperate to efficiently process dHJs that escape BTR-mediated dissolution.

Interactions between MUS81 and EME2 are cell-cycle dependent

In further support of the role of MUS81-EME2 during DNA replication, we found that the interaction between MUS81 and EME2 is cell cycle-regulated and occurs predominantly during S-phase (Figure 4.5). However, given that the level of EME2 is stable throughout the cell cycle, it is unclear how the formation of the MUS81-EME2 complex is prevented (or reduced) during G2 and M phase. Although we could not detect a slower-migrating form of EME2 that would indicate the presence of a cell cycle-dependent phosphorylation, further studies should be aimed at determining whether the cell cycle-specific interaction with MUS81 is modulated by post-translational modifications. In addition, it was surprising to discover that, like MUS81-EME1, MUS81-EME2 can interact with SLX1-SLX4 and XPF-ERCC1 (Figure 4.8). We believe that the low expression level of EME2 has been an impediment for its identification as an SLX4-interacting protein in previous studies. Also, given that MUS81 interacts with SLX4 predominantly during the G2/M phase of the cell cycle, when the level of the MUS81-EME2 complex is low, it is likely that SLX1-SLX4 interacts mainly with MUS81-EME1. However, a smaller fraction of SLX4 interacts with MUS81 during S-phase. Hence, it is likely that, while the majority of SLX1-SLX4 forms a complex with MUS81-EME1 during G2/M, a smaller fraction interacts with MUS81-EME2 during S-phase. Whether the interaction between SLX1-SLX4-XPF-ERCC1 and MUS81-EME2 is cell cycle stage-dependent will be investigated in future studies.

In summary, our results highlight a difference between the biological roles of MUS81-EME1 and MUS81-EME2. It is likely that, while MUS81-EME1 cooperates with SLX1-SLX4 to process intact HJs by a nick and counter-nick mechanism, the activity of MUS81-EME2 is required for the repair of stalled RFs. After prolonged treatments with replication stalling agents (e.g. HU or cisplatin), MUS81-EME2 cleaves stalled RFs to create a one-ended DSB that is required for HR-mediated repair (Figure 6.1). Remarkably, the functional difference observed between

MUS81-EME1 and MUS81-EME2 is consistent with our biochemical analysis, which shows that purified MUS81-EME2 preferentially cleaves 3'-flaps and RF substrates, whereas the nicked HJ is the preferred substrate of MUS81-EME1.

MUS81-EME2, but not MUS81-EME1, appears to be required for telomere maintenance of ALT cells

The activity of the MUS81 endonuclease is required for telomere maintenance of ALT-positive cells, which are characterised by telomere length heterogeneity and by an elevated frequency of T-SCEs (Bryan et al., 1995; Londono-Vallejo et al., 2004). Loss of MUS81 in ALT-positive cells causes telomere loss and a significant decrease in T-SCEs and cell viability (Zeng et al., 2009). Conversely, in accordance with the evidence that MUS81 does not associate with telomeres of telomerase-positive cells, telomere loss was not observed after depletion of MUS81 in HT1080, MCF-7 or mouse embryonic fibroblasts. Our findings reveal that the role of MUS81 in telomere maintenance of ALT-positive cells might be dependent on the activity of MUS81-EME2. In support of this, FISH analysis performed on metaphase spreads from MUS81-, EME1- or EME2-depleted ALT-positive cells showed that loss of EME2 or MUS81 causes an increase in the frequency of telomere-free ends and a significant decrease in the rate of T-SCEs (Figure 5.6, 5.7, 5.9 and 5.10). Conversely, the fraction of EME1-depleted cells containing telomere-free ends and T-SCEs was comparable to that of control-treated cells. Also, in line with what was already observed for MUS81, loss of EME2 did not cause telomeric loss in ALT-negative cells (Figure 5.8), confirming that the function of MUS81-EME2 is specific to cells that use the ALT pathway.

MUS81-EME2 might be required for the processing of stalled RFs at telomeres of ALT cells

Cell cycle distribution analysis of MUS81-, EME1- or EME2-depleted ALT-positive and ALT-negative cells revealed that loss of EME2 causes ALT-positive cells to accumulate in the G2/M phase of the cell cycle (Figure 5.1 and 5.2). Interestingly, a similar phenotype has been observed in RPA-depleted U2OS and GM847 cells and

it correlated with the generation of large telomeric aggregates at the ends of metaphase chromosomes (Grudic et al., 2007). We observed that depletion of EME2 caused a significant increase in chromosome ends carrying multiple telomeric signals (Figure 5.11). This feature has been referred to as telomere fragility and reflects a defect in the replication of telomeric DNA (Sfeir et al., 2009). Telomeres are a difficult substrate for the DNA replication machinery because telomeric repeats promote the formation of G4 quadruplexes. Remarkably, in ALT-positive cells, many chromosome ends display telomere fragility (approximately 2.3%, Figure 5.11) and depletion of proteins involved in the repair of stalled RFs like FEN1, WRN, FANCD2 and MUS81 causes an elevated rate of telomere loss (Crabbe et al., 2004; Fan et al., 2009; Saharia and Stewart, 2009; Zeng et al., 2009). It is likely that ALT-positive cells are more sensitive to defects in the repair of stalled RFs and, given that telomere replication is unidirectional and starts from the sub-telomeric region, unrepaired stalled RFs can cause the loss of the distal telomeric sequences. Therefore, our finding that MUS81-EME2 functions in the repair of stalled RFs upon replication stress might explain the requirement for the MUS81-EME2 complex in telomere maintenance of ALT-positive cells.

The efficient repair of stalled RFs is essential to avoid the accumulation of unreplicated DNA, which constitutes an impediment to the correct chromosome segregation during cell division. Defects in sister chromatid disjunction during anaphase cause genomic instability and induce mitotic aberrations such as lagging chromosomes and DAPI-positive bulky bridges (Figure 5.12). In line with a role of MUS81-EME2 in the repair of stalled RFs at telomeres of ALT-positive cells, we observed that depletion of EME2 in U2OS cells results in an elevated frequency of mitotic aberrations, whereas the number of EME2-depleted HeLa Kyoto cells displaying bridges and laggards was not significantly different from that of cells transfected with luciferase siRNA (Figure 5.13). Interestingly, loss of EME1 caused a significant increase in mitotic aberrations in both ALT-positive and ALT-negative cells, suggesting that the function of EME1 is required for the maintenance of genomic stability and for proper chromosome segregation.

It has been proposed that elongation of telomeres in ALT-positive cells occurs at APBs (Draskovic et al., 2009). We found that both EME1 and EME2 localise to

APBs, indicating a role for MUS81-EME1 and MUS81-EME2 in telomere lengthening (Figure 5.4 and 5.5). We believe that the presence of EME1 at APBs might be related to the function of the MUS81-EME1 complex in the processing of recombination intermediates that are generated during ALT. Also, as described before, processing of stalled RFs by MUS81-EME2 creates a one-ended DSB that triggers HR and the formation of HJs, which are substrates of the SLX-MUS complex.

MUS81-depleted cells exhibit a milder phenotype than EME2-depleted cells

Finally, in all the experiments performed in this study, we observed that the phenotype displayed by EME2-depleted cells was more severe that that of MUS81-depleted cells. Remarkably, we reported that co-depletion of EME2 and MUS81 could rescue both the elevated frequency of endoreduplication in EME2-depleted RPE-1 hTERT cells (Figure 4.7) and the G2/M arrest caused by the loss of EME2 in ALT-positive cells (Figure 5.3). Although a clear explanation for this result is missing, we propose a scenario in which, given that loss of EME2 causes the depletion of the fraction of MUS81 that interacts with EME2, the residual MUS81, in complex with EME1, functions as a dominant negative. Hence, only the complete depletion of MUS81 induces cells to employ other MUS81-independent DNA repair pathways. Furthermore, the observation that loss of EME1 does not trigger a cell cycle arrest may be due to the presence of two redundant mechanisms of HJ resolution in human cells, whereby HJs that have escaped resolution by the SLX-MUS complex are processed by the HJ resolvase GEN1 later in the cell cycle. In conclusion, on the basis of the observation that both MUS81-EME1 and MUS81-EME2 can interact with SLX1-SLX4 and XPF-ERCC1 (Figure 4.8), we believe that future studies should focus on the biological relevance of these two multi-nuclease complexes and on the contribution of SLX1-SLX4 to the activity of MUS81-EME2.

Conclusions

Previous studies conducted to determine the cellular role of the MUS81 endonuclease have often disregarded the existence of two MUS81 complexes in higher eukaryotes: MUS81-EME1 and MUS81-EME2. In this study, we investigate the functional differences between the two human MUS81 heterodimers and we provide evidence for distinct biological roles of MUS81-EME1 and MUS81-EME2: while MUS81-EME1 co-operates with SLX1-SLX4 to resolve joint molecules that are formed during HR-mediated DSB repair, MUS81-EME2 cleaves stalled RFs and creates one-ended DSBs that are substrates for HR-mediated RF repair. Hence, we believe that future studies should be more regardful of the existence of two human MUS81 complexes and should discriminate between the activities of MUS81-EME1 and MUS81-EME2.

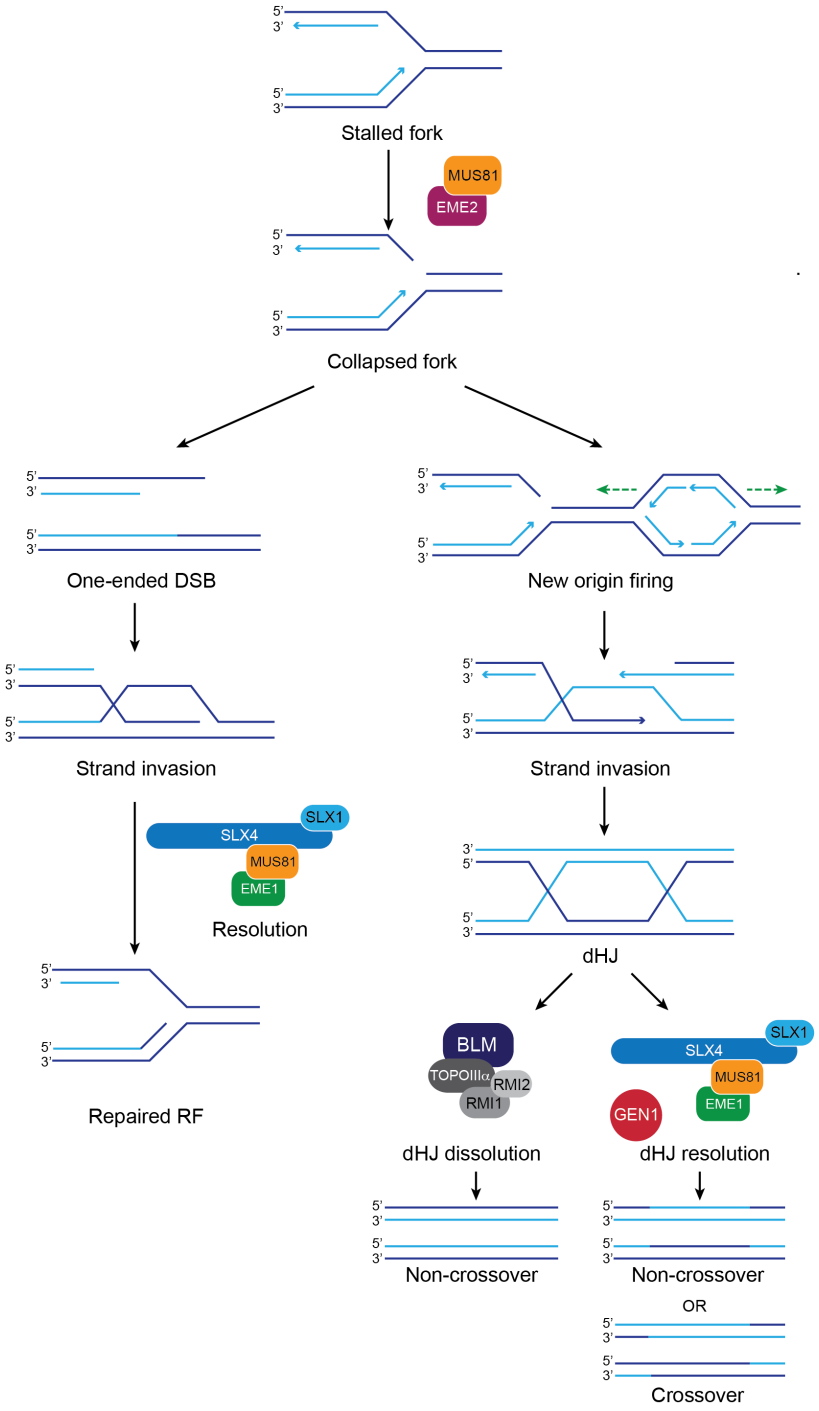

Figure 6.1 Model for MUS81-EME2 and MUS81-EME1 functions in the repair of stalled RFs

MUS81-EME2 cleaves stalled RFs to create a one-ended DSB. RAD51-mediated strand invasion initiates HR and results in the formation of a D-loop structure. Resolution of the single HJ by SLX1-SLX4 and MUS81-EME1 restores the RF and allows DNA replication to restart. In a scenario in which DNA replication restarts by the firing of new origins, RAD51-mediated strand invasion is followed by second-end capture and by the formation of a dHJ, which can be processed by BTR-mediated dissolution or by SLX-MUS/GEN1-mediated resolution.

BIBLIOGRAPHY

Abraham, J., Lemmers, B., Hande, M.P., Moynahan, M.E., Chahwan, C., Ciccia, A., Essers, J., Hanada, K., Chahwan, R., Khaw, A.K.*, et al.* (2003). Eme1 is involved in DNA damage processing and maintenance of genomic stability in mammalian cells. EMBO J *22*, 6137-6147.

Abreu, E., Aritonovska, E., Reichenbach, P., Cristofari, G., Culp, B., Terns, R.M., Lingner, J., and Terns, M.P. (2010). TIN2-tethered TPP1 recruits human telomerase to telomeres in vivo. Mol Cell Biol *30*, 2971-2982.

Adair, G.M., Rolig, R.L., Moore-Faver, D., Zabelshansky, M., Wilson, J.H., and Nairn, R.S. (2000). Role of ERCC1 in removal of long non-homologous tails during targeted homologous recombination. EMBO J *19*, 5552-5561.

Agarwal, S., van Cappellen, W.A., Guenole, A., Eppink, B., Linsen, S.E., Meijering, E., Houtsmuller, A., Kanaar, R., and Essers, J. (2011). ATP-dependent and independent functions of Rad54 in genome maintenance. J Cell Biol *192*, 735-750.

Alt, F.W., Zhang, Y., Meng, F.L., Guo, C., and Schwer, B. (2013). Mechanisms of programmed DNA lesions and genomic instability in the immune system. Cell *152*, 417-429.

Andersen, S.L., Bergstralh, D.T., Kohl, K.P., LaRocque, J.R., Moore, C.B., and Sekelsky, J. (2009). Drosophila MUS312 and the vertebrate ortholog BTBD12 interact with DNA structure-specific endonucleases in DNA repair and recombination. Mol Cell *35*, 128-135.

Araki, M., Masutani, C., Takemura, M., Uchida, A., Sugasawa, K., Kondoh, J., Ohkuma, Y., and Hanaoka, F. (2001). Centrosome protein centrin 2/caltractin 1 is part of the xeroderma pigmentosum group C complex that initiates global genome nucleotide excision repair. J Biol Chem *276*, 18665-18672.

Aravind, L., and Koonin, E.V. (2000). SAP - a putative DNA-binding motif involved in chromosomal organization. Trends Biochem Sci *25*, 112-114.

Aravind, L., and Koonin, E.V. (2001). Prokaryotic homologs of the eukaryotic DNA-end-binding protein Ku, novel domains in the Ku protein and prediction of a prokaryotic double-strand break repair system. Genome Res *11*, 1365-1374.

Arnaudeau, C., Lundin, C., and Helleday, T. (2001). DNA double-strand breaks associated with replication forks are predominantly repaired by homologous recombination involving an exchange mechanism in mammalian cells. J Mol Biol *307*, 1235-1245.

Arnaudeau, C., Tenorio Miranda, E., Jenssen, D., and Helleday, T. (2000). Inhibition of DNA synthesis is a potent mechanism by which cytostatic drugs induce homologous recombination in mammalian cells. Mutat Res *461*, 221-228.

Autexier, C., and Lue, N.F. (2006). The structure and function of telomerase reverse transcriptase. Annu Rev Biochem *75*, 493-517.

Ayoub, N., Rajendra, E., Su, X., Jeyasekharan, A.D., Mahen, R., and Venkitaraman, A.R. (2009). The carboxyl terminus of Brca2 links the disassembly of Rad51 complexes to mitotic entry. Curr Biol *19*, 1075-1085.

Bachrati, C.Z., and Hickson, I.D. (2003). RecQ helicases: suppressors of tumorigenesis and premature aging. Biochem J *374*, 577-606.

Bailey, S.M., Brenneman, M.A., and Goodwin, E.H. (2004). Frequent recombination in telomeric DNA may extend the proliferative life of telomerase-negative cells. Nucleic Acids Res *32*, 3743-3751.

Bailly, A.P., Freeman, A., Hall, J., Declais, A.C., Alpi, A., Lilley, D.M., Ahmed, S., and Gartner, A. (2010). The Caenorhabditis elegans homolog of Gen1/Yen1 resolvases links DNA damage signaling to DNA double-strand break repair. PLoS Genet *6*, e1001025.

Balakrishnan, L., and Bambara, R.A. (2013). Flap endonuclease 1. Annu Rev Biochem *82*, 119-138.

Barber, L.J., Youds, J.L., Ward, J.D., McIlwraith, M.J., O'Neil, N.J., Petalcorin, M.I., Martin, J.S., Collis, S.J., Cantor, S.B., Auclair, M.*, et al.* (2008). RTEL1 maintains genomic stability by suppressing homologous recombination. Cell *135*, 261-271.

Bastin-Shanower, S.A., Fricke, W.M., Mullen, J.R., and Brill, S.J. (2003). The mechanism of Mus81-Mms4 cleavage site selection distinguishes it from the homologous endonuclease Rad1-Rad10. Mol Cell Biol *23*, 3487-3496.

Batzer, M.A., and Deininger, P.L. (2002). Alu repeats and human genomic diversity. Nat Rev Genet *3*, 370-379.

Baumann, C., Korner, R., Hofmann, K., and Nigg, E.A. (2007). PICH, a centromere-associated SNF2 family ATPase, is regulated by Plk1 and required for the spindle checkpoint. Cell *128*, 101-114.

Baumann, P., Benson, F.E., and West, S.C. (1996). Human Rad51 protein promotes ATP-dependent homologous pairing and strand transfer reactions in vitro. Cell *87*, 757-766.

Baumann, P., and Cech, T.R. (2001). Pot1, the putative telomere end-binding protein in fission yeast and humans. Science *292*, 1171-1175.

Bayani, J., and Squire, J.A. (2005). Sister chromatid exchange. Curr Protoc Cell Biol *Chapter 22*, Unit 22 27.

Beattie, T.L., Zhou, W., Robinson, M.O., and Harrington, L. (1998). Reconstitution of human telomerase activity in vitro. Curr Biol *8*, 177-180.

Bechter, O.E., Zou, Y., Walker, W., Wright, W.E., and Shay, J.W. (2004). Telomeric recombination in mismatch repair deficient human colon cancer cells after telomerase inhibition. Cancer Res *64*, 3444-3451.

Bennett, R.J., Dunderdale, H.J., and West, S.C. (1993). Resolution of Holliday junctions by RuvC resolvase: cleavage specificity and DNA distortion. Cell *74*, 1021-1031.

Bennett, R.J., and West, S.C. (1996). Resolution of Holliday junctions in genetic recombination: RuvC protein nicks DNA at the point of strand exchange. Proc Natl Acad Sci U S A *93*, 12217-12222.

Benson, F.E., Baumann, P., and West, S.C. (1998). Synergistic actions of Rad51 and Rad52 in recombination and DNA repair. Nature *391*, 401-404.

Benson, F.E., Stasiak, A., and West, S.C. (1994). Purification and characterization of the human Rad51 protein, an analogue of E. coli RecA. EMBO J *13*, 5764-5771.

Bhattacharyya, S., Keirsey, J., Russell, B., Kavecansky, J., Lillard-Wetherell, K., Tahmaseb, K., Turchi, J.J., and Groden, J. (2009). Telomerase-associated protein 1, HSP90, and topoisomerase IIalpha associate directly with the BLM helicase in immortalized cells using ALT and modulate its helicase activity using telomeric DNA substrates. J Biol Chem *284*, 14966-14977.

Bianchi, A., Smith, S., Chong, L., Elias, P., and de Lange, T. (1997). TRF1 is a dimer and bends telomeric DNA. EMBO J *16*, 1785-1794.

Bianchi, V., Pontis, E., and Reichard, P. (1986). Changes of deoxyribonucleoside triphosphate pools induced by hydroxyurea and their relation to DNA synthesis. J Biol Chem *261*, 16037-16042.

Biffi, G., Tannahill, D., McCafferty, J., and Balasubramanian, S. (2013). Quantitative visualization of DNA G-quadruplex structures in human cells. Nat Chem *5*, 182-186.

Bilaud, T., Brun, C., Ancelin, K., Koering, C.E., Laroche, T., and Gilson, E. (1997). Telomeric localization of TRF2, a novel human telobox protein. Nat Genet *17*, 236-239.

Blais, V., Gao, H., Elwell, C.A., Boddy, M.N., Gaillard, P.H., Russell, P., and McGowan, C.H. (2004). RNA interference inhibition of Mus81 reduces mitotic recombination in human cells. Mol Biol Cell *15*, 552-562.

Blanco, M.G., Matos, J., Rass, U., Ip, S.C., and West, S.C. (2010). Functional overlap between the structure-specific nucleases Yen1 and Mus81-Mms4 for DNA-damage repair in S. cerevisiae. DNA Repair (Amst) *9*, 394-402.

Blasco, M.A., Lee, H.W., Hande, M.P., Samper, E., Lansdorp, P.M., DePinho, R.A., and Greider, C.W. (1997). Telomere shortening and tumor formation by mouse cells lacking telomerase RNA. Cell *91*, 25-34.

Blasco, M.A., Rizen, M., Greider, C.W., and Hanahan, D. (1996). Differential regulation of telomerase activity and telomerase RNA during multi-stage tumorigenesis. Nat Genet *12*, 200-204.

Boboila, C., Alt, F.W., and Schwer, B. (2012). Classical and alternative end-joining pathways for repair of lymphocyte-specific and general DNA double-strand breaks. Adv Immunol *116*, 1-49.

Boddy, M.N., Gaillard, P.H., McDonald, W.H., Shanahan, P., Yates, J.R., 3rd, and Russell, P. (2001). Mus81-Eme1 are essential components of a Holliday junction resolvase. Cell *107*, 537-548.

Boddy, M.N., Lopez-Girona, A., Shanahan, P., Interthal, H., Heyer, W.D., and Russell, P. (2000). Damage tolerance protein Mus81 associates with the FHA1 domain of checkpoint kinase Cds1. Mol Cell Biol *20*, 8758-8766.

Bogliolo, M., Lyakhovich, A., Callen, E., Castella, M., Cappelli, E., Ramirez, M.J., Creus, A., Marcos, R., Kalb, R., Neveling, K.*, et al.* (2007). Histone H2AX and Fanconi anemia FANCD2 function in the same pathway to maintain chromosome stability. EMBO J *26*, 1340-1351.

Bohr, V.A. (2008). Rising from the RecQ-age: the role of human RecQ helicases in genome maintenance. Trends Biochem Sci *33*, 609-620.

Bork, P., Blomberg, N., and Nilges, M. (1996). Internal repeats in the BRCA2 protein sequence. Nat Genet *13*, 22-23.

Brenneman, M.A., Wagener, B.M., Miller, C.A., Allen, C., and Nickoloff, J.A. (2002). XRCC3 controls the fidelity of homologous recombination: roles for XRCC3 in late stages of recombination. Mol Cell *10*, 387-395.

Broccoli, D., Smogorzewska, A., Chong, L., and de Lange, T. (1997). Human telomeres contain two distinct Myb-related proteins, TRF1 and TRF2. Nat Genet *17*, 231-235.

Bryan, T.M., Englezou, A., Gupta, J., Bacchetti, S., and Reddel, R.R. (1995). Telomere elongation in immortal human cells without detectable telomerase activity. EMBO J *14*, 4240-4248.

Bugreev, D.V., Hanaoka, F., and Mazin, A.V. (2007). Rad54 dissociates homologous recombination intermediates by branch migration. Nat Struct Mol Biol *14*, 746-753.

Bugreev, D.V., Mazina, O.M., and Mazin, A.V. (2006). Rad54 protein promotes branch migration of Holliday junctions. Nature *442*, 590-593.

Buis, J., Stoneham, T., Spehalski, E., and Ferguson, D.O. (2012). Mre11 regulates CtIP-dependent double-strand break repair by interaction with CDK2. Nat Struct Mol Biol *19*, 246-252.

Buis, J., Wu, Y., Deng, Y., Leddon, J., Westfield, G., Eckersdorff, M., Sekiguchi, J.M., Chang, S., and Ferguson, D.O. (2008). Mre11 nuclease activity has essential roles in DNA repair and genomic stability distinct from ATM activation. Cell *135*, 85-96.

Bunting, S.F., Callen, E., Wong, N., Chen, H.T., Polato, F., Gunn, A., Bothmer, A., Feldhahn, N., Fernandez-Capetillo, O., Cao, L.*, et al.* (2010). 53BP1 inhibits homologous recombination in Brca1-deficient cells by blocking resection of DNA breaks. Cell *141*, 243-254.

Bzymek, M., Thayer, N.H., Oh, S.D., Kleckner, N., and Hunter, N. (2010). Double Holliday junctions are intermediates of DNA break repair. Nature *464*, 937-941.

Cavenee, W.K., Dryja, T.P., Phillips, R.A., Benedict, W.F., Godbout, R., Gallie, B.L., Murphree, A.L., Strong, L.C., and White, R.L. (1983). Expression of recessive alleles by chromosomal mechanisms in retinoblastoma. Nature *305*, 779-784.

Cejka, P., Plank, J.L., Bachrati, C.Z., Hickson, I.D., and Kowalczykowski, S.C. (2010). Rmi1 stimulates decatenation of double Holliday junctions during dissolution by Sgs1-Top3. Nat Struct Mol Biol *17*, 1377-1382.

Celli, G.B., and de Lange, T. (2005). DNA processing is not required for ATM-mediated telomere damage response after TRF2 deletion. Nat Cell Biol *7*, 712-718.

Cesare, A.J., and Griffith, J.D. (2004). Telomeric DNA in ALT cells is characterized by free telomeric circles and heterogeneous t-loops. Mol Cell Biol *24*, 9948-9957.

Cesare, A.J., and Reddel, R.R. (2010). Alternative lengthening of telomeres: models, mechanisms and implications. Nat Rev Genet *11*, 319-330.

Chaganti, R.S., Schonberg, S., and German, J. (1974). A manyfold increase in sister chromatid exchanges in Bloom's syndrome lymphocytes. Proc Natl Acad Sci U S A *71*, 4508-4512.

Chai, W., Shay, J.W., and Wright, W.E. (2005). Human telomeres maintain their overhang length at senescence. Mol Cell Biol *25*, 2158-2168.

Chan, K.L., North, P.S., and Hickson, I.D. (2007). BLM is required for faithful chromosome segregation and its localization defines a class of ultrafine anaphase bridges. EMBO J *26*, 3397-3409.

Chan, K.L., Palmai-Pallag, T., Ying, S., and Hickson, I.D. (2009). Replication stress induces sister-chromatid bridging at fragile site loci in mitosis. Nat Cell Biol *11*, 753-760.

Chang, J.H., Kim, J.J., Choi, J.M., Lee, J.H., and Cho, Y. (2008). Crystal structure of the Mus81-Eme1 complex. Genes Dev *22*, 1093-1106.

Chapman, J.R., Sossick, A.J., Boulton, S.J., and Jackson, S.P. (2012). BRCA1-associated exclusion of 53BP1 from DNA damage sites underlies temporal control of DNA repair. J Cell Sci *125*, 3529-3534.

Chappell, C., Hanakahi, L.A., Karimi-Busheri, F., Weinfeld, M., and West, S.C. (2002). Involvement of human polynucleotide kinase in double-strand break repair by non-homologous end joining. EMBO J *21*, 2827-2832.

Chen, L., Nievera, C.J., Lee, A.Y., and Wu, X. (2008a). Cell cycle-dependent complex formation of BRCA1.CtIP.MRN is important for DNA double-strand break repair. J Biol Chem *283*, 7713-7720.

Chen, P.L., Chen, C.F., Chen, Y., Xiao, J., Sharp, Z.D., and Lee, W.H. (1998). The BRC repeats in BRCA2 are critical for RAD51 binding and resistance to methyl methanesulfonate treatment. Proc Natl Acad Sci U S A *95*, 5287-5292.

Chen, X.B., Melchionna, R., Denis, C.M., Gaillard, P.H., Blasina, A., Van de Weyer, I., Boddy, M.N., Russell, P., Vialard, J., and McGowan, C.H. (2001). Human Mus81-associated endonuclease cleaves Holliday junctions in vitro. Mol Cell *8*, 1117-1127.

Chen, Y., Yang, Y., van Overbeek, M., Donigian, J.R., Baciu, P., de Lange, T., and Lei, M. (2008b). A shared docking motif in TRF1 and TRF2 used for differential recruitment of telomeric proteins. Science *319*, 1092-1096.

Cheok, C.F., Bachrati, C.Z., Chan, K.L., Ralf, C., Wu, L., and Hickson, I.D. (2005). Roles of the Bloom's syndrome helicase in the maintenance of genome stability. Biochem Soc Trans *33*, 1456-1459.

Chi, P., Van Komen, S., Sehorn, M.G., Sigurdsson, S., and Sung, P. (2006). Roles of ATP binding and ATP hydrolysis in human Rad51 recombinase function. DNA Repair (Amst) *5*, 381-391.

Chun, J., Buechelmaier, E.S., and Powell, S.N. (2013). Rad51 paralog complexes BCDX2 and CX3 act at different stages in the BRCA1-BRCA2-dependent homologous recombination pathway. Mol Cell Biol *33*, 387-395.

Ciccia, A., Constantinou, A., and West, S.C. (2003). Identification and characterization of the human mus81-eme1 endonuclease. J Biol Chem *278*, 25172-25178.

Ciccia, A., Ling, C., Coulthard, R., Yan, Z., Xue, Y., Meetei, A.R., Laghmani el, H., Joenje, H., McDonald, N., de Winter, J.P.*, et al.* (2007). Identification of FAAP24, a Fanconi anemia core complex protein that interacts with FANCM. Mol Cell *25*, 331-343.

Ciccia, A., McDonald, N., and West, S.C. (2008). Structural and functional relationships of the XPF/MUS81 family of proteins. Annu Rev Biochem *77*, 259-287.

Cohen, S.B., Graham, M.E., Lovrecz, G.O., Bache, N., Robinson, P.J., and Reddel, R.R. (2007). Protein composition of catalytically active human telomerase from immortal cells. Science *315*, 1850-1853.

Coin, F., Oksenych, V., and Egly, J.M. (2007). Distinct roles for the XPB/p52 and XPD/p44 subcomplexes of TFIIH in damaged DNA opening during nucleotide excision repair. Mol Cell *26*, 245-256.

Compton, S.A., Choi, J.H., Cesare, A.J., Ozgur, S., and Griffith, J.D. (2007). Xrcc3 and Nbs1 are required for the production of extrachromosomal telomeric circles in human alternative lengthening of telomere cells. Cancer Res *67*, 1513-1519.

Cong, Y.S., Wen, J., and Bacchetti, S. (1999). The human telomerase catalytic subunit hTERT: organization of the gene and characterization of the promoter. Hum Mol Genet *8*, 137-142.

Conomos, D., Stutz, M.D., Hills, M., Neumann, A.A., Bryan, T.M., Reddel, R.R., and Pickett, H.A. (2012). Variant repeats are interspersed throughout the telomeres and recruit nuclear receptors in ALT cells. J Cell Biol *199*, 893-906.

Conway, A.B., Lynch, T.W., Zhang, Y., Fortin, G.S., Fung, C.W., Symington, L.S., and Rice, P.A. (2004). Crystal structure of a Rad51 filament. Nat Struct Mol Biol *11*, 791-796.

Coulthard, R., Deans, A.J., Swuec, P., Bowles, M., Costa, A., West, S.C., and McDonald, N.Q. (2013). Architecture and DNA Recognition Elements of the Fanconi Anemia FANCM-FAAP24 Complex. Structure.

Crabbe, L., Verdun, R.E., Haggblom, C.I., and Karlseder, J. (2004). Defective telomere lagging strand synthesis in cells lacking WRN helicase activity. Science *306*, 1951-1953.

d'Adda di Fagagna, F., Reaper, P.M., Clay-Farrace, L., Fiegler, H., Carr, P., Von Zglinicki, T., Saretzki, G., Carter, N.P., and Jackson, S.P. (2003). A DNA damage checkpoint response in telomere-initiated senescence. Nature *426*, 194-198.

D'Andrea, A.D. (2010). Susceptibility pathways in Fanconi's anemia and breast cancer. N Engl J Med *362*, 1909-1919.

Davies, S.L., North, P.S., and Hickson, I.D. (2007). Role for BLM in replication-fork restart and suppression of origin firing after replicative stress. Nat Struct Mol Biol *14*, 677-679.

de los Santos, T., Hunter, N., Lee, C., Larkin, B., Loidl, J., and Hollingsworth, N.M. (2003). The Mus81/Mms4 endonuclease acts independently of double-Holliday junction resolution to promote a distinct subset of crossovers during meiosis in budding yeast. Genetics *164*, 81-94.

Debatisse, M., Le Tallec, B., Letessier, A., Dutrillaux, B., and Brison, O. (2012). Common fragile sites: mechanisms of instability revisited. Trends Genet *28*, 22-32.

Dehe, P.M., Coulon, S., Scaglione, S., Shanahan, P., Takedachi, A., Wohlschlegel, J.A., Yates, J.R., 3rd, Llorente, B., Russell, P., and Gaillard, P.H. (2013). Regulation of Mus81-Eme1 Holliday junction resolvase in response to DNA damage. Nat Struct Mol Biol *20*, 598-603.

Denchi, E.L., and de Lange, T. (2007). Protection of telomeres through independent control of ATM and ATR by TRF2 and POT1. Nature *448*, 1068-1071.

Dickie, P., McFadden, G., and Morgan, A.R. (1987). The site-specific cleavage of synthetic Holliday junction analogs and related branched DNA structures by bacteriophage T7 endonuclease I. J Biol Chem *262*, 14826-14836.

Diderich, K., Alanazi, M., and Hoeijmakers, J.H. (2011). Premature aging and cancer in nucleotide excision repair-disorders. DNA Repair (Amst) *10*, 772-780.

Dimitrova, N., and de Lange, T. (2009). Cell cycle-dependent role of MRN at dysfunctional telomeres: ATM signaling-dependent induction of nonhomologous end joining (NHEJ) in G1 and resection-mediated inhibition of NHEJ in G2. Mol Cell Biol *29*, 5552-5563.

Dodson, G.E., Limbo, O., Nieto, D., and Russell, P. (2010). Phosphorylation-regulated binding of Ctp1 to Nbs1 is critical for repair of DNA double-strand breaks. Cell Cycle *9*, 1516-1522.

Doe, C.L., Ahn, J.S., Dixon, J., and Whitby, M.C. (2002). Mus81-Eme1 and Rqh1 involvement in processing stalled and collapsed replication forks. J Biol Chem *277*, 32753-32759.

Dominguez-Kelly, R., Martin, Y., Koundrioukoff, S., Tanenbaum, M.E., Smits, V.A., Medema, R.H., Debatisse, M., and Freire, R. (2011). Wee1 controls genomic stability during replication by regulating the Mus81-Eme1 endonuclease. J Cell Biol *194*, 567-579.

Draskovic, I., Arnoult, N., Steiner, V., Bacchetti, S., Lomonte, P., and Londono-Vallejo, A. (2009). Probing PML body function in ALT cells reveals spatiotemporal requirements for telomere recombination. Proc Natl Acad Sci U S A *106*, 15726-15731.

Du, X., Shen, J., Kugan, N., Furth, E.E., Lombard, D.B., Cheung, C., Pak, S., Luo, G., Pignolo, R.J., DePinho, R.A.*, et al.* (2004). Telomere shortening exposes functions for the mouse Werner and Bloom syndrome genes. Mol Cell Biol *24*, 8437-8446.

Dunderdale, H.J., Benson, F.E., Parsons, C.A., Sharples, G.J., Lloyd, R.G., and West, S.C. (1991). Formation and resolution of recombination intermediates by E. coli RecA and RuvC proteins. Nature *354*, 506-510.

Dunham, M.A., Neumann, A.A., Fasching, C.L., and Reddel, R.R. (2000). Telomere maintenance by recombination in human cells. Nat Genet *26*, 447-450.

Echols, H., and Goodman, M.F. (1991). Fidelity mechanisms in DNA replication. Annu Rev Biochem *60*, 477-511.

Ehmsen, K.T., and Heyer, W.D. (2008). Saccharomyces cerevisiae Mus81-Mms4 is a catalytic, DNA structure-selective endonuclease. Nucleic Acids Res *36*, 2182-2195.

Ehmsen, K.T., and Heyer, W.D. (2009). A junction branch point adjacent to a DNA backbone nick directs substrate cleavage by Saccharomyces cerevisiae Mus81-Mms4. Nucleic Acids Res *37*, 2026-2036.

Ellis, N.A., Groden, J., Ye, T.Z., Straughen, J., Lennon, D.J., Ciocci, S., Proytcheva, M., and German, J. (1995). The Bloom's syndrome gene product is homologous to RecQ helicases. Cell *83*, 655-666.

Enzlin, J.H., and Scharer, O.D. (2002). The active site of the DNA repair endonuclease XPF-ERCC1 forms a highly conserved nuclease motif. EMBO J *21*, 2045-2053.

Esashi, F., Christ, N., Gannon, J., Liu, Y., Hunt, T., Jasin, M., and West, S.C. (2005). CDK-dependent phosphorylation of BRCA2 as a regulatory mechanism for recombinational repair. Nature *434*, 598-604.

Fan, Q., Zhang, F., Barrett, B., Ren, K., and Andreassen, P.R. (2009). A role for monoubiquitinated FANCD2 at telomeres in ALT cells. Nucleic Acids Res *37*, 1740-1754.

Fekairi, S., Scaglione, S., Chahwan, C., Taylor, E.R., Tissier, A., Coulon, S., Dong, M.Q., Ruse, C., Yates, J.R., 3rd, Russell, P*., et al.* (2009). Human SLX4 is a Holliday junction resolvase subunit that binds multiple DNA repair/recombination endonucleases. Cell *138*, 78-89.

Feng, Z., Scott, S.P., Bussen, W., Sharma, G.G., Guo, G., Pandita, T.K., and Powell, S.N. (2011). Rad52 inactivation is synthetically lethal with BRCA2 deficiency. Proc Natl Acad Sci U S A *108*, 686-691.

Flott, S., Alabert, C., Toh, G.W., Toth, R., Sugawara, N., Campbell, D.G., Haber, J.E., Pasero, P., and Rouse, J. (2007). Phosphorylation of Slx4 by Mec1 and Tel1 regulates the single-strand annealing mode of DNA repair in budding yeast. Mol Cell Biol *27*, 6433-6445.

Forment, J.V., Blasius, M., Guerini, I., and Jackson, S.P. (2011). Structure-specific DNA endonuclease Mus81/Eme1 generates DNA damage caused by Chk1 inactivation. PLoS One *6*, e23517.

Fouche, N., Cesare, A.J., Willcox, S., Ozgur, S., Compton, S.A., and Griffith, J.D. (2006). The basic domain of TRF2 directs binding to DNA junctions irrespective of the presence of TTAGGG repeats. J Biol Chem *281*, 37486-37495.

Franchitto, A., Pirzio, L.M., Prosperi, E., Sapora, O., Bignami, M., and Pichierri, P. (2008). Replication fork stalling in WRN-deficient cells is overcome by prompt activation of a MUS81-dependent pathway. J Cell Biol *183*, 241-252.

Frankel, F.R., Batcheler, M.L., and Clark, C.K. (1971). The role of gene 49 in DNA replication and head morphogenesis in bacteriophage T4. J Mol Biol *62*, 439-463.

Fricke, W.M., Bastin-Shanower, S.A., and Brill, S.J. (2005). Substrate specificity of the Saccharomyces cerevisiae Mus81-Mms4 endonuclease. DNA Repair (Amst) *4*, 243-251.

Fricke, W.M., and Brill, S.J. (2003). Slx1-Slx4 is a second structure-specific endonuclease functionally redundant with Sgs1-Top3. Genes Dev *17*, 1768-1778.

Froelich-Ammon, S.J., and Osheroff, N. (1995). Topoisomerase poisons: harnessing the dark side of enzyme mechanism. J Biol Chem *270*, 21429-21432.

Fu, D., and Collins, K. (2007). Purification of human telomerase complexes identifies factors involved in telomerase biogenesis and telomere length regulation. Mol Cell *28*, 773-785.

Fugger, K., Chu, W.K., Haahr, P., Nedergaard Kousholt, A., Beck, H., Payne, M.J., Hanada, K., Hickson, I.D., and Storgaard Sorensen, C. (2013). FBH1 co-operates with MUS81 in inducing DNA double-strand breaks and cell death following replication stress. Nat Commun *4*, 1423.

Fuller, L.F., and Painter, R.B. (1988). A Chinese hamster ovary cell line hypersensitive to ionizing radiation and deficient in repair replication. Mutat Res *193*, 109-121.

Gaillard, P.H., Noguchi, E., Shanahan, P., and Russell, P. (2003). The endogenous Mus81-Eme1 complex resolves Holliday junctions by a nick and counternick mechanism. Mol Cell *12*, 747-759.

Gallo-Fernandez, M., Saugar, I., Ortiz-Bazan, M.A., Vazquez, M.V., and Tercero, J.A. (2012). Cell cycle-dependent regulation of the nuclease activity of Mus81-Eme1/Mms4. Nucleic Acids Res *40*, 8325-8335.

Gao, H., Chen, X.B., and McGowan, C.H. (2003). Mus81 endonuclease localizes to nucleoli and to regions of DNA damage in human S-phase cells. Mol Biol Cell *14*, 4826-4834.

Garcia-Higuera, I., Taniguchi, T., Ganesan, S., Meyn, M.S., Timmers, C., Hejna, J., Grompe, M., and D'Andrea, A.D. (2001). Interaction of the Fanconi anemia proteins and BRCA1 in a common pathway. Mol Cell *7*, 249-262.

Gari, K., Decaillet, C., Delannoy, M., Wu, L., and Constantinou, A. (2008a). Remodeling of DNA replication structures by the branch point translocase FANCM. Proc Natl Acad Sci U S A *105*, 16107-16112.

Gari, K., Decaillet, C., Stasiak, A.Z., Stasiak, A., and Constantinou, A. (2008b). The Fanconi anemia protein FANCM can promote branch migration of Holliday junctions and replication forks. Mol Cell *29*, 141-148.

German, J. (1993). Bloom syndrome: a mendelian prototype of somatic mutational disease. Medicine (Baltimore) *72*, 393-406.

Gloeckner, C.J., Boldt, K., Schumacher, A., Roepman, R., and Ueffing, M. (2007). A novel tandem affinity purification strategy for the efficient isolation and characterisation of native protein complexes. Proteomics *7*, 4228-4234.

Golub, E.I., Kovalenko, O.V., Gupta, R.C., Ward, D.C., and Radding, C.M. (1997). Interaction of human recombination proteins Rad51 and Rad54. Nucleic Acids Res *25*, 4106-4110.

Gong, Y., and de Lange, T. (2010). A Shld1-controlled POT1a provides support for repression of ATR signaling at telomeres through RPA exclusion. Mol Cell *40*, 377-387.

Goodhead, D.T. (1989). The initial physical damage produced by ionizing radiations. Int J Radiat Biol *56*, 623-634.

Gravel, S., Chapman, J.R., Magill, C., and Jackson, S.P. (2008). DNA helicases Sgs1 and BLM promote DNA double-strand break resection. Genes Dev *22*, 2767-2772.

Grawunder, U., Wilm, M., Wu, X., Kulesza, P., Wilson, T.E., Mann, M., and Lieber, M.R. (1997). Activity of DNA ligase IV stimulated by complex formation with XRCC4 protein in mammalian cells. Nature *388*, 492-495.

Greider, C.W., and Blackburn, E.H. (1985). Identification of a specific telomere terminal transferase activity in Tetrahymena extracts. Cell *43*, 405-413.

Griffith, J.D., Comeau, L., Rosenfield, S., Stansel, R.M., Bianchi, A., Moss, H., and de Lange, T. (1999). Mammalian telomeres end in a large duplex loop. Cell *97*, 503-514.

Grudic, A., Jul-Larsen, A., Haring, S.J., Wold, M.S., Lonning, P.E., Bjerkvig, R., and Boe, S.O. (2007). Replication protein A prevents accumulation of single-stranded telomeric DNA in cells that use alternative lengthening of telomeres. Nucleic Acids Res *35*, 7267-7278.

Gu, J., Lu, H., Tippin, B., Shimazaki, N., Goodman, M.F., and Lieber, M.R. (2007). XRCC4:DNA ligase IV can ligate incompatible DNA ends and can ligate across gaps. EMBO J *26*, 1010-1023.

Gunz, D., Hess, M.T., and Naegeli, H. (1996). Recognition of DNA adducts by human nucleotide excision repair. Evidence for a thermodynamic probing mechanism. J Biol Chem *271*, 25089-25098.

Haber, J.E., and Heyer, W.D. (2001). The fuss about Mus81. Cell *107*, 551-554.

Halazonetis, T.D., Gorgoulis, V.G., and Bartek, J. (2008). An oncogene-induced DNA damage model for cancer development. Science *319*, 1352-1355.

Hanada, K., Budzowska, M., Davies, S.L., van Drunen, E., Onizawa, H., Beverloo, H.B., Maas, A., Essers, J., Hickson, I.D., and Kanaar, R. (2007). The structure-specific endonuclease Mus81 contributes to replication restart by generating double-strand DNA breaks. Nat Struct Mol Biol *14*, 1096-1104.

Hanada, K., Budzowska, M., Modesti, M., Maas, A., Wyman, C., Essers, J., and Kanaar, R. (2006). The structure-specific endonuclease Mus81-Eme1 promotes conversion of interstrand DNA crosslinks into double-strands breaks. EMBO J *25*, 4921-4932.

Harley, C.B., Futcher, A.B., and Greider, C.W. (1990). Telomeres shorten during ageing of human fibroblasts. Nature *345*, 458-460.

Harrington, J.J., and Lieber, M.R. (1994). Functional domains within FEN-1 and RAD2 define a family of structure-specific endonucleases: implications for nucleotide excision repair. Genes Dev *8*, 1344-1355.

Hartsuiker, E., Neale, M.J., and Carr, A.M. (2009). Distinct requirements for the Rad32(Mre11) nuclease and Ctp1(CtIP) in the removal of covalently bound topoisomerase I and II from DNA. Mol Cell *33*, 117-123.

Helleday, T. (2010). Homologous recombination in cancer development, treatment and development of drug resistance. Carcinogenesis *31*, 955-960.

Heller, R.C., and Marians, K.J. (2006). Replisome assembly and the direct restart of stalled replication forks. Nat Rev Mol Cell Biol *7*, 932-943.

Henson, J.D., Cao, Y., Huschtscha, L.I., Chang, A.C., Au, A.Y., Pickett, H.A., and Reddel, R.R. (2009). DNA C-circles are specific and quantifiable markers of alternative-lengthening-of-telomeres activity. Nat Biotechnol *27*, 1181-1185.

Henson, J.D., Hannay, J.A., McCarthy, S.W., Royds, J.A., Yeager, T.R., Robinson, R.A., Wharton, S.B., Jellinek, D.A., Arbuckle, S.M., Yoo, J.*, et al.* (2005). A robust assay for alternative lengthening of telomeres in tumors shows the significance of alternative lengthening of telomeres in sarcomas and astrocytomas. Clin Cancer Res *11*, 217-225.

Henson, J.D., and Reddel, R.R. (2010). Assaying and investigating Alternative Lengthening of Telomeres activity in human cells and cancers. FEBS Lett *584*, 3800-3811.

Hiyama, T., Katsura, M., Yoshihara, T., Ishida, M., Kinomura, A., Tonda, T., Asahara, T., and Miyagawa, K. (2006). Haploinsufficiency of the Mus81-Eme1 endonuclease activates the intra-S-phase and G2/M checkpoints and promotes rereplication in human cells. Nucleic Acids Res *34*, 880-892.

Ho, C.K., Mazon, G., Lam, A.F., and Symington, L.S. (2010). Mus81 and Yen1 promote reciprocal exchange during mitotic recombination to maintain genome integrity in budding yeast. Mol Cell *40*, 988-1000.

Hoeijmakers, J.H. (2001). Genome maintenance mechanisms for preventing cancer. Nature *411*, 366-374.

Holliday, R. (1964). A mechanism for gene conversion in fungi. Genet Res *89*, 285-307.

Horikawa, I., Cable, P.L., Afshari, C., and Barrett, J.C. (1999). Cloning and characterization of the promoter region of human telomerase reverse transcriptase gene. Cancer Res *59*, 826-830.

Hosfield, D.J., Mol, C.D., Shen, B., and Tainer, J.A. (1998). Structure of the DNA repair and replication endonuclease and exonuclease FEN-1: coupling DNA and PCNA binding to FEN-1 activity. Cell *95*, 135-146.

Howlett, N.G., Taniguchi, T., Olson, S., Cox, B., Waisfisz, Q., De Die-Smulders, C., Persky, N., Grompe, M., Joenje, H., Pals, G.*, et al.* (2002). Biallelic inactivation of BRCA2 in Fanconi anemia. Science *297*, 606-609.

Huertas, P., and Jackson, S.P. (2009). Human CtIP mediates cell cycle control of DNA end resection and double strand break repair. J Biol Chem *284*, 9558-9565.

Hutchinson, F. (1985). Chemical changes induced in DNA by ionizing radiation. Prog Nucleic Acid Res Mol Biol *32*, 115-154.

Imlay, J.A., and Linn, S. (1988). DNA damage and oxygen radical toxicity. Science *240*, 1302-1309.

Interthal, H., and Heyer, W.D. (2000). MUS81 encodes a novel helix-hairpin-helix protein involved in the response to UV- and methylation-induced DNA damage in Saccharomyces cerevisiae. Mol Gen Genet *263*, 812-827.

Ip, S.C., Rass, U., Blanco, M.G., Flynn, H.R., Skehel, J.M., and West, S.C. (2008). Identification of Holliday junction resolvases from humans and yeast. Nature *456*, 357-361.

Ishikawa, G., Kanai, Y., Takata, K., Takeuchi, R., Shimanouchi, K., Ruike, T., Furukawa, T., Kimura, S., and Sakaguchi, K. (2004). DmGEN, a novel RAD2 family endo-exonuclease from Drosophila melanogaster. Nucleic Acids Res *32*, 6251-6259.

Iwasaki, H., Takahagi, M., Nakata, A., and Shinagawa, H. (1992). Escherichia coli RuvA and RuvB proteins specifically interact with Holliday junctions and promote branch migration. Genes Dev *6*, 2214-2220.

Iwasaki, H., Takahagi, M., Shiba, T., Nakata, A., and Shinagawa, H. (1991). Escherichia coli RuvC protein is an endonuclease that resolves the Holliday structure. EMBO J *10*, 4381-4389.

Iyer, V.N., and Szybalski, W. (1963). A Molecular Mechanism of Mitomycin Action: Linking of Complementary DNA Strands. Proc Natl Acad Sci U S A *50*, 355-362.

Jady, B.E., Richard, P., Bertrand, E., and Kiss, T. (2006). Cell cycle-dependent recruitment of telomerase RNA and Cajal bodies to human telomeres. Mol Biol Cell *17*, 944-954.

Jensen, R.B., Carreira, A., and Kowalczykowski, S.C. (2010). Purified human BRCA2 stimulates RAD51-mediated recombination. Nature *467*, 678-683.

Jiang, W.Q., Zhong, Z.H., Henson, J.D., Neumann, A.A., Chang, A.C., and Reddel, R.R. (2005). Suppression of alternative lengthening of telomeres by Sp100-mediated sequestration of the MRE11/RAD50/NBS1 complex. Mol Cell Biol *25*, 2708-2721.

Jiang, W.Q., Zhong, Z.H., Henson, J.D., and Reddel, R.R. (2007). Identification of candidate alternative lengthening of telomeres genes by methionine restriction and RNA interference. Oncogene *26*, 4635-4647.

Joenje, H., Oostra, A.B., Wijker, M., di Summa, F.M., van Berkel, C.G., Rooimans, M.A., Ebell, W., van Weel, M., Pronk, J.C., Buchwald, M.*, et al.* (1997). Evidence for at least eight Fanconi anemia genes. Am J Hum Genet *61*, 940-944.

Johnson, R.D., and Jasin, M. (2000). Sister chromatid gene conversion is a prominent double-strand break repair pathway in mammalian cells. EMBO J *19*, 3398-3407.

Jones, J.M., and Nakai, H. (1999). Duplex opening by primosome protein PriA for replisome assembly on a recombination intermediate. J Mol Biol *289*, 503-516.

Jones, N.J., Cox, R., and Thacker, J. (1987). Isolation and cross-sensitivity of X-ray-sensitive mutants of V79-4 hamster cells. Mutat Res *183*, 279-286.

Kaliraman, V., Mullen, J.R., Fricke, W.M., Bastin-Shanower, S.A., and Brill, S.J. (2001). Functional overlap between Sgs1-Top3 and the Mms4-Mus81 endonuclease. Genes Dev *15*, 2730-2740.

Karow, J.K., Constantinou, A., Li, J.L., West, S.C., and Hickson, I.D. (2000). The Bloom's syndrome gene product promotes branch migration of holliday junctions. Proc Natl Acad Sci U S A *97*, 6504-6508.

Keeney, S., Giroux, C.N., and Kleckner, N. (1997). Meiosis-specific DNA double-strand breaks are catalyzed by Spo11, a member of a widely conserved protein family. Cell *88*, 375-384.

Kemper, B., and Brown, D.T. (1976). Function of gene 49 of bacteriophage T4. II. Analysis of intracellular development and the structure of very fast-sedimenting DNA. J Virol *18*, 1000-1015.

Kim, N.W., Piatyszek, M.A., Prowse, K.R., Harley, C.B., West, M.D., Ho, P.L., Coviello, G.M., Wright, W.E., Weinrich, S.L., and Shay, J.W. (1994). Specific association of human telomerase activity with immortal cells and cancer. Science *266*, 2011-2015.

Kim, Y., Lach, F.P., Desetty, R., Hanenberg, H., Auerbach, A.D., and Smogorzewska, A. (2011). Mutations of the SLX4 gene in Fanconi anemia. Nat Genet *43*, 142-146.

Kim, Y., Spitz, G.S., Veturi, U., Lach, F.P., Auerbach, A.D., and Smogorzewska, A. (2013). Regulation of multiple DNA repair pathways by the Fanconi anemia protein SLX4. Blood *121*, 54-63.

Knipscheer, P., Raschle, M., Smogorzewska, A., Enoiu, M., Ho, T.V., Scharer, O.D., Elledge, S.J., and Walter, J.C. (2009). The Fanconi anemia pathway promotes replication-dependent DNA interstrand cross-link repair. Science *326*, 1698-1701.

Kratz, K., Schopf, B., Kaden, S., Sendoel, A., Eberhard, R., Lademann, C., Cannavo, E., Sartori, A.A., Hengartner, M.O., and Jiricny, J. (2010). Deficiency of FANCD2-associated nuclease KIAA1018/FAN1 sensitizes cells to interstrand crosslinking agents. Cell *142*, 77-88.

Kunkel, T.A. (1995). DNA-mismatch repair. The intricacies of eukaryotic spell-checking. Curr Biol *5*, 1091-1094.

Kuzminov, A., and Stahl, F.W. (1999). Double-strand end repair via the RecBC pathway in Escherichia coli primes DNA replication. Genes Dev *13*, 345-356.

Laemmli, U.K. (1970). Cleavage of structural proteins during the assembly of the head of bacteriophage T4. Nature *227*, 680-685.

Lam, Y.C., Akhter, S., Gu, P., Ye, J., Poulet, A., Giraud-Panis, M.J., Bailey, S.M., Gilson, E., Legerski, R.J., and Chang, S. (2010). SNMIB/Apollo protects leading-strand telomeres against NHEJ-mediated repair. EMBO J *29*, 2230-2241.

Lang, M., Jegou, T., Chung, I., Richter, K., Munch, S., Udvarhelyi, A., Cremer, C., Hemmerich, P., Engelhardt, J., Hell, S.W.*, et al.* (2010). Three-dimensional organization of promyelocytic leukemia nuclear bodies. J Cell Sci *123*, 392-400.

Latrick, C.M., and Cech, T.R. (2010). POT1-TPP1 enhances telomerase processivity by slowing primer dissociation and aiding translocation. EMBO J *29*, 924-933.

Lau, L.M., Dagg, R.A., Henson, J.D., Au, A.Y., Royds, J.A., and Reddel, R.R. (2013). Detection of alternative lengthening of telomeres by telomere quantitative PCR. Nucleic Acids Res *41*, e34.

Lei, M., Baumann, P., and Cech, T.R. (2002). Cooperative binding of single-stranded telomeric DNA by the Pot1 protein of Schizosaccharomyces pombe. Biochemistry *41*, 14560-14568.

Li, X., Stith, C.M., Burgers, P.M., and Heyer, W.D. (2009). PCNA is required for initiation of recombination-associated DNA synthesis by DNA polymerase delta. Mol Cell *36*, 704-713.

Lieber, M.R. (2010). The mechanism of double-strand DNA break repair by the nonhomologous DNA end-joining pathway. Annu Rev Biochem *79*, 181-211.

Lilley, D.M., and White, M.F. (2001). The junction-resolving enzymes. Nat Rev Mol Cell Biol *2*, 433-443.

Lin, W., Sampathi, S., Dai, H., Liu, C., Zhou, M., Hu, J., Huang, Q., Campbell, J., Shin-Ya, K., Zheng, L.*, et al.* (2013). Mammalian DNA2 helicase/nuclease cleaves G-quadruplex DNA and is required for telomere integrity. EMBO J *32*, 1425-1439.

Lindahl, T. (1993). Instability and decay of the primary structure of DNA. Nature *362*, 709-715.

Lindahl, T., and Wood, R.D. (1999). Quality control by DNA repair. Science *286*, 1897-1905.

Liu, D., Safari, A., O'Connor, M.S., Chan, D.W., Laegeler, A., Qin, J., and Songyang, Z. (2004). PTOP interacts with POT1 and regulates its localization to telomeres. Nat Cell Biol *6*, 673-680.

Liu, T., Ghosal, G., Yuan, J., Chen, J., and Huang, J. (2010). FAN1 acts with FANCI-FANCD2 to promote DNA interstrand cross-link repair. Science *329*, 693-696.

Liu, Y., Snow, B.E., Hande, M.P., Yeung, D., Erdmann, N.J., Wakeham, A., Itie, A., Siderovski, D.P., Lansdorp, P.M., Robinson, M.O.*, et al.* (2000). The telomerase reverse transcriptase is limiting and necessary for telomerase function in vivo. Curr Biol *10*, 1459-1462.

Loayza, D., and De Lange, T. (2003). POT1 as a terminal transducer of TRF1 telomere length control. Nature *423*, 1013-1018.

Loeb, L.A., and Kunkel, T.A. (1982). Fidelity of DNA synthesis. Annu Rev Biochem *51*, 429-457.

Lok, B.H., Carley, A.C., Tchang, B., and Powell, S.N. (2013). RAD52 inactivation is synthetically lethal with deficiencies in BRCA1 and PALB2 in addition to BRCA2 through RAD51-mediated homologous recombination. Oncogene *32*, 3552-3558.

Londono-Vallejo, J.A., Der-Sarkissian, H., Cazes, L., Bacchetti, S., and Reddel, R.R. (2004). Alternative lengthening of telomeres is characterized by high rates of telomeric exchange. Cancer Res *64*, 2324-2327.

Lorenz, A., West, S.C., and Whitby, M.C. (2010). The human Holliday junction resolvase GEN1 rescues the meiotic phenotype of a Schizosaccharomyces pombe mus81 mutant. Nucleic Acids Res *38*, 1866-1873.

Lovejoy, C.A., Li, W., Reisenweber, S., Thongthip, S., Bruno, J., de Lange, T., De, S., Petrini, J.H., Sung, P.A., Jasin, M.*, et al.* (2012). Loss of ATRX, genome instability, and an altered DNA damage response are hallmarks of the alternative lengthening of telomeres pathway. PLoS Genet *8*, e1002772.

Ma, Y., Lu, H., Tippin, B., Goodman, M.F., Shimazaki, N., Koiwai, O., Hsieh, C.L., Schwarz, K., and Lieber, M.R. (2004). A biochemically defined system for mammalian nonhomologous DNA end joining. Mol Cell *16*, 701-713.

Ma, Y., Pannicke, U., Schwarz, K., and Lieber, M.R. (2002). Hairpin opening and overhang processing by an Artemis/DNA-dependent protein kinase complex in nonhomologous end joining and V(D)J recombination. Cell *108*, 781-794.

Ma, Y., Schwarz, K., and Lieber, M.R. (2005). The Artemis:DNA-PKcs endonuclease cleaves DNA loops, flaps, and gaps. DNA Repair (Amst) *4*, 845-851.

Machwe, A., Xiao, L., Lloyd, R.G., Bolt, E., and Orren, D.K. (2007). Replication fork regression in vitro by the Werner syndrome protein (WRN): holliday junction formation, the effect of leading arm structure and a potential role for WRN exonuclease activity. Nucleic Acids Res *35*, 5729-5747.

MacKay, C., Declais, A.C., Lundin, C., Agostinho, A., Deans, A.J., MacArtney, T.J., Hofmann, K., Gartner, A., West, S.C., Helleday, T.*, et al.* (2010). Identification of KIAA1018/FAN1, a DNA repair nuclease recruited to DNA damage by monoubiquitinated FANCD2. Cell *142*, 65-76.

Makarov, V.L., Hirose, Y., and Langmore, J.P. (1997). Long G tails at both ends of human chromosomes suggest a C strand degradation mechanism for telomere shortening. Cell *88*, 657-666.

Mankouri, H.W., Ashton, T.M., and Hickson, I.D. (2011). Holliday junction-containing DNA structures persist in cells lacking Sgs1 or Top3 following exposure to DNA damage. Proc Natl Acad Sci U S A *108*, 4944-4949.

Masson, J.Y., Tarsounas, M.C., Stasiak, A.Z., Stasiak, A., Shah, R., McIlwraith, M.J., Benson, F.E., and West, S.C. (2001). Identification and purification of two distinct complexes containing the five RAD51 paralogs. Genes Dev *15*, 3296-3307.

Matos, J., Blanco, M.G., Maslen, S., Skehel, J.M., and West, S.C. (2011). Regulatory control of the resolution of DNA recombination intermediates during meiosis and mitosis. Cell *147*, 158-172.

Matos, J., Blanco, M.G., and West, S.C. (2013). Cell-cycle kinases coordinate the resolution of recombination intermediates with chromosome segregation. Cell Rep *4*, 76-86.

Mazin, A.V., Alexeev, A.A., and Kowalczykowski, S.C. (2003). A novel function of Rad54 protein. Stabilization of the Rad51 nucleoprotein filament. J Biol Chem *278*, 14029-14036.

Mazina, O.M., and Mazin, A.V. (2008). Human Rad54 protein stimulates human Mus81-Eme1 endonuclease. Proc Natl Acad Sci U S A *105*, 18249-18254.

McCulloch, S.D., and Kunkel, T.A. (2008). The fidelity of DNA synthesis by eukaryotic replicative and translesion synthesis polymerases. Cell Res *18*, 148-161.

McElhinny, S.A., Havener, J.M., Garcia-Diaz, M., Juarez, R., Bebenek, K., Kee, B.L., Blanco, L., Kunkel, T.A., and Ramsden, D.A. (2005). A gradient of template dependence defines distinct biological roles for family X polymerases in nonhomologous end joining. Mol Cell *19*, 357-366.

McElligott, R., and Wellinger, R.J. (1997). The terminal DNA structure of mammalian chromosomes. EMBO J *16*, 3705-3714.

McIlwraith, M.J., Vaisman, A., Liu, Y., Fanning, E., Woodgate, R., and West, S.C. (2005). Human DNA polymerase eta promotes DNA synthesis from strand invasion intermediates of homologous recombination. Mol Cell *20*, 783-792.

McIlwraith, M.J., Van Dyck, E., Masson, J.Y., Stasiak, A.Z., Stasiak, A., and West, S.C. (2000). Reconstitution of the strand invasion step of double-strand break repair using human Rad51 Rad52 and RPA proteins. J Mol Biol *304*, 151-164.

McPherson, J.P., Lemmers, B., Chahwan, R., Pamidi, A., Migon, E., Matysiak-Zablocki, E., Moynahan, M.E., Essers, J., Hanada, K., Poonepalli, A.*, et al.* (2004). Involvement of mammalian Mus81 in genome integrity and tumor suppression. Science *304*, 1822-1826.

Meetei, A.R., Medhurst, A.L., Ling, C., Xue, Y., Singh, T.R., Bier, P., Steltenpool, J., Stone, S., Dokal, I., Mathew, C.G.*, et al.* (2005). A human ortholog of archaeal DNA repair protein Hef is defective in Fanconi anemia complementation group M. Nat Genet *37*, 958-963.

Meetei, A.R., Yan, Z., and Wang, W. (2004). FANCL replaces BRCA1 as the likely ubiquitin ligase responsible for FANCD2 monoubiquitination. Cell Cycle *3*, 179-181.

Mimitou, E.P., and Symington, L.S. (2008). Sae2, Exo1 and Sgs1 collaborate in DNA double-strand break processing. Nature *455*, 770-774.

Mimori, T., and Hardin, J.A. (1986). Mechanism of interaction between Ku protein and DNA. J Biol Chem *261*, 10375-10379.

Mitchell, D.L., and Nairn, R.S. (1989). The biology of the (6-4) photoproduct. Photochem Photobiol *49*, 805-819.

Mizuuchi, K., Kemper, B., Hays, J., and Weisberg, R.A. (1982). T4 endonuclease VII cleaves holliday structures. Cell *29*, 357-365.

Modesti, M., Ristic, D., van der Heijden, T., Dekker, C., van Mameren, J., Peterman, E.J., Wuite, G.J., Kanaar, R., and Wyman, C. (2007). Fluorescent human RAD51 reveals multiple nucleation sites and filament segments tightly associated along a single DNA molecule. Structure *15*, 599-609.

Moggs, J.G., Yarema, K.J., Essigmann, J.M., and Wood, R.D. (1996). Analysis of incision sites produced by human cell extracts and purified proteins during nucleotide excision repair of a 1,3-intrastrand d(GpTpG)-cisplatin adduct. J Biol Chem *271*, 7177-7186.

Mohaghegh, P., Karow, J.K., Brosh, R.M., Jr., Bohr, V.A., and Hickson, I.D. (2001). The Bloom's and Werner's syndrome proteins are DNA structure-specific helicases. Nucleic Acids Res *29*, 2843-2849.

Monnat, R.J., Jr. (2010). Human RECQ helicases: roles in DNA metabolism, mutagenesis and cancer biology. Semin Cancer Biol *20*, 329-339.

Moser, J., Kool, H., Giakzidis, I., Caldecott, K., Mullenders, L.H., and Fousteri, M.I. (2007). Sealing of chromosomal DNA nicks during nucleotide excision repair requires XRCC1 and DNA ligase III alpha in a cell-cycle-specific manner. Mol Cell *27*, 311-323.

Moynahan, M.E., Chiu, J.W., Koller, B.H., and Jasin, M. (1999). Brca1 controls homology-directed DNA repair. Mol Cell *4*, 511-518.

Mu, D., Hsu, D.S., and Sancar, A. (1996). Reaction mechanism of human DNA repair excision nuclease. J Biol Chem *271*, 8285-8294.

Mullen, J.R., Kaliraman, V., Ibrahim, S.S., and Brill, S.J. (2001). Requirement for three novel protein complexes in the absence of the Sgs1 DNA helicase in Saccharomyces cerevisiae. Genetics *157*, 103-118.

Munoz, I.M., Hain, K., Declais, A.C., Gardiner, M., Toh, G.W., Sanchez-Pulido, L., Heuckmann, J.M., Toth, R., Macartney, T., Eppink, B.*, et al.* (2009). Coordination of structure-specific nucleases by human SLX4/BTBD12 is required for DNA repair. Mol Cell *35*, 116-127.

Munoz-Galvan, S., Tous, C., Blanco, M.G., Schwartz, E.K., Ehmsen, K.T., West, S.C., Heyer, W.D., and Aguilera, A. (2012). Distinct roles of Mus81, Yen1, Slx1-Slx4, and Rad1 nucleases in the repair of replication-born double-strand breaks by sister chromatid exchange. Mol Cell Biol *32*, 1592-1603.

Muntoni, A., Neumann, A.A., Hills, M., and Reddel, R.R. (2009). Telomere elongation involves intra-molecular DNA replication in cells utilizing alternative lengthening of telomeres. Hum Mol Genet *18*, 1017-1027.

Murfuni, I., Nicolai, S., Baldari, S., Crescenzi, M., Bignami, M., Franchitto, A., and Pichierri, P. (2013). The WRN and MUS81 proteins limit cell death and genome instability following oncogene activation. Oncogene *32*, 610-620.

Nabetani, A., and Ishikawa, F. (2009). Unusual telomeric DNAs in human telomerase-negative immortalized cells. Mol Cell Biol *29*, 703-713.

Naim, V., and Rosselli, F. (2009). The FANC pathway and BLM collaborate during mitosis to prevent micro-nucleation and chromosome abnormalities. Nat Cell Biol *11*, 761-768.

Naim, V., Wilhelm, T., Debatisse, M., and Rosselli, F. (2013). ERCC1 and MUS81-EME1 promote sister chromatid separation by processing late replication intermediates at common fragile sites during mitosis. Nat Cell Biol *15*, 1008-1015.

Nakamura, K., Sakai, W., Kawamoto, T., Bree, R.T., Lowndes, N.F., Takeda, S., and Taniguchi, Y. (2006). Genetic dissection of vertebrate 53BP1: a major role in non-homologous end joining of DNA double strand breaks. DNA Repair (Amst) *5*, 741-749.

Nandakumar, J., Bell, C.F., Weidenfeld, I., Zaug, A.J., Leinwand, L.A., and Cech, T.R. (2012). The TEL patch of telomere protein TPP1 mediates telomerase recruitment and processivity. Nature *492*, 285-289.

Neumann, A.A., Watson, C.M., Noble, J.R., Pickett, H.A., Tam, P.P., and Reddel, R.R. (2013). Alternative lengthening of telomeres in normal mammalian somatic cells. Genes Dev *27*, 18-23.

Newman, M., Murray-Rust, J., Lally, J., Rudolf, J., Fadden, A., Knowles, P.P., White, M.F., and McDonald, N.Q. (2005). Structure of an XPF endonuclease with and without DNA suggests a model for substrate recognition. EMBO J *24*, 895-905.

Nicolette, M.L., Lee, K., Guo, Z., Rani, M., Chow, J.M., Lee, S.E., and Paull, T.T. (2010). Mre11-Rad50-Xrs2 and Sae2 promote 5' strand resection of DNA double-strand breaks. Nat Struct Mol Biol *17*, 1478-1485.

Niedernhofer, L.J. (2007). The Fanconi anemia signalosome anchor. Mol Cell *25*, 487-490.

Nimonkar, A.V., Genschel, J., Kinoshita, E., Polaczek, P., Campbell, J.L., Wyman, C., Modrich, P., and Kowalczykowski, S.C. (2011). BLM-DNA2-RPA-MRN and EXO1-BLM-RPA-MRN constitute two DNA end resection machineries for human DNA break repair. Genes Dev *25*, 350-362.

Nimonkar, A.V., Ozsoy, A.Z., Genschel, J., Modrich, P., and Kowalczykowski, S.C. (2008). Human exonuclease 1 and BLM helicase interact to resect DNA and initiate DNA repair. Proc Natl Acad Sci U S A *105*, 16906-16911.

Nishimoto, H., Takayama, M., and Minagawa, T. (1979). Purification and some properties of deoxyribonuclease whose synthesis is controlled by gene 49 of bacteriophage T4. Eur J Biochem *100*, 433-440.

Nishino, T., Komori, K., Ishino, Y., and Morikawa, K. (2003). X-ray and biochemical anatomy of an archaeal XPF/Rad1/Mus81 family nuclease: similarity between its endonuclease domain and restriction enzymes. Structure *11*, 445-457.

O'Donovan, A., Davies, A.A., Moggs, J.G., West, S.C., and Wood, R.D. (1994). XPG endonuclease makes the 3' incision in human DNA nucleotide excision repair. Nature *371*, 432-435.

Oettinger, M.A., Schatz, D.G., Gorka, C., and Baltimore, D. (1990). RAG-1 and RAG-2, adjacent genes that synergistically activate V(D)J recombination. Science *248*, 1517-1523.

Oganesian, L., and Karlseder, J. (2011). Mammalian 5' C-rich telomeric overhangs are a mark of recombination-dependent telomere maintenance. Mol Cell *42*, 224-236.

Ogawa, T., Yu, X., Shinohara, A., and Egelman, E.H. (1993). Similarity of the yeast RAD51 filament to the bacterial RecA filament. Science *259*, 1896-1899.

Ögrünc, M., and Sancar, A. (2003). Identification and characterization of human MUS81-MMS4 structure-specific endonuclease. J Biol Chem *278*, 21715-21720.

Oliver, A.W., Swift, S., Lord, C.J., Ashworth, A., and Pearl, L.H. (2009). Structural basis for recruitment of BRCA2 by PALB2. EMBO Rep *10*, 990-996.

Olovnikov, A.M. (1971). [Principle of marginotomy in template synthesis of polynucleotides]. Dokl Akad Nauk SSSR *201*, 1496-1499.

Olovnikov, A.M. (1973). A theory of marginotomy. The incomplete copying of template margin in enzymic synthesis of polynucleotides and biological significance of the phenomenon. J Theor Biol *41*, 181-190.

Osman, F., Dixon, J., Doe, C.L., and Whitby, M.C. (2003). Generating crossovers by resolution of nicked Holliday junctions: a role for Mus81-Eme1 in meiosis. Mol Cell *12*, 761-774.

Painter, R.B., and Young, B.R. (1980). Radiosensitivity in ataxia-telangiectasia: a new explanation. Proc Natl Acad Sci U S A *77*, 7315-7317.

Palm, W., and de Lange, T. (2008). How shelterin protects mammalian telomeres. Annu Rev Genet *42*, 301-334.

Palmer, D., Lallu, S., Matheson, P., Bethwaite, P., and Tompson, K. (2007). Karyomegalic interstitial nephritis: a pitfall in urine cytology. Diagn Cytopathol *35*, 179-182.

Parsons, C.A., Stasiak, A., Bennett, R.J., and West, S.C. (1995). Structure of a multisubunit complex that promotes DNA branch migration. Nature *374*, 375-378.

Parsons, C.A., Tsaneva, I., Lloyd, R.G., and West, S.C. (1992). Interaction of Escherichia coli RuvA and RuvB proteins with synthetic Holliday junctions. Proc Natl Acad Sci U S A *89*, 5452-5456.

Parsons, C.A., and West, S.C. (1993). Formation of a RuvAB-Holliday junction complex in vitro. J Mol Biol *232*, 397-405.

Patel, K.J., Yu, V.P., Lee, H., Corcoran, A., Thistlethwaite, F.C., Evans, M.J., Colledge, W.H., Friedman, L.S., Ponder, B.A., and Venkitaraman, A.R. (1998). Involvement of Brca2 in DNA repair. Mol Cell *1*, 347-357.

Pavlov, Y.I., Minnick, D.T., Izuta, S., and Kunkel, T.A. (1994). DNA replication fidelity with 8-oxodeoxyguanosine triphosphate. Biochemistry *33*, 4695-4701.

Perez-Burgos, L., Peters, A.H., Opravil, S., Kauer, M., Mechtler, K., and Jenuwein, T. (2004). Generation and characterization of methyl-lysine histone antibodies. Methods Enzymol *376*, 234-254.

Perrem, K., Colgin, L.M., Neumann, A.A., Yeager, T.R., and Reddel, R.R. (2001). Coexistence of alternative lengthening of telomeres and telomerase in hTERT-transfected GM847 cells. Mol Cell Biol *21*, 3862-3875.

Perry, J.J., Yannone, S.M., Holden, L.G., Hitomi, C., Asaithamby, A., Han, S., Cooper, P.K., Chen, D.J., and Tainer, J.A. (2006). WRN exonuclease structure and molecular mechanism imply an editing role in DNA end processing. Nat Struct Mol Biol *13*, 414-422.

Petermann, E., and Helleday, T. (2010). Pathways of mammalian replication fork restart. Nat Rev Mol Cell Biol *11*, 683-687.

Petermann, E., Orta, M.L., Issaeva, N., Schultz, N., and Helleday, T. (2010). Hydroxyurea-stalled replication forks become progressively inactivated and require two different RAD51-mediated pathways for restart and repair. Mol Cell *37*, 492-502.

Petronczki, M., Siomos, M.F., and Nasmyth, K. (2003). Un menage a quatre: the molecular biology of chromosome segregation in meiosis. Cell *112*, 423-440.

Pierce, A.J., Johnson, R.D., Thompson, L.H., and Jasin, M. (1999). XRCC3 promotes homology-directed repair of DNA damage in mammalian cells. Genes Dev *13*, 2633-2638.

Plank, J.L., Wu, J., and Hsieh, T.S. (2006). Topoisomerase IIIalpha and Bloom's helicase can resolve a mobile double Holliday junction substrate through convergent branch migration. Proc Natl Acad Sci U S A *103*, 11118-11123.

Popanda, O., and Thielmann, H.W. (1992). The function of DNA polymerases in DNA repair synthesis of ultraviolet-irradiated human fibroblasts. Biochim Biophys Acta *1129*, 155-160.

Poser, I., Sarov, M., Hutchins, J.R., Heriche, J.K., Toyoda, Y., Pozniakovsky, A., Weigl, D., Nitzsche, A., Hegemann, B., Bird, A.W*., et al.* (2008). BAC TransgeneOmics: a high-throughput method for exploration of protein function in mammals. Nat Methods *5*, 409-415.

Potts, P.R., and Yu, H. (2007). The SMC5/6 complex maintains telomere length in ALT cancer cells through SUMOylation of telomere-binding proteins. Nat Struct Mol Biol *14*, 581-590.

Poulet, A., Buisson, R., Faivre-Moskalenko, C., Koelblen, M., Amiard, S., Montel, F., Cuesta-Lopez, S., Bornet, O., Guerlesquin, F., Godet, T*., et al.* (2009). TRF2 promotes, remodels and protects telomeric Holliday junctions. EMBO J *28*, 641-651.

Rafferty, J.B., Sedelnikova, S.E., Hargreaves, D., Artymiuk, P.J., Baker, P.J., Sharples, G.J., Mahdi, A.A., Lloyd, R.G., and Rice, D.W. (1996). Crystal structure of DNA recombination protein RuvA and a model for its binding to the Holliday junction. Science *274*, 415-421.

Rahman, N., Seal, S., Thompson, D., Kelly, P., Renwick, A., Elliott, A., Reid, S., Spanova, K., Barfoot, R., Chagtai, T*., et al.* (2007). PALB2, which encodes a BRCA2-interacting protein, is a breast cancer susceptibility gene. Nat Genet *39*, 165-167.

Ralf, C., Hickson, I.D., and Wu, L. (2006). The Bloom's syndrome helicase can promote the regression of a model replication fork. J Biol Chem *281*, 22839-22846.

Rass, U., Compton, S.A., Matos, J., Singleton, M.R., Ip, S.C., Blanco, M.G., Griffith, J.D., and West, S.C. (2010). Mechanism of Holliday junction resolution by the human GEN1 protein. Genes Dev *24*, 1559-1569.

Raynard, S., Bussen, W., and Sung, P. (2006). A double Holliday junction dissolvasome comprising BLM, topoisomerase IIIalpha, and BLAP75. J Biol Chem *281*, 13861-13864.

Regairaz, M., Zhang, Y.W., Fu, H., Agama, K.K., Tata, N., Agrawal, S., Aladjem, M.I., and Pommier, Y. (2011). Mus81-mediated DNA cleavage resolves replication forks stalled by topoisomerase I-DNA complexes. J Cell Biol *195*, 739-749.

Reid, S., Schindler, D., Hanenberg, H., Barker, K., Hanks, S., Kalb, R., Neveling, K., Kelly, P., Seal, S., Freund, M*., et al.* (2007). Biallelic mutations in PALB2 cause Fanconi anemia subtype FA-N and predispose to childhood cancer. Nat Genet *39*, 162-164.

Rich, T., Allen, R.L., and Wyllie, A.H. (2000). Defying death after DNA damage. Nature *407*, 777-783.

Richardson, C., and Jasin, M. (2000). Frequent chromosomal translocations induced by DNA double-strand breaks. Nature *405*, 697-700.

Ristic, D., Wyman, C., Paulusma, C., and Kanaar, R. (2001). The architecture of the human Rad54-DNA complex provides evidence for protein translocation along DNA. Proc Natl Acad Sci U S A *98*, 8454-8460.

Rizzo, A., Salvati, E., Porru, M., D'Angelo, C., Stevens, M.F., D'Incalci, M., Leonetti, C., Gilson, E., Zupi, G., and Biroccio, A. (2009). Stabilization of quadruplex DNA perturbs telomere replication leading to the activation of an ATR-dependent ATM signaling pathway. Nucleic Acids Res *37*, 5353-5364.

Roberts, J.J., and Pascoe, J.M. (1972). Cross-linking of complementary strands of DNA in mammalian cells by antitumour platinum compounds. Nature *235*, 282-284.

Rodrigue, A., Coulombe, Y., Jacquet, K., Gagne, J.P., Roques, C., Gobeil, S., Poirier, G., and Masson, J.Y. (2013). The RAD51 paralogs ensure cellular protection against mitotic defects and aneuploidy. J Cell Sci *126*, 348-359.

Rothkamm, K., Kruger, I., Thompson, L.H., and Lobrich, M. (2003). Pathways of DNA double-strand break repair during the mammalian cell cycle. Mol Cell Biol *23*, 5706-5715.

Roy, R., Chun, J., and Powell, S.N. (2012). BRCA1 and BRCA2: different roles in a common pathway of genome protection. Nat Rev Cancer *12*, 68-78.

Ruden, M., and Puri, N. (2013). Novel anticancer therapeutics targeting telomerase. Cancer Treat Rev *39*, 444-456.

Saharia, A., and Stewart, S.A. (2009). FEN1 contributes to telomere stability in ALT-positive tumor cells. Oncogene *28*, 1162-1167.

Saintigny, Y., Delacote, F., Vares, G., Petitot, F., Lambert, S., Averbeck, D., and Lopez, B.S. (2001). Characterization of homologous recombination induced by replication inhibition in mammalian cells. EMBO J *20*, 3861-3870.

Saleh-Gohari, N., Bryant, H.E., Schultz, N., Parker, K.M., Cassel, T.N., and Helleday, T. (2005). Spontaneous homologous recombination is induced by collapsed replication forks that are caused by endogenous DNA single-strand breaks. Mol Cell Biol *25*, 7158-7169.

Salewsky, B., Schmiester, M., Schindler, D., Digweed, M., and Demuth, I. (2012). The nuclease hSNM1B/Apollo is linked to the Fanconi anemia pathway via its interaction with FANCP/SLX4. Hum Mol Genet *21*, 4948-4956.

San Filippo, J., Sung, P., and Klein, H. (2008). Mechanism of eukaryotic homologous recombination. Annu Rev Biochem *77*, 229-257.

Sapir, E., Gozaly-Chianea, Y., Al-Wahiby, S., Ravindran, S., Yasaei, H., and Slijepcevic, P. (2011). Effects of BRCA2 deficiency on telomere recombination in non-ALT and ALT cells. Genome Integr *2*, 9.

Sargent, R.G., Brenneman, M.A., and Wilson, J.H. (1997). Repair of site-specific double-strand breaks in a mammalian chromosome by homologous and illegitimate recombination. Mol Cell Biol *17*, 267-277.

Sartori, A.A., Lukas, C., Coates, J., Mistrik, M., Fu, S., Bartek, J., Baer, R., Lukas, J., and Jackson, S.P. (2007). Human CtIP promotes DNA end resection. Nature *450*, 509-514.

Sasaki, K., Murakami, T., and Takahashi, M. (1989). [Flow cytometric analysis of cell proliferation kinetics using the anti-BrdUrd antibody]. Gan To Kagaku Ryoho *16*, 2338-2344.

Saugar, I., Vazquez, M.V., Gallo-Fernandez, M., Ortiz-Bazan, M.A., Segurado, M., Calzada, A., and Tercero, J.A. (2013). Temporal regulation of the Mus81-Mms4 endonuclease ensures cell survival under conditions of DNA damage. Nucleic Acids Res.

Schreiber, V., Hunting, D., Trucco, C., Gowans, B., Grunwald, D., De Murcia, G., and De Murcia, J.M. (1995). A dominant-negative mutant of human poly(ADP-ribose) polymerase affects cell recovery, apoptosis, and sister chromatid exchange following DNA damage. Proc Natl Acad Sci U S A *92*, 4753-4757.

Schwacha, A., and Kleckner, N. (1995). Identification of double Holliday junctions as intermediates in meiotic recombination. Cell *83*, 783-791.

Schwartz, E.K., Wright, W.D., Ehmsen, K.T., Evans, J.E., Stahlberg, H., and Heyer, W.D. (2012). Mus81-Mms4 functions as a single heterodimer to cleave nicked intermediates in recombinational DNA repair. Mol Cell Biol *32*, 3065-3080.

Seigneur, M., Bidnenko, V., Ehrlich, S.D., and Michel, B. (1998). RuvAB acts at arrested replication forks. Cell *95*, 419-430.

Setlow, R.B. (1966). Cyclobutane-type pyrimidine dimers in polynucleotides. Science *153*, 379-386.

Sfeir, A. (2012). Telomeres at a glance. J Cell Sci *125*, 4173-4178.

Sfeir, A., and de Lange, T. (2012). Removal of shelterin reveals the telomere end-protection problem. Science *336*, 593-597.

Sfeir, A., Kosiyatrakul, S.T., Hockemeyer, D., MacRae, S.L., Karlseder, J., Schildkraut, C.L., and de Lange, T. (2009). Mammalian telomeres resemble fragile sites and require TRF1 for efficient replication. Cell *138*, 90-103.

Shah, R., Bennett, R.J., and West, S.C. (1994a). Activation of RuvC Holliday junction resolvase in vitro. Nucleic Acids Res *22*, 2490-2497.

Shah, R., Bennett, R.J., and West, S.C. (1994b). Genetic recombination in E. coli: RuvC protein cleaves Holliday junctions at resolution hotspots in vitro. Cell *79*, 853-864.

Shahid, M.J., Khouri, F.P., and Ballas, S.K. (1972). Fanconi's anaemia: report of a patient with significant chromosomal abnormalities in bone marrow cells. J Med Genet *9*, 474-478.

Shao, X., and Grishin, N.V. (2000). Common fold in helix-hairpin-helix proteins. Nucleic Acids Res *28*, 2643-2650.

Shay, J.W., and Bacchetti, S. (1997). A survey of telomerase activity in human cancer. Eur J Cancer *33*, 787-791.

Sheaff, R., Ilsley, D., and Kuchta, R. (1991). Mechanism of DNA polymerase alpha inhibition by aphidicolin. Biochemistry *30*, 8590-8597.

Sidorova, J.M., Li, N., Folch, A., and Monnat, R.J., Jr. (2008). The RecQ helicase WRN is required for normal replication fork progression after DNA damage or replication fork arrest. Cell Cycle *7*, 796-807.

Sigurdsson, S., Van Komen, S., Bussen, W., Schild, D., Albala, J.S., and Sung, P. (2001). Mediator function of the human Rad51B-Rad51C complex in Rad51/RPA-catalyzed DNA strand exchange. Genes Dev *15*, 3308-3318.

Sigurdsson, S., Van Komen, S., Petukhova, G., and Sung, P. (2002). Homologous DNA pairing by human recombination factors Rad51 and Rad54. J Biol Chem *277*, 42790-42794.

Siitonen, H.A., Sotkasiira, J., Biervliet, M., Benmansour, A., Capri, Y., Cormier-Daire, V., Crandall, B., Hannula-Jouppi, K., Hennekam, R., Herzog, D.*, et al.* (2009). The mutation spectrum in RECQL4 diseases. Eur J Hum Genet *17*, 151-158.

Singer, B. (1975). The chemical effects of nucleic acid alkylation and their relation to mutagenesis and carcinogenesis. Prog Nucleic Acid Res Mol Biol *15*, 219-284.

Singh, T.R., Ali, A.M., Busygina, V., Raynard, S., Fan, Q., Du, C.H., Andreassen, P.R., Sung, P., and Meetei, A.R. (2008). BLAP18/RMI2, a novel OB-fold-containing protein, is an essential component of the Bloom helicase-double Holliday junction dissolvasome. Genes Dev *22*, 2856-2868.

Smogorzewska, A., Desetty, R., Saito, T.T., Schlabach, M., Lach, F.P., Sowa, M.E., Clark, A.B., Kunkel, T.A., Harper, J.W., Colaiacovo, M.P.*, et al.* (2010). A genetic screen identifies FAN1, a Fanconi anemia-associated nuclease necessary for DNA interstrand crosslink repair. Mol Cell *39*, 36-47.

Smogorzewska, A., Matsuoka, S., Vinciguerra, P., McDonald, E.R., 3rd, Hurov, K.E., Luo, J., Ballif, B.A., Gygi, S.P., Hofmann, K., D'Andrea, A.D.*, et al.* (2007). Identification of the FANCI protein, a monoubiquitinated FANCD2 paralog required for DNA repair. Cell *129*, 289-301.

Stavropoulos, D.J., Bradshaw, P.S., Li, X., Pasic, I., Truong, K., Ikura, M., Ungrin, M., and Meyn, M.S. (2002). The Bloom syndrome helicase BLM interacts with TRF2 in ALT cells and promotes telomeric DNA synthesis. Hum Mol Genet *11*, 3135-3144.

Stoepker, C., Hain, K., Schuster, B., Hilhorst-Hofstee, Y., Rooimans, M.A., Steltenpool, J., Oostra, A.B., Eirich, K., Korthof, E.T., Nieuwint, A.W.*, et al.* (2011). SLX4, a coordinator of structure-specific endonucleases, is mutated in a new Fanconi anemia subtype. Nat Genet *43*, 138-141.

Strumberg, D., Pilon, A.A., Smith, M., Hickey, R., Malkas, L., and Pommier, Y. (2000). Conversion of topoisomerase I cleavage complexes on the leading strand of ribosomal DNA into 5'-phosphorylated DNA double-strand breaks by replication runoff. Mol Cell Biol *20*, 3977-3987.

Sugasawa, K., Ng, J.M., Masutani, C., Iwai, S., van der Spek, P.J., Eker, A.P., Hanaoka, F., Bootsma, D., and Hoeijmakers, J.H. (1998). Xeroderma pigmentosum group C protein complex is the initiator of global genome nucleotide excision repair. Mol Cell *2*, 223-232.

Sugiyama, T., Zaitseva, E.M., and Kowalczykowski, S.C. (1997). A single-stranded DNA-binding protein is needed for efficient presynaptic complex formation by the Saccharomyces cerevisiae Rad51 protein. J Biol Chem *272*, 7940-7945.

Sundquist, W.I., and Klug, A. (1989). Telomeric DNA dimerizes by formation of guanine tetrads between hairpin loops. Nature *342*, 825-829.

Svendsen, J.M., Smogorzewska, A., Sowa, M.E., O'Connell, B.C., Gygi, S.P., Elledge, S.J., and Harper, J.W. (2009). Mammalian BTBD12/SLX4 assembles a Holliday junction resolvase and is required for DNA repair. Cell *138*, 63-77.

Sy, S.M., Huen, M.S., and Chen, J. (2009). PALB2 is an integral component of the BRCA complex required for homologous recombination repair. Proc Natl Acad Sci U S A *106*, 7155-7160.

Szakal, B., and Branzei, D. (2013). Premature Cdk1/Cdc5/Mus81 pathway activation induces aberrant replication and deleterious crossover. EMBO J *32*, 1155-1167.

Szostak, J.W., Orr-Weaver, T.L., Rothstein, R.J., and Stahl, F.W. (1983). The double-strand-break repair model for recombination. Cell *33*, 25-35.

Takakura, M., Kyo, S., Kanaya, T., Hirano, H., Takeda, J., Yutsudo, M., and Inoue, M. (1999). Cloning of human telomerase catalytic subunit (hTERT) gene promoter and identification of proximal core promoter sequences essential for transcriptional activation in immortalized and cancer cells. Cancer Res *59*, 551-557.

Takata, M., Sasaki, M.S., Sonoda, E., Fukushima, T., Morrison, C., Albala, J.S., Swagemakers, S.M., Kanaar, R., Thompson, L.H., and Takeda, S. (2000). The Rad51 paralog Rad51B promotes homologous recombinational repair. Mol Cell Biol *20*, 6476-6482.

Takata, M., Sasaki, M.S., Sonoda, E., Morrison, C., Hashimoto, M., Utsumi, H., Yamaguchi-Iwai, Y., Shinohara, A., and Takeda, S. (1998). Homologous recombination and non-homologous end-joining pathways of DNA double-strand break repair have overlapping roles in the maintenance of chromosomal integrity in vertebrate cells. EMBO J *17*, 5497-5508.

Takata, M., Sasaki, M.S., Tachiiri, S., Fukushima, T., Sonoda, E., Schild, D., Thompson, L.H., and Takeda, S. (2001). Chromosome instability and defective recombinational repair in knockout mutants of the five Rad51 paralogs. Mol Cell Biol *21*, 2858-2866.

Tan, T.L., Essers, J., Citterio, E., Swagemakers, S.M., de Wit, J., Benson, F.E., Hoeijmakers, J.H., and Kanaar, R. (1999). Mouse Rad54 affects DNA conformation and DNA-damage-induced Rad51 foci formation. Curr Biol *9*, 325-328.

Taniguchi, T., Garcia-Higuera, I., Andreassen, P.R., Gregory, R.C., Grompe, M., and D'Andrea, A.D. (2002). S-phase-specific interaction of the Fanconi anemia protein, FANCD2, with BRCA1 and RAD51. Blood *100*, 2414-2420.

Tarsounas, M., Munoz, P., Claas, A., Smiraldo, P.G., Pittman, D.L., Blasco, M.A., and West, S.C. (2004). Telomere maintenance requires the RAD51D recombination/repair protein. Cell *117*, 337-347.

Tay, Y.D., and Wu, L. (2010). Overlapping roles for Yen1 and Mus81 in cellular Holliday junction processing. J Biol Chem *285*, 11427-11432.

Taylor, E.R., and McGowan, C.H. (2008). Cleavage mechanism of human Mus81-Eme1 acting on Holliday-junction structures. Proc Natl Acad Sci U S A *105*, 3757-3762.

Tejera, A.M., Stagno d'Alcontres, M., Thanasoula, M., Marion, R.M., Martinez, P., Liao, C., Flores, J.M., Tarsounas, M., and Blasco, M.A. (2010). TPP1 is required for TERT recruitment, telomere elongation during nuclear reprogramming, and normal skin development in mice. Dev Cell *18*, 775-789.

Teoule, R. (1987). Radiation-induced DNA damage and its repair. Int J Radiat Biol Relat Stud Phys Chem Med *51*, 573-589.

Thompson, L.H., Brookman, K.W., Dillehay, L.E., Carrano, A.V., Mazrimas, J.A., Mooney, C.L., and Minkler, J.L. (1982). A CHO-cell strain having hypersensitivity to mutagens, a defect in DNA strand-break repair, and an extraordinary baseline frequency of sister-chromatid exchange. Mutat Res *95*, 427-440.

Thorslund, T., McIlwraith, M.J., Compton, S.A., Lekomtsev, S., Petronczki, M., Griffith, J.D., and West, S.C. (2010). The breast cancer tumor suppressor BRCA2 promotes the specific targeting of RAD51 to single-stranded DNA. Nat Struct Mol Biol *17*, 1263-1265.

Tomas-Loba, A., Flores, I., Fernandez-Marcos, P.J., Cayuela, M.L., Maraver, A., Tejera, A., Borras, C., Matheu, A., Klatt, P., Flores, J.M.*, et al.* (2008). Telomerase reverse transcriptase delays aging in cancer-resistant mice. Cell *135*, 609-622.

Tomaska, L., Nosek, J., Kramara, J., and Griffith, J.D. (2009). Telomeric circles: universal players in telomere maintenance? Nat Struct Mol Biol *16*, 1010-1015.

Tomlinson, R.L., Ziegler, T.D., Supakorndej, T., Terns, R.M., and Terns, M.P. (2006). Cell cycle-regulated trafficking of human telomerase to telomeres. Mol Biol Cell *17*, 955-965.

Tripsianes, K., Folkers, G., Ab, E., Das, D., Odijk, H., Jaspers, N.G., Hoeijmakers, J.H., Kaptein, R., and Boelens, R. (2005). The structure of the human ERCC1/XPF interaction domains reveals a complementary role for the two proteins in nucleotide excision repair. Structure *13*, 1849-1858.

Trujillo, J.P., Mina, L.B., Pujol, R., Bogliolo, M., Andrieux, J., Holder, M., Schuster, B., Schindler, D., and Surralles, J. (2012). On the role of FAN1 in Fanconi anemia. Blood *120*, 86-89.

Tsaneva, I.R., Muller, B., and West, S.C. (1992). ATP-dependent branch migration of Holliday junctions promoted by the RuvA and RuvB proteins of E. coli. Cell *69*, 1171-1180.

Tsujimoto, Y., and Ogawa, H. (1978). Intermediates in genetic recombination of bacteriophage T7 DNA. Biological activity and the roles of gene 3 and gene 5. J Mol Biol *125*, 255-273.

van Brabant, A.J., Ye, T., Sanz, M., German, I.J., Ellis, N.A., and Holloman, W.K. (2000). Binding and melting of D-loops by the Bloom syndrome helicase. Biochemistry *39*, 14617-14625.

van der Heijden, T., Seidel, R., Modesti, M., Kanaar, R., Wyman, C., and Dekker, C. (2007). Real-time assembly and disassembly of human RAD51 filaments on individual DNA molecules. Nucleic Acids Res *35*, 5646-5657.

Van Dyck, E., Stasiak, A.Z., Stasiak, A., and West, S.C. (2001). Visualization of recombination intermediates produced by RAD52-mediated single-strand annealing. EMBO Rep *2*, 905-909.

van Heemst, D., Brugmans, L., Verkaik, N.S., and van Gent, D.C. (2004). End-joining of blunt DNA double-strand breaks in mammalian fibroblasts is precise and requires DNA-PK and XRCC4. DNA Repair (Amst) *3*, 43-50.

Vannier, J.B., Pavicic-Kaltenbrunner, V., Petalcorin, M.I., Ding, H., and Boulton, S.J. (2012). RTEL1 dismantles T loops and counteracts telomeric G4-DNA to maintain telomere integrity. Cell *149*, 795-806.

Venteicher, A.S., Abreu, E.B., Meng, Z., McCann, K.E., Terns, R.M., Veenstra, T.D., Terns, M.P., and Artandi, S.E. (2009). A human telomerase holoenzyme protein required for Cajal body localization and telomere synthesis. Science *323*, 644-648.

Venteicher, A.S., Meng, Z., Mason, P.J., Veenstra, T.D., and Artandi, S.E. (2008). Identification of ATPases pontin and reptin as telomerase components essential for holoenzyme assembly. Cell *132*, 945-957.

Verdun, R.E., and Karlseder, J. (2006). The DNA damage machinery and homologous recombination pathway act consecutively to protect human telomeres. Cell *127*, 709-720.

Vermote, C.L., and Halford, S.E. (1992). EcoRV restriction endonuclease: communication between catalytic metal ions and DNA recognition. Biochemistry *31*, 6082-6089.

Wang, R.C., Smogorzewska, A., and de Lange, T. (2004). Homologous recombination generates T-loop-sized deletions at human telomeres. Cell *119*, 355-368.

Watson, J.D. (1972). Origin of concatemeric T7 DNA. Nat New Biol *239*, 197-201.

Wechsler, T., Newman, S., and West, S.C. (2011). Aberrant chromosome morphology in human cells defective for Holliday junction resolution. Nature *471*, 642-646.

Weinrich, S.L., Pruzan, R., Ma, L., Ouellette, M., Tesmer, V.M., Holt, S.E., Bodnar, A.G., Lichtsteiner, S., Kim, N.W., Trager, J.B.*, et al.* (1997). Reconstitution of human telomerase with the template RNA component hTR and the catalytic protein subunit hTRT. Nat Genet *17*, 498-502.

West, S.C. (1997). Processing of recombination intermediates by the RuvABC proteins. Annu Rev Genet *31*, 213-244.

West, S.C. (2003). Molecular views of recombination proteins and their control. Nat Rev Mol Cell Biol *4*, 435-445.

West, S.C., Cassuto, E., Mursalim, J., and Howard-Flanders, P. (1980). Recognition of duplex DNA containing single-stranded regions by recA protein. Proc Natl Acad Sci U S A *77*, 2569-2573.

West, S.C., Countryman, J.K., and Howard-Flanders, P. (1983). Enzymatic formation of biparental figure-eight molecules from plasmid DNA and their resolution in E. coli. Cell *32*, 817-829.

Whitby, M.C., Osman, F., and Dixon, J. (2003). Cleavage of model replication forks by fission yeast Mus81-Eme1 and budding yeast Mus81-Mms4. J Biol Chem *278*, 6928-6935.

Williams, R.S., and Tainer, J.A. (2005). A nanomachine for making ends meet: MRN is a flexing scaffold for the repair of DNA double-strand breaks. Mol Cell *19*, 724-726.

Williamson, J.R., Raghuraman, M.K., and Cech, T.R. (1989). Monovalent cation-induced structure of telomeric DNA: the G-quartet model. Cell *59*, 871-880.

Winkler, G.S., Araujo, S.J., Fiedler, U., Vermeulen, W., Coin, F., Egly, J.M., Hoeijmakers, J.H., Wood, R.D., Timmers, H.T., and Weeda, G. (2000). TFIIH with inactive XPD helicase functions in transcription initiation but is defective in DNA repair. J Biol Chem *275*, 4258-4266.

Wold, M.S. (1997). Replication protein A: a heterotrimeric, single-stranded DNA-binding protein required for eukaryotic DNA metabolism. Annu Rev Biochem *66*, 61-92.

Wong, A.K., Pero, R., Ormonde, P.A., Tavtigian, S.V., and Bartel, P.L. (1997). RAD51 interacts with the evolutionarily conserved BRC motifs in the human breast cancer susceptibility gene brca2. J Biol Chem *272*, 31941-31944.

Wood, R.D. (2010). Mammalian nucleotide excision repair proteins and interstrand crosslink repair. Environ Mol Mutagen *51*, 520-526.

Wooster, R., Bignell, G., Lancaster, J., Swift, S., Seal, S., Mangion, J., Collins, N., Gregory, S., Gumbs, C., and Micklem, G. (1995). Identification of the breast cancer susceptibility gene BRCA2. Nature *378*, 789-792.

Wright, W.E., Pereira-Smith, O.M., and Shay, J.W. (1989). Reversible cellular senescence: implications for immortalization of normal human diploid fibroblasts. Mol Cell Biol *9*, 3088-3092.

Wright, W.E., Piatyszek, M.A., Rainey, W.E., Byrd, W., and Shay, J.W. (1996). Telomerase activity in human germline and embryonic tissues and cells. Dev Genet *18*, 173-179.

Wu, F., Liu, S.Y., Tao, Y.M., Ou, D.P., Fang, F., and Yang, L.Y. (2008). Decreased expression of methyl methansulfonate and ultraviolet-sensitive gene clone 81 (Mus81) is correlated with a poor prognosis in patients with hepatocellular carcinoma. Cancer *112*, 2002-2010.

Wu, F., Shirahata, A., Sakuraba, K., Kitamura, Y., Goto, T., Saito, M., Ishibashi, K., Kigawa, G., Nemoto, H., Sanada, Y.*, et al.* (2011). Downregulation of Mus81 as a novel prognostic biomarker for patients with colorectal carcinoma. Cancer Sci *102*, 472-477.

Wu, G., Lee, W.H., and Chen, P.L. (2000). NBS1 and TRF1 colocalize at promyelocytic leukemia bodies during late S/G2 phases in immortalized telomerase-negative cells. Implication of NBS1 in alternative lengthening of telomeres. J Biol Chem *275*, 30618-30622.

Wu, L., and Hickson, I.D. (2003). The Bloom's syndrome helicase suppresses crossing over during homologous recombination. Nature *426*, 870-874.

Wu, P., Takai, H., and de Lange, T. (2012). Telomeric 3' overhangs derive from resection by Exo1 and Apollo and fill-in by POT1b-associated CST. Cell *150*, 39-52.

Wu, P., van Overbeek, M., Rooney, S., and de Lange, T. (2010). Apollo contributes to G overhang maintenance and protects leading-end telomeres. Mol Cell *39*, 606-617.

Wyatt, H.D., S., S., J., M., and S.C., W. (2013). Coordinated actions of SLX1-SLX4 and MUS81-EME1 for Holliday junction resolution in human cells. Molecular Cell *in press*.

Wyatt, H.D., West, S.C., and Beattie, T.L. (2010). InTERTpreting telomerase structure and function. Nucleic Acids Res *38*, 5609-5622.

Xia, B., Sheng, Q., Nakanishi, K., Ohashi, A., Wu, J., Christ, N., Liu, X., Jasin, M., Couch, F.J., and Livingston, D.M. (2006). Control of BRCA2 cellular and clinical functions by a nuclear partner, PALB2. Mol Cell *22*, 719-729.

Yang, W., Lee, J.Y., and Nowotny, M. (2006). Making and breaking nucleic acids: two-Mg2+-ion catalysis and substrate specificity. Mol Cell *22*, 5-13.

Ye, J.Z., Donigian, J.R., van Overbeek, M., Loayza, D., Luo, Y., Krutchinsky, A.N., Chait, B.T., and de Lange, T. (2004a). TIN2 binds TRF1 and TRF2 simultaneously and stabilizes the TRF2 complex on telomeres. J Biol Chem *279*, 47264-47271.

Ye, J.Z., Hockemeyer, D., Krutchinsky, A.N., Loayza, D., Hooper, S.M., Chait, B.T., and de Lange, T. (2004b). POT1-interacting protein PIP1: a telomere length regulator that recruits POT1 to the TIN2/TRF1 complex. Genes Dev *18*, 1649-1654.

Yeager, T.R., Neumann, A.A., Englezou, A., Huschtscha, L.I., Noble, J.R., and Reddel, R.R. (1999). Telomerase-negative immortalized human cells contain a novel type of promyelocytic leukemia (PML) body. Cancer Res *59*, 4175-4179.

Ying, S., Minocherhomji, S., Chan, K.L., Palmai-Pallag, T., Chu, W.K., Wass, T., Mankouri, H.W., Liu, Y., and Hickson, I.D. (2013). MUS81 promotes common fragile site expression. Nat Cell Biol.

Yoshihara, T., Ishida, M., Kinomura, A., Katsura, M., Tsuruga, T., Tashiro, S., Asahara, T., and Miyagawa, K. (2004). XRCC3 deficiency results in a defect in recombination and increased endoreduplication in human cells. EMBO J *23*, 670-680.

Yu, C.E., Oshima, J., Fu, Y.H., Wijsman, E.M., Hisama, F., Alisch, R., Matthews, S., Nakura, J., Miki, T., Ouais, S.*, et al.* (1996). Positional cloning of the Werner's syndrome gene. Science *272*, 258-262.

Yu, X., Jacobs, S.A., West, S.C., Ogawa, T., and Egelman, E.H. (2001). Domain structure and dynamics in the helical filaments formed by RecA and Rad51 on DNA. Proc Natl Acad Sci U S A *98*, 8419-8424.

Yuan, S.S., Lee, S.Y., Chen, G., Song, M., Tomlinson, G.E., and Lee, E.Y. (1999). BRCA2 is required for ionizing radiation-induced assembly of Rad51 complex in vivo. Cancer Res *59*, 3547-3551.

Zakharyevich, K., Ma, Y., Tang, S., Hwang, P.Y., Boiteux, S., and Hunter, N. (2010). Temporally and biochemically distinct activities of Exo1 during meiosis: double-strand break resection and resolution of double Holliday junctions. Mol Cell *40*, 1001-1015.

Zakharyevich, K., Tang, S., Ma, Y., and Hunter, N. (2012). Delineation of joint molecule resolution pathways in meiosis identifies a crossover-specific resolvase. Cell *149*, 334-347.

Zeng, S., Xiang, T., Pandita, T.K., Gonzalez-Suarez, I., Gonzalo, S., Harris, C.C., and Yang, Q. (2009). Telomere recombination requires the MUS81 endonuclease. Nat Cell Biol *11*, 616-623.

Zhang, F., Fan, Q., Ren, K., and Andreassen, P.R. (2009). PALB2 functionally connects the breast cancer susceptibility proteins BRCA1 and BRCA2. Mol Cancer Res *7*, 1110-1118.

Zhong, F.L., Batista, L.F., Freund, A., Pech, M.F., Venteicher, A.S., and Artandi, S.E. (2012). TPP1 OB-fold domain controls telomere maintenance by recruiting telomerase to chromosome ends. Cell *150*, 481-494.

Zhong, Z.H., Jiang, W.Q., Cesare, A.J., Neumann, A.A., Wadhwa, R., and Reddel, R.R. (2007). Disruption of telomere maintenance by depletion of the MRE11/RAD50/NBS1 complex in cells that use alternative lengthening of telomeres. J Biol Chem *282*, 29314-29322.

Zhou, W., Otto, E.A., Cluckey, A., Airik, R., Hurd, T.W., Chaki, M., Diaz, K., Lach, F.P., Bennett, G.R., Gee, H.Y.*, et al.* (2012). FAN1 mutations cause karyomegalic interstitial nephritis, linking chronic kidney failure to defective DNA damage repair. Nat Genet *44*, 910-915.

Zhu, Z., Chung, W.H., Shim, E.Y., Lee, S.E., and Ira, G. (2008). Sgs1 helicase and two nucleases Dna2 and Exo1 resect DNA double-strand break ends. Cell *134*, 981-994.

Zijlmans, J.M., Martens, U.M., Poon, S.S., Raap, A.K., Tanke, H.J., Ward, R.K., and Lansdorp, P.M. (1997). Telomeres in the mouse have large inter-chromosomal variations in the number of T2AG3 repeats. Proc Natl Acad Sci U S A *94*, 7423-7428.